

# **Modelling soil erosion in a small catchment on the Chinese Loess Plateau**



Nederlandse Geografische Studies 307

Modelling soil erosion in a small catchment on  
the Chinese Loess Plateau  
Applying LISEM to extreme conditions

Rudi Hessel

Utrecht 2002

Koninklijk Nederlands Aardrijkskundig Genootschap /  
Faculteit Ruimtelijke Wetenschappen Universiteit Utrecht

This publication has been submitted as Ph.D. thesis in partial fulfillment of the requirements for the award of the degree of Doctor at Utrecht University, The Netherlands, 18 November 2002.

Promotor: Prof. Dr. P.A. Burrough  
Faculty of Geographical Sciences, Utrecht University

Co-promotores: Dr. V.G. Jetten  
Dr. Th.W.J. van Asch  
Faculty of Geographical Sciences, Utrecht University

Examination: Committee	Prof. Dr. R.P.C. Morgan	Cranfield University
	Prof. Dr. G. Govers	Katholieke Universiteit Leuven
	Prof. Dr. J.D. Nieuwenhuis	Delft University
	Prof. Dr. S.M. de Jong	Utrecht University
	Dr. C.J. Ritsema	Alterra Green World Research

This research was financially supported by the INCO-DEV Programme of the European Commission through the research project EROCHINA (Contract IC18-CT97-0158): A participatory approach for soil and water conservation planning, integrating soil erosion modeling and land evaluation, to improve the sustainability of land use on the Loess Plateau in China.

ISBN 90-6809-343-6

Copyright © Rudi Hessel, p/a Faculty of Geographical Sciences, Utrecht University, 2002.

Niets uit deze uitgave mag worden vermenigvuldigd en/of openbaar gemaakt door middel van druk, fotokopie of op welke andere wijze dan ook zonder voorafgaande schriftelijke toestemming van de uitgevers.

All rights reserved. No part of this publication may be reproduced in any form, by print or photo print, microfilm or any other means, without written permission by the publishers.

Printed in the Netherlands by Labor Grafimedia b.v. – Utrecht



*'God's voice thunders in marvellous ways;  
he does great things beyond our understanding.  
He says to the snow, 'Fall on the earth,'  
and to the rain shower, 'Be a mighty downpour.'*

(Job 37: 5 and 6, NIV translation of The Bible)

To my parents



# CONTENTS

List of figures	10
List of tables	13
List of appendices	14
Acknowledgements	17
1 Introduction	19
1.1 Introduction	19
1.2 The Loess Plateau	19
1.3 The EROCHINA project	23
1.4 Aims of this thesis	23
2 Theory of soil erosion modelling	25
2.1 Introduction	25
2.2 Flow velocity and flow routing	25
2.3 Sediment transport	27
2.4 High concentrations	33
2.5 Gullies	34
2.6 Erosion modelling	38
2.7 LISEM	43
2.8 Conclusions	50
3 The Danangou catchment	51
3.1 The Loess Plateau	51
3.2 Catchment choice	56
3.3 Geology and soils	58
3.4 Geomorphology	60
3.5 Climate and hydrology	68
3.6 Land use	70
3.7 Event erosion	74
3.8 Conclusions	76
4 Field methods and data	77
4.1 LISEM field measurements	77
4.2 Rainfall	83
4.3 Soil physical properties	86
4.4 Discharge measurement	89

4.5	Measurement of soil erosion	105
4.6	Conclusions	110
5	Sediment concentration	113
5.1	Introduction	113
5.2	Causes of high concentrations	115
5.3	Consequences of high concentrations	117
5.4	Streamflow in the Danangou catchment	125
5.5	Overland flow in the Danangou catchment	129
5.6	Conclusions	132
6	Flow velocity	133
6.1	Introduction	133
6.2	Experimental setup	136
6.3	Results	140
6.4	Discussion	143
6.5	Conclusions	151
7	Transport capacity	161
7.1	Introduction	161
7.2	Study area	164
7.3	Use of the LISEM model	164
7.4	Transport equations	165
7.5	Catchment results	172
7.6	Discussion of catchment results	175
7.7	Discussion of catchment methods	179
7.8	Overland flow	183
7.9	Conclusions	189
8	Gullies	193
8.1	Introduction	193
8.2	Gully types and processes	193
8.3	Stability model	199
8.4	Model results and discussion	203
8.5	Sediment balance	206
8.6	Conclusions	218
9	LISEM changes and settings	219
9.1	Introduction	219
9.2	Effects of LISEM changes	219
9.3	Cell size and time step length	226

9.4	Conclusions	235
10	LISEM calibration and validation	237
10.1	Introduction	237
10.2	Catchment outlet calibration	238
10.3	Additional events	254
10.4	Erosion pattern evaluation	259
10.5	Conclusions	265
11	Land use scenarios	267
11.1	Introduction	267
11.2	Methods	268
11.3	Results	273
11.4	Choice of storm	277
11.5	Parameter sensitivity	282
11.6	Discussion	283
11.7	Conclusions	284
12	Synthesis	285
	Summary	289
	Samenvatting (Dutch Summary)	295
	摘要(Chinese Summary)	301
	References	307
	Curriculum vitae	317

## FIGURES

1.1	Distribution of loess in China	20
1.2	Map of the Yellow River basin	21
1.3	Typical landscape of the hilly part of the Loess Plateau, northern Shaanxi	22
2.1	Simplified flow chart of the LISEM soil erosion model	44
2.2	c and d coefficients as a function of median grainsize (D50)	46
2.3	Transport capacity as function of stream power for different grainsizes	47
3.1	Elevation map of the Danangou catchment. The position of the Danangou catchment on the Chinese Loess Plateau is also indicated	57
3.2	Slope map (°) of the Danangou catchment	58
3.3	Red loess gully with secondary calcareous concretions derived from the loess in the foreground. The depth of the gully is about 50 m.	60
3.4	Lithological map of the Danangou catchment.	61
3.5	Geomorphological map of the Danangou catchment	62
3.6	Slump in the Danangou catchment. Several gully complexes are also visible	63
3.7	Conceptual model of yellow loess gully development	65
3.8	Soil fall in a yellow loess gully.	66
3.9	Rill in soybean field, September 1998	68
3.10	Monthly rainfall at Ansai over the period 1971-1998.	69
3.11	Daily rainfall amount as a function of return period, Yan'an. A partial series technique has been used on all daily rainfall amounts over 13 mm	69
3.12	Ploughing with an ox on a steep slope	71
3.13	Farmers grinding maize with a millstone. A mule is used to rotate the upper millstone. The mule is blindfolded to prevent it from becoming dizzy	72
3.14	Land use map of the Danangou catchment, 1999	73
3.15	Runoff in the Danangou catchment during an event that occurred on July 20 <sup>th</sup> , 1999. Picture taken just before peak runoff	75
3.16	Evidence of flowing water in a woodland after the event of August 29 <sup>th</sup> , 2000.	76
4.1	Measurement locations in 1999. The 1999 land use map (figure 3.14) is used as background.	79
4.2	Plant height in 1998 (May – October) and 1999 (April – September)	80
4.3	Random Roughness in 1998 (May – October) and 1999 (April – September)	81
4.4	Soil moisture content in 1998 (May – October) and 1999 (April – September)	82
4.5	Average daily rainfall in the Danangou catchment, April to September 2000.	85
4.6	Measured water level and concentration for all six events	96
4.7	Rainfall arrival times for the different rain gauges, event of August 29 <sup>th</sup> , 2000	98
4.8	The weir on August 30 <sup>th</sup> , 2000. The supporting construction of the ultrasonic water level sensor as well as the sensor itself were destroyed by the event of 000829.	99
4.9	Sediment plot in 1999. The crop is pearl millet	103
4.10	Rill erosion maps of 1998 and 2000	107
5.1	Dynamic viscosity as function of sediment concentration. Viscosity is expressed as the fluid viscosity divided by clear water viscosity. Values are for 15 degree centigrade fluid.	120

5.2	Settling velocity as a function of sediment concentration. Settling velocity is expressed as fraction of the clear water settling velocity.	122
5.3	Sediment delivery ratio as a function of catchment size.	123
5.4	Measured discharge and concentration & sediment corrected discharge for the event of July 20 <sup>th</sup> , 1999	129
5.5	Thick sediment layer (about 10 cm) in the gully-flume after the event of 980715.	131
5.6	Measured water level, estimated sediment level and corrected water level for the event of 990710, sediment plot	131
6.1	Setup of measurement 3 of the second series (2000).	137
6.2	Manning's n and Darcy-Weisbach f as functions of Reynolds number. Data for all cropland runs of the second series.	140
6.3.	Cropland Manning's n as a function of slope, data per plot. Data for 1999 and 2000 combined.	141
6.4	Velocity as a function of slope for cropland and woodland, all data	142
6.5	R and h as function of flowwidth	144
6.6	Manning's n as a function of slope for croplands, data of second series. The squares represent the original data, the triangles the data with slope correction.	145
6.7	Manning's n versus sediment volume in the bucket at the downstream end of the plot. Data for the second series are shown.	146
6.8	Velocity as a function of discharge. Measurements are compared with the relationship developed by Govers (1992) and given in equation 6.4 and with equation 6.5. Data for all cropland runs of 1999 and 2000 are shown	148
7.1	Clean water concentration as function of clean water discharge for all 5 events at the Danangou weir combined	170
7.2	Results of different transport equations, event of 990720. Maximum possible clear water concentration was 1060 g/l	173
7.3	Transport capacities predicted by different transport equations for t= 10 minutes (during heavy rain). Clear water transport capacities range from 0 (black) to 1060 (white) g/l	174
7.4	LISEM simulation results for the sediment plot, 990710, 000707 and 000829 events	186
7.5	Amount of sediment in downslope buckets of manning measurements as function of slope and discharge. Cropland plots only	188
7.6	Concentration as a function of stream power. Data for cropland plot measurements only. Transport capacity (for D50 = 35 $\mu$ m) according to the Govers (1990) equations is also shown	189
8.1	Lithological map of the Danangou catchment. The position of the gully headcuts from table 8.2 is also shown in the map; red loess gully headcuts are shown with a 4-point star, yellow loess gullies with a 5-point star	195
8.2	Left: red Loess gully complex containing red loess gully heads 2, 4 and 5 of table 8.2. The position of gully heads 2 and 4 is indicated with arrows; gully head 5 is not included in the picture. Right: yellow loess gully 4 of table 8.2 (indicated with arrow)	196
8.3	Loose soil material in one of the gullies of the Danangou catchment before (left) and after (right) the runoff event of July 20 <sup>th</sup> , 1999	198
8.4	Relationship between residual gravimetric soil water content and c, $\phi$ for remoulded (weathered) loess	201

8.5	Measured headcut heights (A) and simulated headcut heights (B) for the Danangou catchment	204
8.6	Simulated 10-run average daily soil fall amount (line with triangles) and average measured rainfall minus simulated runoff (bars), May to October 1998	205
8.7	Grainsize distribution of samples taken at the weir during the event of august 11 <sup>th</sup> , 2000	214
8.8	D50 as a function of concentration, all 5 events combined	214
8.9	Sediment concentration as a function of discharge, 980801 event	216
8.10	Sediment concentration as function of discharge, 980823 event	216
9.1	Effect of slope correction: smaller water depth and longer flow distance	220
9.2	Predicted discharge with LISEM 163 and using a slope correction	221
9.3	Comparison of sediment concentration predicted with a version of LISEM 163 that incorporated the slope correction, without and with settling correction added. Event of 990720.	223
9.4	Loose material map of a small part of the Danangou catchment before (left) and after (right) LISEM simulation.	224
9.5	Areas occupied by different slope classes in the Danangou catchment.	225
9.6	Effect of grid size on simulated discharge, 15-second time step, 990720 event	228
9.7	Effect of grid size on simulated concentration, 15-second time step, 990720 event	228
9.8	Predicted sediment concentration for different time step lengths, calibrated dataset of 990720, 10-metre grid	231
10.1	Calibration results for the five events that were measured at the weir	245
10.2	Validation results for the 990720 event.	248
10.3	Validation results for the 000829 event.	249
10.4	Simulated and measured concentration for the 980801 event	249
10.5	Simulated concentration for the 000829 event as function of cohesion	251
10.6	Simulated concentration for different values of D50, 990720 event	252
10.7	Relationship between D50 of the suspension and clear water discharge, all 5 events combined	252
10.8	Observed rainfall and simulated discharge for 6 events	256
10.9	A) Mapped rill erosion of 1999. B) LISEM simulation results for the 990720 event. This map gives a classified map of the net erosion (erosion-deposition).	261
11.1	Simplified land use map for 1998	269
11.2	Scenario land use (15-degree cropland limit) for the Danangou catchment	271
11.3	Classified LISEM erosion map for the present land use and the august 1 <sup>st</sup> 1998 storm	274
11.4	Results for the present land use with biological conservation measures (scenario 0a) on cropland/fallow	275
11.5	Predicted erosion for the scenario land use with 15-degree cropland slope limit (scenario 3)	276
11.6	Predicted hydrographs for different land use scenarios	277
11.7	Decrease in total soil loss for the different scenarios, 980801 and 000829 storm	280
11.8	Effect of multiplication factors on simulated total soil loss	283



## TABLES

2.1	Input data for LISEM version 1.63, with the use of the SWATRE infiltration submodel but without the use of a wheeltrack network	48
3.1	Stratigraphy of Chinese loess	52
3.2	Areas occupied by the areal features of the geomorphological map.	63
3.3	Land use (%) in the Danangou catchment, 1998-2000	74
4.1	Selected fields of 1998 and 1999	78
4.2	Yearly averages (week 21 to 39) of plant and soil characteristics in 1998 and 1999.	83
4.3	Monthly rainfall (mm), May to September. The values for Danangou are average values from 6 tipping bucket rain gauges.	84
4.4	Summary of events used in this study. Maximum intensities are given in mm/h for 1-minute intervals.	84
4.5	Soil physical parameters measured in the Danangou catchment.	86
4.6	Bulk densities for different soil types	86
4.7	Grain size distribution of different lithologies	87
4.8	Chemical compound contents (%) of different lithologies from Danangou, Gaolanshan, Ariendorf and Vicksburg.	88
4.9	Equipment performance and available data for all known events	94
4.10	Overview of the runoff events measured at the weir.	94
4.11	Results from the gully-flume, 1998-2000	101
4.12	Overview of the runoff events measured at the sediment plot	103
4.13	Erosion rates (tonnes/km <sup>2</sup> ) for different rill erosion classes	108
4.14	Results of pin measurements in gullies	109
5.1	Characteristics of different types of flow	114
6.1	Literature values of Manning's n	134
6.2	Plot characteristics. The soil surface for the cropland plots showed slight crusting, unless otherwise stated.	139
6.3	Average values of Manning's n for the first (1999) series	141
7.1	Selected transport equations: main equation and conversion to transport capacity	167
7.2	Selected transport equations: secondary equations and transport threshold	168
7.3	Simulated detachment and deposition for different transport capacity equations. Maximum possible clear water concentration was 1060 g/l	175
7.4	Simulation results for different maximum possible clear water concentrations and different storms	180
7.5	Available data and simulation results for the sediment plot events	184
8.1	Properties of different types of loess.	194
8.2	Measured and estimated headcut heights (m) of red loess and yellow loess gullies and estimated volume of loose soil material below the headcut, May 1999	194
8.3	Pin length change over a 2-year period (October 1998 – September 2000).	197
8.4	Sediment sources of gully catchments on the Loess Plateau	207
8.5	Sources of soil erosion in small catchments (0.18 – 70.7 km <sup>2</sup> ) in the gullied hilly part of the Loess Plateau	208

8.6	Measured and simulated (in italics) total event erosion (tonne) in the Danangou catchment.	211
8.7	Measured and estimated erosion rates (tonnes) in the Danangou catchment, 1998-2000	212
9.1	Effect of using a slope dependent Manning's n	222
9.2	Effects of different grid sizes (m) on catchment characteristics and simulation results	227
9.3	Effect of time step length (seconds) on LISEM simulations. Calibrated dataset of the event of 990720 is used	230
9.4	Summary of time step length results	231
10.1	Multiple regression equations used for predicting initial moisture content	238
10.2	Event characteristics	241
10.3	Correction factors for prediction of initial moisture content	241
10.4	Measured LISEM input dataset (plant and soil characteristics) for the 990720 event	242
10.5	Peak discharge calibrated values for all events	243
10.6	Nash-Sutcliffe coefficients for LISEM 163 and LISEM LP for the 5 events used for LISEM calibration	244
10.7	Simulated peak discharge using the calibrated data sets for the different events	247
10.8	Summary of the total discharge calibration results	248
10.9	Simulation summary	250
10.10	Correction factors for prediction of initial moisture content	255
10.11	Result for additional storms	255
10.12	Average observed rill erosion rates (with sheet erosion rates added) and approximate boundaries between classes of rill erosion severity, 1999 data	260
10.13	Distribution of erosion (tonnes) according to LISEM simulation.	262
11.1	Summary of land use scenarios	270
11.2	Areas (%) occupied by the different land uses for the different land use maps. Catchment area is 3.52 square kilometres	271
11.3	LISEM input data set for the event of August 1 <sup>st</sup> , 1998	272
11.4	Effects of conservation measures on LISEM input parameters	272
11.5	Classification scheme for LISEM erosion maps. Erosion is given in tonnes ha <sup>-1</sup>	273
11.6	Erosion (tonnes) for different land use scenarios	276
11.7	Summary of simulation results for the catchment outlet, 980801 event	278
11.8	Effect of storm size (given as multiplication factor) on scenario result	279
11.9	Summary of simulation results for the catchment outlet, 000829 event	281

## APPENDICES

4.1	Number of measurements for the different parameters	112
6.1	Data for all Manning's n measurements	152
7.1	List of symbols used in chapter 7	191





## ACKNOWLEDGEMENTS

When you are waiting for rain on a dry and dusty hilltop in the middle of the Chinese Loess Plateau, you will see the same brown hills extending to the horizon in all directions. It is like the rest of China: not always beautiful, but always impressive. And, at times, it seems inconceivable that it ever rains here. Under such circumstances, it might seem a lonely job to work on a Ph.D. thesis on soil erosion modelling there. Nevertheless, looking back at the end of the project, I find that it has been a good time, not in the least because of the help and support I received from various people whom I want to thank here.

To start at the beginning I would like to thank Theo van Asch and Steven de Jong for giving me the opportunity to undertake this project. They, at times, seemed to have more confidence in the success of the project than I did myself. Theo went on to become one of my daily supervisors, but Steven soon made place for Victor Jetten, whom I also want to thank. He and Theo formed a formidable pair of daily supervisors without whom I would not have been able to finish this thesis. I was often amazed at their speed of thinking and at Victor's vast knowledge of the (in)famous LISEM model.

I would also like to thank my supervisor, Peter Burrough. With his large experience in guiding Ph.D. students, he was able to support me in ways that Victor and Theo could not.

Over the years, I have always found the atmosphere at the department of Physical Geography quite stimulating. I thank all my colleagues and former colleagues for that but would like to mention by name Rutger Dankers, Karin Pfeffer, Harry Blijenberg, Thom Bogaard, Maarten Kleinhans, Raymond Sluiter, Derek Karssenberg, Kor de Jong, Antoine Wilbers, Kim Cohen and Leonie van der Maesen. Furthermore, I thank Kees Klawer and Marieke van Duin for the help they gave me in getting a number of soil analyses done, Jaap van Barneveld for his help with equipment, Annina Andriessen and Irene Esser for their support in practical matters, and finally Maarten Zeijlmans for his help with Arc/Info and unix. I also gratefully acknowledge the help I received from the (former) students who came with me to the Danangou catchment: Judith Snepvangers, Erik van de Giessen, Hiddo Huitzing, Ronny Vergouwe, Suzan Vos and Leanne Reichard. They not only did their part of the job, but also made my stay in Ansai much more pleasant, as did a couple of students from Wageningen University, Hogeschool Larenstein and the Swedish University of Agricultural Sciences (SUAS).

Since this thesis is the result of an international project called Erochina, I would also like to thank a number of colleagues from several institutes in China, the Netherlands and Sweden.

I have always found the collaboration with Alterra Green World Research (the former Winand Staring Centre) very pleasant. I thank Kim Trouwborst for the vital role he played during the first years of the project. I thank Jannes Stolte and Erik van den Elsen for our joint fieldwork and for their assistance by telephone and e-mail at other times. I must add, though, that I never understood why they talked so much about McDonalds. Finally, I thank Coen Ritsema for the support he gave me as project coordinator. However, the

Alterra story should not end here because in March 2001, I became a part-time colleague of the people mentioned above. They, and my other colleagues, especially Simone van Dijck, have always understood the complexities that come with having another job when finishing a Ph.D. thesis.

From SUAS, I would like to thank Ingmar Messing, Minh Ha Hoang Fagerström and Magnus Carlsson for their companionship during their stay at Ansai, and for the good collaboration in the project.

The first Chinese Institute to mention is Beijing Normal University (BNU). Over the 3 years of the project I have worked closely together with a number of people, ranging from students to professors: Liu Baoyuan, Wu Yongqiu, Ma Xiujun, Zhang Qingchun, Zhang Yan, Cai Yongming, Zhang Wenbo and Fu Suhua. They all proved to be very enthusiastic, helpful and hard working.

Another Chinese Institute that played a vital role is the Institute of Soil and Water Conservation (ISWC) in Yangling. They were very helpful in arranging my stays at Ansai Field Station. I especially want to thank: Li Rui, Liu Guobin, Yang Qinke, Xu Mingxiang, Wen Zhongming, Zhang Guanghui and Zhang Qiaoping. Furthermore, I thank the staff of Ansai Field Station for their kindness and I am much ashamed to have to admit that even after 3 years I still was not able to remember all their names. Nevertheless, returning to the field station after spending the winter in Holland was almost like arriving at home.

From the Research Center of Eco-Environmental Sciences (RCEES) in Beijing I thank: Fu Bojie, Chen Liding, Wang Jun, Zhang Shurong, Meng Qinghua and especially Qiu Yang (now at BNU), who translated the summary of the thesis into Chinese.

Another group that should not be forgotten are the farmers of the Danangou catchment. They graciously accepted the presence of a bunch of crazy foreigners, who insisted on running up and down the hills, who carried large amounts of water around in plastic buckets only to throw it on the ground later (and even paid good prices to do that), who thought it necessary to walk in their fields to pick leaves from their crops and who were not able to speak anything comprehensible. What shocked them most, however, is that when heavy rain started we all ran out to do silly things like throwing bottles in the river. Nevertheless, they always offered us fruit and noodles and made us feel welcome.

Finally, I would like to thank my parents and my brother for all the support they have given me over the years.

Utrecht, September 2002

# 1 INTRODUCTION

## 1.1 Introduction

Flooding on China's largest and most important river, the Yangtze, is frequently reported in the press due to the almost annual occurrence of monsoon-related floods. In addition, the Three Gorges Dam being built to harness power from the Yangtze is also a matter of hot debate. In contrast, China's second river, the Yellow River (Huanghe) is not often in the news, yet this river probably poses a greater threat to the people living around it than the Yangtze does. It has been estimated that major floods on the Yellow River could threaten the lives of 150 million people: it is not by chance that the Yellow River has earned the name 'China's sorrow'. The threat posed by the Yellow River is caused by a major peculiarity: its huge sediment content, which has caused rapid sedimentation in its lower course. This, in turn has in the past led to regular major changes in its course. Since the early 1950's, however, the river has been harnessed but continuing sedimentation has raised the river bed to several metres above the surrounding landscape, so that breaching of the dikes could result in disaster. The Yellow river basin has been studied intensively by Chinese scientists for over 50 years and the Chinese government is well aware of the problems posed by the river and seems committed to combat them. Since the Loess Plateau is the source of about 90% of all the sediment that enters the Yellow River (Douglas, 1989; Zhaohui Wan & Zhaoyin Wang, 1994), much attention is being directed at decreasing the erosion rates in this important part of the Yellow River catchment. Reducing the erosion rates on the Loess Plateau should decrease downstream sedimentation problems while at the same time reducing the loss of agricultural land on the Loess Plateau itself.

## 1.2 The Loess Plateau

### 1.2.1 Introduction

Loess is defined by Pye (1987) as a terrestrial windblown silt deposit that forms in semi-arid continental climates. It consists mostly of quartz, feldspar, mica, clay minerals and carbonate grains with the clay minerals and carbonate acting as cementation material. The proportions of the constituents may vary widely from place to place. Most loess deposits were formed during the Pleistocene. More than 6 % of China is covered by loess: the Loess Plateau of central China has an area of about 300,000 km<sup>2</sup> (Tan, 1988; Muxart et al., 1994). According to Derbyshire et al. (1991), this is the area having a minimum loess thickness of 10 metres. Other authors therefore mention larger areas. The maximum loess thickness is about 300 metres. The Loess Plateau is situated in the Yellow River basin, in northern China and covers large parts of the Gansu, Ningxia, Shaanxi and Shanxi provinces. Figure 1.1 shows the location of loess in China, while figure 1.2 shows a map of the Yellow River basin.

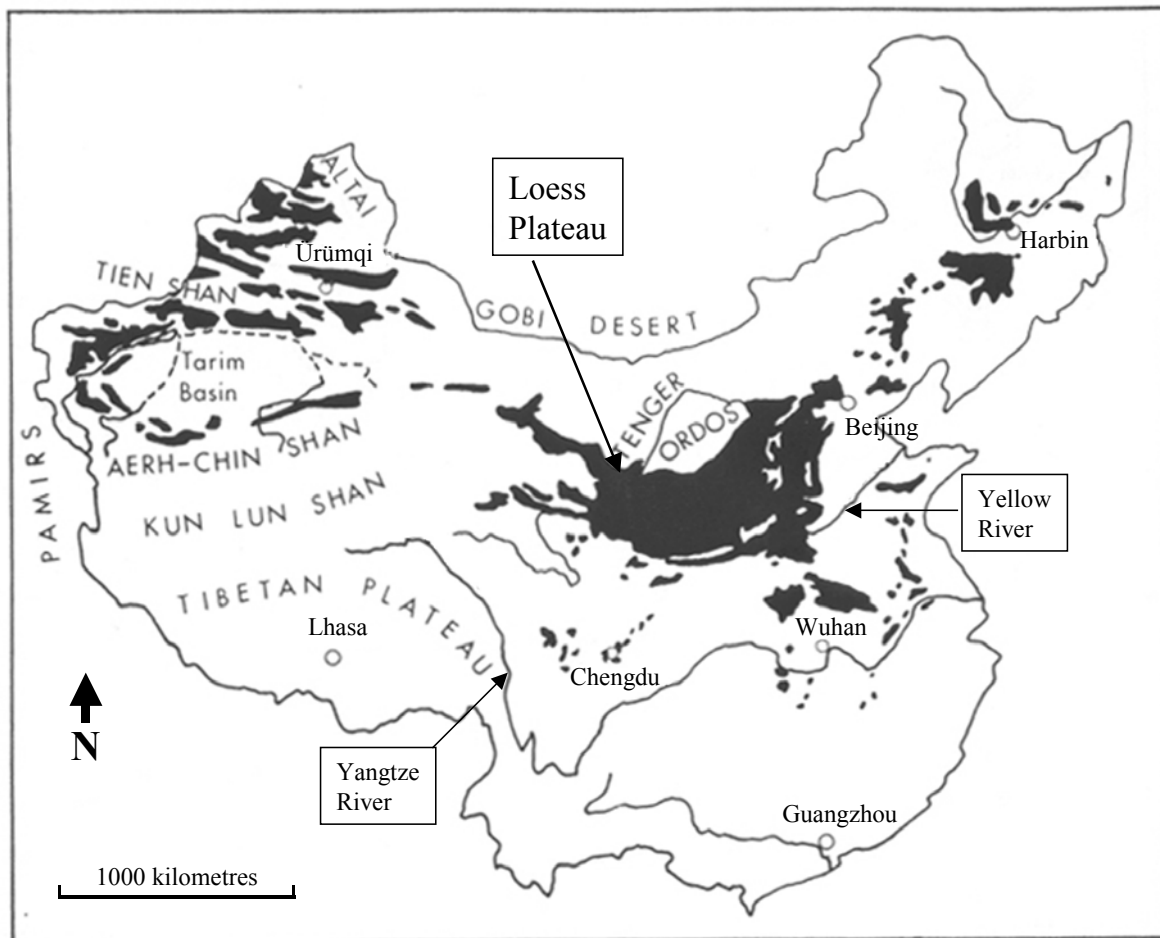


Figure 1.1 Distribution of loess in China. Adapted from Pye (1987)

### 1.2.2 Loess erosion

#### *Basin-wide erosion*

The Loess Plateau has some of the highest erosion rates on the entire planet. Some of the table lands of the Loess Plateau are very dissected by gullies, but the region with the highest erosion rates is generally considered to be the hilly part of the Loess Plateau, which is also very dissected by gullies. This region is mostly located in the northern part of Shanxi and Shaanxi Provinces. Figure 1.3 shows a typical landscape for the hilly part of the Loess Plateau. Jiang Deqi et al. (1981) estimated that erosion rates may be as much as 18,000 tonnes per square kilometre per year for the hilly loess region of the Wuding catchment, which is one of the main Loess Plateau tributaries of the Yellow River (figure 1.2). Sediment concentrations in runoff on the Loess Plateau of over 1000 g/l have been recorded regularly. There are several reasons for these very high erosion rates:

- First, the loess is very erodible, especially when wet.
- Second, the area's rainfall is characterized by heavy storms in summer (mainly July and August). Single storms can produce 10% of yearly precipitation and 40% of erosion (Gong Shiyang & Jiang Deqi, 1979, Zhang et al., 1990). Though the



saturated conductivity of the loess is generally higher than rainfall intensity, crusting prevents that all water infiltrates (Douglas, 1989). Muxart et al. (1994) found that as much as 95% of rainfall can become runoff due to crusting.

- Third, the area has considerable relief. Continuing uplift is an important factor in causing this.
- Finally, vegetation cover is generally sparse. This is partly caused by a semi-arid climate with cold winters, but also by deforestation and grazing (Jiang Deqi et al., 1981).

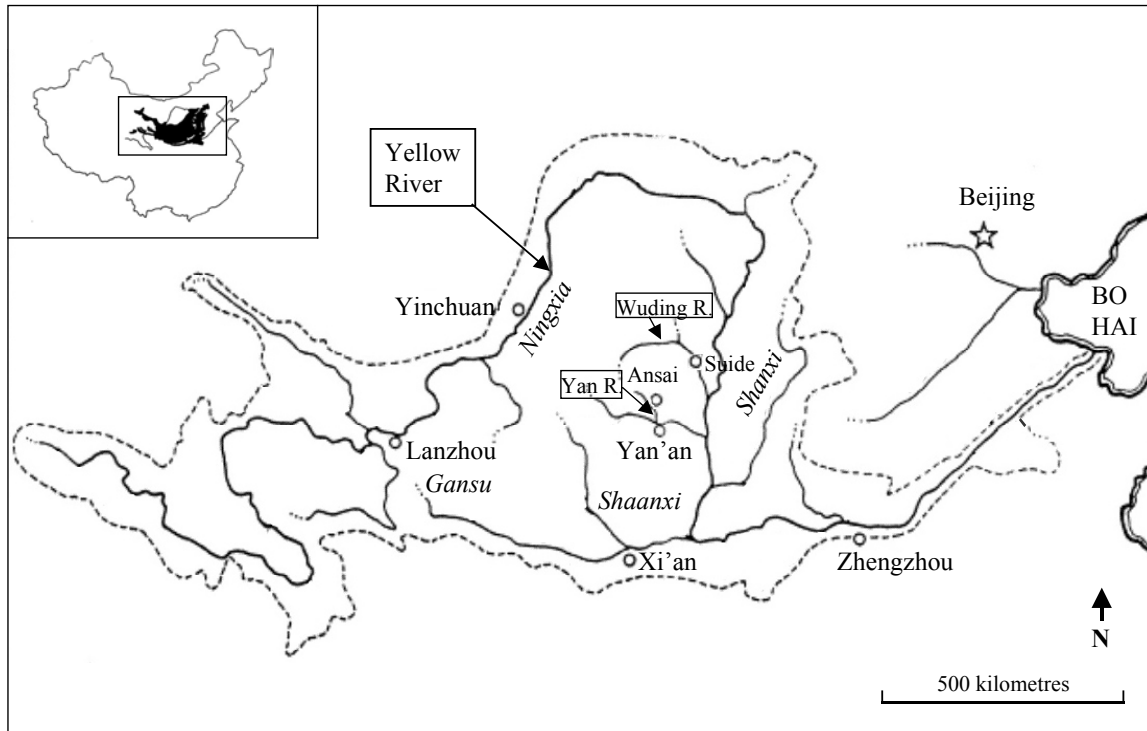


Figure 1.2 Map of the Yellow River basin. Adapted from Xu Jiongxin (1999a) and Pye (1987)

Erosion rates have not always been so high. Rem Mei-e & Zhu Xianmo (1994) showed how different kinds of information (written records, Yellow River delta volumes) indicate that the serious soil erosion on the Loess Plateau started at about 1000 AD. Xu Jiongxin (2001) found that bank breaching of the Yellow River increased in frequency from the 10<sup>th</sup> century AD. According to him, breaching frequency depends on sediment load, which apparently increased because erosion on the Loess Plateau was increased by destruction of the natural vegetation. Such destruction greatly reduces the high natural permeability of loess as well as the resistance to erosion. Rainfall experiments reported by Rem Mei-e & Zhu Xianmo (1994) also show the much higher erosion rates of bare soils, which have resulted in a large extension of the gullied area and also increased the relative relief of the area. Headcut retreat rates are at present sometimes as high as 3 meters per year. On the other hand, Long Yuqian & Xiong Guishu (1981) reported that historic literature from the Eastern Han Dynasty (25-220 AD) already recorded very high sediment contents: ‘the silt occupied six tenths of the volume in one barrel of water

sampled'. Nevertheless, such observations seem to have been exception rather than rule before about 1000 AD.



Figure 1.3 Typical landscape of the hilly part of the Loess Plateau, northern Shaanxi

Discharging all the sediment delivered to the Yellow River requires substantial river flow, which puts limits on the amount of water that can be used for irrigation, even though irrigation with dirty water has been successfully applied in places. Aggradation of the river bed has already caused the river to flow 5-10 meters above the surrounding area along its lower reaches (Douglas, 1989; Zhang et al., 1990; Zhu et al., 1997). Long Yuqian & Xiong Guishu reported annual sedimentation rates of 4 to 7 centimetres over the period 1951-1977, which causes, as already noted, a major flooding risk. Before the Yellow River was harnessed (from 1946 on), it changed course once every century and flooded every 2 out of 3 years (Zhang et al., 1990).

#### *Combating erosion*

Reducing the flooding risk and using the Yellow River water for agriculture and industry requires a large reduction in the sediment content. The most effective way of doing this is to decrease the erosion rate on the Loess Plateau because this is the major sediment source in the Yellow River basin. A major project has therefore been started to reduce erosion on the Loess Plateau, mainly by check-dams and terrace building. According to Jiang Deqi et al. (1981) the sediment discharge of the Wuding catchment decreased by 28% between 1957 and 1978. However, most of this decrease was due to reservoirs and dams, which have limited capacity. Afforestation and terracing should result in more permanent decreases in sediment production, while grasses such as Jiji grass might be used to stabilise gullies. Fang Zhengsan et al. (1981) reported that terracing can decrease

erosion by as much as 95%. They also described several methods that have been used to create terraces. Terrace building had already started several hundred years ago and is now widespread on the Loess Plateau. Terraces are effective against erosion because they have low slope angles, which reduce water velocity and increase infiltration. However, they require a high level of maintenance and are prone to gully erosion when they are not properly constructed. Other measures that reduce water velocity and increase infiltration should also be effective in combating erosion. Removal of the soil crust seems to be a good option, though Muxart et al. (1994) found that cracks in soil crusts caused by drying out of the soil did not disappear due to swelling on rewetting, but instead had to be filled with sediment before runoff across the cracks could occur. Therefore, the net effect of crusts might not always be as clear as expected.

Despite all efforts to reduce erosion rates, the Loess Plateau is likely to remain an area having considerable erosion. It will remain a high-relief, low vegetation-cover area with heavy storms on erodible soils. Since the gully erosion has very markedly increased local relief, it is unrealistic to think that proper conservation methods will reduce erosion rates to pre-deforestation levels. Nevertheless, such conservation methods could achieve large reductions of current erosion rates. The best place to implement conservation measures is at the sediment source.

### **1.3 The EROCHINA Project**

In 1998, a European project called EROCHINA started, in which several European and several Chinese partners participated. Its aim was to find ways to decrease erosion rates in a small catchment on the Loess Plateau. The project used a participatory approach in the sense that farmers were involved in the process of identification and design of solutions to erosion related problems. All farmers were interviewed to find out their opinions on soil erosion, on economical problems and on possible solutions. The results of the participatory approach have been discussed elsewhere (Messing & Hoang Fagerström, 2001; Hoang Fagerström et al., in press). Based on data obtained from the farmers, on government policy and on data collected in the catchment a number of land use scenarios were developed. The effects of these scenarios in terms of soil erosion were investigated using the process based erosion model LISEM (Limburg Soil Erosion Model, De Roo et al., 1996a; Jetten & De Roo, 2001). The research described in this thesis was part of the EROCHINA project and focused on process based erosion modelling in the selected catchment.

### **1.4 The aims of this thesis**

Soil erosion modelling is potentially a powerful tool for combating soil erosion. It helps us better to understand erosion, better to locate erosion hotspots, to predict erosion and to evaluate the effect of different soil and water conservation methods. Even though research on the Loess Plateau has been intense for the past 50 years, process based

erosion models have not often been applied. Instead, more attention has been given to monitoring.

The presence of loess on steep slopes requires special attention in erosion modelling, and the Loess Plateau has several characteristics that specifically need to be addressed:

- Slopes in the erodible loess can be very steep, which may have consequences for flow velocity and transport capacity of the flow.
- Sediment concentrations in runoff may be extremely high. At such concentrations the fluid properties might differ from those of clear water.
- The area is heavily dissected by gullies. Thus, erosion models should be able to cope with gully erosion, or at least with gullies as a source of sediment.

The aims of this thesis are:

- 1) To evaluate what are the effects of these particular characteristics of the Loess Plateau on soil erosion processes.
- 2) To evaluate whether or not process based erosion models in general, and LISEM in particular, can deal with those characteristics.
- 3) To adapt the LISEM model to Loess Plateau conditions if this proves necessary.
- 4) To calibrate and validate the LISEM model for a small catchment on the Chinese Loess Plateau.
- 5) To simulate the effect that different soil and water conservation methods have on soil erosion.

Chapter 2 examines the abilities of current erosion models to deal with the characteristics of the Loess Plateau. Chapter 3 describes the study area, a small catchment on the Loess Plateau, in more detail. Chapter 4 lists the methods used in the field as well as the measurement results. The Loess Plateau characteristics of steep slopes, high concentrations and presence of gullies are discussed one by one in chapters 5 to 8. The effects of these changes on the LISEM simulations are evaluated in chapter 9. Finally, Lisem is calibrated in chapter 10 and used to simulate the effect of soil and water conservation methods in chapter 11.

## 2 THEORY OF SOIL EROSION MODELLING

### 2.1 Introduction

In chapter 1 some characteristics peculiar to catchments on the Chinese Loess Plateau were identified:

1. Slope angles are steep. This can have consequences for both velocity and transport capacity of the flow.
2. Sediment concentrations in runoff can be very high.
3. Large permanent gullies are common.

This chapter will discuss the erosion processes that are operating on the Loess Plateau, and especially those that are relevant to the characteristics mentioned above. The chapter will also explore to what extent these processes are at present being taken into account in soil erosion modelling. Chapters 5 to 8 will then, in turn, discuss the implications of each of these characteristics for the study area.

### 2.2 Flow velocity and flow routing

Two dimensionless numbers are used in hydrology to classify flow type. These are the Reynolds number (Re) and the Froude number (Fr). The Reynolds number is used to determine whether a flow is laminar, turbulent or something in between (transitional). The Froude number is used to determine whether flow is sub-critical or super-critical.

The Reynolds number is given by:

$$\text{Re} = \frac{4 \cdot V \cdot R}{\nu} \quad (2.1)$$

Where:  $V$  = flow velocity (m/s)  
 $R$  = hydraulic radius (m)  
 $\nu$  = kinematic viscosity ( $\text{m}^2/\text{s}$ )

At what Reynolds number flow will be laminar, transitional or turbulent is not clearly defined. However, the boundary between laminar and transitional flow is usually placed between 1500 and 2000 (e.g. Emmett, 1970, Abrahams et al., 1986, Ven Te Chow et al., 1988, Li & Abrahams, 1997), while the same authors placed the boundary between transitional and turbulent flow at 6000 to 10000. The main difference between laminar flow and turbulent flow is the velocity distribution over depth that results from different degrees of vertical mixing. In laminar flow the flow can be envisioned as parallel layers that move over each other, but that do not mix. This results in a clear velocity gradient from bottom to top of the flow, where average velocity of the flow is theoretically 0.67 times the surface velocity (e.g. Emmett, 1970). In turbulent flow eddies are formed that disturb the velocity distribution of the flow and that cause energy loss. The result is that the velocity gradient is less than for laminar flow, and the average velocity is about 0.8 times the surface velocity (Emmett, 1970).

The Froude number is given by:

$$Fr = \frac{V}{\sqrt{g \cdot h}} \quad (2.2)$$

Where:  $g$  = gravitational acceleration ( $m/s^2$ )  
 $h$  = water depth (m)

For Froude numbers below 1 flow is sub-critical, while for values above 1 it is super-critical. In super-critical flow any disturbances of the flow can only propagate in the downstream direction. Using the Reynolds and Froude number flows can be classified as being laminar-sub-critical, laminar-super-critical, turbulent-sub-critical or turbulent-super-critical.

Water velocity in erosion models is usually calculated with empirical formulae such as the Manning equation or the Darcy-Weisbach equation. Such velocity equations might or might not be applicable to some kinds of flow. It is, for example, sometimes stated that the Manning equation may only be applied to turbulent flow (e.g. Ven Te Chow et al., 1988). The velocity equations incorporate the slope angle, but were not developed for such steep slope angles as present in the Loess Plateau catchments. Since the equations are of empirical nature one should be careful with using them for conditions outside those for which they were developed. Therefore, the applicability of these equations will be evaluated in chapter 6.

To route flow to the catchment outlet a continuity equation as well as a flux-concentration equation are needed (Singh, 2002). For water flow the velocity equation (Manning, Chezy, Darcy-Weisbach) is the flux-concentration equation. Either of these equations is a specific form of the following equation:

$$A = \alpha \cdot Q^\beta \quad (2.3)$$

Where  $A$  is the cross-sectional area of the flow,  $Q$  is the discharge,  $\alpha$  is a parameter and  $\beta$  a coefficient. Both  $\alpha$  and  $\beta$  are often assumed constant, but might in reality vary spatially and with flow conditions (Singh, 2002). When the Manning equation is used  $\beta$  would be 0.6 and  $\alpha$  would be:

$$\alpha = \left( \frac{n \cdot P^{2/3}}{S^{1/2}} \right)^{0.6} \quad (2.4)$$

Where  $P$  is the wetted perimeter,  $S$  the energy slope and  $n$  Manning's  $n$ . The continuity equation, in its basic 1-dimensional form, is given by:

$$\frac{\partial Q}{\partial x} + \frac{\partial A}{\partial t} = q \quad (2.5)$$

Where  $q$  is lateral inflow, which in case of overland flow would be defined as rainfall minus infiltration. Equations 2.3 and 2.5 can be combined to give (Ven Te Chow et al., 1988):

$$\frac{\partial Q}{\partial x} + \alpha \cdot \beta \cdot Q^{\beta-1} \cdot \frac{\partial Q}{\partial t} = q \quad (2.6)$$

This is the kinematic wave equation. According to Singh (2002) the kinematic wave can be applied to both overland flow and channel flow. According to him, kinematic waves are dominant for Froude numbers below one, while for higher Froude numbers dynamic waves are more dominant. The assumption behind the kinematic wave is that the friction slope is equal to the bed slope. This assumption is more realistic for steeper slopes (Fread, 1985; 1993; Singh, 2002). If the assumption is not realistic, or if Froude numbers are high, more complete versions of the Saint Venant equation, such as the diffusion wave and dynamic wave, should be used. The kinematic wave equation is usually solved by numerical methods. These methods transform the governing partial differential equation into a set of finite-difference equations by using a Taylor series expansion (Ven Te Chow et al., 1988). This transformation introduces several types of error:

- Truncation error. The higher order derivatives are dropped from the Taylor series expansion.
- Rounding error. Only a certain number of significant digits are used.
- Numerical errors that are generated because the continuous partial differential equation is transformed into a set of finite difference equations that are only valid for the grid points in the x-t plane. Between grid points, values are obtained by linear interpolation.

If these errors do not amplify during successive time steps the solution is stable (Ven Te Chow et al., 1988). Stability of the solution, however, does not guarantee that the solution is also accurate. Although the kinematic wave equation does not allow for wave attenuation, attenuation will occur because of the numerical errors associated with the finite difference solution of the kinematic wave (Fread, 1993).

## 2.3 Sediment transport

### 2.3.1 Introduction

Sediment transport is an important process in studies on soil erosion. Through this process eroded sediment is removed from the catchment. The ratio between sediment transported out of the catchment and sediment eroded in the catchment is called the sediment delivery ratio. The sediment delivery ratio usually decreases with increasing catchment area because in larger catchment there is more opportunity for sediment storage, e.g. in floodplains. By far the most important transporting agent on the hilly part of the Chinese Loess Plateau is flowing water, which can also be a major cause of erosion. Flowing water exerts a force on its bed that, in terms of stress, can be expressed as:

$$\tau = \rho_f \cdot g \cdot R \cdot S \quad (2.7)$$

Where:  $\tau$  = shear stress ( $\text{kg m}^{-1} \text{s}^{-2} = \text{N/m}^2$ )  
 $\rho_f$  = fluid density ( $\text{kg m}^{-3}$ )  
 $g$  = gravitational acceleration ( $\text{m s}^{-2}$ )  
 $R$  = hydraulic radius (m)  
 $S$  = energy slope ( $\text{m m}^{-1}$ )

Another important parameter of the flow with respect to sediment transport is stream power. It can be expressed in many different ways (see Rhoads, 1987). The stream power per unit wetted area (or mean stream power, Rhoads, 1987) is given by:

$$\Omega = \rho_f \cdot g \cdot R \cdot S \cdot V = \tau \cdot V \quad (2.8)$$

Where:  $\Omega$  = stream power per unit wetted area ( $\text{kg s}^{-3}$ )  
 $V$  = flow velocity (m/s)

The product of  $S$  and  $V$  is called unit stream power. It represents the power per unit weight of water. The energy slope  $S$  is equal to the sine of the slope angle (Rhoads, 1987; Ven Te Chow et al., 1988; Flanagan et al., 2001), and can only be equated with tangent for gentle slopes.

Water can transport sediment in several ways. The total sediment load of flowing water is usually subdivided into bedload and suspension load. Suspended load is sometimes subdivided into suspended bed material load and wash load. Hsieh Wen Shen & Julien (1993) give the following characteristics of these types of load:

*Bedload*: sediment particles moving along the streambed in the processes of rolling, sliding, and/or hopping.

*Suspended load*: sediment particles that are supported by the turbulent motion of the flow. Suspended load has a vertical distribution in the flow. Concentrations are larger at the bed than at the surface. This distribution is caused by a balance between falling due to gravity and upward transport due to turbulence. The finer the particles and the more turbulent the flow, the more evenly the distribution of particles over depth will be.

*Suspended bed material load*: suspended load in which the particles are large enough to be seen on the streambed.

*Wash load*: suspended load in which the particles are so small that they cannot be easily seen individually on the streambed. Wash load does not depend directly on flow conditions, but more on supply rate. Wash load is almost uniformly distributed over depth.

The concentration of suspended sediment in water can be defined in several different ways. First, the amount of sediment can be expressed as volume of sediment or as mass of sediment. Second, the amount of water can be defined as the total amount of fluid or as the amount of clear water. Hence, the following definitions may be used:



$$C_f = C_{vf} \cdot \rho_s = \frac{V_s}{V_f} \cdot \rho_s = \frac{V_s}{V_s + V_w} \cdot \rho_s \quad (2.9)$$

$$C_w = C_{vw} \cdot \rho_s = \frac{V_s}{V_w} \cdot \rho_s \quad (2.10)$$

Where:  $C_f$  = fluid concentration (g/l) = dirty water concentration  
 $C_{vf}$  = volumetric fluid concentration  
 $C_w$  = clear water concentration (g/l)  
 $C_{vw}$  = volumetric clear water concentration  
 $V_s$  = volume of solids  
 $V_f$  = volume of fluid  
 $V_w$  = volume of water  
 $\rho_s$  = density of solids ( $\text{kg/m}^3$ , which is numerically equal to g/l)

Most authors use  $C_f$ , but  $C_w$  is also sometimes used. Unfortunately, authors do not always state which definition they use. This can have large implications when concentrations are large, as on the Chinese Loess Plateau. The amount of bedload that is moving is usually not expressed as a concentration, but as a sediment flux:

$$q_s = q_b \cdot \rho_s \quad (2.11)$$

Where  $q_b$  is volumetric bedload transport per unit width of flow ( $\text{m}^2/\text{s}$ ) and  $q_s$  is the sediment transport rate in  $\text{kg m}^{-1} \text{s}^{-1}$ . Thus, the amount of sediment is explicitly linked to the amount of water for suspended load, but not for bedload. For bedload the link is more implicit, since  $q_b$  will be determined by shear stress or stream power of the flow, which depends on discharge.

### 2.3.2 Concept of transport capacity

Present day process based soil erosion models like WEPP (Flanagan et al., 2001), KINEROS2 (Smith et al., 1995), EUROSEM (Morgan et al., 1998a,b) and LISEM (Jetten & De Roo, 2001) use the concept of transport capacity to determine sediment transport rates in overland flow and streamflow. Smith et al. (1995) defined transport capacity as the amount of sediment that a given flow can carry at steady state conditions in equilibrium with a loose bed. Detachment and deposition are then functions of transport capacity:

$$D = a \cdot (TC - C) \quad (2.12)$$

Where:  $TC$  = transport capacity  
 $C$  = concentration  
 $a$  = rate control constant  
 $D$  = detachment or deposition

If transport capacity exceeds concentration net erosion will occur at rate  $a$ . If concentration exceeds transport capacity net deposition will occur at rate  $a$ . The rate control constant might be different for erosion and deposition, e.g. because it will depend on soil cohesion in the case of detachment. If equation 2.12 is used, transport capacity becomes the controlling factor in determining whether net erosion or net deposition occurs. There are several potential limitations to this concept:

- 1) Huang et al. (1999) argued that equation 2.12 is based on the assumption that there is a coupling between transport and detachment. It can be easily seen from equation 2.12 that if  $TC-C$  increases  $D$  will increase. They stated that this approach does not do justice to the fact that there might be a limit to  $D$  that depends not on  $TC-C$  but on some other factor like cohesion or soil strength. In equation 2.12 the rate control constant  $a$  might depend on cohesion, so that  $D$  is also cohesion dependent, but despite that  $D$  will always increase if  $TC-C$  increases. Therefore, equation 2.12 cannot cope with situations where transport is detachment limited instead of transport limited. Huang et al. do not seem to have taken into account that  $D$  is a net rate (Morgan et al., 1998a) and cannot be equated with either deposition or detachment rate since both will occur simultaneously in reality. Therefore, in the case of net erosion,  $D$  might continue to increase with increasing  $TC-C$  even if erosion rate has reached its upper limit. Nevertheless, a method that calculates erosion and deposition independently, as suggested by Huang et al. is conceptually clearer. Rose (1985) described such a method. In his method there is no need for an a priori definition of transport capacity, instead a 'transport capacity' will automatically emerge when detachment equals deposition. Such an approach, however, does not allow a check for impossible concentrations. Rose (1985) found that in practice the prediction is not much different from the results obtained with a method that explicitly uses transport capacity.
- 2) Transport capacity is a predefined number that depends on flow and sediment characteristics, but not on sediment concentration. It will be shown in chapter 5 that in the case of the Loess Plateau transport capacity might depend on concentration. One way around this might be to treat both erosion and deposition independently (as described above) and to calculate transport as the sum of both. Another option would be to redefine transport capacity to incorporate effects of concentration. Huang et al. (1999) found that transport capacity also depends on surface hydrologic conditions such as drainage and seepage.
- 3) The concept of transport capacity might not be useful for wash load (grain size below about 50  $\mu\text{m}$ ), since the concentration of wash load depends mainly on availability of material and not on flow conditions (e.g. Hsieh Wen Shen & Julien, 1993, Reid et al., 1997). Wash load can apparently be transported in almost limitless quantities (Van Rijn, 1993). Using separate sediment classes with different transport capacity might circumvent this problem. The finest material could then be given a very high transport capacity. This also results in a shift of grain size distribution of transported sediment in comparison to the original soil. The Rose (1985) and WEPP models currently use different sediment size classes.

Thus, the concept of transport capacity is not without problems. Nevertheless the approach of using transport capacity as the controlling factor in net erosion and net deposition seems valid, though it might be necessary to apply transport capacity equations that take local circumstances into account.

### 2.3.3 Transport equations

Many, mostly empirical, equations have been developed to predict sediment transport from flow characteristics, slope and material characteristics. These equations often use a threshold value for stream power, shear stress or discharge. Below this threshold no sediment transport will take place. A distinction is often made between channel flow and overland flow. Overland flow usually has much steeper slopes and much lower discharge than channel flow. Another distinction in equations is that in bedload equations and total load equations. Neither type specifically includes wash load. Some authors claim (Borges et al, 1995, Smart & Jaeggi, 1983, Rickenmann, 1991) that their formula is applicable to steep slopes, but this usually means up to slopes of only about 20%. Furthermore, almost all formulae for channel flow are bedload formula. Some equations for channel flow and rill flow will be discussed in chapter 7.

For overland flow less equations are available. Huang (1995) studied soil loss from 1.2-m soil pans with slopes ranging from 4-30%. He found that concentration was best predicted using stream-power based polynomials of the form:

$$C = D_1 \cdot q^2 \cdot S^2 + D_2 \cdot q \cdot S + D_3 \quad (2.13)$$

Where the  $q$  is discharge,  $S$  is slope and  $D_1$  to  $D_3$  are coefficients depending on soil type.

Everaert (1991) performed measurement in a very small flume (0.05 by 0.3 m) to test transport capacity for interrill conditions with laminar flow regime. Slopes ranging from 1 to 10 degrees were used, while discharge was between 0.2 and 2.5 cm<sup>2</sup>/s. He used several grainsizes, the smallest of those was 33 μm. The results were best predicted with effective stream power (depth corrected stream power), but good results could also be obtained with shear velocity, unit stream power and a combination of  $q$  and  $S$ . His unit stream power equation for a grainsize of 33 μm is:

$$\log(q_s) = -1.31 + 1.51 \cdot \log(S \cdot V) \quad (2.14)$$

Where  $V$  is given in cm/s and  $q_s$  is predicted in g cm<sup>-1</sup> s<sup>-1</sup>.

Neither Huang (1995) nor Everaert (1991) discussed whether or not the small plot size used by them is large enough to reach transport rates that equal transport capacity.

As Beschta (1987) noted each equation has usually been developed for a limited range of conditions and when used in field application the estimated transport rates for the different equations may vary over several orders of magnitude. There is no such thing as

a universally applicable transport equation. Many studies have evaluated the use of different transport equations under different circumstances (e.g. channel flow: Van den Berg & Van Gelder, 1993, Van Rijn, 1993, Hossain & Rahman, 1998; overland flow: Alonso et al., 1981, Govers, 1992a, Guy et al., 1992; flume data: Low, 1989, Lu et al., 1989). Almost all studies reached different conclusions about the suitability of certain equations. Some of the studies mentioned here will be discussed in more detail in chapter 7. In this section, some attention will be given to the more theoretical evaluation of transport equations by Julien & Simons (1985) and Prosser & Rustomji (2000).

Prosser and Rustomji (2000) reason that discharge ( $q$ ) and slope ( $S$ ) are the basic controlling factors in sediment transport and that other parameters such as shear stress and stream power are derived from these two basic parameters. Therefore, they expressed a large number of equations in terms of  $q$  and  $S$  to make comparison possible:

$$TC = A \cdot q^a \cdot S^b \quad (2.15)$$

To express the different equations in this way it is necessary to neglect the threshold values in the equations. The  $a$  and  $b$  coefficients were calculated with different methods (q&S, shear stress, stream power) and compared. The results showed that the resulting  $a$  and  $b$  coefficients depended on the method used, but that  $a$  and  $b$  were comparable for all types of experiment (lab-plot, plot, river). Only flume-studies gave slightly different results. The median of both  $a$  and  $b$  was found to be 1.4, and both ranged between about 1.0 and 1.8. Any equation with coefficients within this range would be valid if the choice for that particular equation can be justified for the specific conditions to which it is applied.

Julien & Simons (1985) reviewed a number of bedload equations for their applicability to overland flow. They rewrote the equations to a form similar to that of equation 2.15 and compared the exponents of slope ( $b$ ) and discharge ( $a$ ) with equations developed for laminar flow. They assumed that overland flow is laminar and found that the discharge exponent ( $a$ ) varies with type of flow, but that the slope exponent ( $b$ ) is fairly constant. The discharge exponent of streamflow equations (turbulent flow) is generally lower than that of overland flow equations (laminar flow). Only the equations by Engelund-Hansen and Barekyan were found to be relevant to overland flow.

A number of transport equations will be evaluated for the Danangou catchment in chapter 7. An equation that could not be tested, but that is nevertheless interesting was developed by Abrahams et al. (2001). In recognition of the fact that the use of transport equations is often hampered by the limited range of conditions for which they were developed, Abrahams et al. (2001) used a very large data set obtained from flume experiments to develop a total load transport equation for interrill flow. Experiments were conducted in a 5.2 metre long flume and were performed under a wide range of conditions with respect to: flow depth and velocity, Reynolds number, Froude number, slope, sediment size, sediment concentration, roughness concentration and diameter, flow density and viscosity. Based on a dimensional analysis the following transport equation was obtained:

$$q_b = a \cdot D \cdot U_* \cdot Y \cdot \left(1 - \frac{Y_c}{Y}\right)^b \cdot \left(\frac{V}{U_*}\right)^c \cdot \left(\frac{w_i}{U_*}\right)^d \quad (2.16)$$

$$w_i = \left(\frac{g \cdot (\rho_f - \rho_s) \cdot D}{\rho_f}\right)^{0.5} \quad (2.17)$$

Where:

- $q_s$  = sediment transport rate (m<sup>2</sup>/s)
- $D$  = median grainsize (m)
- $U_*$  = shear velocity (m/s, see equation 7.4)
- $Y$  = Shields parameter (see equation 7.3)
- $Y_c$  = critical value of Shields parameter
- $V$  = flow velocity (m/s)
- $w_i$  = inertial fall velocity (m/s)
- $g$  = gravitational acceleration (m/s<sup>2</sup>)
- $\rho_f$  = fluid density (kg/m<sup>3</sup>)
- $\rho_s$  = sediment density (kg/m<sup>3</sup>)
- $a-d$  = coefficients

This equation is interesting since it was developed using data obtained under a range of conditions. For application on the Loess Plateau especially maximum volumetric concentration (0.3), minimum grain size (98  $\mu$ ) and maximum slope (10 degrees) are relevant. These values compare favourably with those of some other transport equations (see chapter 7), but grain size is still too large and slope angle too low for Loess Plateau conditions.

## 2.4 High concentrations

The effects of high concentrations on streamflow and sediment transport have traditionally been studied more in the context of hydraulics than of hydrology. Flows with extreme concentrations such as debris flows have received much attention and have been modelled with different degrees of success. Flow of debris flows is very different from channel flow. Soil erosion models, however, have not paid any specific attention to high sediment concentrations. For most regions, concentrations in runoff will not be very high, so that no special attention is needed. For the Loess Plateau, however, very high concentrations have been reported regularly. These kinds of flow occupy intermediate positions between clear water flow and debris flow and could have properties that differ significantly from clear water flow. More specifically high sediment concentrations could change density, viscosity, resistance to flow, velocity profile and transport capacity. This subject, therefore, requires special attention in the case of the Loess Plateau, and will be discussed in chapter 5.

## 2.5 Gullies

### 2.5.1 Introduction

Nordström (1988) summarised several definitions of gullies. She mentioned the following characteristics of gullies: a steep incised channel, often with a headcut, no permanent water, evidence of present or past rapid extension and the incision is mainly formed in unconsolidated materials. Gully erosion can have major effects, both on-site (due to soil loss) and off-site (due to sediment). On-site agricultural land can be lost, while off-site the major consequences are flooding and silting up of reservoirs.

### 2.5.2 Channel head

Dietrich & Dunne (1993) defined the channel head as the upstream boundary of concentrated flow between definable banks. The upper gully head will therefore often (though not always) coincide with the channel head. The position of the channel head in the landscape has been a topic of investigation for a long time in theoretical geomorphology. Channel initiation by overland flow can be viewed in two ways (Dietrich & Dunne, 1993, Montgomery & Dietrich, 1994, Kirkby, 1994, Prosser & Dietrich, 1995, Bull & Kirkby, 1997): as a balance between erosion and infilling and as a threshold phenomenon.

The first approach is called the instability view by Kirkby (1994) and Prosser & Dietrich (1995). It was developed by Smith & Bretherton (1972). This approach assumes that at every point of a slope incision processes and diffusion processes are operating. On the higher parts of the slopes diffusion processes will dominate because incision is limited by lack of water. Further downslope incision dominates. Channel initiation is then assumed to occur at the point where incision starts to dominate over dissipation. This will usually be around the inflexion point. Valleys tend to be without a sharp edge.

The second approach (the threshold view) assumes that for channel initiation to occur a threshold must be exceeded. In other words, erosivity of overland flow must surpass resistance of the soil. This threshold is usually expressed in term of shear stress or stream power. The critical shear stress (or critical stream power) will depend on the properties of the soil. Shear stress itself is related to discharge and slope. In the case of Hortonian overland flow, discharge should be proportional to drainage area. Valleys tend to have sharp edges and headcuts. This concept was proposed by Horton (1945). The threshold approach can also be applied to other processes such as sapping and mass movements (Montgomery & Dietrich, 1994). Gerits et al. (1987) used a threshold approach to explain piping on badland slopes. The link between threshold and process might not always be straightforward as reaction time and relaxation time can also play a role, so that the system could still be reacting to some threshold exceedance in the past.

Several authors (Montgomery & Dietrich, 1994; Kirkby, 1994; Rauws, 1987) mentioned the compatibility of these two views. No incision will occur until the threshold is exceeded; afterwards incision and diffusive processes will both operate. Kirkby (1994) stated that threshold behaviour is likely to dominate over instability behaviour in semi-arid areas,

while the reverse is true for humid areas. Prosser & Dietrich (1995) reasoned that the threshold approach is most appropriate for materials with cohesion, while the instability approach should be used in the case of cohesionless materials.

### *2.5.3 Gully processes*

The main difference between rills and gullies is their size but processes operating in gullies can also differ from processes in rills. Imeson and Kwaad (1980) stated that gullies resemble river valleys, while rills resemble river channels in their behaviour. Kalman (1976) stated that rills are in principle self-stabilising, while gullies are not. Rills are most likely formed by overland flow erosion, but gullies can develop in several ways.

#### *Role of overland flow*

Overland flow is likely to play a role in gully formation in semi-arid regions since infiltration excess overland flow (or hortonian overland flow) is likely to be important in semi-arid regions because of high rainfall intensities. The assumption of hortonian overland flow can however also be used in other regions, for example on soils with low permeability. It has the advantage that drainage area can be used instead of discharge (at least in steady state conditions), which is much harder to measure. Vandaele et al. (1996) used upslope drainage area and slope gradient to predict the initiation of rills and gullies. They found that larger drainage areas were necessary for rill initiation when there was more stone cover or vegetation. Antecedent moisture conditions proved also to be important. Overland flow is concentrated because of small accidental variations in topography (Bryan, 1987). Because of concentration shear stress will increase rapidly. Overland flow shear stress (or stream power) must exceed a threshold value, the value of which is determined by surface material properties (such as cohesion, texture and aggregate stability) and by vegetation. Rauws (1987), for example, found the following thresholds for rill initiation: slopes of more than 2 degrees and flow velocities of more than 3 - 3.5 cm/s. According to Prosser & Dietrich (1995) and Prosser (1996) vegetation can increase the threshold shear stress several times. It is often assumed that this threshold will be exceeded when flow becomes turbulent (Loch & Thomas, 1987), while it is also often stated that the flow must be able to transport all particle sizes (the flow is non-selective) for a rill to form (Bryan, 1987, Torri et al, 1987, Rauws, 1987, Crouch & Novruzi, 1989). When a rill is formed transport capacity increases greatly. The rill can grow into a gully when it is not removed by hillslope processes (diffusive) or management by man. Because of headcut migration the gully can retreat into un-rilled areas, thereby obliterating the rills that preceded its formation. Gullies formed by overland flow tend to be v-shaped. If a gully is u-shaped, seepage flow probably plays a role, even though overland flow might still be dominant (Imeson & Kwaad, 1980).

#### *Role of piping*

Piping can be caused by two mechanisms. Firstly, a pipe can be formed by animal activity or plant root decay. Alternatively, it can be formed because of seepage. Seepage erosion (also called sapping) sensu stricto can only occur in cohesionless materials, because the process involves liquefaction (Montgomery & Dietrich, 1994). Pipes can, however, also be formed in cohesive material. Chemistry often plays an important role, as it controls swelling/shrinking properties of materials. Swelling/shrinking and dispersion are mainly

controlled by the type and amount of clay. Bocco (1990) mentioned the following factors to be helpful in piping: high soil dispersion, soil cracking, steep hydraulic gradients and a convex slope profile. Most of these factors are also mentioned by Nordström (1988). Pipes can collapse to form lines of sinkholes and ultimately gullies. Pipe directions are mainly controlled by subsoil properties, such as geology and the direction of joints and faults, and can therefore differ from surface water directions.

#### *Role of mass movements*

Mass movements can be important in gully development because gully side slopes can be quite steep. Undercutting and seepage can both be important. Collison (1996) found that most material from gullies is produced by head and wall instability. He assumes that instability of the gully head is enhanced by overland flow infiltrating into cracks near the edge of the gully. Govers (1987) assumed that rill widening is caused by mass movements and rill deepening by overland flow incision. Rill incision thus creates the opportunity for mass movements to occur on the rill walls, but the actual mass movements on the rill/gully walls need not occur at the time of the storm. Govers (1987) viewed mass movements as delayed reactions to gully incision by water flow. Water distribution in the soil is important for stability, and this process takes time.

The above-mentioned processes are not all equally effective in producing gullies. Sapping, for example, is most effective when a free face is present. As a result sapping is more efficient in headcut migration than in actually forming a new gully on an undisturbed slope.

#### *2.5.4 Gully development*

To be able to predict the future behaviour of gullies it is necessary to understand the development of gullies over time. Gully heads tend to migrate because of e.g. plunge-pools, seepage, mass wasting and headcut erosion by flowing water. This decreases the upstream area of the gully head, which should eventually result in stabilisation of the gully head because less water is available at the headcut. Side slope processes will however continue and will dominate over incision. The upstream area of the gully outlet will remain constant, because as flow over the headscarp is decreased flow over the sidewalls is increased (Burkard and Kostaschuk, 1997). All material that is delivered to the gully must be transported by the water flowing into the gully. If sediment transport is decoupled from sediment production stabilisation can occur (Harvey, 1994). Imeson and Kwaad (1980) also stressed this balance between sediment production in gullies and sediment removal from gullies. Coupling is likely to decrease with growing gully size. Gully erosion should therefore become a transport-limited process, and stabilisation could occur. The sequence of events can also be important in gully development. Moderate rainfall events might for example be capable of enlarging existing gullies, without being able to form new ones. If loose material is produced between rainfall events, the first storm after a dry period might produce much sediment, while later storms of equal magnitude produce less sediment. It also means that a series of small events might cause no overland flow erosion, but could result in for example mass movements. This makes it harder to relate rainfall amount or rainfall intensity to the observed amount of erosion. Ultimately, gully development will,



however, be controlled by base level. If base level remains constant, sidewall stabilisation will occur eventually.

#### 2.5.5 *Gully erosion and soil conservation*

From the foregoing discussion, it should be clear that soil conservation methods should be adapted to the soil erosion process that is operating. If, for example, incision by overland flow is the dominant process methods should be aimed at increasing infiltration. But this will only aggravate the problem if piping is the dominant process (Bocco, 1990). Another example of the complexities of conservation measures is described by Nir & Klein (1974), who suggested that introducing contour ploughing increased gully erosion. Because of the contour ploughing field erosion was decreased and sediment content of water entering the gully system was lower than before, which made the water more erosive. Kalman (1976) performed field experiments on rill erosion in Morocco and found that rills were self-stabilising. He applied a certain discharge and observed progressively lower sediment concentrations that finally approached zero. Erosion after that only occurred when a higher discharge was applied. Kalman did not discuss the causes of this but the implication of his result is that erosion rates in his case will be higher when rills are removed than when they are left alone. This shows that a thorough knowledge of local erosion processes is necessary. Gullies did not show this self-stabilising behaviour. These examples show that erosion-restricting measures should be well thought out.

#### 2.5.6 *Gully erosion in loess areas*

Loess is an erodible material that is nevertheless able to form vertical walls that can be 10 metres or more in height. This is mainly due to bonds between the silt particles and to tension (Derbyshire, 1989). When loess becomes wet, however, it loses much of its strength because the bonds that exist between the primary silt particles are destroyed. Loess is therefore said to be a collapsible (or metastable) material (e.g. Handy, 1973). Erosion of loess can therefore be a major problem and gullies commonly occur (Leger, 1990).

In the loess area of central Belgium a distinction is commonly made between ephemeral gullies and bank gullies (e.g. Poesen, 1993; Poesen et al., 1998). Ephemeral gullies occur where overland flow concentrates, such as in thalwegs or along linear landscape elements. Bank gullies occur where concentrated flow encounters an earth bank. Bank gullies depend more on local conditions than ephemeral gullies and less on overland flow intensity. The distinction in ephemeral gullies and bank gullies is useful for gently sloping agricultural loess areas (such as in Belgium), but loses its relevance for other loess areas where gullies are much larger.

Large loess gullies, with depths of over 50 metres, have been reported from areas with a continental climate, such as Ukraine (Leger, 1990), China and Nebraska, USA (Pye & Sherwin, 1999). These very large gullies are often more like small valleys, and in fact, there are no clear criteria to distinguish between large gullies and small valleys. Sidewalls are often almost vertical near the top and headcuts can be several tens of metres in height.

Leger (1990) noted the role of desiccation cracks in causing the detachment of blocks of material in such large gullies. Derbyshire et al. (2000) found that the Chinese loess is prone to slab development that is due to tensional stresses in the loess. They also confirmed the findings of Lohnes & Handy (1968) that stability analysis can be used to show that loess slopes would have near vertical slopes at the top (70-85°) and slopes of 51-59° lower down. These gullies can cause severe dissection of previously low relief areas by headcut retreat. A well-known example of this is the retreat into the tablelands of the Chinese Loess Plateau.

Loess is not only susceptible to gully erosion, but also to sheet and rill erosion. Not only is it an erodible material, it is also prone to sealing and crusting. Cerdan et al. (2002), for example, found that sealing was important on loessic soils in Normandy, France. They measured maximum concentrations in runoff of about 100 g/l. These concentrations are much lower than those found elsewhere (e.g. on the Chinese Loess Plateau), but the slope angles in Normandy were gentle (1-10%).

## **2.6 Erosion modelling**

### *2.6.1 Introduction*

Morgan & Quinton (2001) and Doe & Harmon (2001) distinguished two broad model categories: predictive models and research models. Predictive models are used in practical applications, e.g. to assist in making land management decisions, while research models primarily aim to increase process understanding. In practice, this distinction is not so clear-cut, but it clearly shows that different models should be used for different aims. Therefore, the starting point of modelling should be a clear statement of objective (Morgan & Quinton, 2001). In this thesis, the focus will be on process understanding and research models.

Many models have been developed for simulating soil erosion. These models range from simple empirical models to very complicated process based models. Process based models apply as much process-knowledge as is available and use general laws or principles such as conservation of mass (continuity), Newton's second law of motion (momentum) and the first law of thermodynamics (energy) (Doe & Harmon, 2001). Process based models may, in principle, be used for conditions outside those tested since the laws on which they are based must be obeyed in all circumstances. Empirical models, on the other hand, do not necessarily model the right process and can only be used for the range of conditions for which they were developed. Which type of model is most suited to any particular situation depends on what the purpose of modelling is as well as on time and funds that are available. Complex process based models do not always give better predictions than simple models for several reasons: 1) Not all processes of soil erosion are sufficiently understood, so that the model structure might be flawed and empirical components are still used. 2) The more complex the model the more input data is required. Since input parameters are often difficult to determine accurately, uncertainty regarding the model input will increase with model complexity (Brazier et al., 2000,

Jetten et al., in press). Favis-Mortlock et al. (2001) showed that for more complex models error propagation becomes more important too. 3) Often, there are no unique input parameter sets, so that different input parameter sets can result in equally good predictions. This is called equifinality. On the other hand, process based models are the only type of model that can help us to better understand the processes that are operating. Besides, if physical processes are correctly incorporated in the model this would increase the reliability of predictions regarding the effects of management and landscape change (Brazier et al., 2000). Finally, though process based models might not give better predictions than empirical models they do give additional information, e.g. regarding the spatial and temporal distribution of erosion (Morgan & Quinton, 2001).

Erosion models can also be subdivided in those that simulate erosion for single storms and those that simulate erosion for longer time periods (continuous models). The first type depends on accurate data about model parameters at the start of an event (the initial conditions), while the latter models these parameters in between events. Thus, what happens in between events is not relevant for storm based models, as long as the initial conditions for the next event are correctly specified, but should be modelled by models operating on longer time scales. Processes that should be dealt with in continuous models include plant growth, evapotranspiration, percolation and the seasonal change of soil properties. Therefore, continuous models need much more data than event based models.

A third subdivision of soil erosion models is that in lumped and distributed models. Lumped models use only a few spatial elements for any application, while in distributed models the number of spatial elements can be in the tens of thousands. Obviously, lumped models can only predict the amount of soil loss leaving the study area, while distributed models should be able to give spatial predictions of erosion and deposition, but at the cost of having larger data need and computing time.

Scale issues play a role in soil erosion modelling in several ways. First, it is possible that at different spatial scales different processes are operating, or that they are operating in different ways. For any particular study, a model should therefore be chosen that is relevant to the scale of the problem being studied. Generally, a finer time and space resolution requires more detailed process knowledge, so that modelling at catchment scale is inevitably a compromise between detailed process understanding and reasonable computation times (Kirkby, 1998). At the same time, however, additional processes might appear at larger scales. Gully erosion, for example, does not operate at plot scale, but only on hillslope or catchment scale. Secondly, models usually require the use of effective parameter values that are representative values for the spatial units of the model. In most cases, the values of effective parameters are scale dependent. Another problem is that measurement scale of these parameters is often different from model scale. Most measurements of soil characteristics, for example, are point based (King et al, 1998), and might therefore not be representative for the larger model units. Finally, the way in which the actual landscape is represented in the model can also influence the model results. For grid-based models, for example, the results depend on grid size. This issue will be further discussed in chapter 9.

This section will briefly discuss some of the present day soil erosion models. LISEM will be discussed in section 2.7. Some models that have been developed with the specific purpose of simulating gully erosion will also be discussed.

### *2.6.2 Soil erosion models*

#### *USLE*

The Universal Soil Loss Equation (Wischmeier & Smith, 1978) is an empirical equation developed for the United States. It is based on a large number of Wischmeier plot measurements and predicts average annual erosion for plots or fields. Deposition is neglected. The basic equation is a simple multiplication of a number of factors. As shown by Haan et al. (1994), the individual factors can, however, be calculated in complex ways, especially in the revised version (RUSLE, Renard et al., 1997). The USLE has later been adapted to other areas as well. Since the plot scale is not the appropriate scale to study gully erosion the model is not capable of simulating gully erosion.

#### *WEPP*

The Water Erosion Prediction Project (Flanagan et al., 2001) is a process-based erosion model that simulates erosion for hillslope profiles. By combining several profiles with channel segments and impoundments small catchments can also be modelled. The model structure is described by NSERL (1995). WEPP is a continuous simulation model that can also be used for single storms. Since it is a continuous model it needs many parameters that are not needed in event-based models. For example, one needs to take into account soil management and changes of soil properties over the season. The minimum number of input parameters required to run the model is about 100 (Brazier et al., 2000).

Infiltration is simulated with the Green-Ampt Mein-Larson equation. Overland flow is divided into rill and interrill flow. Friction factors are calculated as the sum of partial friction factors, such as surface residue friction, bare soil friction and so on. Rill density must be specified beforehand and it is further assumed that all rills have equal discharge. Sediment transport is calculated with a modified Yalin equation. Water routing is in principle done with the kinematic wave, but to limit computation time approximations are used instead. For erosion calculation the steady-state runoff is used, which in practice means that the peak runoff is calculated and used in the erosion calculations. The runoff duration is adapted to a so-called effective duration to ensure that the total runoff volume remains constant. WEPP uses 5 sediment classes: clay, silt, sand, small aggregates and large aggregates. Transport and deposition are calculated separately for these classes. Gullies cannot be modelled.

#### *EUROSEM*

EUROSEM (Morgan et al., 1998a,b) is a process based soil erosion model developed to operate on event basis. The model was developed to overcome some of the problems and limitations of the USLE. The main problem of the USLE is that it is a model that gives only mean annual soil loss, while for the European circumstances it is more important to model within single storms (Morgan et al., 1998a,b). Some newer American models, such

as CREAMS (Knisel, 1991) and WEPP can be run for individual storms, but still they only model total storm soil loss. To model individual events a dynamic model is needed. EUROSEM therefore uses a 1-minute time step. Catchments are divided in a series of planes and channels that are supposed to be internally homogeneous. The main problem with a distributed, storm-based model is that many data about initial conditions are required.

In EUROSEM, all flow is assumed to be turbulent, which makes the use of the Manning equation possible. Morgan et al. (1998a,b) discussed the value of Manning's  $n$  for overland flow and channel flow. Theoretically, Manning's  $n$  should be higher for overland flow, but Morgan and co-workers argued that surges in velocity and presence of sediment could counterbalance this. They therefore use the same Manning's  $n$  for both overland flow and channel flow. Sediment is detached by both rainsplash and flow erosion and transported by flow. Rill erosion is modelled explicitly, but rill position has to be specified in advance. The sediment concentration in the flow is modelled as a balance between erosion and deposition (which both operate continuously). Transport capacity for rills is modelled with the use of transport equations developed by Govers (1990) and for interrill flow with those of Everaert (1991). Both equations use stream power to calculate transport capacity for different median grainsizes.

EUROSEM cannot be considered to be a fully distributed model as the possible amount of planes and channel segments is limited. Rill position has to be specified in advance. Gully erosion is at present not included explicitly and can only be modelled if the gullies can be either seen as large rills or as small channels. If different processes are operating in gullies these cannot be modelled. In addition, the location of gullies has to be specified in advance.

### *2.6.3 Gully erosion models*

#### *RILLGROW*

Favis-Mortlock et al. (1998) developed the RILLGROW model to simulate the initiation of rill systems and their subsequent development. The only input is detailed micro topography data (which are not always available). The micro topography is adapted during the simulation run according to the calculated erosion. Erosion is calculated with a stream power based equation. This method appears promising for very small areas, but it is unlikely that it can be used for catchment scale or even field scale as the data requirement and the computational demands will be too large for that.

#### *EGEM*

The Ephemeral Gully Erosion Model (EGEM), as described by Woodward (1999), was especially developed to simulate ephemeral gully erosion, in particular in the USA. EGEM consists of a hydrology and an erosion component. Erosion is driven by peak discharge and runoff volume, where peak discharge is assumed to occur as long as there is runoff. Gully depth is assumed to be constant along the length of the gully. It is assumed that the gully will erode vertically downwards until a less erodible layer is

reached. The maximum allowed depth is 46 cm (18 inches) because deeper gullies are considered to be 'classical' gullies instead of ephemeral gullies. When the maximum depth is reached the gully will widen. Nachtergaele et al. (2001) tested the model for mediterranean conditions in southern Portugal and southern Spain. They found that the ephemeral gully volume was predicted well, but this proved to be caused by the fact that gully length is also an input parameter of EGEM. In fact, the relationship between gully length and gully volume had a higher  $R^2$  than the EGEM-predicted volumes with measured volumes. EGEM assigns values for a number of soil parameters (like shear stress, grain size) based on soil type and tillage method. This method might not be accurate for the stony soils in the mediterranean study areas (Nachtergaele et al., 2001). The theory underlying EGEM was also not based on mediterranean conditions and might therefore not apply in this case.

### *GULTEM*

Sidorchuk and Sidorchuk (1998) developed the three-dimensional hydraulic GULTEM model to simulate the first stage of gully development. This first stage is the phase in which there is incision of the gully floor (gullies are assumed to be rectangular) with mass movements after the runoff events (resulting in a trapezoidal gully cross-section). The system develops rapidly during this stage. Flow width and depth are calculated from discharge using empirical equations developed for the Yamal Peninsula in arctic Russia. Particle detachment is calculated using the product of bed shear stress and average velocity. The output of the model is gully depth, width and volume. The main limitation of the model seems to be that the final gully length has to be specified beforehand. Headcut retreat is not modelled. Later Sidorchuk (1999) also presented a model for the second, so called stable, stage of gully development. During this stage, there is negligible erosion and deposition along the gully bed and the gully's bottom and walls are morphologically stable. Crucial in this model is how to specify the channel-forming discharge, since the stable condition implies that the threshold for transport is exceeded, but the threshold for erosion not reached. These thresholds depend on discharge. Sidorchuk reasoned that each discharge produces channel transformation and that therefore each discharge should be used as well as the return period for the particular discharges.

#### *2.6.4 Discussion*

In the previous sections only a few of the large number of available soil erosion models (see e.g. Jetten et al, 1999; Morgan & Quinton, 2001) have been discussed. It is clear that the models presented here do not take into account the effects of very steep slopes or high concentrations.

Gully erosion has received more attention, but up until now no erosion model can model gully erosion accurately. The more recent soil erosion models do, however, perform some sort of rill erosion calculation. It is, however, generally necessary to specify beforehand where the rills or gullies will develop. Even in a model such as the Ephemeral Gully Erosion Model (EGEM), which was especially designed to model ephemeral gullies, one has to specify the estimated depth and final length before simulation (Woodward, 1999). It

seems likely that the trend towards incorporating gully erosion into erosion modelling will continue as field measurements have shown how important gully erosion can be. At the moment none of these models can model for example mass movements on gully walls or headcut retreat (Poesen et al., 1998). Haan et al. (1994), however, report the development of models that take at least one of these processes into account.

Another trend is to use the grid based Digital Elevation Model (DEM) to estimate the amount of water at a certain point and to use a threshold concept to model concentrated flow erosion. From the DEM a slope map and a map of drainage direction can be calculated. Several authors (e.g. Ludwig et al., 1996; Takken et al., 1999 and Van Dijck, 2000) have recognised that tillage direction can change the runoff direction. Ludwig et al. create a drainage direction map by combining slope, tillage direction and linear features such as field boundaries. They assume that water is more likely to follow the slope on steeper slopes and more likely to follow the tillage direction on gentle slopes. Thresholds of upstream area and slope length are subsequently used to predict where concentrated flow erosion will occur.

The way in which to model gully erosion depends on what exactly one wants to model. Do we want a geomorphological model or an erosion model? In the first case we are trying to model the shape of the gully, in the second case only the amount of eroded material. So, geomorphological modelling would require adaptation of the DEM after each time step. In the second case the DEM maybe does not need to change and it might be possible to model the process of gully erosion by just indicating if a gully is present in any particular model unit.

Gully development is also a process that operates on several timescales. We can for example assume that loose material will be produced by mass movements between storms. Initial conditions and throughflow are also better modelled on a daily basis than on a storm basis. Produced material will then be removed during a storm. Incorporating these 'slow' processes into storm-based erosion models does not seem logical, since this would take too much computing time. It would be preferable to link storm-based erosion models to another model that simulates gully processes operating on longer timescales. In the case of the Chinese Loess Plateau this means modelling on a daily basis with a soil water model and modelling with a storm-based erosion model during storms.

## **2.7 LISEM**

Water erosion on the Chinese Loess Plateau almost exclusively occurs during the few heavy storms that occur in a year. This makes the choice for a storm-based model logical. LISEM (Limburg Soil Erosion Model) was used in this study because it is not only a storm-based model, but it is also raster based and can therefore simulate detailed spatial patterns of erosion. Many soil erosion models do not pay much attention to simulating erosion patterns. The principles of LISEM have been described in several papers (De Roo et al. 1994; 1996a,b; Jetten and De Roo, 2001). LISEM is also a process based model, so that any new process knowledge can be incorporated where necessary. A practical

advantage of LISEM is that it has been integrated with a Geographical Information System (GIS). It reads GIS-maps as input and produces GIS-maps as output. As GIS PCRaster is used (Wesseling et al., 1996). PCRaster is a grid-based GIS that has been specifically designed at Utrecht University to perform spatial calculations. Both LISEM and PCRaster are written in the C++ programming language.

### 2.7.1 Model structure

Figure 2.1 shows a simplified flow chart of the LISEM model. LISEM can be divided into two parts: a water part and an erosion part. Rainfall is the basic input of the water part. Interception is subtracted from the rainfall. The remaining rainfall reaches the soil surface, where it can infiltrate or form a surface storage. Since LISEM is a storm-based model the infiltrated water is essentially a loss of water in the sense that infiltrated water cannot resurface. Infiltration can be simulated using one of several available equations. Partly empirical equations such as the Green&Ampt and Holtan equations can be chosen as well as the physically based Richards equation (using the SWATRE sub model, Belmans et al., 1983). Surface storage will result in surface runoff once a certain threshold is exceeded. Flow velocity is calculated with the Manning equation and surface runoff is routed over the landscape with the kinematic wave equation. The effects of steep slopes on flow velocity are not specifically considered. The user can specify separate wheeltrack and channel networks. Overland flow and flow from wheeltracks can flow into the channel and is then routed to the catchment outlet as channel flow.

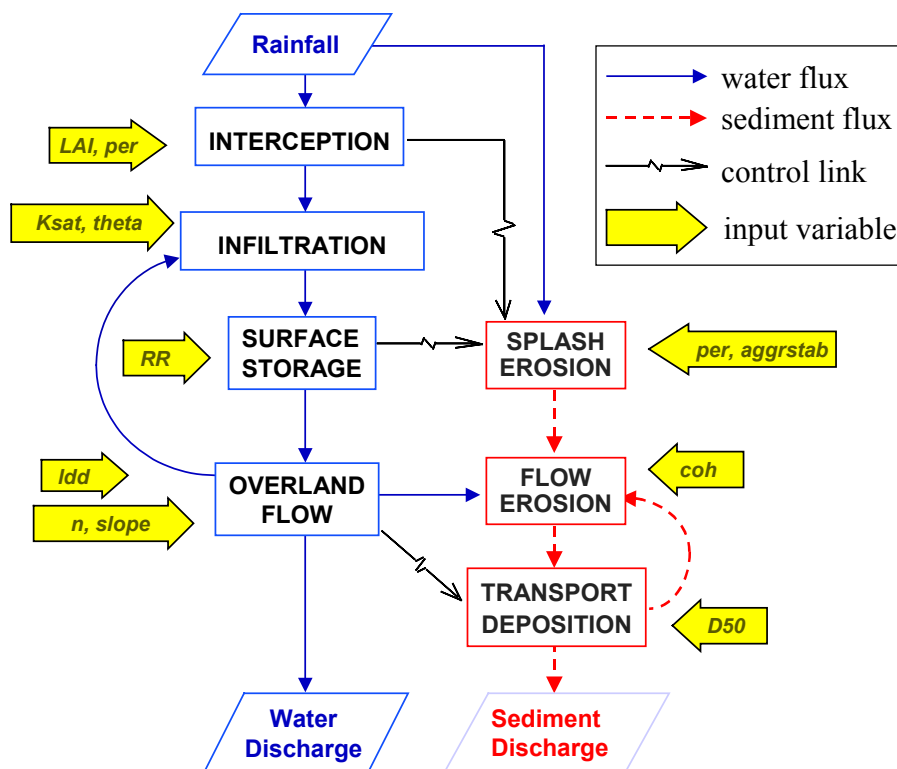


Figure 2.1 Simplified flow chart of the LISEM soil erosion model



Overland flow and channel flow are both routed with the kinematic wave, which is solved by a 4-point finite difference solution. An implicit method is used, so that the solution is usually stable and the choice of time step length and grid size is more important for accuracy than for stability. To solve the equation a linear scheme is used to obtain a first estimate of discharge, while iteration proceeds thereafter using a non-linear scheme and the Newton method (Ven Te Chow et al., 1988). The present version of LISEM (version 1.63) does not perform a kinematic wave for sediment. Instead, the sediment is redistributed according to the redistribution of water as determined with the kinematic wave. This procedure seems to introduce some error and a mass balance correction is used for the sediment to overcome this problem. In this correction the mass balance error of sediment is redistributed over the network according to the sediment output of the different pixels. Future versions of LISEM might include a separate kinematic wave for sediment in which discharge is routed first and the results from the discharge routing are used to route the sediment.

LISEM simulates erosion by rainfall and erosion by overland flow and channel flow. Rain splash erosion is calculated as a function of rainfall kinetic energy and depth of the surface water layer. Sediment transport only occurs by overland flow and channel flow. For both overland flow and channel flow, LISEM uses the transport equation developed by Govers (1990) for slopes of up to 12 degrees. The equation is based on a stream power approach:

$$TC = c(SV - SV_{cr})^d \cdot \rho_s \quad (2.18)$$

Where:  $TC$  = transport capacity (g/l)  
 $S$  = slope (m/m)  
 $V$  = mean velocity (cm/s)  
 $SV_{cr}$  = critical unit stream power (cm/s)  
 $\rho_s$  = density of solids (kg/m<sup>3</sup>)  
 $c, d$  are coefficients

According to Govers the critical unit stream power is 0.4 cm/s. The coefficients  $c$  and  $d$  depend on grainsize and can be calculated with equations 7.17 and 7.18. Figure 2.2 shows  $c$  and  $d$  as function of median grainsize (D50), while figure 2.3 shows transport capacities calculated with equation 2.17. Figure 2.3 shows that transport capacities increase with decreasing grainsize. Net flow detachment and deposition are calculated with an equation derived from the EUROSEM model (Morgan et al, 1998a,b), but reformulated for use with pixels:

$$D_f = y \cdot (TC - C) \cdot \omega \cdot w \cdot DX \cdot dt \quad (2.19)$$

Where:  $D_f$  = net detachment/deposition flow (kg)  
 $y$  = efficiency coefficient  
 $TC$  = transport capacity (g/l)  
 $C$  = concentration (g/l)

$\omega$  = settling velocity (m/s)  
 $w$  = flow width (m)  
 $DX$  = pixel length (m)  
 $dt$  = time step length (s)

The efficiency coefficient ( $\gamma$ ) is 1 for deposition and smaller than 1 for detachment. In case of detachment the value of  $\gamma$  depends on cohesion. After detachment and deposition are calculated with equation 2.19 a check is performed to ensure that no physically impossible situations occur. This is necessary because using equation 2.19 detachment and deposition might become larger than  $TC-C$ . Therefore, detachment is limited to that amount of detachment that would just fill all available transport capacity, while deposition is restricted to the total amount of sediment present in the flow.

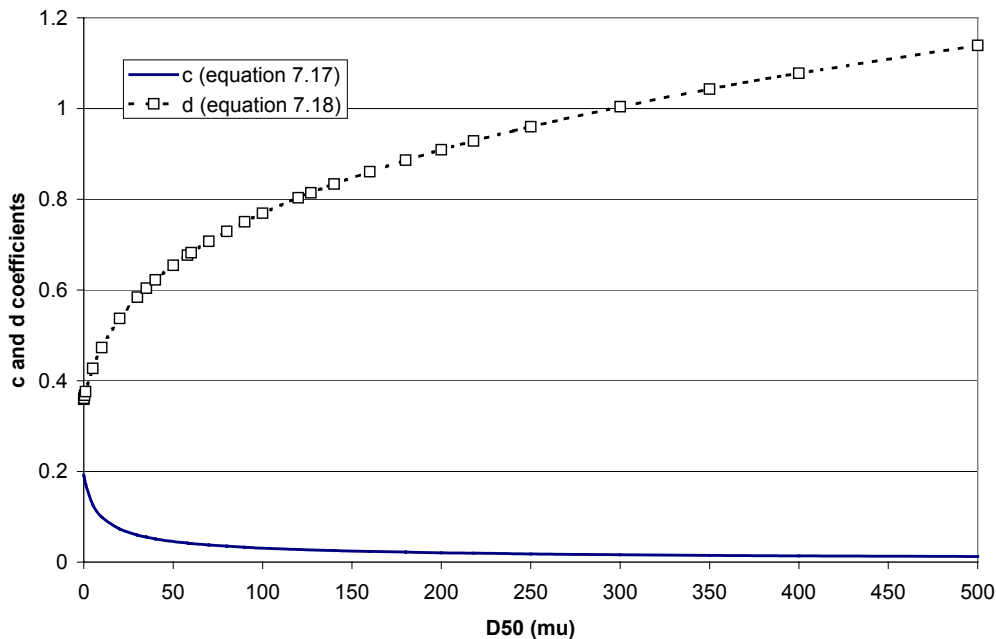


Figure 2.2. c and d coefficients as a function of median grainsize (D50)

Like the other erosion models LISEM does not take the effect of high concentrations into account. Fluid density is assumed to be constant, and predicted water discharge is a clear water discharge. Neither is gully erosion explicitly modelled by LISEM.

### 2.7.2 LISEM input and output

As a process based model LISEM requires a significant amount of input. The input differs from one infiltration equation to the other. Table 2.1 shows the input that is required by LISEM if the Richards equation is used for infiltration, and when the wheeltrack option is not used. All names with extension .map are PCRaster maps. Provided that field data are available almost all maps can be derived from the 3 basic maps: DEM, land use map and soil map. Table 2.1 also shows how these data can be obtained.

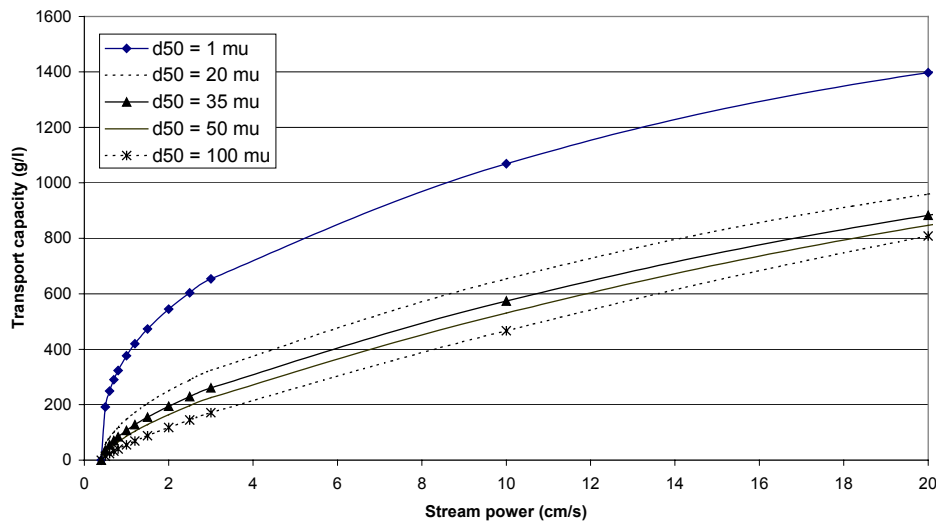


Figure 2.3. Transport capacity as function of stream power for different grainsizes

As can be seen from table 2.1 there is a number of parameters that should be measured in the field, either once or repeatedly. How these parameters were determined will be discussed in chapter 4. Table 2.1 only shows which data are needed to actually run the model. To test the model result additional field data are needed. Those data are at least runoff and sediment concentration at the outlet of the catchment, and preferably also data about the actual distribution of erosion in the catchment. Those data will also be discussed in chapter 4.

The standard output of LISEM consists of several ASCII files that can be used to prepare hydrographs and sedigraphs for a maximum of 3 different points in a catchment as well as several maps. Apart from an erosion map (tonnes/ha) and a deposition map (tonnes/ha) a number of runoff maps (l/s) is created for user-specified times. One of the ASCII-files gives a summary for the outlet of the catchment.

In this thesis Windows version 1.63 of LISEM is used. This version will be referred to as LISEM 163. In the course of the thesis 2 adaptations of LISEM 163 were developed. For sake of clarity these versions will be called LISEM LP (Loess Plateau) and LISEM TC (Transport Capacity).

### 2.7.3 LISEM calibration and validation

LISEM was developed for the province of Limburg, The Netherlands, and has been previously calibrated and validated for several catchments in the Loess region of northwestern Europe. De Roo et al. (1996b) performed a sensitivity analyses and found that the most sensitive variable in the prediction of runoff is saturated conductivity. For

Table 2.1 Input data for LISEM version 1.63, with the use of the SWATRE infiltration sub model but without the use of a wheeltrack network.

Parameter	Name <sup>b</sup>	Method <sup>a</sup>	Unit
<u>Basin characteristics</u>			
Catchment area	area.map	derive from DEM	-
Drainage direction	ldd.map	derive from DEM	-
Slope gradient	grad.map	derive from DEM	tangent
Catchment outlet	outlet.map	derive from DEM	-
Position rain gauges	id.map	mapping	-
Rainfall data	*.tbl	measure continuously	mm/h
<u>Soil and land use</u>			
Plant cover	per.map	measure repeatedly	-
Plant height	ch.map	measure repeatedly	m
Leaf area index	lai.map	measure repeatedly	-
Random roughness	rr.map	measure repeatedly	cm
Aggregate stability	aggrstab.map	measure repeatedly	-
Soil cohesion	coh.map	measure repeatedly	kPa
Added cohesion roots	cohadd.map	estimate	kPa
Manning's n	n.map	measure once	-
Median grain size	d50.map	measure once	µm
Splash delivery ratio	-	estimate	-
Stone cover fraction	stonefrc.map	measure once	-
Width grass strips	grasswid.map	measure once	m
Manning's n grass strip	-	estimate/measure	-
Road width	roadwidt.map	measure once	m
<u>Channels</u>			
Drainage direction	lddchan.map	derive from ldd.map	-
Channel gradient	changrad.map	derive from grad.map	tangent
Manning's n channel	chanman.map	measure once/estimate	-
Cohesion channel	chancoh.map	measure/estimate	kPa
Channel width	chanwidt.map	measure once	m
Channel shape	chanside.map	field observation	-
<u>SWATRE infiltration</u>			
Soil profile map	profile.map	derive from soil map	-
Soil profile table	profile.inp	derive from soil map	-
Initial pressure head	inithead.*	measure repeatedly	cm
K-unsat tables	*.tbl	laboratory meas.(once)	cm/day
Crust fraction	crustfrc.map	measure	-
Crust profile map	profcrst.map	profile description	-
Grass strip profile map	profgras.map	profile description	-

<sup>a</sup> Once and repeatedly refer to a frequency in time, not space. Measurements should be performed in a sufficient number of places to be able to create a map.

<sup>b</sup> When no name is specified the value of the parameter applies to the entire catchment and should be specified in the LISEM interface.

the prediction of soil erosion LISEM was most sensitive to changes in Manning's  $n$  and transport capacity. De Roo et al. (1996b) found that LISEM gave reasonable results for 60% of the storms that were modelled. They attributed the discrepancy for the other 40% to spatial and temporal variability in saturated conductivity and initial moisture content and to differences between summer storms and winter storms. De Roo & Jetten (1999) identified saturated conductivity, suction at the wetting front and initial moisture content as sensitive parameters. Takken et al. (1999) showed that LISEM predicted catchment runoff reasonably well, but failed to reproduce observed erosion and deposition patterns inside a catchment.

#### 2.7.4 *LISEM and the Loess Plateau*

Some of the main algorithms of LISEM are only valid for a given range of circumstances. Since the circumstances on the Loess Plateau are very different from the circumstances for which LISEM was developed it is possible that application limits will be encountered when applying LISEM to the Loess Plateau. Gullies play a much more dominant role than in northwestern Europe and they may function both as sinks and source of sediment. Likewise, the combination of steep slopes with small-scale land use, might provide an environment that LISEM is not able to simulate. Some important characteristics of LISEM that might affect its application on the Loess Plateau will be discussed briefly here.

The first characteristic is the way in which transport capacity is calculated. LISEM calculates flow velocity with Manning's equation and subsequently calculates stream power and transport capacity. Since stream power is the product of the velocity and the (energy) slope, the slope angle influences the stream power considerably. According to Govers (1990) the transport capacity equation derived from stream power is valid for slope angles up to 20%, and this will pose one of the largest potential problems in the application of LISEM to this area. The erosion and deposition are modelled as transport deficits and surpluses and are therefore also strongly determined by the flow conditions.

Another important characteristic of LISEM is that it is a grid-based model. Flow circumstances are determined locally in each grid cell and inertia of water is not taken into account. Thus while in reality sediment remains in suspension when the slope angle changes abruptly, LISEM may simulate sudden deposition because it assumes that the transport capacity decreases radically. It is therefore possible that the presence of gullies with extreme changes in slope pose problems for the kinematic wave that is used in LISEM to route the water and sediment. Such problems are likely to be more pronounced for steeper areas. On the other hand, models that do not use a grid based approach cannot model spatial distribution of erosion at all.

A final feature of LISEM that may be important is that concentrated flow in ditches and ephemeral streambeds can be simulated as a separate process, by defining these features as 'channels'. The channels are assumed impermeable and the channel dimensions and characteristics influence the hydrograph shape considerably.

This study must be seen as a performance test of a process based distributed model under extreme circumstances.

## **2.8 Conclusions**

The specific characteristics of the Chinese Loess Plateau that have been identified have so far not been studied in the context of soil erosion modelling.

Both the velocity equations and the sediment transport equations that are commonly used in erosion models have not been developed for such steep slopes as those of the Chinese Loess Plateau. The effect of slope angle on flow velocity and sediment transport has not been evaluated for such models either. Likewise, the effect of sediment concentration on flow properties has not received any particular attention in erosion modelling.

Gully erosion is a topic that has received more attention in erosion modelling. Some of the present day erosion models do simulate some sort of gully erosion, but even models that have been specifically developed to model gully erosion require that some properties of the gullies be set in advance.

The LISEM model is an up to date erosion model that is in principle suitable for simulating erosion on the Loess Plateau for several reasons. LISEM is storm-based, so that it should be able to handle the storm-dominated water erosion of the Plateau. LISEM is also a distributed model, so that spatial predictions of erosion inside a catchment are possible. Finally, LISEM is a process based model. This means that process descriptions in the model can be adapted if the specific characteristics of the Loess Plateau require this. At present LISEM does not specifically take into account the effects of steep slopes, high sediment concentrations and the presence of gullies.

### 3 THE DANANGOU CATCHMENT

Chapter 1 introduced the Loess Plateau and the characteristics that make it different from most areas where so far erosion modelling has been applied. Chapter 2 showed that these characteristics potentially have implications for erosion modelling, and that the current process based erosion models do not consider these implications. In this chapter, more attention will be given to the development and erosion of the Loess Plateau. Thereafter, the study area will be introduced and described. The aim is not only to describe the area, but also to determine if the specific Loess Plateau characteristics of steep slopes, high concentrations and the presence of gullies are equally characteristic for the study area.

#### 3.1 The Loess Plateau

##### 3.1.1 *Loess deposition*

###### *Source*

The loess deposits of central China show increasing clay content and decreasing sand content towards the southeast. Loess thickness decreases from northwest to southeast. Likewise, trace elements like zinc, manganese and cobalt all increase in concentration towards the southeast (Wen Qizhong et al., 1987). This suggests that the source of the loess was in the northwest. There appear to have been several sources of loess (Derbyshire et al., 1993). Most of the loess of the Loess Plateau originated from the deserts of northwestern China. Mechanical weathering in these deserts formed silt size particles. Another important source were large alluvial fans at the foot of the mountain ranges of western China (Derbyshire & Meng, 2000). There was also some silt formed by glacial grinding and mechanical weathering on the Tibetan Plateau (Figure 1.1). The material from the Tibetan Plateau was probably transported to basins north of the Tibetan Plateau by fluvial processes. Different degrees of rounding and weathering support this hypothesis (Derbyshire et al., 1993). The silt from the deserts and the basins was then entrained by dust storms and transported to the southeast by the westerly jet stream and by the winter monsoon (Huang et al., 2000). The monsoon circulation was probably stronger during the Pleistocene than it is today (Linyuan et al., 1991), especially during glacials, when the equator-pole temperature gradient was much larger than it is now (Huang et al., 2000). This wind-blown material was deposited on the Loess Plateau, which is also situated in a basin north of the Tibetan Plateau. The entire Loess Plateau is rising, but the Tibetan Plateau rises faster. The area of loess deposition is bordered by mountains on the east and south. This resulted in massive deposition of loess, with maximum loess thickness of over 300 metres. Deposition started in the early Pleistocene and continued intermittently through most of the Quaternary (Lin & Liang, 1982). Though the Tibetan Plateau should not be seen as the major source of silt, its rise has been very important to the loess deposition. The rise of the Tibetan Plateau progressively blocked the flow of moist air from the southeast, which gave rise to the present day monsoonal circulation and to deposition of loess on what is now the Loess Plateau (Huang et al., 2000). The rate of uplift of the Tibetan Plateau is, however, a matter of

debate (Derbyshire et al., 2000). It is therefore also uncertain when the Tibetan Plateau reached an altitude high enough to enhance the monsoon system. According to Pye (1987) the plateau rose about 2000 meters during the Pleistocene. As a result conditions became much dryer, which enhanced silt formation and loess deposition. Palaeosols indicate that the loess deposition was episodic. According to Huang et al. (2000) pedogenesis occurred when the climate was dominated by the wet southeasterly summer monsoon, while loess deposition occurred when the climate was dominated by the dry northwesterly winter monsoon. Even today deposition from dust storms continues, but erosion dominates over deposition (Linyuan et al., 1991).

### *Stratigraphy*

The loess of the Loess Plateau is underlain by Cretaceous bedrock and Upper Pliocene red clays from the Linxia formation (Derbyshire et al., 1993, Kukla & An, 1989, Huang et al., 2000). This clay layer has been deposited in a lacustrine environment and can attain magnitudes of up to 50 metres in some places on the Loess Plateau. The Pleistocene loess deposits themselves can be subdivided into three parts. From old to young these are: Wucheng, Lishi and Malan loess (table 3.1).

Table 3.1 Stratigraphy of Chinese loess. After Lin & Liang (1982)

Geological Age		Name of stratum		Remarks
Holocene	Recent		New Loess (Yellow loess)	Mostly collapsible, often highly compressible
	Early			Collapsible
Pleistocene	Late	Malan	Old Loess (Red loess)	Non-collapsible, except sometimes in upper layers
	Middle	Lishi		
	Early	Wucheng		

Wucheng and Lishi loess are often together called Old loess and the Malan loess is called New loess. For reasons explained in section 3.3, in this thesis the Old Loess will be called Red loess and the New Loess will be called Yellow loess. The old loess has undergone alterations, which have made it relatively compact and stable. Clay content has increased and secondary carbonate concretions have formed. Several palaeosols have formed in it. These are darker coloured and have a carbonate layer at their bottom (Kukla & An, 1989). The loess/soil sequence has been subdivided using colour, carbonate content, degree of bioturbation, humus content and low magnetic susceptibility (Kukla & An, 1989). It was also dated by several methods such as vertebrate palaeontology, radiocarbon dating, thermoluminescence and paleomagnetism. The dated sequence closely resembles the  $^{18}\text{O}/^{16}\text{O}$  curves obtained from deep-sea drilling (Kukla & An, 1989, Huang et al., 2000, Lu & Sun, 2000), including the Milankovitch cyclicities.

### *Properties*

According to Pye & Sherwin (1999) typical loess is a unimodal, poorly sorted, fine skewed sediment that may contain up to 10% fine sand and up to 20% clay. The grain size distribution of loess can, however, vary widely from place to place. For China, Pye and Sherwin report median grain sizes between 16 and 33  $\mu\text{m}$ . Pye & Sherwin also give data on the composition of loess. For loess from Lanzhou, China, they report the following



mean composition: Quartz (51%), feldspar (21%), calcite (12%), dolomite (7%) and mica (10%). The clay fraction was dominated by illite, with about 60%. More information on the chemical composition of loess is given in chapter 4. Apart from its composition, loess has several characteristics that are important to understand its behaviour:

- Loess, and especially Malan loess, has very loose packing. Its mechanical properties are entirely determined by the bonds between the particles, as the larger particles do not touch each other (Tan, 1988). For Malan loess the cementation is weak (Derbyshire & Meng, 2000). Porosity of Malan loess can be 50% (Tan, 1988 and Miao & Wang, 1991) or more and unit weight is about 1.4–1.5 g/cm<sup>3</sup>. Older loess has been more compacted and has lower porosity, more cementation and larger strength.
- Loess is very sensitive to water as the bonds between the larger particles contain soluble salts, calcium carbonate and clay minerals (Tan, 1988, Pye & Sherwin, 1999). This can cause collapse of the structure of the loess skeleton upon wetting. This process is called hydroconsolidation. The tendency of loess to collapse is inversely related to its clay content (Pye, 1987). The clay content of the loess increases from northwest to southeast (away from the source) and the thickness of the Malan loess decreases in that direction. The collapsibility of the loess therefore decreases towards the southeast (Lin & Liang, 1982). Handy (1973) investigated the collapsibility of loess in Iowa, USA. He used the ratio between liquid limit and saturated water content to determine whether the loess is collapsible or not. If liquid limit is lower than saturated water content the loess is collapsible. Old loess is non-collapsible (table 3.1), but still loses strength upon wetting.
- Loess shows creep behaviour of its skeleton (Tan, 1988), meaning that when it is loaded it can gradually deform without structural collapse.
- Loess is erodible. According to Morgan (1996) silts and fine sands are the least resistant to erosion. Smaller particles have more cohesion, while the entrainment of larger particles requires greater force due to the larger weight of the particles. Morgan (1996) also showed that soils with organic matter content below about 3.5% are more erodible. Organic matter content of Loess Plateau soils is usually well below this value.
- Loess is often closely jointed. Joints are often sub-vertical and can be formed by a variety of processes, including geological forces, stress release and wetting/drying cycles. These joints enable water to penetrate to great depth, which would otherwise not be possible (Derbyshire et al., 2000).

### *Landform*

The loess was deposited on a pre-existing landscape, which is likely to influence present landform in areas where the loess deposits are not very thick (Derbyshire et al., 1993). Other factors that influenced the present morphology of the Loess Plateau were climatic alternations during the Quaternary, uneven uplift of the Plateau and several thousand years of agriculture (Leger, 1990). The loess-landscapes of the Loess Plateau can be roughly subdivided into 3 parts. These are plateau landforms (yuan), ridge landforms (liang) and rounded hills (mao). The latter landform can also be called the hilly loess area. These different landforms can represent different stages in denudation. Rounded

hills would than develop from plateaus via ridges. This view of landform development is, however, complicated by the influence of the underlying bedrock and by the episodic nature of loess deposition (Derbyshire et al., 2000), so that not all mao and liang landforms are necessarily developed from yuan landforms. Figure 1.3 shows a typical landscape of the hilly part of the Loess Plateau of northern Shaanxi province.

### 3.1.2 Loess erosion

As shown in chapter 1 the Loess Plateau is subject to large erosion rates because of its steep slopes, high intensity rainfall, low vegetation cover and erodible material. Several types of erosion are important on the Loess Plateau.

#### Overland flow erosion

Overland flow erosion ranges from sheet erosion on hillslopes to large-scale gully erosion. Several empirical erosion equations have been developed to predict storm erosion on various parts of the Loess Plateau. These equations are usually developed using erosion monitoring on plots. Barrels are often used to collect water and sediment, so that there is information about total storm erosion, but not about the change of concentration over time. Zhang Cunfu (cited in Fang Zhengsan et al., 1981) developed the following equation for Suide, which is inside the Wuding catchment (figure 1.2):

$$E = 526 \cdot I^{0.434} \cdot Q^{1.39} \cdot S^{0.687} \cdot 0.324^c \quad (3.1)$$

Where:  $E$  = erosion (tonne/km<sup>2</sup>)  
 $I$  = average intensity of the storm (mm/min)  
 $Q$  = runoff depth (mm)  
 $S$  = slope (%)  
 $c$  = plant cover (%)

Jiang Zhongshan (Fenli Zheng, personal communication) developed the following equation for erosion on fallow slope land near Ansai, Shaanxi province:

$$E = 5.097 \cdot P^{0.999} \cdot I_{30}^{2.637} \cdot S^{0.880} \cdot L^{0.286} \quad (3.2)$$

Where:  $E$  = erosion (tonne/km<sup>2</sup>)  
 $P$  = total event precipitation (mm)  
 $I_{30}$  = max 30 minute intensity (mm/min)  
 $S$  = slope (°)  
 $L$  = slope length (m)

Mou Jinze (1981) discussed results from plot studies on soil erosion of the Loess Plateau. He used large plots because small plots will not give results that are representative of the processes on hillslopes. This is because gully erosion provides most of the sediment on natural hillslopes, and gully erosion will not occur on small erosion plots. Mou Jinze found that because of the very high transport capacity of overland flow sediment

concentrations continuously increased along flowlines on hillslopes. As a result, erosion per unit area increased with increasing plotsize and could be calculated with a rating equation:

$$E = a \cdot Q_{tot}^b \quad (3.3)$$

Where  $Q_{tot}$  is total event discharge in mm,  $E$  is erosion in tonnes/ha and  $a$  &  $b$  are coefficients.

Apart from plot studies of soil erosion, there are also a number of experimental catchments on the Loess Plateau. Zhu et al. (1997), for example, studied runoff generation in a 20 ha catchment in Shanxi province. They found that the amount of runoff showed low correlation with rainfall amount, but a clear relationship with rainfall intensity. Rainfall intensity needed to produce runoff varied with soil type, but was on average about 0.2 mm/min. Crusts developed on cultivated lands decreased conductivity from 0.6-0.7 to 0.2-0.3 mm/min. Because of this, the difference in runoff generated on cultivated lands and on wastelands decreased during the season from 1/6 to 1/2. Increasing infiltration seems to be the best way to diminish erosion. The crust on cultivated lands is sometimes broken by hoeing, but this is not general practice. Billard et al. (2000) also demonstrated the importance of crusting on Chinese loess soils. They, however, also showed that desiccation cracks in old crusts are very persistent, and can reduce runoff compared to fresh crusts.

In these experimental catchments, discharge and sediment concentration is usually measured. This is also the case for several rivers on the Loess Plateau. Such measurements have revealed extreme concentrations and very high annual soil loss. Jiang Deqi et al. (1981), for example reported annual soil losses of 18,000 tonne/km<sup>2</sup> for large parts of the Wuding catchment, while for the gullied areas of smaller catchments they found values of over 30,000 tonne/km<sup>2</sup>. Such values are the aggregated result of several sediment sources (rills, gullies, pipes etc).

### *Piping*

Piping is a widespread phenomenon in the western part of the Loess Plateau (Muxart et al., 1994), where the loess is sandier than in the southeast. Nevertheless, piping can occur everywhere on the Loess Plateau.

Zhu (1997) and Zhu et al. (2002) studied hydrology and erosion of tunnel systems in the small Yangdaogou catchment in Shanxi Province. Runoff and sediment concentration were monitored for the tunnel systems in the catchment as well as for the catchment outlet and on a few plots without tunnels. The tunnels were too far underground to get any water from infiltration. Instead, the water flowing through them entered the system through a number of pipe inlets and is essentially underground overland flow. The tunnel systems showed a rapid reaction to rainfall. Tunnel runoff generally increased during the rainy season as the initial events lost water through infiltration from the tunnels, but later events did not. The tunnel runoff data showed evidence of tunnels becoming temporarily blocked by tunnel collapse. On the other hand, new inlets might be formed during events.

Tunnel discharge and sediment yield from tunnels are therefore far more erratic than is the case for overland flow. Zhu et al. (2002) reported sediment concentrations in tunnel runoff of up to 890 g/l. Concentrations in tunnel runoff were, on average, equal to those in runoff from the entire catchment, but higher than those measured on slopes without tunnels. On average, the tunnel systems produced 57% of total sediment yield from the catchment, but this percentage varied widely from storm to storm. This value, however, does not seem to take into account that the water entering the tunnel system will already carry sediment. Thus, the contribution of tunnels themselves is not known exactly. Tunnel connectivity was repeatedly investigated using smoke bombs. It was found that many tunnel inlets are not connected to tunnel outlets. Water flowing into these inlets will infiltrate and can recharge the ground water.

### *Stability*

The loess karst pipes can increase infiltration. Another important source of water can be irrigation of the arable land. The infiltrating water can progressively weaken the loess by eluviation and it can also result in higher pore pressures. The result can be instability and mass movements, sometimes of catastrophic proportions. Earthquakes can be important triggers, but mass movements can also occur just because the loess is progressively weakened by eluviation. Mass movements often occur at the end of the rainy season in wet years, indicating the importance of water in stability of the loess.

As discussed in chapter 2, dry loess can form near vertical walls. Tensile stresses near the top of the wall can result in the formation of joints. Joints can also form parallel to the ground surface because of unloading. According to Pye (1987) these processes make loess walls of more than about 5 meters high potentially unstable. Handy (1973) related the geomorphology of loess-gullies to the collapsibility of loess. He argued that the presence of headcuts of up to 10 metres high indicates that failure occurs in unsaturated conditions and that this is likely to be caused by water contents above the liquid limit in a zone at the base of the headwall and the sidewalls of the gully. According to him loess is an underconsolidated and potentially collapsible material that is metastable. Only excess water is needed to make it unstable.

## **3.2 Catchment choice**

The Danangou catchment (figure 3.1) is located close to the small town of Ansai and is about 40 km north of Yan'an, Shaanxi Province, China. According to Douglas (1989) the region north of Yan'an has the highest erosion rates of the Loess Plateau. The catchment belongs to the hilly part of the Loess Plateau, which is the most severely eroded part.

The Danangou catchment was selected for several reasons (scientific as well as practical):

- Since a process based erosion model (LISEM) was used, the catchment could not be too large. The bigger a catchment is the larger the spatial units of the model will have to be, which means that the real situation is represented less well. Furthermore, the larger the number of spatial units in the model the more difficult it will be to get enough input data.

- Since the Erochina project as a whole aimed at defining alternative land use scenario's a catchment that was as yet not much influenced by soil conservation methods had to be chosen.
- To obtain good results with the participatory approach the catchment needed to have enough inhabitants.
- The catchment had to be close to one of the research stations that are situated on the Loess Plateau.

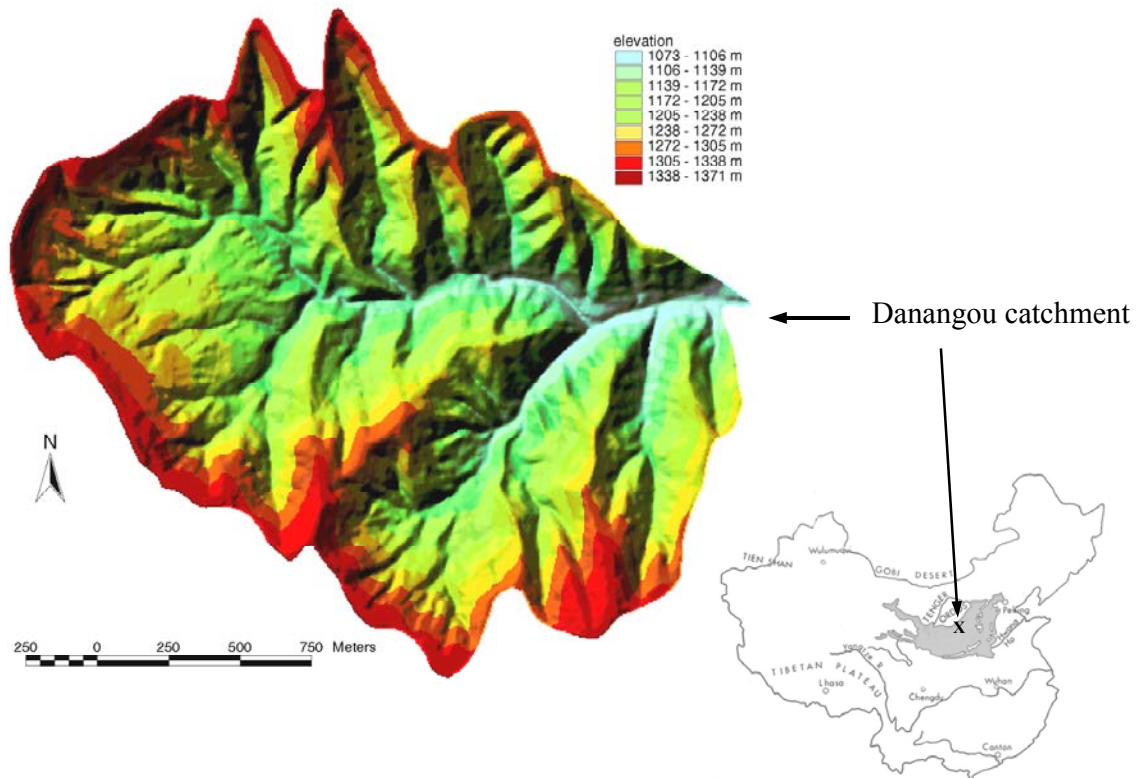


Figure 3.1 Elevation map of the Danangou catchment. Shading has been used to give the relief better visibility. The position of the Danangou catchment on the Chinese Loess Plateau is also indicated. The map of China was adapted from Pye (1987)

From the available options the Danangou catchment matched these requirements best:

- The catchment has an area of about 3.5 km<sup>2</sup> and was therefore not too large to model with a process based model.
- The only conservation methods at present are a few large terraces and some reforestation. The catchment is very different from the surrounding catchments, since in the other catchments large scale terracing has been applied as part of a World Bank Project.
- A total number of about 50 families live in the catchment. There are two small villages in the catchment, so that there were good opportunities to involve the farmers in the project though a participatory approach.

- The Danangou catchment is located about 5 km north from the small town of Ansai. In Ansai a research station of the Institute for Soil and Water Conservation (ISWC) is located.

The Danangou catchment has an area of 3.58 km<sup>2</sup>. Elevation ranges from 1075 to 1370 metres and slope angles are steep (figure 3.2). Maximum slope angles derived from the topographical map are 70 degrees, while in the field almost vertical walls of several tens of metres can be observed. Figure 3.1 shows a Digital Elevation model of the catchment as well as the position of the catchment on the Chinese Loess Plateau. The catchment drains into the Yan river, which in turn drains into the Yellow river (figure 1.2).

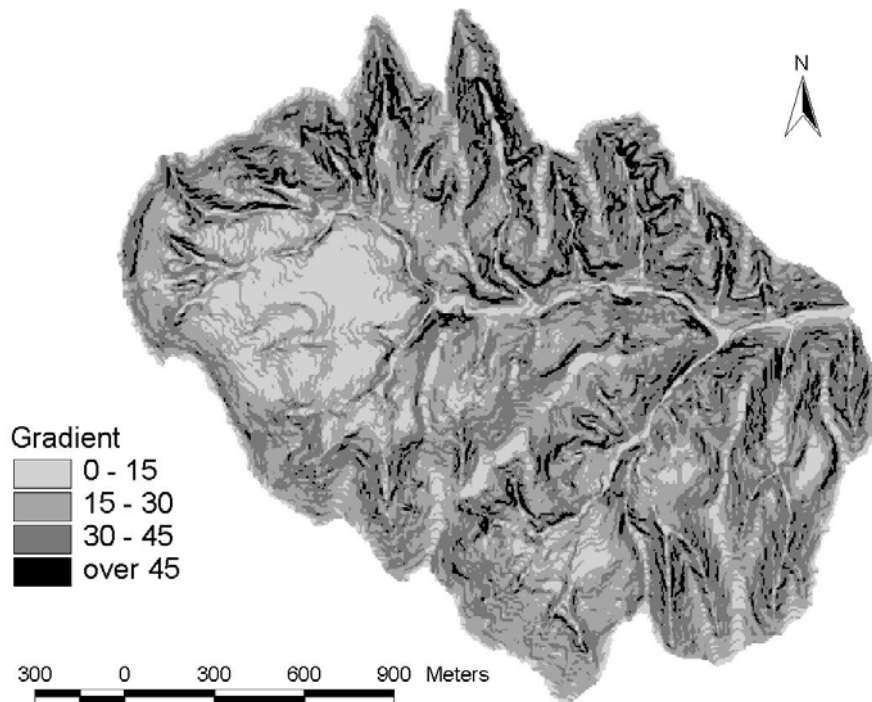


Figure 3.2 Slope map (°) of the Danangou catchment

### 3.3 Geology and soils

Along the main channels in the Danangou catchment an alternation of Cretaceous sandstones and siltstones crops out. The bedrock is not folded, but in the sandstones multiple vertical faults are present. There is generally no displacement along these faults. Most faults trend in a southwest-northeast direction. These faults are likely to continue in the siltstones as well, but are much harder to observe because these rocks generally have a platy structure. The sandstones, on the other hand, form massive banks with a thickness of several metres. The top of these Cretaceous deposits is sometimes very weathered. The weathered bedrock is quite variable in properties from one location to the next; in some

places it is essentially composed of small rock fragments that can usually be crushed by hand, while in other places it has weathered into clays.

The Loess sequence is deposited on top of the bedrock and weathered bedrock. From other parts of the Loess Plateau a late Pliocene red clay layer of lacustrine origin is often reported (Derbyshire et al., 1993; Kukla & An, 1989). In the Danangou catchment, however, a clayey layer between Cretaceous bedrock and Quaternary Loess was only observed in a few places. The appearance of this layer is different from the Lingxia formation as observed near Lanzhou. Since it is by no means certain that the Tertiary lakes were distributed over the whole region of the present Loess Plateau this absence of Tertiary Red clay can easily be explained.

The Loess sequence consists of Wucheng, Lishi and Malan Loess, which are respectively of early, middle and late Pleistocene age. Field observations suggest that the loess deposits can more easily be subdivided into two parts: red loess and yellow loess. This classification is taken to be more or less in line with the distinction in old loess and new loess that has been used by other authors (e.g. Lin & Liang, 1982). Like old loess, red loess consists of Wucheng and Lishi loess, while Yellow loess mainly consists of Malan loess, but could include the upper part of the Lishi loess as well as some loess of Holocene age (table 3.1). Nevertheless, the classification into red loess and yellow loess is strictly speaking not a chronostratigraphic classification, but a lithostratigraphic one. The main reason to use the names Yellow loess and Red loess is that this a distinction that can be observed in the field, while old and new are characteristics that cannot be observed directly. Apart from colour, the properties of red loess and yellow loess differ in several ways:

- The red loess is much harder and also has a higher bulk density
- The red loess contains layers of secondary calcareous concretions that are usually associated with paleosols (Kukla & An, 1989).
- The grainsize distribution of red loess and yellow loess is different.

All these differences should be interpreted as being caused by changes after loess deposition. At deposition the Wucheng, Lishi and Malan loess were probably quite similar. The red loess has, however, undergone alteration due to weathering. This has resulted in a higher percentage of clay-sized particles, higher bulk density, secondary concretions and it also explains the colour difference (which is probably caused by iron). The concretions can reach several decimetres in size, as can be seen from figure 3.3. The red loess can have a thickness of about 150 metres, while the maximum thickness of the yellow loess is only about 10 metres. Figure 3.3 shows a large red loess gully with secondary calcareous concretions derived from the loess in the foreground. Both red loess and yellow loess are closely jointed by mostly vertical joints.

Figure 3.4 shows a lithological map of the catchment. The small areas of red clay mentioned in the map should not be interpreted as Tertiary Red clay. Bulk density and grainsize analysis suggested that they are part of the red loess, and that the main difference was a slightly brighter red colour. Table 4.8, however, shows that there were differences in chemical composition between red loess and red clay, so the origin of the red clay remains unclear.



Figure 3.3 Red loess gully with secondary calcareous concretions derived from the loess in the foreground. The depth of the gully is about 50 m. The relatively flat area in the foreground is formed by deposition behind a dam built by farmers

Loessial soils are predominant in the catchment and cover about 95% of the catchment area. They have large porosity and a large water storage capacity. Messing et al. (in press a) reported the results of nutrient analysis. The soils are highly calcareous, but contain very little organic matter (below 1%) and nutrients like phosphorus (below 0.06%) and nitrogen (below 0.06%). pH is very high, generally above 8.5. According to the FAO classification system the loessial soils of the catchment classify as calcaric regosols and calcaric/chromic cambisols (Messing et al., in press a). Local farmers distinguish four different types of loessial soil based on colour, hardness and structure (Messing et al., in press a). Where the bedrock is close to the surface there is not much soil.

### **3.4 Geomorphology**

The Danangou catchment is located in the hilly part of the Loess Plateau. Geomorphically it is dominated by the presence of many large permanent gullies. These gullies can have vertical headcuts of about 30 metres high, while the total gully depth is much larger than



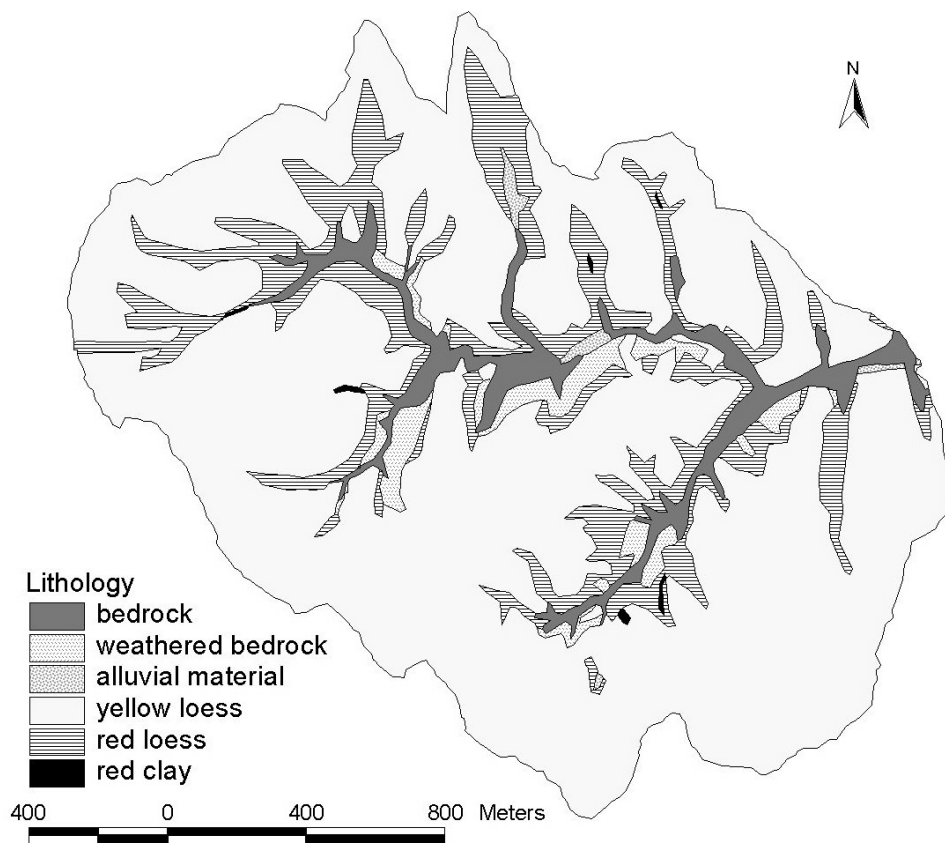


Figure 3.4 Lithological map of the Danangou catchment

that. Figure 3.3 shows one of the largest gullies in the catchment. The loess hills are of the liang (ridge) and mao (rounded hill) types. Yuan landforms do not occur in this part of the Loess Plateau. Figure 3.5 shows a geomorphological map of the catchment. The map shows large areas that are gullied. It also shows the gully edge boundary line, which is the boundary line between the un-gullied hilltops (interfluves) and the gullies below. The edge is often a clear break in slope angle. This line is often used in Chinese literature on the Loess Plateau to distinguish gullied land from the interfluves. However, not all land downslope of the gully boundary line is necessarily gullied (figure 3.5). Table 3.2 shows the area occupied by the areal features of the geomorphological map.

Geomorphology and geology are linked. The gorge cut into the bedrock by the main stream has a total depth of several tens of metres, which indicates that the valleys cannot have formed since the completion of the loess sequence; instead there must have been an interplay between geomorphological development and loess deposition. Comparison of figures 3.4 and 3.1 for example shows that in some parts of the catchment Yellow loess is found well inside the main valley. This cannot always be explained by post-depositional processes such as mass movements. Instead, it seems to indicate that at least the main valleys already existed during deposition of the Malan Loess. Channel materials are also found in the hillslopes along the main stream, often at elevations several tens of metres

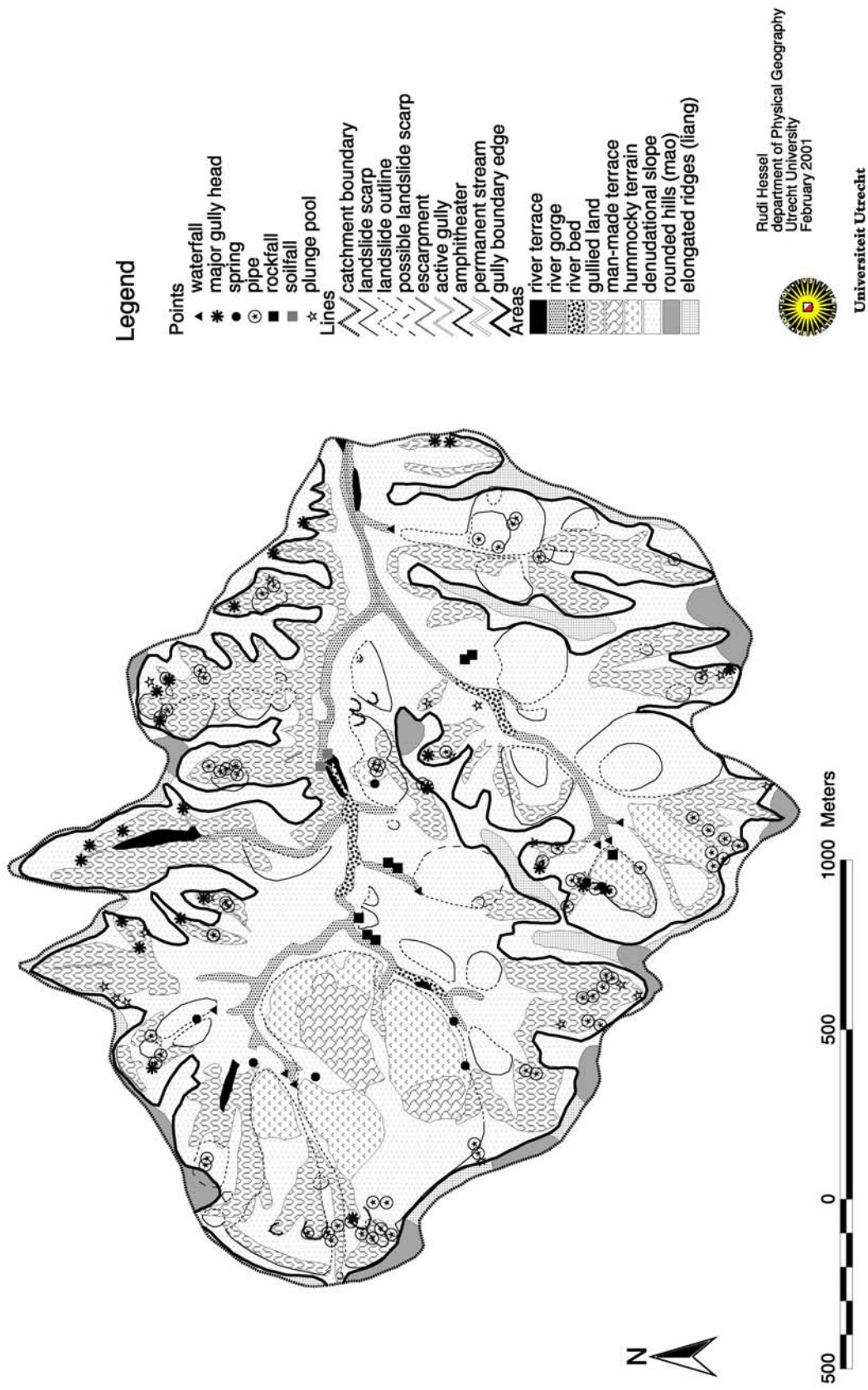


Figure 3.5 Geomorphological map of the Danangou catchment

above the present level of the channel bed. On top of these channel deposits loess has also accumulated.

Table 3.2 Areas occupied by the areal features of the geomorphological map.

	m <sup>2</sup>	%
River terrace	16725	0.5
River gorge	99300	2.8
River bed	22850	0.7
Gullied land	823750	23.6
Man-made terrace	72725	2.1
Hummocky terrain	207500	5.9
Denudational slope	1957950	56.0
Mao (rounded hills)	112700	3.2
Liang (ridge)	182300	5.2
Total	3495800	100



Figure 3.6 Slump in the Danangou catchment. Several gully complexes are also visible

#### 3.4.1 Mass movements

On the steep gully slopes many mass movements have occurred, as indicated in figure 3.5. According to the farmers the most recent large mass movement occurred in 1994. These mass movements are often of considerable size (several hundred metres) and are of

the slump type. The occurrence of these mass movements can probably be related to hydrological conditions at the bedrock-loess boundary. From other parts of the Loess Plateau earthquakes are often mentioned as a cause. In the Danangou catchment there is no evidence of past earthquakes and the farmers also never mentioned them. Figure 3.6 shows a large slump in the Danangou catchment. Some of these mass-movements are likely to have blocked the drainage system for some time, until erosion of the lobes occurred. Such lobes can provide sediment to the runoff during events for many years. Also, mass movement scarps might form starting points of gully erosion because of their steep slope.

### 3.4.2 Gullies

The differences in characteristics of red loess and yellow loess are reflected in different characteristics of gullies developed in red and yellow loess. Red loess gullies are generally much larger. Red loess is more resistant than yellow loess and can therefore support higher vertical headcuts. Besides, the maximum thickness of the yellow loess is only about 10 m. Since red loess is at lower elevation than yellow loess, red loess gullies are also usually more directly connected to the channel network. In fact, red loess gullies can often be seen as steep-sided valleys instead of gullies. Yellow loess gullies on the other hand are often situated high on the hills and do not have a direct connection with the channel network. Figure 3.8 shows a typical example of a yellow loess gully. Many yellow loess gullies have plunge pools below their headcuts. These plungepools can be several metres deep and are generally inaccessible. From field observations it is, however, clear that they have underground drainage. For such large plunge pools to form it is necessary that the soil can also be removed via underground drainage. Exit holes of this underground flow are however hard to find. The development of yellow loess gullies can be envisioned as follows (figure 3.7):

- 1) An initial small (sub)vertical headcut is formed by concentrated overland flow erosion during a runoff event.
- 2) Such an initial headcut can grow in size due to parallel retreat of the headcut by soil fall along vertical cracks and by flow erosion. Since the gully floor usually has a lower slope than the surrounding undisturbed slope this will result in an increase of gully depth.
- 3) With increasing gully size more material from headcut and gully walls falls into the gully in between events due to soil falls along vertical cracks in the loess. This fallen material will be (partly) removed during runoff events.
- 4) The resulting gully shape is an elongated trench with vertical sides and headcut, while the gully bottom is being filled in with material from the gully walls. This accumulation of material can reach magnitudes of several metres.
- 5) Since the runoff has considerable energy, it will start forming a depression below the headcut. This depression is in the essentially loose material that has previously fallen in the gully. If the water finds a pathway through the loose infill (maybe along the original surface) water will flow underground and the gully floor downstream of the headcut will no longer be eroded.

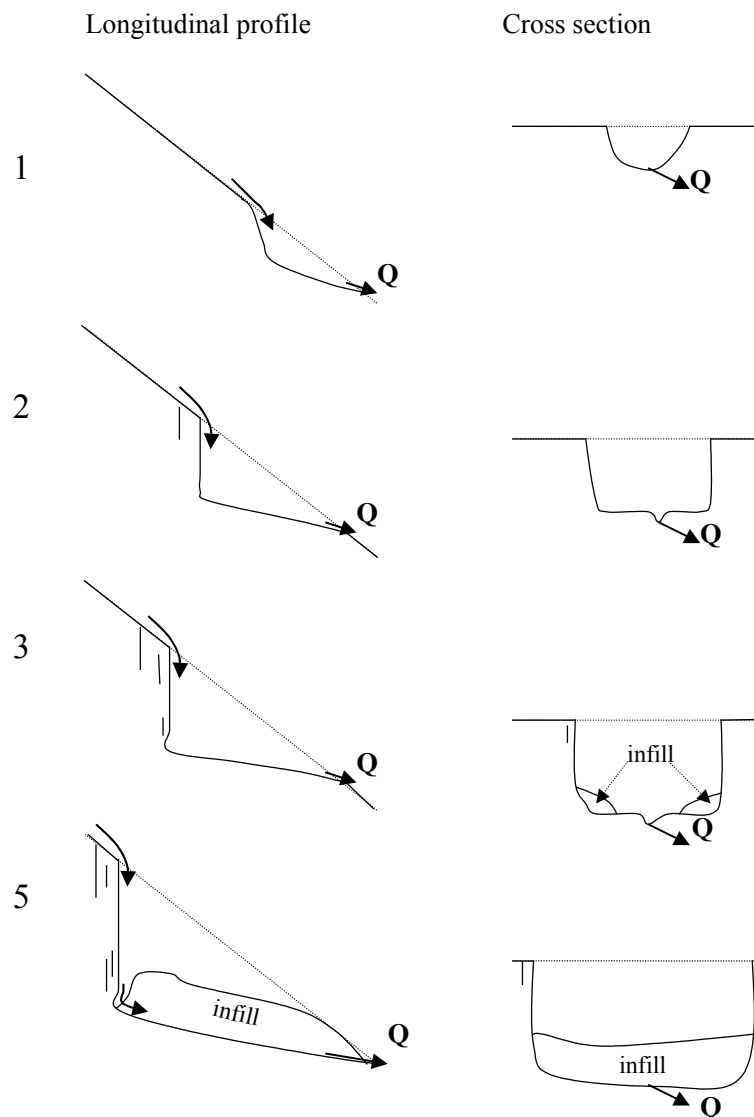


Figure 3.7 Conceptual model of yellow loess gully development

Field observations suggest that most gullies (yellow & red loess) do not perceptibly change shape during single storms. Many of the headcuts and gully sides are only active intermittently and none shows signs of rapid retreat. Most yellow loess headcuts are covered by black algae, so they cannot be very active at present (though algae covered parts can collapse). During small events some material from croplands upstream can be deposited in the vegetation around the fringe of gully. During larger storms part of the infill of the gully might be removed by flowing water. Soil falls on the gully walls and headcut can occur in between event or during the latter part of events, when the soil becomes very wet. The headcuts of both yellow and red loess gullies generally show evidence of dripping water. As soon as there is significant runoff, however, the water will fall freely, without touching or eroding the headcut. Field observations after storms



confirm this hypothesis since it was observed that vegetation about one metre into some gullies got dirty from falling water. Therefore, water erosion can only erode the headcut when discharge is small. If there is only some dripping water there might even be some deposition of sediment, rather than erosion.

Only in a few red loess gullies close to the bedrock boundary is there any evidence of sapping. This is the case at the places called amphitheater in the map (figure 3.5) and at some of the springs. Most gullies are, however, wetter than the surrounding area. There is generally more vegetation in the gullies (especially trees) than outside. The cause of this is probably that water infiltrates easily in the gully-fill, while evaporation is limited due to the more sheltered position of the gully bottoms. This larger wetness is therefore likely to be a result of gully erosion rather than a cause.



Figure 3.8 Soil fall in a yellow loess gully. Backpack (top-middle) for scale

### 3.4.3 Pipes

Figure 3.5 shows the location of a number of pipes. The dots should be interpreted as representing an area with pipes rather than individual pipes. Field observations suggest that almost all pipes occur in places that have previously been disturbed by other processes, e.g.:

- Inside the valley fills in the gullies (as discussed above)
- In association with mass movements, either along fissures that are likely to develop into future head scarps or in between mass movement lobes.

Pipes in apparently undisturbed loess are rare. As discussed in section 3.1 pipes can increase infiltration if the water does not resurface further down the slope. If it just flows underground for some distance, and then resurfaces, the behaviour of the pipe flow is

similar to that of other kinds of concentrated flow. Its reaction to rainfall is rapid, though potentially erratic (Zhu, 1997) and flow from pipes can therefore not be distinguished in the hydrograph obtained at the catchment outlet.

#### 3.4.4 *Rills*

Rills are usually found on steeper parts of the cultivated slopes and also in places where surface runoff concentrates, like on the slopes of topographical depressions. Figure 3.9 shows a rill in a soybean field. Croplands downslope of fallow land seem to be more susceptible to rill erosion than other croplands. The fallow land usually has a more or less stable crust (which seems to become more stable over time). The fallow land is therefore likely to produce significant amounts of surface runoff, without showing much evidence of rilling itself. When this water reaches less crusted, less resistant agricultural land rills develop. Rills can start within a few meters from the drainage divide. The severity of rill erosion will then increase downslope until rills start to combine to form larger rills. The unploughed loess below the tillage layer is more resistant and prevents the formation of very deep rills. In the end, the water will concentrate in the depressions between small mounds on the slope, thus forming a few large rills with typical widths and depths of about 20 cm, which could be called ephemeral gullies. The severity of rill erosion can then decrease in the downslope direction, as the water that has already concentrated into the large rills is no longer available to form new rills in the inter-rill area. The situation is complicated by the presence of small escarpments between adjacent fields. These escarpments are probably the result of ploughing, are mostly about 1 – 1.5 meters high and they seem to increase rill erosion on the field downstream. Rill erosion rates can be high since croplands have low cohesion and occur on steep slopes. Also, crop cover is generally low.

#### 3.4.5 *Channels*

The main channels have incised into the bedrock. The lowest elevation in the catchment is at about 1075 m, while the top of the bedrock is approximately at 1200 m. The actual channel is often located in a gorge cut into the sandstone. Bedrock surfaces in some parts of the channel, but in other parts there is an infill with bed material with a thickness of up to 2 metres.

Based on the foregoing data and field observations one can arrive at the following model of erosion in the Danangou catchment:

The large gullies are at present fairly stable. Occasional large landslides on the gully walls can provide large amounts of essentially loose material to the valley floor. These events occur infrequently, but can provide large amounts of sediment during runoff events for years to come. Soil falls on the gully walls occur more frequently and also provide loose sediment to the valley floor. It usually builds up in the channel itself and can thus be removed as soon as there is any runoff. The croplands can also provide large amounts of sediment during events through rill erosion.



Figure 3.9 Rill in soybean field, September 1998

### 3.5 Climate and hydrology

The climate in the area is semi-arid and continental, with occasional heavy thunderstorms in summer. At Ansai town, 5 km from the Danangou catchment, total average yearly rainfall was 513 mm over the period 1971-1998 (data from Ansai County Meteorological Station). Most of the rain (72%) fell in the period June-September, and all heavy storms occur in that period. Only during these large storms will runoff occur in the catchment. On average, three to four storms each year are large enough to cause runoff, but the actual number varies widely from year to year. Figure 3.10 shows the average monthly rainfall amount at Ansai. It shows the concentration of rain between June and September and also shows high standard deviations, which indicates large inter-annual variability. The large inter-annual variability is partly caused by the influence of the front of the summer monsoon, which does not advance equally far inland in all years. Figure 3.11 shows the daily rainfall amounts at Yan'an for different return periods. The climate at Yan'an is comparable to that at Danangou, which is only 40 km away. Elevation and topographical location are also similar. Data were provided by Beijing Normal University and cover the period 1971-1995. The partial duration series technique (Ven Te Chow et al., 1988, p 383) was used to get information on return intervals for all days with rain of more than 13



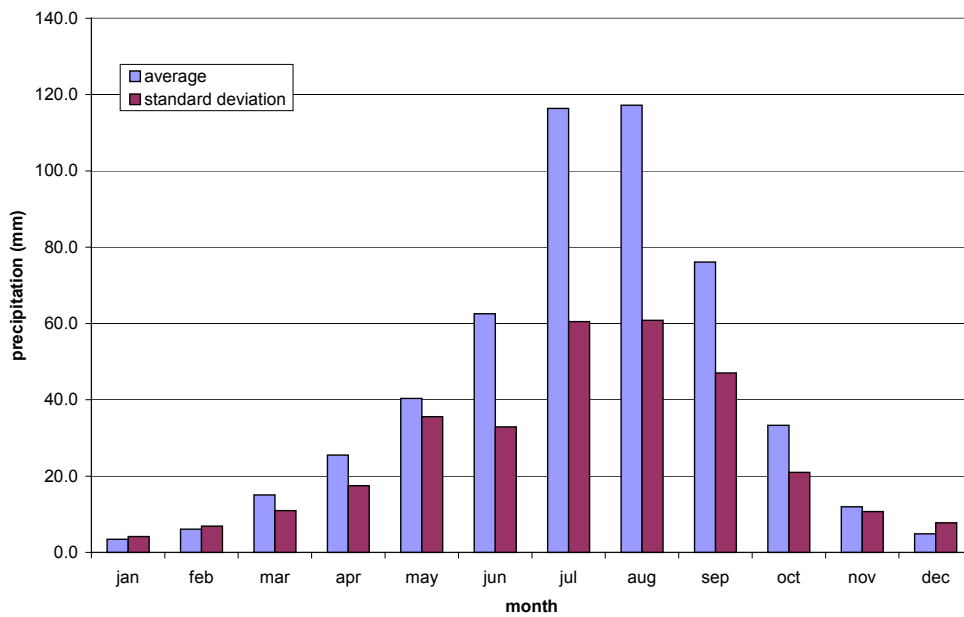


Figure 3.10 Monthly rainfall at Ansai over the period 1971-1998. Data from Ansai County Meteorological Station

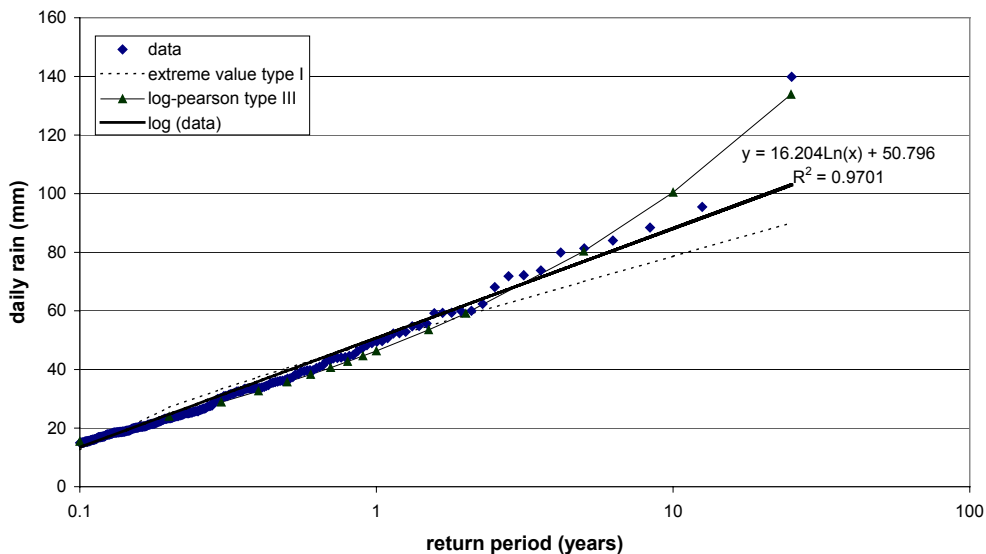


Figure 3.11 Daily rainfall amount as a function of return period, Yan'an. Based on data provided by Beijing Normal University. A partial series technique has been used on all daily rainfall amounts over 13 mm

mm, instead of only on the maximum daily rain of each year. Figure 3.11 shows different types of distributions that have been fitted to the data. From the chart it is apparent that the lognormal distribution gives the best results. It gives a good fit to the data, except for the largest daily rainfall amount. This is normal; since the length of the data series does not allow for calculated return intervals of more than 25 years, while in reality an event

with larger return interval might well occur in such a period. From the chart the return period of a daily rainfall of certain magnitude can be read. For example, a daily rainfall amount of 50 mm will occur once every year. No data on storm rainfall are available, so that daily rainfall amounts have to be used. This limits the usefulness of the chart considerably, since storms that have equal amounts of rain might have very different intensities and thus very different return periods.

Winters are dry (figure 3.10) and cold because of the influence of the Siberian high-pressure system that causes the winter monsoon (Huang et al., 2000). Data from the Ansai County Meteorological Station show that over the period 1971-1998 the average temperature in January was  $-6.8$  degrees centigrade. Over the same period the average temperature in the warmest month (July) was  $22.4$  degrees, and yearly average temperature was  $8.9$  degrees.

The loess soils of the Danangou catchment are in principle permeable. Infiltration rates will however be significantly reduced by sealing and crusting of the soil surface. The loess soils also have high porosity and have a good water holding capacity (Messing et al., in press a). This means that if water infiltrates it is likely that most remains in the upper part of the soil, so that it can later be used by plants. Deep drainage of water into the loess probably only occurs along fissures in the loess (these are common) and by sporadically occurring soil pipes. The existence of a small groundwater reservoir is indicated by a very small, but continuous, leakage of water along the bedrock planes and along the bedrock-loess boundary. In some places there is dripping water, while in others there are wet zones that show deposition of salt crystals from the evaporating water. The farmers have built several cisterns that collect the dripping or seeping water. During very wet years water pressure might build up sufficiently to induce large mass movements, probably aided by progressive weathering of material along the bedrock-loess boundary. In most places the water table is at great depth (several tens of metres at least).

During rainfall events only overland flow (and pipe flow) will reach the outlet. Infiltrated water will probably not reach the outlet at all, as indicated above, and given the fact that potential yearly evapotranspiration is several times higher than yearly precipitation.

## **2.6 Land use**

Agricultural land is cultivated in a labour intensive way. The reasons for this are both economical and environmental. The farmers generally lack funds and cannot afford any mechanical equipment. Fertiliser is applied on a limited scale, but essentially all farm work has to be done by human or animal power. Besides, the steep slopes make mechanisation almost impossible. For ploughing donkeys or oxen are used, weeding and harvesting are done manually. Figure 3.12 shows ploughing with an ox on a steep slope, while figure 3.13 shows grinding of corn by a mule.

Croplands are mainly located on the flatter areas along the hilltops and also on the flatter areas lower down. Some families also have alluvial land along the Yan river. The

Danangou stream drains into the Yan river. The alluvial land is not located inside the Danangou catchment itself. The alluvial land is the best land, because it is level and can be irrigated with water from the Yan river. In the catchment itself the farmers prefer the plots closest to their home, so that croplands on top of the ridges are more likely to be left fallow. Still, plots on slopes of up to about 60% are used as arable land. Plots are of small size. The main crops in the catchment are pearl millet, foxtail millet, soy bean, potato, buckwheat and maize. Several other crops are also present: black beans, green beans, hemp, sorghum, and sunflower. At present about 40% of the catchment is used for growing crops. This area is likely to decrease in the future as the Chinese government has formulated new policies about the Loess Plateau that aim at reducing the maximum permissible slope angle for cropland to 15 degrees.

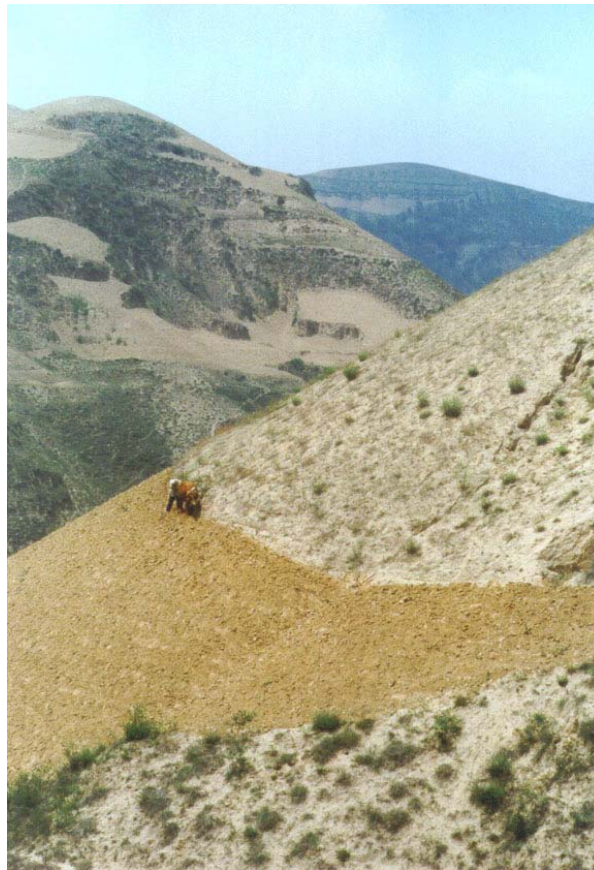


Figure 3.12 Ploughing with an ox on a steep slope

About 40% of the catchment is wasteland. Until recently it was used for grazing goats, but this practice has virtually ceased after it was prohibited by the Chinese government as part of a new Loess Plateau policy that aims at erosion reduction. The wastelands are generally rather poorly vegetated grasslands with small shrubs and they are located on the steepest slopes in the catchment. These are the slopes of the main gullies, which can be as steep as 70 degrees.

The remaining 20% of the catchment is occupied by woodland, orchard, fallow land, vegetable gardens and houses. Some of the upper gullied valleys have been revegetated with woodland in an attempt to limit erosion. The most common trees are willows and locusts. Orchards are located at low elevation. Apple is most common, but pear, apricot, peach and Chinese date are also present. The new Loess Plateau policy aims at increasing woodland and orchard areas. Vegetables are usually irrigated either by hand (buckets) or using small channels that start at the springs in the catchment.



Figure 3.13 Farmers grinding maize with a millstone. A mule is used to rotate the upper millstone. The mule is blindfolded to prevent it from becoming dizzy

Figure 3.14 shows a land use map made in 1999, while table 3.3 shows the areas occupied by the different land use types from 1998 to 2000. In 1998 the land use mapping was conducted by RCEES (Research Centre for Eco-Environmental Sciences, Beijing, China), in 1999 and 2000 by UU (Utrecht University, The Netherlands). Mapping by different persons explains some of the differences between 1998 and 1999 & 2000, e.g. concerning orchard and forests. Table 3.3 shows a clear decrease in cropland area accompanied by a similar increase in fallow area. This change is probably caused by a combination of weather conditions and government policy. During dry years less land is cultivated than during wet years, while the crop types are also different. In 1998 the different crop types were not distinguished during mapping, but the 1999 and 2000 mapping revealed that the 10% decrease in cropland area between those years was largely due to a decrease of soy bean (6%), foxtail millet (1.6%) and maize (1.2%). Farmers confirmed that they did not sow soy bean in 2000 because they expected a dry year. Other



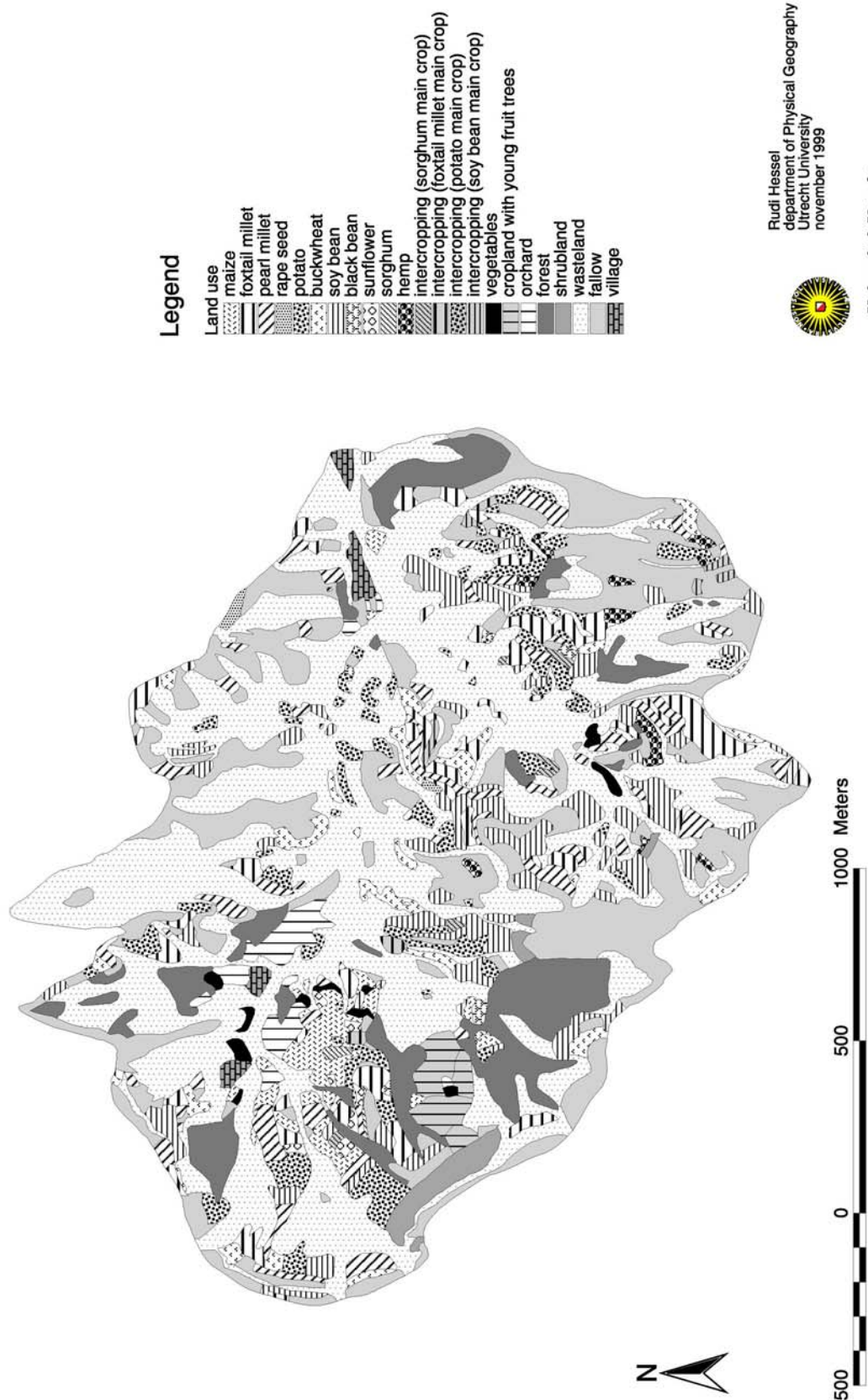


Figure 3.14 Land use map of the Danangou catchment, 1999

crops, like potato, buckwheat and pearl millet were not reduced in area. Buckwheat and pearl millet are sowed late (June), at that time some rain had fallen in 2000. Another cause can be the new government policy, since this policy was presented to the farmers in late 1999 or early 2000. As shown above, this policy is intended to result in a lasting decrease in cropland area, accompanied by increases in forest and orchard areas.

Table 3.3 Land use (%) in the Danangou catchment, 1998-2000

Land use	1998	1999	2000
Cropland	35.8	25.5	15.8
Cropland with small fruit trees	1.1	1.2	1.5
Vegetables	0.1	0.5	0.7
Fallow	7.3	19.9	27.7
Orchard	2.4	1.4	1.4
Shrubland	1.2	1.0	1.1
Forest	11.7	7.9	8.1
Young locust trees	0.0	0.0	0.4
Wasteland	40.5	41.9	42.7
Village	*	0.6	0.6
Total	100	100	100

\* Not mapped separately in 1998

### 3.7 Event Erosion

Erosion almost exclusively occurs during heavy storms in summer. Wind erosion seems to be negligible in this part of the Loess Plateau. Summer storms can have rainfall intensities of 1-3 mm/minute (Zhaohui Wan & Zhaoyin Wang, 1994) during short intervals. Though loess is in principle a permeable material these intensities are high enough to cause flash floods. Nevertheless, even during large storms at least 80% of all rainfall infiltrates (table 4.10). Soil surface sealing and crusting are also likely to play an important role. During these events runoff rates from the catchment may sometimes reach over 15 m<sup>3</sup>/s. Sediment concentrations in the runoff are often several hundred grams per litre, so that huge amounts of sediment are removed during large events. As an example of what happens during a storm a description of an event that occurred on July 20<sup>th</sup>, 1999 is useful.

July 20<sup>th</sup>, 1999 started cloudless and hot. Clouds started coming in from about 12:00. Rainfall of the 990720 event started at about 13:30. It was accompanied by violent wind and by lightning. The rain came from the southeast and consequently produced much more rainfall in the southeastern part of the catchment than elsewhere. At the eastern boundary of the catchment 23.8 mm of rain fell in 20 minutes. The storm was also accompanied by a temperature drop of about 10 degrees centigrade. Within seconds of the onset of heavy rain, water started to flow on the roads and paths. Channel flow started at about 13:46 and increased very rapidly to 3.7 m<sup>3</sup>/s within 10 minutes. Water gushed

from all tributaries and from the fields along the channel. The road turned into a river, with water depths of close to 50 cm in places. Figure 3.15 shows the weir that was used to measure discharge (section 4.4) shortly before peak discharge. Since the rainfall was concentrated in the eastern part of the catchment and the measurement location (figure 4.1) is situated in the middle the worst part of the event could not be measured.



Figure 3.15 Runoff in the Danangou catchment during an event that occurred on July 20<sup>th</sup>, 1999. Picture taken just before peak runoff

Observations as well as later computer simulations indicate that the maximum runoff from the entire 3.5 km<sup>2</sup> catchment was about 10 m<sup>3</sup>/s. Average dirty water sediment concentrations at the measurement location were about 200 g/l, while maximum measured concentrations were almost 400 g/l. Observation of the stream bed after the event indicated that boulders with diameters of several tens of centimetres had also been transported. The Yan river was not in flood at the time of the event and a 'delta' mainly consisting of boulders extended several metres into the main river after the event. This shows that bedload transport was also large. The whole event ended at approximately 14:40. LISEM-simulations indicated that about 3340 tonnes of sediment left the catchment in about an hour.

Figure 3.16 shows evidence of water flow in a woodland after an event that occurred on August 29<sup>th</sup>, 2000. As can be seen from the picture flow width could be easily estimated after the event. The picture also shows that there was not much erosion or deposition in the woodland. The flow merely flattened the herbs and draped them with a thin sediment layer. All events that occurred will be further discussed in chapter 4.





Figure 3.16 Evidence of flowing water in a woodland after the event of August 29<sup>th</sup>, 2000. Flow width can be estimated easily and the picture also shows that there has not been much erosion or deposition

### 3.8 Conclusions

From literature data (chapters 1 and 2) it was concluded that three characteristics of the Loess Plateau are likely to require attention in erosion modelling. These characteristics were found to apply to the Danangou catchment too:

1. Slope angles are very high. Croplands occur on slopes of up to about 60 %, wastelands on slopes of up to 250 % and the steepest parts of the gully walls are even steeper.
2. Sediment concentrations are high. High sediment concentrations could have pronounced effects on both water flow and transport capacity.
3. There are many very large permanent gullies. In such gullies erosion processes will be different from erosion processes operating on 'normal slopes'

The Danangou catchment is therefore representative for the hilly part of the Loess Plateau. Since these conditions differ from conditions elsewhere in the world it is necessary to adapt the present soil erosion models so that they can cope with these particular circumstances.



## 4 FIELD METHODS AND DATA

Several types of data were collected. Obviously, it was necessary to collect the LISEM input data. These data included field measurements of plant and soil characteristics, rainfall and some soil physical data measured on samples taken in the field. Some additional soil physical and chemical data were collected to explore the differences between red loess and yellow loess. Furthermore, discharge data were needed to calibrate LISEM and to evaluate its performance. Finally, erosion data were also needed to calibrate LISEM and to evaluate its performance, both for the catchment outlet and spatially. This chapter discusses how these data were measured, and what the results of these measurements were.

### 4.1 LISEM field measurements

#### 4.1.1 *Methods*

To be able to model soil erosion with the LISEM model several plant and soil data are needed. Table 2.1 shows which plant and soil characteristics are needed as input for the LISEM model. For practical reasons these characteristics were measured on a number of fields that were assumed representative for the different land uses of the Danangou catchment. Both in 1998 and in 1999, 17 fields were selected to do the field measurements on. The distribution of fields was, however, different in 1998 and 1999. Table 4.1 gives an overview of the land use on the selected fields in 1998 and 1999. As can be seen from table 4.1 cropland was measured much more extensively than other land uses. In 1999 more care was taken to select croplands with different types of crop. Figure 4.1 shows the location of the fields that were used in 1999 to measure the LISEM input.

In 1999, a field was selected for each major crop. To get a representative input for the LISEM model care has been taken to select fields in different geographical positions (as far as the limited amount of fields allowed this). In principle, the measurements described in this section were repeated every two weeks. In 1998 all measurements were done every two weeks. The results showed that some parameters did not change much over time. Some parameters were therefore measured less frequently in 1999. In 2000 the measurements could not be continued.

Appendix 4.1 gives the number of measurements that were performed for each parameter during each visit to the selected fields. As can be seen from the appendix, the choice for a relatively high temporal resolution and a relatively large number of fields limited, for some parameters, the number of measurements that could be performed on each field during each visit.

Table 4.1 Selected fields of 1998 and 1999

	1998		1999	
	Land use	Crop	Land use	Crop
1	cropland	millet & soybean	cropland	foxtail millet
2	fallow		wasteland	
3	wasteland		wasteland	
4	cropland	soybean (& maize)	orchard	
5	orchard		woodland	
6	woodland		cropland	pearl millet (& soybean)
7	cropland	soybean (& rape seed)	cropland	foxtail millet
8	cropland	soybean	fallow	
9	fallow		orchard	
10	wasteland		woodland	
11	shrubland		cropland	maize & soybean
12	-		cropland	potato
13	cropland	maize, sunflower & soybean	cropland	soybean
14	woodland		cropland	foxtail millet & soybean
15	cropland		fallow	
16	cropland	maize & soybean	shrubland	
17	orchard		cropland	buckwheat
18	cropland	maize & soybean	-	

#### *Plant Height*

LISEM uses plant height for leaf drip calculation. The higher a crop is, the more energy dripping water will have and the more splash erosion the leaf drip can cause. Plant height was measured with tape. In the case of trees, triangulation was used.

#### *Plant cover*

LISEM uses plant coverage for the calculation of interception. It was estimated by looking straight down when plant height allowed this.

#### *Leaf Area Index*

Leaf area index (LAI) is used by LISEM to calculate water storage on the leaves. It is expressed as area of leaves per area of ground, and therefore has no dimension. It can range from 0 to about 6. There are several methods to calculate LAI. The one used here distinguished between plants and trees, but did not distinguish between different plant or tree species. The procedure followed was meant to calculate the total area of leaves on a certain area from the use of 20 representative leaves. If different species occurred, care was taken to produce a weighted estimate of average leaf area. Total area of the 20 representative leaves was determined using a scanner. The average leaf area was then multiplied by the total number of leaves (which was estimated) to give the total leaf area for a certain area. If the plant cover was below 0.1 LAI was not determined, but was assumed to be equal to plant cover.

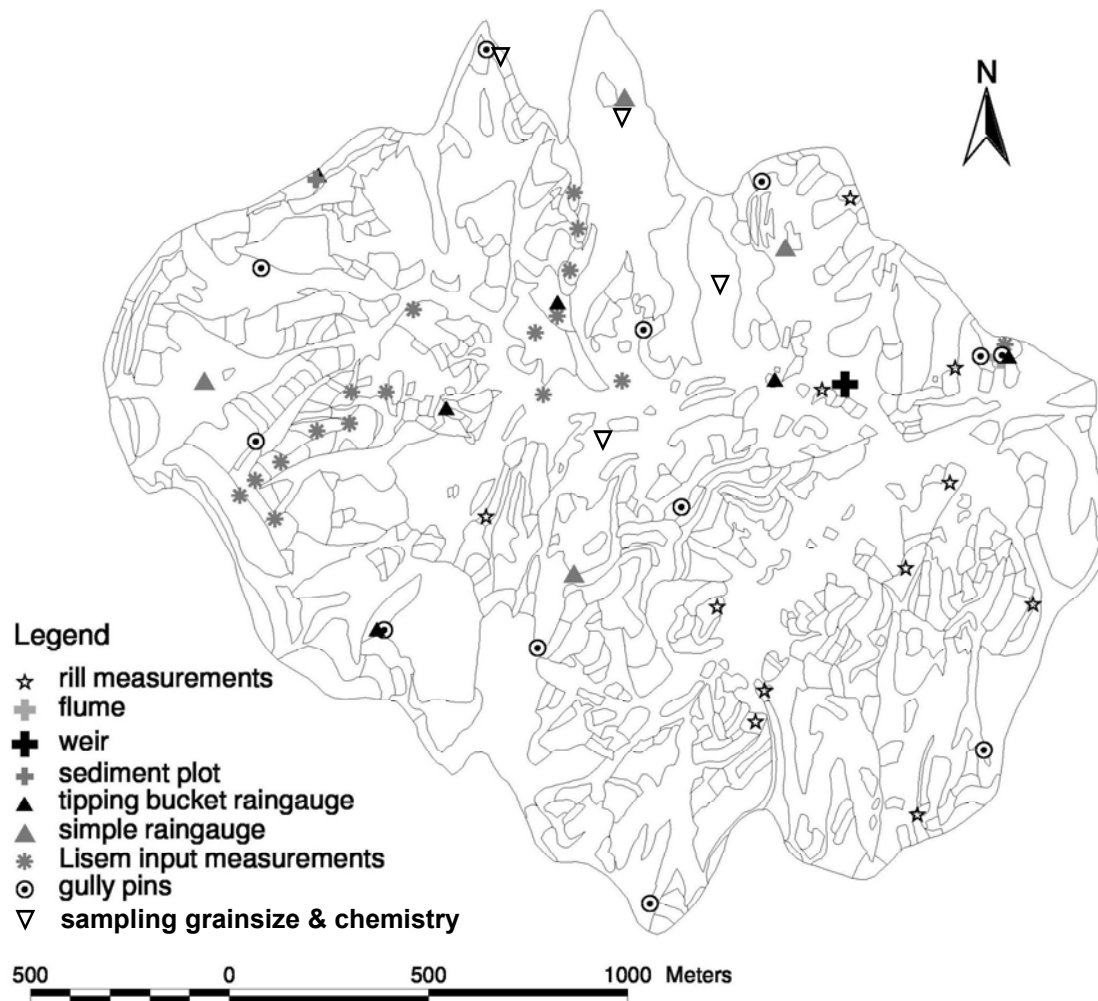


Figure 4.1 Measurement locations in 1999. The 1999 land use map (figure 3.14) is used as background.

#### *Random Roughness*

LISEM uses random roughness to calculate water storage on the soil surface and the start of overland flow. As the name suggests random roughness is considered to be random. It should therefore not be used for rills or land management operations. For the measurement a pin meter (e.g. Wagner & Yiming Yu, 1991) was used. Because all pins have equal length, the soil surface profile is reproduced by the tops of the pins. Digital pictures were taken and pin positions were calculated with the PMPPROJ software (developed by J. Kilpelainen, Agricultural Research Centre, Jokioinen, Finland). Random roughness is defined as the standard deviation of pin positions. 294 pins were used for each field.

### Aggregate stability

Aggregate stability is used to calculate the amount of splash erosion. The test that was used here (the drip test of Low, 1954) aims at simulating the impact of falling rain on an aggregate. To be able to compare the results from different tests, the moisture content of the aggregates was standardised before measurement. The median number of drops needed to destroy the aggregates was used. In the tests at least 20 aggregates were measured for each plot.

### Cohesion

LISEM uses cohesion to calculate erosion caused by overland flow. The cohesion at saturation is therefore critical and care must be taken to measure very wet soils. Cohesion was measured with a Torvane. As part of the aim of the project was to model gully erosion, cohesion of the second soil layer was also measured. A small 20 cm deep pit with was dug with a small shovel to perform these measurements.

### Moisture content

The initial moisture content at the start of a LISEM simulation must be specified. As initial moisture content is very important in determining soil conductivity this is vital information for LISEM. Especially the moisture content of the upper soil layers is important in this respect. For the LISEM simulation the initial water content must be specified for each soil layer. Moisture content was measured in auger holes with a portable TDR at depths of 5, 15, 25, 45 and 75 cm.

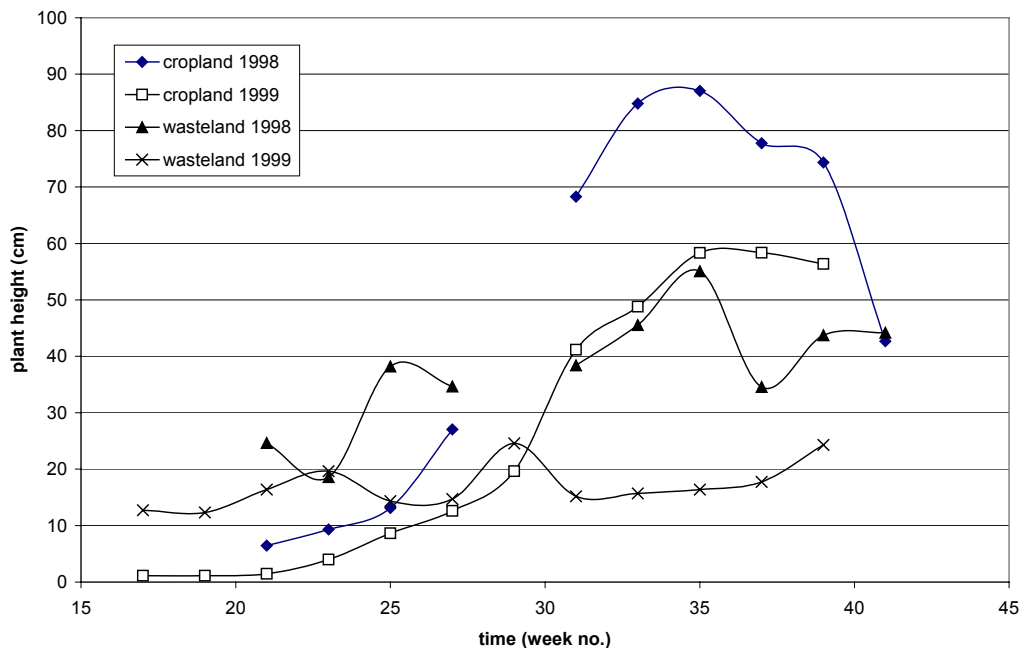


Figure 4.2 Plant height in 1998 (May – October) and 1999 (April – September). The mean standard deviation of field averages (method 3 of appendix 4.1) was 69% of the average for cropland and 60% for wasteland

Apart from the periodical measurements discussed above LISEM needs Manning's n for fields and channels, cohesion for channels, channel width, crust fraction and stone cover. Only the crust fraction was determined every 2 weeks. The Manning's n measurements will be discussed in chapter 6. Channel cohesion, channel width and stone cover were estimated or measured in the field once. No grass strips or roads were present in the area, so their width was zero.

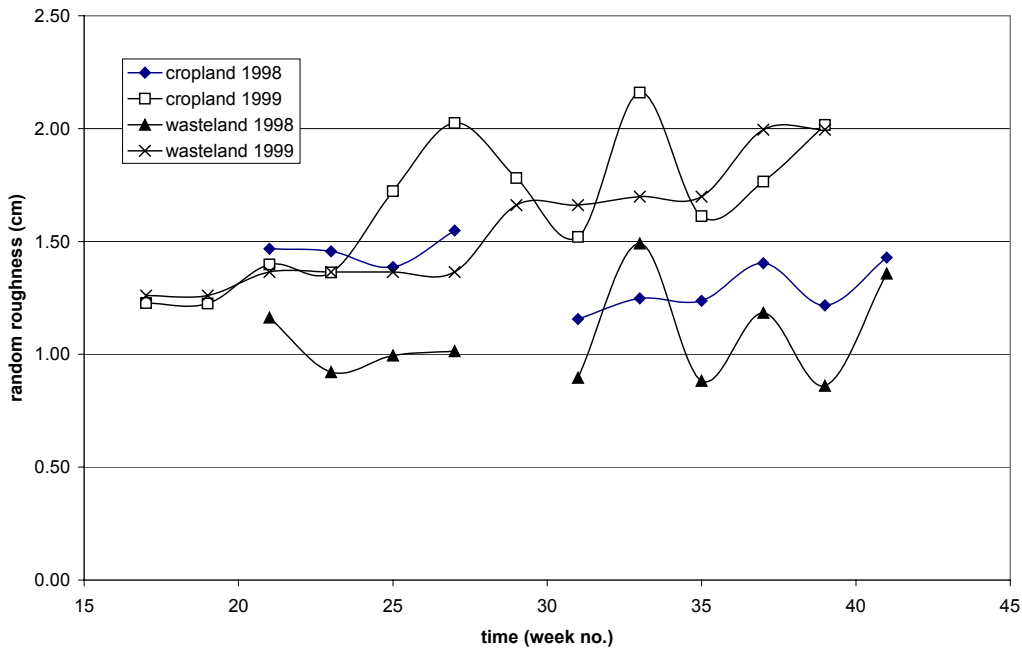


Figure 4.3 Random Roughness in 1998 (May – October) and 1999 (April – September). The mean standard deviation of field averages (method 3 of appendix 4.1) was 22% of the average for cropland and 46% for wasteland

#### 4.1.2 Results

Figure 4.2 shows an example of the results of the bi-weekly measurements. It shows the plant height in 1998 and 1999 for two land uses. The chart clearly shows the effect of the growing season. In 1998 cropland also showed a clear decrease in plant height in October (week 41) due to harvesting. In 1999 the measurements stopped before harvesting. Wasteland exhibited a much less pronounced change over time than cropland. Figure 4.2 also shows that in 1998 plant height was larger than in 1999. Part of the reason is that 1998 was a wetter year than 1999, but the 1998 field selection also contained more croplands with tall crops such as maize. Note that the differences between the different fields were large, which is reflected in large standard deviations. The other plant characteristics (cover and leaf area index) gave similar results. Figure 4.3 shows random roughness results for 1998 and 1999. Random roughness did not show a clear trend during the year, only some variation that can probably be ascribed to the measurement itself. Apparently, random roughness was somewhat higher in 1999 than in 1998, although this difference is not statistically significant due to large standard deviations.

Generally speaking, the plant variables showed a temporal trend, while the soil surface characteristics did not. From the soil characteristics only the cropland cohesion measurements of 1999 showed a trend. From April to June 1999 cohesion decreased because more and more of the measurement fields were ploughed during this period. After that, cohesion increased again due to compaction of the plough layer as well as the formation of a soil crust. One would expect other soil surface characteristics to show a temporal trend as well, e.g. random roughness might be expected to show a decrease over time for croplands since crust formation can be expected to smooth the surface, but the data did not show this trend (figure 4.3).

From the gathered input data LISEM input data sets were produced on a bi-weekly basis, which means that when a storm occurred there were always data available that were collected within two weeks before the storm.

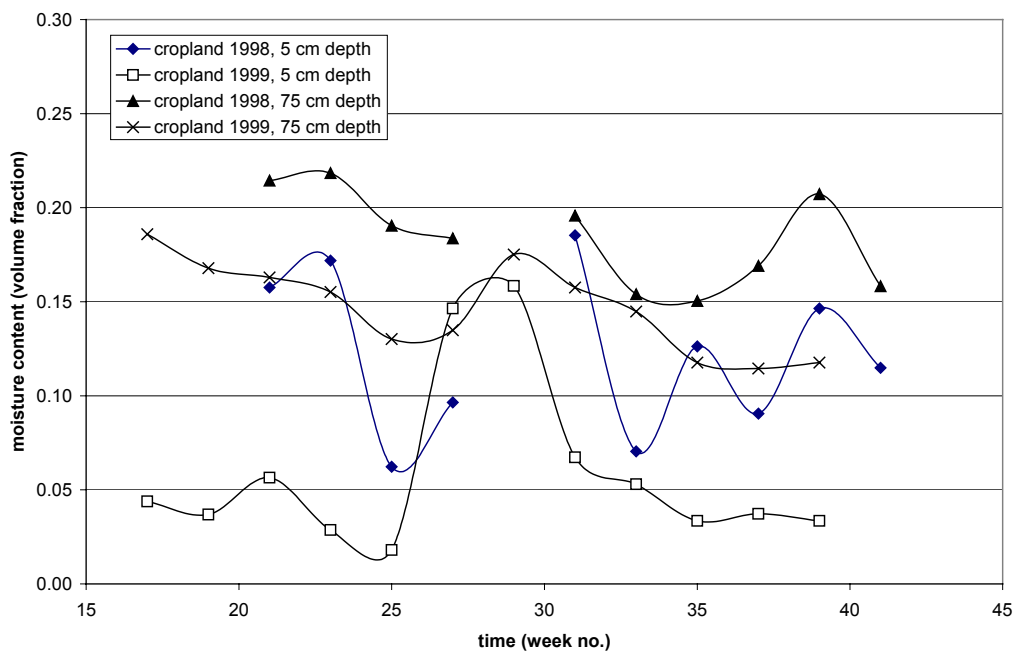


Figure 4.4 Soil moisture content in 1998 (May – October) and 1999 (April – September). The mean standard deviation of field averages (method 3 of appendix 4.1) was 30% of the average at 5 cm depth and 27% at 75 cm depth

The moisture content measurements showed a clear reaction to rainfall. Figure 4.4 shows the variation in moisture content for croplands. It shows several interesting features:

- The variation in moisture content at the surface (5 cm depth) was much larger than at 75 cm depth. This was to be expected. Nevertheless, the moisture content at 75 cm depth still showed the rainfall influence, albeit damped and maybe shifted in time. The measured variation in moisture content at the surface was more than 0.1 in both 1998 and 1999.
- The measurements at 75 cm depth showed a decrease of water content over time, both in 1998 and in 1999. The reason was probably water extraction by growing plants.

- The average moisture content increased with depth.
- Moisture contents in 1998 were clearly higher than in 1999, which was caused by the much larger amount of rain in 1998 (table 4.3). Surface moisture contents in 1999 were very low.

This study focused on the simulation of surface runoff, so that the moisture content variations in the uppermost part of the soil were much more important than those lower down.

Table 4.2 summarises the plant and soil data. To make comparison between 1998 and 1999 possible the average values of the different parameters were calculated for the period that was covered by the measurements in both years, namely week 21 to week 39 (May – September) of each year. Table 4.2 confirms the data presented in figures 4.2 to 4.4 and gives additional information regarding differences between land uses. For land use with trees (orchard and woodland) the plant characteristics are probably more influenced by the difference in position of measurement field than by differences between the years.

Table 4.2 Yearly averages (week 21 to 39) of plant and soil characteristics in 1998 and 1999

	Crop		Fallow		Orchard		Wasteland		Woodland	
	98	99	98	99	98	99	98	99	98	99
Plant height (cm)	50	31	33	14	344	310	37	18	739	1362
Plant cover (-)	0.21	0.12	0.14	0.12	0.29	0.27	0.44	0.25	0.78	0.44
Leaf area index (-)	1.07	0.59	0.57	0.20	2.80	1.32	1.04	0.39	5.00	1.71
Aggregate stability (-)	10.6	6.4	7.3	5.6	10.4	8.5	12.5	12.8	13.5	9.1
Dry cohesion (kg/cm <sup>2</sup> )	0.08	0.05	0.13	0.08	0.12	0.09	0.24	0.12	0.14	0.18
Wet cohesion (kg/cm <sup>2</sup> )	0.08	0.06	0.11	0.09	0.11	0.08	0.19	0.14	0.13	0.17
Cohesion at 20 cm (kg/cm <sup>2</sup> )	0.10	0.09	0.11	0.09	0.13	0.09	0.17	0.21	0.12	0.16
Random roughness (cm)	1.35	1.74	1.09	1.10	1.32	1.45	1.05	1.62	0.74	0.97
Moisture content at 5 cm (-)	0.12	0.06	0.09	0.05	0.15	0.06	0.13	0.06	0.15	0.07
Moisture content at 15 cm (-)	0.15	0.09	0.12	0.08	0.15	0.08	0.13	0.09	0.13	0.08
Moisture content at 25 cm (-)	0.16	0.11	0.13	0.10	0.16	0.09	0.13	0.09	0.14	0.09
Moisture content at 45 cm (-)	0.17	0.13	0.16	0.11	0.15	0.09	0.13	0.10	0.14	0.09
Moisture content at 75 cm (-)	0.19	0.14	0.17	0.13	0.17	0.09	0.14	0.11	0.15	0.10

## 4.2 Rainfall

Rainfall was measured with six calibrated tipping bucket rain gauges. The gauges had 0.2 mm accuracy. The bucket tips after every 0.2 mm of rain and the time of the tipping was recorded. These data could thus be used to calculate rainfall intensities. An additional six simple rain gauges were installed in 1999. These consist of bottle and funnel and could therefore only give rainfall totals. The position of both kinds of rain gauge is for 1999 given in figure 4.1.

Table 4.3 Monthly rainfall (mm), May to September. The values for Danangou are average values from 6 tipping bucket rain gauges

	Danangou			Ansai County 1971-1998	
	1998	1999	2000	mean	stdev
May	144.7 <sup>a</sup>	30.4	3.7	40.4	35.6
June	38.6	9.7	79.0	62.5	32.9
July	154.7	110.4	47.2	116.4	60.5
August	87.6	15.8	104.7	117.2	60.8
September	55.0	35.3	10.1 <sup>b</sup>	76.1	47.1
May-September	480.6	201.6	244.7	412.6	96.0

a from May 5<sup>th</sup>

b until September 21<sup>st</sup>

Table 4.4 Summary of events used in this study. Maximum intensities (max I) are given in mm/h for 1-minute intervals

a) 1998

	980705	980712	980715	980801	980823
Time start rain	12:15	2:26	14:12	13:43	20:41
Time end rain	14:39	3:41	15:19	14:31	21:56
Total event rain (mm)	20.8	22.3	28.7	15.1	13.0
Max I (catchment average)	41.3	59.4	66.2	69.9	47.2
Max I (single rain gauge)	60.3	71.6	108.5	107.5	70.9
Time max I	12:57	2:53	14:20	14:05	20:48
Gauge max I	A	C	B	C	D

b) 1999 and 2000

	990710	990720	990721	000807	000811	000829
Time start rain	14:50	13:30	2:42	10:01	18:28	21:37
Time end rain	15:15	14:30	3:00	16:09	19:35	22:06
Total event rain (mm)	10.7	15.8	3.5	18.7	11.6	16.8
Max I (catchment average)	67.7	55.6	35.8	18.2	49.5	84.9
Max I (single rain gauge)	107.5	130.0	72.4	24.1	83.6	189.1
Time max I	15:10	13:34	2:47	multiple	18:35	21:49
Gauge max I	E	D	B	multiple	E	D



### Results

Monthly rainfall during the summer period is given in table 4.3. Comparison with the data of the Ansaï County Meteorological Station (also in table 4.3) shows that 1998 had above average rainfall during the summer period, while 1999 and 2000 both had rainfall amounts that were far below average. Figure 4.5 shows the average daily rainfall from April to September 2000. During this period the total amount of rain was only about 250 mm, while the long-term average over this period is 438 mm.

From the event rainfall data 1-minute rainfall intensities were calculated for use in LISEM. Summary data of the events used in this study are shown in table 4.4. The storms in table 4.4 include all the storms that are known to have produced runoff. Besides, a few storms that might have produced runoff as well as a few storms that did not produce runoff have been included. Total daily rainfall was generally a few mm higher than event rainfall. Comparison with figure 3.11 suggests that all events had recurrence intervals of less than one year. This certainly shows that much larger storms are possible. On the other hand, it can be expected that recurrence interval not only depends on rainfall total, but also on rainfall intensity. Table 4.4, for example, shows that the event of August 29<sup>th</sup>, 2000 had much higher intensities than the other events, while its total rainfall amount is not much higher. This storm was thus of very high intensity but short duration. Such a storm is likely to have a larger recurrence interval than other storms with comparable amounts of rainfall. This indicates that the available data are insufficient to determine recurrence interval with any precision.

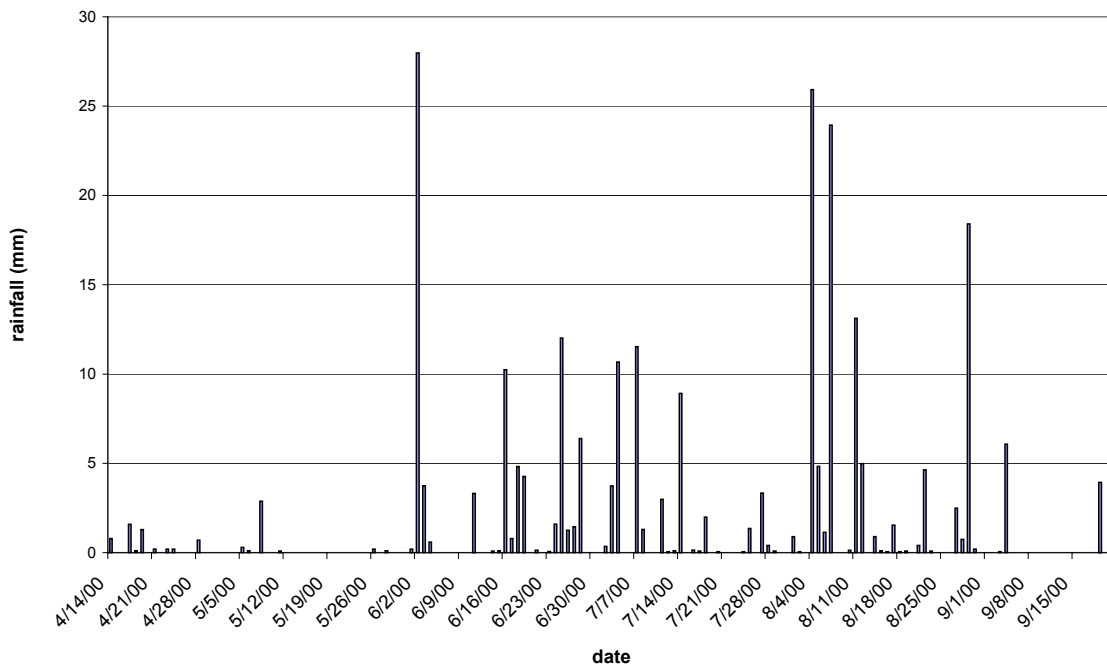


Figure 4.5 Average daily rainfall in the Danangou catchment, April to September 2000

### 4.3 Soil physical properties

#### 4.3.1 Hydraulic conductivity

Saturated hydraulic conductivity was measured with the constant head method using samples taken from the field ( $K_{sat_m}$ ). Sample size was 8 cm across and 10 cm high. The Wind evaporation method was used to measure soil moisture content with corresponding suction at different depths in soil samples. From these data relationships between moisture content, suction and conductivity were obtained by fitting the Mualem-Van Genuchten parameters. By extrapolating these relationships to saturated conditions fitted values for  $K_{sat}$  were obtained ( $K_{sat_f}$ ). Measurements as well as results have been described by Stolte et al. (in press). The number of measurements is given in appendix 4.1 and a summary of the data is shown in table 4.5. The table shows that saturated conductivities determined with the constant head method and from the Wind evaporation method were clearly different. According to Stolte et al. (in press) the true value should be in between the values obtained with the two methods.

Table 4.5 Soil physical parameters measured in the Danangou catchment.

	$K_{sat_m}$ (cm/d)	$K_{sat_f}$ (cm/d)	Alpha	n	l	$\theta_r$	$\theta_{sat}$
Cropland	55.9	1	0.0075	1.925	0.1	0.120	0.425
Orchard	96.9	25	0.0052	2.700	0.5	0.0	0.459
Woodland	122.1	13.2	0.0030	3.058	0.5	0.1	0.450
Shrubland	163.7	10	0.0062	3.207	0.5	0.1	0.350
Wasteland	153.4	0.59	0.0067	2.331	0.5	0.1	0.391
10-20 cm	21.3	0.92	0.0059	2.137	0.5	0.0	0.396
20-100 cm	97.0	20	0.0044	2.595	0.5	0.1	0.350

Table 4.6 Bulk densities for different soil types

	Yellow loess plough layer		Yellow loess		Red loess plough layer		Red loess	
	Mean	Stdev	Mean	Stdev	Mean	Stdev	Mean	Stdev
Field bulk density (kg/m <sup>3</sup> )	1257	118	1399	91	1298	206	1882	48
Dry bulk density (kg/m <sup>3</sup> )	1167	76	1270	58	1167	126	1570	67
Saturated bulk density (kg/m <sup>3</sup> )	1675	75	1777	51	1682	105	2018	35
Porosity	51	2	51	2	51	2	45	5
Number of measurements	31		14		9		10	

### 4.3.2 Bulk density

Table 4.6 shows the results of bulk density and porosity measurements for red and yellow loess. It shows clear differences between plough layer and undisturbed loess and also a clear difference between yellow loess and red loess. The red loess plough layer was sampled at two sites that proved to have quite different properties (hence the large standard deviations). No difference was found between the yellow loess plough layer and the red loess plough layer.

### 4.3.3 Grainsize analysis

Grainsize analyses were performed both with laserdiffractometry and with the traditional sieve-pipette method. A Coulter LS 230 was used for the laserdiffractometry, with a wavelength of 750 nm. As suggested by Beuselinck et al. (1998), the Fraunhofer theory was applied. After boiling the samples with hydrogen peroxide and hydrochloric acid the samples were dried and pulverised. A small subsample (0.1 – 0.3 g) was taken and suspended, after which three repeat measurements were performed with the Coulter. The sieve pipette method was applied with full treatment of hydrogen peroxide and hydrochloric acid and also with minimum treatment. The minimum treatment was supposed to better represent natural conditions. Measurements were done for the different lithologies present in the area, as well as for a number of samples taken at the outlet of the catchment during runoff events. The results for the catchment outlet will be discussed

Table 4.7 Grain size distribution of different lithologies

	Weathered bedrock	Yellow loess	Red loess	Red clay
<i>Sieve/pipette minimum treatment</i>				
D50 (mu)	853	35	23	5
Sand (%)	69.8	20.2	28.1	8.2
Silt (%)	26.6	70.4	55.3	53.8
Clay (%)	3.6	9.5	16.5	38.0
<i>Sieve/pipette full treatment</i>				
D50 (mu)	200	35	7	7
Sand (%)	65.4	29.1	13.5	7.5
Silt (%)	27.6	60.0	55.5	56.5
Clay (%)	7.0	10.9	31.1	36
<i>Coulter LS 230</i>				
D50 (mu)	54	42	20	17
Sand (%)	48.3	31.0	12.6	11.7
Silt (%)	46.8	63.9	79.0	80.0
Clay (%)	4.9	5.1	8.4	8.3

∞ Table 4.8 Chemical compound contents (%) of different lithologies from Danangou, Gaolanshan (Derbyshire & Meng, 2000), Ariendorf (Pye, 1987) and Vicksburg (Pye, 1987). Derbyshire & Meng used inductively coupled plasma atomic emission spectrometry (ICP-AES); Pye used X-ray fluorescence spectrometry (XRFS).

Element	Danangou (China)				Gaolanshan (China)			Ariendorf (Germany)	Vicksburg (USA)	
	Weathered bedrock	Red clay	Red loess	Yellow loess	Wucheng loess	Lishi loess	Malan loess	Un- weathered loess	Un- weathered loess (2K)	Weathered loess (2A)
SiO <sub>2</sub>	56.65	61.30	56.92	61.98	57.66	58.48	59.30	63.56	61.72	74.24
Al <sub>2</sub> O <sub>3</sub>	17.87	15.91	13.04	11.28	11.84	11.46	11.34	8.53	7.92	11.02
Fe <sub>2</sub> O <sub>3</sub> , FeO	8.08	6.14	5.05	4.13	4.21	4.04	3.98	3.10	3.02	4.30
CaO	1.89	2.17	7.86	7.80	8.20	8.11	8.13	9.78	8.26	0.69
MgO	2.50	2.91	2.86	2.35	3.01	3.02	3.14	1.45	4.23	0.76
K <sub>2</sub> O	2.79	2.76	2.11	2.18	2.30	2.27	2.24	1.69	1.86	2.26
Na <sub>2</sub> O	1.58	0.88	1.30	1.91	2.08	2.12	1.92	0.98	1.28	1.17
MnO	0.13	0.09	0.08	0.08	0.08	0.09	0.09	0.08	0.07	0.12
P <sub>2</sub> O <sub>5</sub>	0.16	0.06	0.11	0.12	0.18	0.16	0.14	0.08	0.13	0.18
TiO <sub>2</sub>	0.87	0.74	0.65	0.58	0.66	0.61	0.60	0.59	0.62	0.74

in chapter 8. The results for the different lithologies are shown in table 4.7 for all three methods. All three methods were applied to sub-samples of the same sample (sampling location is given in figure 4.1). Table 4.7 shows that results obtained with the 3 methods are different. Beuselinck et al. (1998) discussed the differences between the sieve pipette method and laserdiffractometry. The main difference is that both methods use different principles and assumptions. The sieve/pipette method yields mass% and assumes equivalent spherical particles, while the Coulter gives volume% and uses optical diameter. Which method is better is hard to say since there is no independent way to determine real grainsize distribution. Table 4.7 shows that most of the material that is of clay fraction according to the sieve pipette method belongs to the silt fraction according to laserdiffractometry.

#### 4.3.4 Chemical analysis

The chemical composition of several lithologies was determined on samples taken at the surface, using X-ray fluorescence spectrometry (XRFS). Sub-samples of the samples taken for grainsize analysis were used. Table 4.8 shows the results together with results reported by Derbyshire & Meng (2000) and Pye (1987). Table 4.8 shows that the Gaolanshan loess from Gansu province (western part of the Loess Plateau) has a chemical composition that is similar to that in Danangou, though some of the minerals occur in slightly higher percentages in the Gansu loess (e.g. CaO, MgO). It further shows that the different types of loess are not very different chemically. The chemical composition of unweathered loess from Germany and the USA, as reported by Pye (1987), is also similar to that of the Chinese loess. There are some differences, e.g. in Al<sub>2</sub>O<sub>3</sub>, Na<sub>2</sub>O and MgO, but these differences are small. The weathered loess from the USA, however, contains far less CaO and MgO. According to Pye (1987) Ca and Mg will be lost first during weathering. The loss of Ca and Mg has also resulted in some enrichment of other elements. This shows that the Danangou loess is unweathered, despite the fact that it is at the soil surface. Both weathered bedrock and red clay were found to be different from loess since both contain more iron and far less calcium than the Chinese loess. Their iron content is also far higher than for the loess from Germany and the USA.

## 4.4 Discharge measurement

*Partly based on: Van den Elsen, E., R. Hessel, Baoyuan Liu, K.O. Trouwborst, J. Stolte, C.J. Ritsema & H. Blijenberg (in press) Discharge measurements at the outlet of a watershed on the Loess Plateau of China. Catena.*

### 4.4.1 Introduction

In the Danangou catchment discharge was measured with a weir that had a triangular cross-section. Discharge measurement with measurement structures is based on a relationship between water level and discharge. Water level is measured and converted to discharge. To do this, equations have been derived for various types of measurement structures. Bos (1989) discussed many of these structures. The discharge equations are

usually based on the law of Bernoulli, but they can also be empirical. If energy-losses can be considered negligible the law of Bernoulli is valid. The total energy head can be expressed in terms of specific energy (that is taking the bottom of the flow as reference level). This is only allowed if the streamlines are straight and parallel, which ensures that there is a hydrostatic pressure distribution. The specific energy is:

$$He = h + \frac{V^2}{2 \cdot g} \quad (4.1)$$

Where:  $He$  = specific energy (m)  
 $h$  = water level (m)  
 $V$  = flow velocity (m/s)

As  $V = Q/A$  it is possible to write:

$$He = h + \frac{Q^2}{2 \cdot g \cdot A^2} \quad (4.2)$$

Where:  $Q$  = discharge (m<sup>3</sup>/s)  
 $A$  = cross sectional area of the flow (m<sup>2</sup>)

Water level is usually measured some distance upstream of the structure. It is then assumed that the water velocity can be neglected. The alternative is to measure water level at the point where the flow becomes critical. At this point, there is a unique relationship between  $h$  and  $Q$ . At all other points, two different discharges would be possible for a given  $h$ , depending on whether flow is sub-critical or super-critical. For critical flow  $dHe/dh = 0$ . Because  $A$  also depends on  $h$  this gives:

$$0 = 1 - \frac{Q^2}{g \cdot A^3} \cdot \frac{dA}{dh} \quad (4.3)$$

As  $dA = Bdh$  it follows that:

$$Q = \sqrt{\frac{g \cdot A^3}{B}} \quad (4.4)$$

Where:  $B$  = width of the flow (m)  
 $g$  = gravitational acceleration (m/s<sup>2</sup>)

For weirs with triangular cross section width ( $B$ ) and area ( $A$ ) are:

$$B = 2 \cdot h \cdot \tan\left(\frac{\theta}{2}\right) \quad (4.5)$$

$$A = \frac{B \cdot h}{2} \quad (4.6)$$

Where:  $\theta$  = total angle of the weir (°)

Equation 4.4 thus becomes:

$$Q = C \cdot \sqrt{\frac{g}{2}} \cdot h_c^{5/2} \cdot \tan\left(\frac{\theta}{2}\right) \quad (4.7)$$

Where:  $h_c$  = critical water level (m)  
 $C$  = a correction factor

The correction factor  $C$  is in general made up of two parts:  $C_d$  and  $C_v$ .  $C_d$  is a correction factor that is called discharge coefficient. It has to be applied because effects such as viscosity, turbulence and a non-uniform flow distribution (Bos, 1989). These effects cause energy-loss. As the equation was derived under the assumption of no energy loss (Bernoulli) a correction must be made. The discharge coefficient depends on shape and type of measurement structure, but is generally between 0.93 and 1.02 (Bos, 1989).  $C_v$  is a correction for neglecting the velocity in the approach channel. Normally the water level is measured upstream of the measurement structure. When this is done, it has to be assumed that the water velocity upstream of the structure is 0. As this is normally not the case a correction must be applied.  $C_v$  is given by:

$$C_v = \left(\frac{H_1}{h_1}\right)^u \quad (4.8)$$

Where:  $H_1$  = the total upstream energy head  
 $h_1$  = the upstream water level  
 $u$  = the power of h in the head-discharge equation  
(2.5 for a triangular cross-section)

If the critical water level is measured directly, as was attempted in this study, this correction is not necessary and  $C_v$  equals 1.

Weirs can be subdivided into broad-crested, short-crested and sharp-crested. The width at the top is used for this: sharp-crested weirs have widths of maximum 2 mm, broad-crested weirs have widths of several meters and short-crested weirs are in between sharp-crested and broad-crested weirs. For short-crested weirs another correction factor applies than for broad-crested weirs because streamline curvature can no longer be neglected (Bos, 1989). Discharge will be higher than for broad-crested weirs (so  $C_d$  will be higher).

#### 4.4.2 *The Danangou weir*

Several criteria played a role in selecting the site of the Danangou weir. The first was that the catchment area of the weir should be as large as possible. The second was that a site should be selected where it was possible to ensure stability of the weir. Finally, the local farmers had to agree with the site. After selection of the site the local farmers built a weir with triangular cross-section. The position of the weir is indicated in figure 4.1, while the weir itself is shown in figure 4.8. A dam with a width of 2 meters was built. The height of the dam was also 2 metres, 1 metre of which was below the previous river bed. On top of the dam the actual weir was built. Locally available sandstone was used to build both the dam and the weir. The length of the weir (which is equal to the width of the stream) was about 10 meters and water levels up to 1.7 meters could be accommodated. The water level measurement was done about 80 cm upstream of the overflow point. It was assumed that flow would become critical there. The weir had a triangular cross-section with an angle of 140 degrees ( $\theta/2 = 70$ ). These dimensions mean that discharges of up to about  $20\text{m}^3/\text{s}$  could be measured. The width of the weir was 0.5 meters at the top, but a steel plate with a thickness of 6 mm was inserted at the top of the weir. The Danangou weir was therefore short crested. Bos (1989) gives rating tables for short-crested v-notch weirs. Combining these data with data on  $C_v$ , which are also given by Bos, suggests a  $C_d$  of about 0.95. It would be preferable to calibrate the  $C$ -factor of equation 4.7 by measuring discharge at known water levels. This calibration would however be very difficult, because of the very short duration of discharge peaks and the high discharges (up to maybe  $20\text{ m}^3/\text{s}$ ). The area is also inaccessible during major storms. Calibration is therefore virtually impossible. There is thus a considerable uncertainty in the value of  $C$ . High sediment concentrations have implications for the discharge measurement as well. These effects will be discussed in chapter 5.

#### 4.4.3 *Measuring equipment*

Initially a horizontal support for the water level sensor was built over the stream with supporting beams upstream and downstream of the dam. The sensor was mounted on the horizontal support. This construction did not survive the first large storm (July 15<sup>th</sup>, 1998), however, and a new 'doorpost' like construction had to be built from the remains of the first one. The disadvantage of this construction was that in some storms floating material would be caught behind the poles, which might partially obstruct the water flow.

An Ultrasonic level sensor (Endress + Hauser, type FMU-230E) was installed over the weir to measure the water level. An ultrasonic sensor emits an ultrasonic sound signal and measures the reflection time of the sound signal. It was chosen because the measurement is not influenced by presence of sediment in the runoff and because the measurements do not disturb the flow. The instrument gave water level values that were accurate to within about 0.5-1.0 cm. It was connected to a Campbell CR500 data logger, together with a small rain gauge. Because the whole system was powered by two small 12V batteries (recharged by a solar panel), the system had to use as little power as possible. Therefore, the level sensor was only switched on after the rain gauge detected rain. The level sensor would then start doing level measurements once every minute, and would continue for



half an hour or until the water level fell below 0.2 m. Measurement details are given by Van den Elsen et al. (in press b).

As a back-up system a pressure transducer was installed in 1999. A pressure transducer measures the pressure of the fluid suspension above the sensor. In order to derive the exact water level from the measured pressure, the sediment concentration at the moment of measurement needs to be taken into account. This is necessary because the sediment concentration determines the density of the fluid. The pressure transducer measured continuously at 1-minute intervals. Power was supplied by a car battery that had to be changed periodically. The pressure transducer was installed in a stilling well a few meters upstream of the weir. Its zero-level is 32 cm above the overflow point of the weir. As a second back up a local farmer was hired to manually record the water level during runoff events. To do this a staff gauge was painted on the rock visible in figure 3.15. The staff gauge is in between ultrasonic sensor and pressure transducer. It allowed water level to be recorded with about 1-cm accuracy.

The farmer also took surface samples to determine the sediment content of the flow. Teams from UU (Utrecht University, The Netherlands) and Alterra (Alterra Green World Research, The Netherlands) also recorded water levels and took samples when possible. In 1998 a turbidity sensor was installed, but it could only measure sediment concentrations to 100 g/l. Since this was not enough this sensor was replaced in 1999 by an IMCO automatic water sampler. This sampler was triggered by water level measurements from the pressure transducer and could take 24 samples during an event. Power was supplied by the same battery that was used for the pressure transducer. The inlet of the suction tube was at a fixed position.

#### *4.4.4 Measurement results*

Table 4.9 shows how the different measurement devices performed during the events that occurred at the dam. It shows that at least partial data were collected during 6 events. A large event that occurred on July 15<sup>th</sup>, 1998 was completely missed. Rainfall data indicated that 2 more events might have occurred before July 15<sup>th</sup>, 1998. No data about these events exist because the ultrasonic sensor did not yet function at that time. Once it started working, however, it produced at least partial data during all 6 subsequent events. The pressure transducer also worked well, but the data obtained with that sensor were more difficult to interpret since the water pressure not only depends on water height but also on fluid density. Table 4.9 also shows that the most complete data set was obtained during the event of July 20<sup>th</sup>, 1999. Table 4.10 gives a summary of the data that have been collected at the weir.

Table 4.10 shows that the data on the different events are consistent: the more rain, the higher the recorded maximum intensity and the higher the discharge. The table further suggests that about 11.5 mm of high intensity rain is needed to produce runoff at the weir. The only exception is the event of 990721, which had very little rain, but still produced some discharge. This is probably due to the fact that the soil was still very wet because of the event of 990720. It must also be kept in mind that the rainfall given in the table is a

non-weighted average. Events that are localised in space might have lower average rainfall amounts, but still could produce runoff. On the other hand, the event of 990710 had about 10.5 mm of high intensity rain but did not produce runoff at the weir. All events at the dam will be discussed briefly in order to get insight in the quality of the data obtained during these events.

Table 4.9 Equipment performance and available data for all known events.

Data source	980715	980801	980823	990720	990721	000811	000829
Ultrasonic sensor	X	=	+	+	+	+	=
Pressure transducer	-	-	-	+	+	-	+
Farmer-level	-	-	+	=	-	-	O
UU-level	-	-	-	=	-	+	-
Turbidity sensor	X	-	-	-	-	-	-
Automatic sampler	-	-	-	+	X	-	X
Farmer-samples	-	-	+	=	-	-	+
UU-samples	-	-	-	X	-	+	-
Alterra-samples	-	+	-	-	-	-	-

X: no data collected, O: imperfect data collected, =: partial data collected, +: good data collected, -: not applicable

Table 4.10. Overview of the runoff events measured at the weir.

	980801	980823	990720	990721	000811	000829
Event rainfall (mm)	15.1	13.0	14.1	3.5	11.6	17.8
Max 1-minute intensity (mm/h) <sup>a</sup>	69.9	47.2	66.2	35.8	49.5	84.9
Time to peak (minutes) <sup>c</sup>	15	34	19	32	31	15
Peak level (m)	1.02	0.45	0.89	0.37	0.28	1.29 <sup>b</sup>
Peak discharge (m <sup>3</sup> /s)	5.1	0.7	3.6	0.5	0.2	8.7
Total discharge (mm)	1.9	0.4	1.7	0.2	0.1	2.9
Q/P (%)	12.6	3.0	12.1	5.7	0.9	16.3
Total soil loss (tonne)	1280	96	770	n.a.	16	2630
Soil loss (tonne/ha)	6.2	0.5	3.7	n.a.	0.1	12.7
Mean clear water concentration (g/l)	321	131	235	n.a.	80	446
Max dirty water concentration (g/l)	361	154	371	n.a.	129	498

<sup>a</sup> This is a catchment-average. Maximum intensities for individual rain gauges were much higher, with maximum 1-minute rainfall intensity during the 000829 storm of 190 mm/h

<sup>b</sup> This value was estimated from the pressure transducer data

<sup>c</sup> The time difference between catchment averaged peak rainfall intensity and peak discharge

### 980801

As can be seen from table 4.9 and figure 4.6 only a partial data series of discharge was obtained at the dam. Water samples were taken by Alterra.

### *980823*

Between the 980801 and 980823 events, the staff-gauge was finished and a farmer was hired to write down the levels and to collect water samples. The data obtained from the ultrasonic water level sensor had erroneous times due to resetting of the equipment, but a satisfactory fit with the level data from the farmer was easily obtained just by shifting the time. The data collected by the farmer and by the sensor then matched each other closely, as can be seen in figure 4.6.

### *990720*

In early 1999 the pressure transducer and automatic water sampler were installed. Almost all equipment functioned properly during the event of 990720. The only data that lack are sediment concentrations for the rising stage of the hydrograph. These data were lost because of problems with the sampler. Figure 4.6 shows that the water levels as determined with different methods closely corresponded to each other. Nevertheless, there were some clear differences. The most obvious was that during the later stages of the falling limb the levels started deviating significantly. As mentioned before the manual measurements were done 3 metres upstream of the dam, while the pressure transducer was 5 metres upstream of the dam. The level of the river bed in those places was unknown, but was certainly higher than at the dam. Furthermore, the width of the river might be larger and the velocity might be different. Since these factors were unknown (and might change during an event) a correction was not possible. The level measurement from the ultrasonic sensor was therefore the most reliable and was used during subsequent analysis.

### *990721*

A small event occurred early on July 21<sup>st</sup>, 1999. The total amount of rainfall was very small, and the only reason that any discharge was produced was probably that the soils in the catchment were still very wet from the event of 990720. Figure 4.6 shows water levels measured with the ultrasonic sensor and with the pressure transducer. It shows that both methods agreed on the timing of discharge, but it also shows that measured levels did not correspond. As mentioned before the 0-level of the pressure transducer was at a level of 32 cm above the overflow point of the weir. The level of the channel bed was, however, unknown. An additional problem was that for this event no concentration data were available, so that the actual water level could not be determined from the pressure data. The ultrasonic level sensor data were therefore more reliable.

### *000811*

For this event, the water level was barely above the minimum of the ultrasonic water level sensor and did not reach the minimum of the pressure transducer. The water level time series from the ultrasonic water level sensor could be supplemented with manual recordings (figure 4.6). Water samples were also taken. Observations after the event as well as analysis of the rainfall data suggested that most discharge came from the large gullies in the northern part of the catchment.

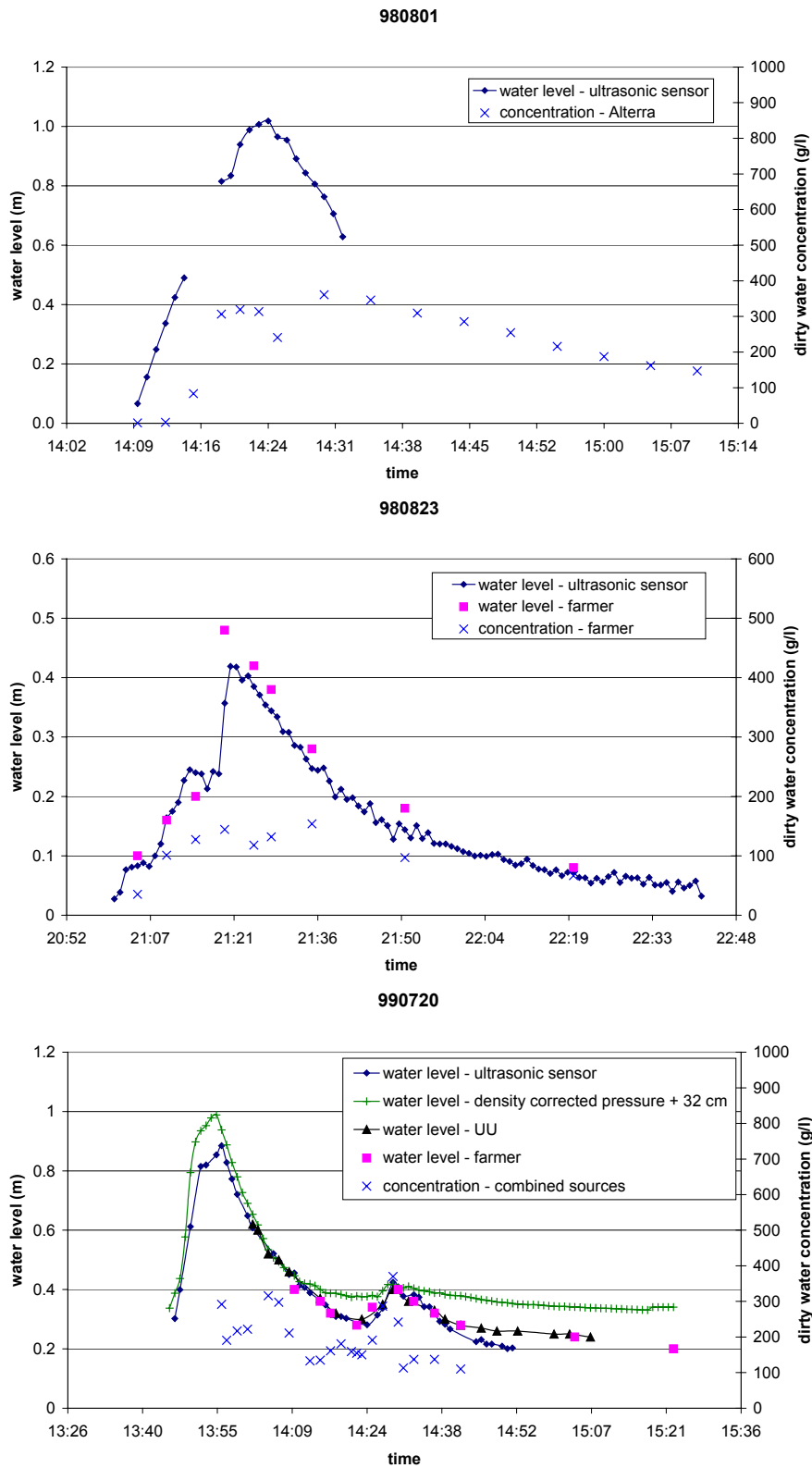


Figure 4.6 Measured water level and concentration for all six events

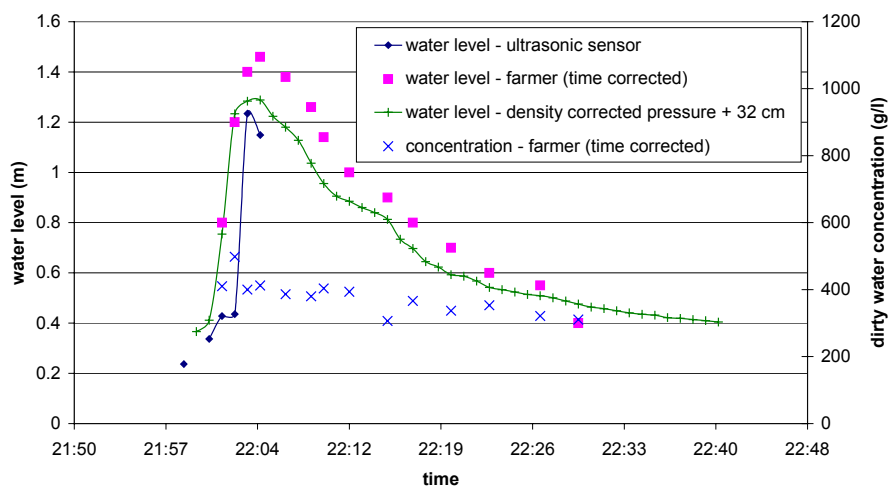
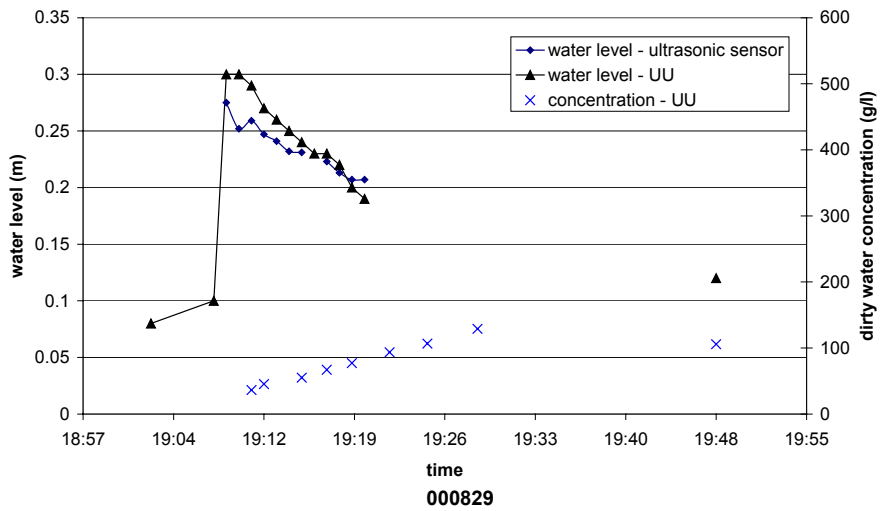
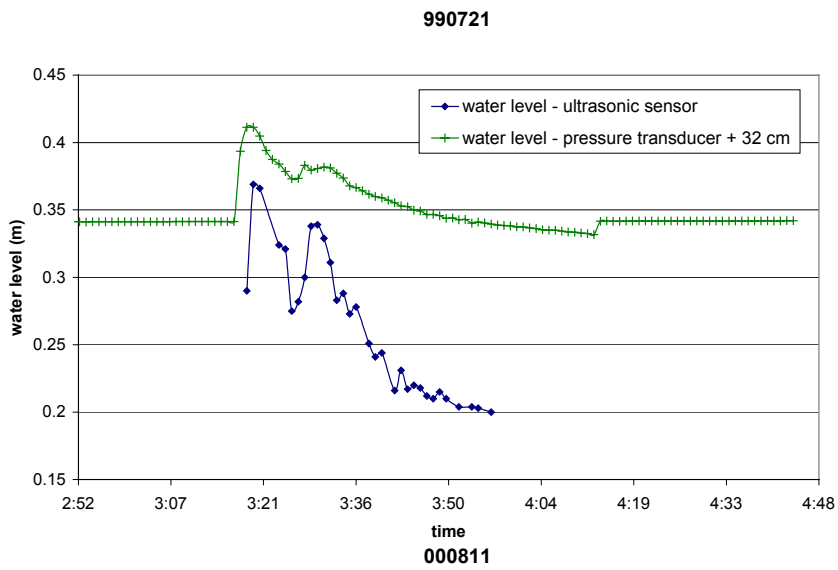


Figure 4.6 (continued)

000829

The 000829 event occurred at a very inconvenient time (22:00) and was of short duration but of very high intensity. Catchment averaged rainfall intensities were above 60 mm/hour for 9 consecutive minutes, while the recorded peak intensity for a 1-minute interval was 190 mm/h at rain gauge D. Farmers at Leipingta village reported hailstones of about 3 cm. Next morning the water of the Yan river was extremely cold and hail impact craters could be seen throughout the upper part of the Danangou catchment. At the weir only the hired farmer was present. He took water samples and recorded water levels from the staff gauge. The supporting construction of the ultrasonic sensor collapsed and the sensor was destroyed (figure 4.8) in the course of the event. The original construction can be seen in figure 3.15. The pressure transducer functioned properly. Both the pressure transducer data and the (few) ultrasonic sensor data contradicted the time recorded by the farmer, but matched each other (figure 4.6). Analysis of the rainfall data showed that the time recordings by the farmer could not be right. Figure 4.7 shows the rainfall arrival

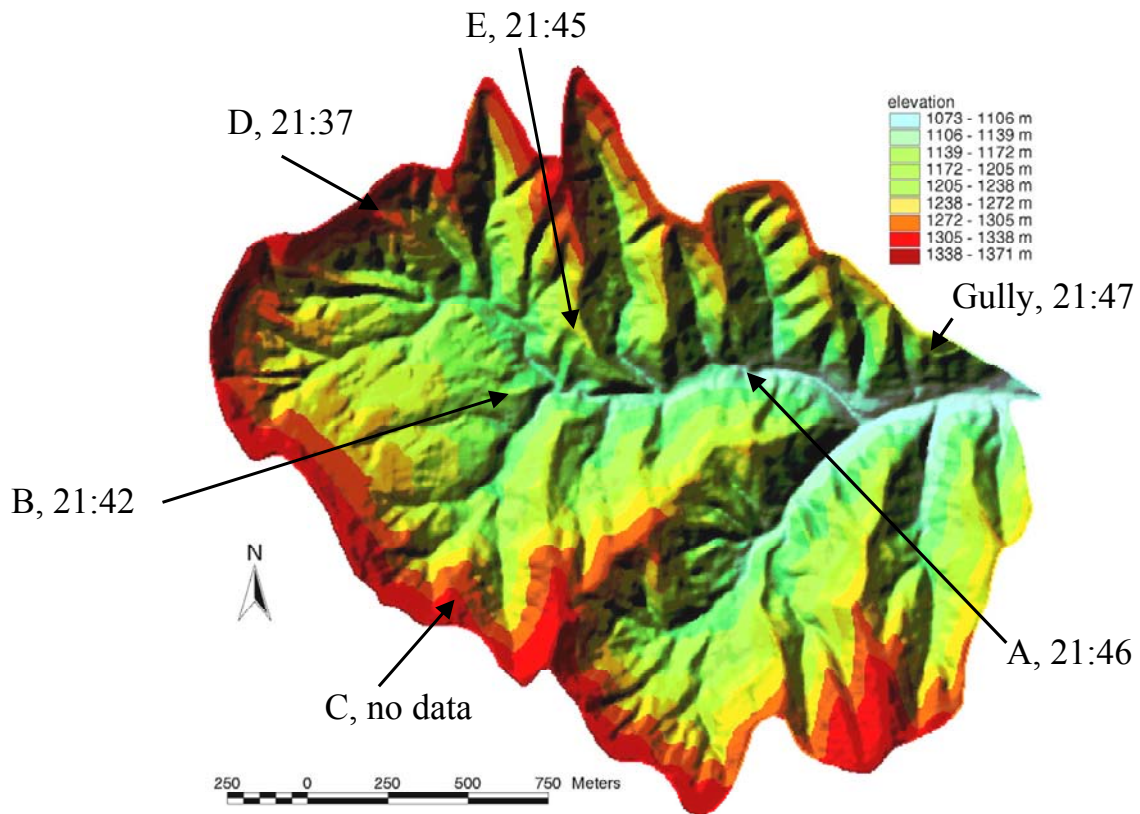


Figure 4.7 Rainfall arrival times for the different rain gauges, event of August 29<sup>th</sup>, 2000

times at the different rain gauges in the catchment. Heavy rain started some minutes after that. The map clearly shows that the rainstorm came from the northwest. As the farmer lives in the east rain would certainly not have arrived at his home before 21:47 and probably later (since the gully rain gauge had 5 minute time resolution rain can have arrived there from 21:47 to 21:52). The rainfall data therefore indicated that:

- The farmer cannot have been at the dam when he says he arrived (before 21:54).

- Since heavy rain started at 21:47 there cannot have been discharge at the dam at 21:54.

Both the pressure transducer and the ultrasonic water level sensor indicated that runoff started at about 22:00, which is much more likely in view of the rainfall data.

Therefore, the pressure transducer data were used and the time of sampling of the farmer was adapted to the time of the pressure transducer by using the manual level recordings of the farmer. Consequently there is considerable uncertainty about the precise water levels during the event.



Figure 4.8 The weir on August 30<sup>th</sup>, 2000. The supporting construction of the ultrasonic water level sensor as well as the sensor itself were destroyed by the event of 000829. Note the large amount of plant material around the pipes and around the pipe of the pressure transducer (background). Water level during the event was close to the top of the V-shaped weir.

#### *Discussion*

Table 4.9 shows that, thanks to several backup systems, at least partial data were collected for all events that occurred after 980715. The results that were obtained with the different methods can, however, not always be compared directly.

Water levels were measured with an ultrasonic sensor, a pressure transducer and using a staff gauge. Of these measurements, the ultrasonic sensor was the most reliable since it measured closest to the weir. Even so, there is no guarantee that the assumption that the ultrasonic level sensor measured critical water level is true. The point where flow becomes critical might well vary with water level. The measured levels might therefore deviate

somewhat from true critical water depth, but this error is likely to be relatively small, probably 0.1 m at most.

Both the staff gauge and the pressure transducer suffered from the fact that they could for practical reasons not be installed very close to the weir; the staff gauge was about 3 m upstream and the pressure transducer 5 m. Figure 4.6 shows that this resulted in unreliable results for low water levels. The most important cause for this was that the level of the streambed was different from that at the weir. For example, adding 32 cm to the levels measured with the pressure transducer is unrealistic for low water levels, as clearly shown for the event of 990721. The data for the events of 990720 and 000829 show that this error was much smaller for higher water levels, which indicates that the slope of the water surface at the weir decreased with increasing discharge. This was because for higher water levels the weir would cause a pond to develop, so that the water slope became smaller than the bed slope. Other factors that might have influenced the results of staff gauge and pressure transducer were differences in channel width and differences in flow velocity, while for low discharge flow might not even have occupied the entire width of the channel. All these problems would reduce significantly if a pond could be maintained just upstream of the weir. This was, however, impossible due to the remote location of the weir and due to large sediment transport that would require regular removal of material.

Interpretation of the pressure transducer data was further complicated by the fact that its measurement depends on flow density, which is a function of sediment concentration. This problem will be discussed in chapter 5.

Measurements of concentration were complicated by the fact that concentrations were well above the range that could be measured with a turbidity sensor. Therefore, two sources of data remained: samples taken by the automatic sampler at a fixed height and surface samples taken by people present at the weir. Since the automatic sampler took samples at fixed height, the relative depth at which it samples changed as a function of water level. Concentration is likely to be a function of relative water level, but to be able to use the measurement results it was necessary to assume that concentration was equal throughout the depth of the flow. This can have introduced errors, but since the suspension load mainly consisted of fine-grained silt these errors might be fairly small. Another potential problem with automatic samplers is that the sediment might clog the inlet tube when sediment concentrations are high (Cantón et al., 2001). This was not observed in the Danangou catchment, but the inlet tube was found to have burst where it was compressed by the pump. This probably happened during the 990720 event.

Table 4.9 shows that for most events there was no choice about which data to use. Sediment data were always scarce, even for the 990720 event, where there was only partial overlap between data collected automatically and manually. For some events there were water level data from several sources. In those cases the data collected by the ultrasonic sensor were preferred over the others.



#### 4.4.5 Gully-flume

In the Danangou catchment a 2-foot H-flume was also installed to measure the discharge from a single gully. The discharge equation of the flume was (Bos, 1989):

$$\log Q = 0.0237 + 2.4918 \cdot \log h + 0.2605 \cdot (\log h)^2 \quad (4.9)$$

Where:  $h$  = water level (m)  
 $Q$  = discharge (m<sup>3</sup>/s)

The area draining to the flume was about 0.2 ha. Water level in the flume was measured with an Endress & Hauser ultrasonic sensor in a way similar to the method used at the weir. Sediment concentration was measured with a turbidity sensor. The total amount of discharge was collected in a series of 3 barrels downstream from the flume. The divisor system used 5 holes (1<sup>st</sup> barrel) and 11 holes (2<sup>nd</sup> barrel). Rainfall was measured with a tipping bucket rain gauge. It measured the amount of rain for 5-minute intervals. The measurement methods are more fully described in Van den Elsen et al. (in press a).

Table 4.11 Results from the gully-flume, 1998-2000.

	P(tot) (mm)	Max I. (mm/h)	Q-peak (l/s)	Q-tot sensor (l)	Q-tot sensor cor (l)	Q-tot barrels (l)	Q/P (%)	C-av dirty (g/l)
980705	22.2	50	1.6	3018				
980712	19.0	46	23.1	13269				
980715	23.4	67	14.5	6651				
980801	18.8	96	23.9	7850				
980823	13.6	34	6.7	3347				
990720	30.0	113	70.1*	11931	25954	2540	44	598
000829	10.8	51	11.5	2725	1305	1212	6.2	61

\* estimated, highest measured value was 63.1

#### Results

Unfortunately, the selected gully proved not to be a very representative one, so the data obtained there will not be much used in this thesis. The collected data were, however, reported by Van den Elsen et al. (in press a) and table 4.11 gives a summary. Table 4.11 shows that sediment concentrations measured at the plot were almost 600 g/l for the event of July 20<sup>th</sup>, 1999, while they were about 60 g/l for the event of August 29<sup>th</sup>, 2000. Before 1999, the divisor was not yet in place and no data on total discharge was therefore available. The maximum intensity given in table 4.11 is of 5-minute duration. It is therefore likely that 1-minute maximum intensities were considerably higher.

Interpretation of the data collected at the flume was difficult for two reasons: 1) To spare

battery power the system could not continuously measure with high frequency. Instead, high frequency measurements (every 20 or 30 seconds) were triggered by measured water levels, which were usually measured every 5 minutes. The gully area was small and hence its reaction to rainfall was rapid. Therefore, the 5 minute measuring interval repeatedly caused the rising limb of the hydrograph to be missed. 2) Sediment layers built up in the flume in the later stages of events. These layers influenced measured runoff, as explained for the sediment plot in section 5.5. For 1999 and 2000 data on sediment levels were available, so that a corrected discharge could be calculated. This correction included an estimate of the rising limb of the hydrograph, and also removed measured values that were obviously highly unlikely. The results show a good match for 000829, but a very large unexplained difference for 990720.

#### 4.4.6 Sediment plot

In 1999 a single sediment plot was installed in order to measure runoff and erosion from a field. Its position is shown in figure 4.1. The plot started at the hilltop and had a length of 34.2 metres, the width was about 6.5 metres on average, so that the area was about 200 m<sup>2</sup>. On the sides small walls made of loess were built. At the downstream end of the plot 2 3.5 metre gutters were installed. Both gutters drained into a single 1-foot HS-flume. Water level in the HS-flume was measured with an OTT Thalimedes. The Thalimedes is a system that consist of float, pulley and counter weight. The rotation of the pulley was transformed in a water level recording and stored in the data logger once every minute. The measured water level can be converted into discharge with the following equation (Bos, 1989):

$$\log Q = -0.4382 + 2.4193 \cdot \log h + 0.1790 \cdot (\log h)^2 \quad (4.10)$$

Where:  $h$  = water level (m)  
 $Q$  = discharge (m<sup>3</sup>/s)

The total amount of runoff was stored in 2 barrels downstream of the flume. The first barrel had 11 holes, 1 of which drained into the second barrel. Rainfall was measured with a tipping bucket rain gauge. Figure 4.9 shows the sediment plot setup. The crop was pearl millet in both 1999 and 2000. When an event occurred the sediment plot was always visited within a day to collect the data from the Thalimedes sensor and from the barrels, and to clean the equipment. The total amount of water was corrected for rain falling on gutter, flume and barrels. To determine sediment concentration, water samples of known volume were taken from the barrels after stirring thoroughly. Sediment levels in gutters and flume were also measured. The density of these sediment layers was measured on samples taken in the flume. From these data runoff and soil loss from the plot were calculated.

In the period June 1999 – September 2000 only 5 storms occurred at the sediment plot, 4 of them small. The results for these 5 storms are given in table 4.12. Table 4.12 shows that there were problems with the data collected at the sediment plot. For some events, the total amount of runoff determined from the sensor signal was very different from the

total amount of runoff determined from the barrels. All events will be discussed briefly to assess the reliability of the data.



Figure 4.9 Sediment plot in 1999. The crop was pearl millet

Table 4.12 Overview of the runoff events measured at the sediment plot

	990710	990721	000707	000811	000829
Event rainfall (mm)	10.6 <sup>a</sup>	5.0	16.3	12.0	16.7
Max 1-minute intensity (mm/h)	59.1 <sup>a</sup>	47.8	71.6	59.1	189.1
Peak level (cm)	2.9	7.6	2.3	1.0	20.3
Peak discharge (l/s)	0.18	1.20	0.12	0.03	9.4
Total discharge from level (l) <sup>b</sup>	42.1	119.0	84.6	6.0	2143
Total corrected discharge barrels (at sensor) (l)	50.7	224.6	111.9	51.3	1871
Total corrected discharge barrels (from plot) (l)	33.7	216.7	83.1	31.9	1845
Total soil loss (kg)	24.8	162.1	27.9	1.3	659
Soil loss (tonne/ha)	1.3	8.4	1.4	0.1	34.0
Average dirty water concentration (g/l)	736	748	336	39	357
Average sediment level in flume (cm)	1.35	2.03	1.88	0.18	1.20
Discharge/Rainfall (%)	1.6	21.7	2.5	1.3	55.2

<sup>a</sup> rain gauge at the plot did not work; value reported here is from the next-closest rain gauge

<sup>b</sup> total discharge is difficult to calculate from the sensor data because of sedimentation in the flume, and also because for some events the falling limb of the hydrograph is clearly incorrect.

*990710*

No rainfall data could be collected at the plot, so data from another gauge (about 500 m away) were used. There was also uncertainty about the water level in the barrel before the event occurred. Considering these difficulties, it is concluded that the system itself worked properly during this event.

*990721*

The rain gauge at the plot did work, and the values recorded here more or less matched the values from other rain gauges. Over the period 14/7 to 22/7, however, this rain gauge only recorded 56% of the average rainfall recorded by other gauges. This, in itself, is possible, also because most of the difference was caused by the event of 990720 for which only 3 mm was recorded at the plot. Nevertheless, there is doubt about the performance of this rain gauge, but not to such a degree that it could explain the very small rainfall amount that apparently caused the second-largest runoff event. Also, the Thalimedes sensor did not record any discharge during the 990720 event, which confirmed the rain gauge data since it indicated that there cannot have been much rain then. As for the entire catchment, the fact that the soil was still wet from the storm of 990720 might have played a role. Concluding: it seems possible that the actual amount of rainfall was higher, but not by a large amount. The difference between total runoff determined from the Thalimedes sensor and the total discharge determined from the barrels was very large. Even if one takes into account that there was uncertainty about pre-event levels in the barrel it was not possible to match the data which each other. Data for this event are therefore unreliable (except for barrel data).

*000707*

The same rain gauge as before was used, but during the time of the event the system seemed to work properly.

*000811*

The rain gauge was changed, so that rainfall data should be trustworthy. The 100 g counter-weight was, however, stolen and temporarily replaced by a 122 g adjustable spanner. It is unclear in how far this influenced the measurement. The falling limb of the hydrograph was corrected because it appeared from the data that the float remained artificially high and then went down very rapidly (maybe counterweight or float got stuck). Data from this event are probably unreliable.

*000829*

The adjustable spanner was replaced by a 103 g counterweight before the event occurred. The falling limb of the hydrograph showed a gradual decrease over several hours. The cause is unknown. From an estimate of overland flow velocity (0.15 m/s) and maximum distance (40 m) one can deduce that runoff should stop within 5 minutes of the end of high intensity rain. The hydrograph was corrected along these lines. This event was also the only one in which the second barrel was used. The first barrel had 11 holes, 1 of which drained into the second barrel. Such a procedure relies heavily on the assumption that flow through all holes is equal, which is not necessarily the case. Observations after

the event suggested that flow was larger on one side than on the other, but the hole that drained into the second barrel was in the middle and probably produced a good average.

### *Discussion*

From analysing the data gathered during these five events it is clear that the data collected should be regarded with caution. Several potential problems became apparent:

- Sediment levels in the flume always posed a problem because it is unknown when this sediment was deposited. It is therefore difficult to correct for this. In this study it was assumed that the sediment level was gradually build up after the discharge peak. This is also discussed in chapter 5.5.
- For the first 3 events the rainfall data were probably unreliable.
- For some of the events the signal stored by the Thalimedes sensor contained errors. By making certain assumptions some of these errors were remediated, but nevertheless, it leaves some doubt about the reliability of the system. It is possible that during very rapid changes in water level the float did not react quickly enough, especially when the level was falling.
- When water levels were low, the water did not form a continuous level in the flume. Instead, it occupied only part of the flume width. For small events the flow might thus have bypassed the stilling well with the float. The size of events would thus be underestimated by the sensor. This might, for example, have happened with the 000811 event.
- For the smaller events it is necessary to have fairly accurate data about water levels in the barrel before the event occurred.

All events measured suffered from one or more of these problems, so that in analysis one should be aware that the collected data might be unreliable.

In general, the barrel data were more reliable than the sensor data. It therefore seems that concentrations in runoff were much higher in 1999 than in 2000. Even though both years were extremely dry, the crop cover in 2000 was significantly larger than in 1999. This is the only obvious difference between the 2 years and might be the cause of the observed difference in concentration. In 1999 the concentrations measured at the sediment plot were higher than were ever measured at the dam. If the plot were representative of steep croplands, this would indicate that erosion for other land uses must have been lower or that deposition occurred further downstream.

## **4.5 Measurement of soil erosion**

### *4.5.1 Introduction*

Sound modelling is only possible when there are sufficient measurement data for model input, but also to check the model results. To check model results, measurements of soil erosion are needed, preferably for the different erosion processes separately. Field observations should provide the process understanding necessary to decide where, when and how to measure. Measuring the different erosion processes might then give vital clues to the relative importance of these different processes. This will give the

opportunity to focus on the processes that are most important during modelling. The final aim is to be able to model sediment yield from the catchment. Observations in the Danangou catchment suggested that erosion on fields (both rill and interrill) as well as gully erosion and land degradation by mass movements occur in the Danangou catchment.

#### 4.5.2 *Interrill erosion*

Interrill erosion is difficult to measure in the field. The most suitable method would be to use erosion pins, but these cannot be used on agricultural land as the stability of the pins can never be guaranteed. Securing the stability of the pins would mean changing land management and the measurement would no longer be representative. Interrill erosion rates were therefore estimated using data from the erosion plot. At the plot total erosion was measured. Interrill erosion was then calculated as total erosion minus rill erosion. Because of practical reasons the plot could not extend to the lower field boundary. Since the lower parts of most fields are less steep it can be expected that some sedimentation would occur there. Field observations supported this assumption. As a result a field-delivery ratio had to be applied to the results from the sediment plot. For 1999 a field-delivery ratio of 0.3 was used. For 2000, 0.5 was used because it was apparent that the much larger storm of 000829 had a higher delivery ratio.

#### *Results*

Data from the sediment plot are shown in table 4.13 under the rill erosion class 'no rills'. The value given is the total plot erosion minus the observed rill erosion on the plot, and multiplied by the sediment delivery ratio. The table shows that the field erosion was much larger in 2000 than in 1999. This is in accordance with observations on other fields.

#### 4.5.3 *Rill erosion*

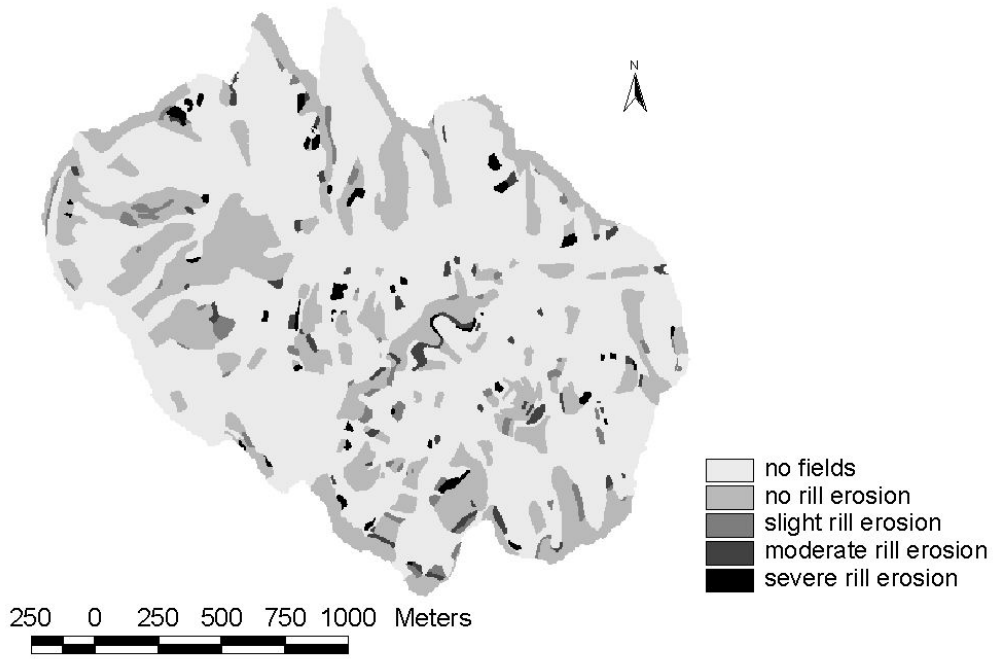
Rill erosion can be measured after storms by calculating rill volume from measurements of rill depth and width. These measurements can be carried out with tape and ruler. The problem is how to get a representative value of the entire area. Two methods were adopted:

- 1) Repeated rill measurements at certain representative fields should give information about rill erosion over time.
- 2) At the end of each rainy season rill erosion intensity was mapped over the entire catchment. Rill spacing, depth and width were measured on transects. This allows one to estimate the total amount of rill erosion for a certain year.

#### *Results*

The repeated rill measurements were attempted in 1999 and 2000. Both years were very dry and in both years only one major storm occurred, so that no information of rill development over time could be obtained. The rill mapping was conducted in 1998, 1999 and 2000. Rill erosion severity was visually classified in 4 classes: no rill erosion, slight rill erosion, moderate rill erosion and severe rill erosion. Rill measurements were performed to be able to quantify rill erosion rates for these classes, so that a catchment

A) 1998



B) 2000

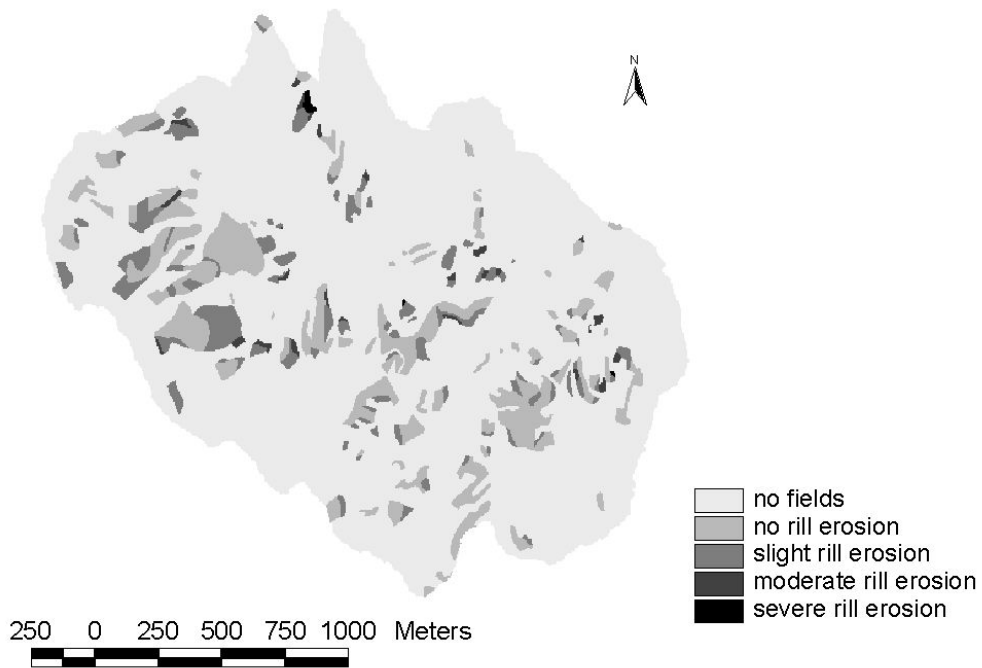


Figure 4.10 Rill erosion maps of 1998 and 2000

wide rill erosion amount could be estimated. The measurement locations for 1999 are shown in figure 4.1. The resulting erosion rates for the different rill erosion classes are shown in table 4.13. The values correspond well with those used by Zhang et al. (1997). They found yearly erosion rates of 500 tonnes/km<sup>2</sup> for slight sheet and rill erosion, 4500 tonnes/km<sup>2</sup> for moderately severe sheet and rill erosion, 8584 tonnes/km<sup>2</sup> for severe sheet and rill erosion and 15851 tonnes/km<sup>2</sup> for very severe sheet and rill erosion.

Table 4.13 Erosion rates (tonnes/km<sup>2</sup>) for different rill erosion classes

	1998	1999	2000
No rills	483 <sup>a</sup>	251	1501
Slight	1950	1199	585
Moderate	4989	4571	1926
Severe	13648	16944	7821

<sup>a</sup> this value was not based on data from the sediment plot, but on a single measurement of small erosion features in a field.

Table 4.13 shows that the measured rates for 1998 and 1999 were similar, but that the rates for 2000 were much lower for corresponding classes. Why this happened is not clear, but it does not affect the results since each rill erosion map was only used in conjunction with its corresponding erosion rate. As can be seen from the table the no rill erosion class had a higher erosion rate in 2000 than the slight rill erosion class. Since the rill mapping only gave information about rill erosion itself it was assumed that the no rill erosion rate should be added to all other rates. The difference between the different years then decreased somewhat. On the other hand, field observations after the storm of August 29<sup>th</sup> 2000 indicated that sheet erosion rates during that event were indeed very high. In places, potatoes were exposed, even though no rills had formed. It seems strange that the largest event that occurred did not produce many rills. Interestingly, Lu et al. (1989) observed that in their flume experiments rills developed especially when there was no rain applied but only runoff. This might suggest that very heavy rain could prevent rills from developing. However, the lack of rills might also be due to other circumstances, such as time of the year. The resulting rill erosion maps are given in figure 4.10 for 1998 and 2000, and in figure 10.9a for 1999. Figure 10.9a clearly shows the effect of rainfall that was localised in the southeastern part of the catchments. The maps in figure 4.10 show a more even distribution of rill erosion.

#### 4.5.4 Gully erosion

Soil erosion is often measured on erosion plots but these are not suited to measuring gully erosion, as the slope length is too short for that. Imeson and Kwaad (1980) mention several of the following methods that can be used to measure gully erosion:

1. Measuring the output of water and sediment from the gully. There are several ways to do this, ranging from hand readings and hand sampling to fully automated systems. Bedload material can be collected using a sediment trap. Suspended load is



calculated by multiplying the measured discharge with the measured sediment concentration.

2. Measuring the amount of headcut retreat with the use of for example sequential air photographs or by repeated survey. According to Crouch (1987) this is the best way to determine average erosion rates, as short-term observations (of for example a few years) will not be representative due to the inherent episodic character of gully erosion. High-resolution air photos are of course required to be able to accurately measure the position of the gully head over time.
3. The use of markers such as metal pins. The pin length is measured periodically. Pins should remain fixed and they should also not disturb the erosion processes too much (Loughran, 1989).
4. Level, tape and staff can be used to measure the gully volume. This is the method that is also most often used to measure rill erosion.

A single gully was selected and discharge & turbidity were measured (section 4.4.5). Unfortunately, due to practical considerations, the gully that was chosen for this purpose was not really representative of gully erosion in the Danangou catchment. Repeated observations showed that there is no visible headcut retreat for most gullies in the Danangou catchment. Almost all gullies in the Danangou catchment are far too large to measure with level, tape and staff. Therefore, the only other option was to measure gully erosion by using erosion pins. These pins should be placed in transects. It was impossible to measure all gullies in this way and a selection was therefore made. A total of 201 erosion pins was made from bicycle spokes and inserted in 12 gullies spread throughout the catchment (figure 4.1). Care was taken to select gullies of different size and exposition. Nevertheless, the large red loess gullies could not be measured in this way, so that the measurements were more representative of the smaller yellow loess gullies. In addition, the method is more suitable for gradual retreat than for soil fall. In the case of soil fall the pin would just disappear. This gives information about the erosion process, but such information is very hard to quantify. A survey of gully headcut size and available loose material was also carried out and is reported in chapter 8.

Table 4.14 Results of pin measurements in gullies

Position	Number of pins	Average change (cm)	Stdev (cm)
Gully bottom	28	-0.95	2.08
Headcut top	16	0.16	2.34
Headcut wall	37	0.89	2.62
Sidewall top	40	-0.00	1.08
Sidewall wall	80	0.41	1.45

### *Results*

Pins were classified according to their position on headcut top, headcut wall, sidewall top, sidewall wall and gully bottom. Exposed pin lengths were measured 5 times between

October 1998 and September 2000. Sometimes pins were clearly disturbed or had even disappeared, while it was clear that this was not caused by erosion. Suspect pin lengths were removed from the data set and the total difference in exposed pin length over the 2-year period was calculated for all pins. Table 4.14 shows the results.

A negative sign in table 4.14 means that the exposed pin length had decreased. The data therefore suggested that there was erosion on the gully walls, no change around the gully edge and deposition on the gully floor. One should, however, be careful not to read too much into the data because:

- 1) Standard deviations were always much higher than average pin length changes. This is because single pins dominated the average change. This can be due to real erosion or to disturbance that was not noticed during data collection.
- 2) Obviously, pin lengths on gully walls cannot decrease since deposition in these areas is impossible.
- 3) Trampling by goats occurred frequently. On gully edge and bottom this could push the pins into the soil, but on gully walls it can only cause erosion.

Nevertheless, the picture emerging from the pin data was confirmed by qualitative field observations (chapter 3). As shown in section 4.2 both 1999 and 2000 were very dry, which might have implications for the gully head retreat rate that was measured.

#### 4.5.5 *Mass movements*

The volume of mass movements can mostly only be guessed at. One needs to know width, length and depth, and especially the last one is difficult to measure. Apart from this there is another problem: after a soil mass has failed it will take considerable time before all material is removed from the catchment (if this ever happens). Mass movements act more as a mechanism for providing readily available sediment than as a process that actually removes sediment from the catchment. The best approach is to map the mass movements and to assess whether or not there is loose material available that could be removed during a runoff event.

#### *Results*

The geomorphological map (figure 3.5) shows the positions of all major mass movements in the Danangou catchment. Most mass movements are relatively old and are not connected to the channel system in such a way that they will produce very large amounts of erosion during events. The main exception is the most recent mass movement, which is located in the southeastern part of the catchment (outside the catchment of the weir) and which has a clear lobe that fills the valley. Several active gullies cut through this lobe and this particular mass movement will continue to deliver large amounts of sediment during storms for years to come.

## 4.6 **Conclusions**

This chapter mainly served to present the data that have been collected in the Danangou catchment from 1998 to 2000. Most of these data will be used in subsequent chapters, so

that conclusions about those data can better be drawn there. There are, however, also some conclusions that can be drawn here.

The input data for LISEM were collected in 1998 and 1999 by repeated measurements on a number of fields. These data showed that the plant characteristics changed in the course of the summer season, while the soil characteristics remained more or less the same. The data also showed that the LISEM input parameters were different for the dry year 1999 and the normal to wet year 1998.

Soil physical and chemical data show that yellow loess and red loess are of comparable chemical composition. Red loess, however, has higher bulk density and lower D50.

Discharge and sediment loss were measured at several positions in the Danangou catchment, with the use of several methods. These data suggested that the most reliable way to automatically measure water level is to use an ultrasonic sensor. For sediment concentration, however, it appears that the most reliable measurements were obtained by hand sampling, since both turbidity sensor and automatic sampler suffered from the effects of high concentrations. For both discharge and concentration it is advisable to use one or more backup systems.

Comparison of rainfall data with runoff data showed that runoff in the Danangou catchment is related to the intensity of the rainfall, rather than the amount. The data suggested that about 11.5 mm of high intensity rain was needed before runoff from the catchment occurred.

#### Appendix 4.1 Number of measurements for the different parameters

Parameter	Number of measurements	Remarks
<i>Measurements on the selected fields (tables 4.1 and 4.2)</i>		
Plant height	10	for each plant layer separately
Plant cover	1	for each plant layer separately & combination
Leaf area index	20	leaves for each plant layer
Aggregate stability	20-50	aggregates
Dry cohesion	10-20	
Wet cohesion	10-20	
Cohesion at 20 cm	5-10	
Random roughness	6	6 pictures, $6 \cdot 49 = 294$ pins
Moisture at 5 cm	5	
Moisture at 10 cm	5	
Moisture at 25 cm	5	
Moisture at 45 cm	3	
Moisture at 75 cm	2	
<i>Measurements based on land use (tables 4.5 and 6.3)</i>		
K <sub>sat,m</sub>	10	2 for deeper soil layers
K <sub>sat,f</sub>	1	As discussed by Stolte et al. (in press) 2-4 samples were taken for each land use. The samples with highest range of data and best fit were selected
Alpha	1	
n	1	
l	1	
$\theta_r$	1	
$\theta_{sat}$	1	
Manning's n	2-16	number of plots, see table 6.3
<i>Measurements based on lithology (tables 4.6, 4.7 and 4.8)</i>		
Bulk density	9-31	only red loess and yellow loess
Porosity	9-31	only red loess and yellow loess
Grainsize	1	different methods all applied to sub-samples of the same sample
Chemistry	1	same sample as used for grainsize

The average value for the parameters measured on the selected fields was calculated for each field, after which the average value for the different land uses was obtained by taking the average of the different fields with that particular land use. Because of this method there were several ways to calculate standard deviations: 1) from all measured values for a certain land use, 2) as an average of standard deviations for the different fields (neglecting between field variance) and 3) from the average values that were obtained for the different fields (neglecting within field variance). Since not all raw data were available method 3 was sometimes the only option, but, as table 4.1 shows, this means that the standard deviations in those cases were, for most land uses, based on two values only.

## 5 SEDIMENT CONCENTRATION

*'The concentration is so high that eroded sediment can be easily carried away by the flow'* Zhaohui Wan & Zhaoyin Wang, 1994

### 5.1 Introduction

Large sediment concentrations in runoff might significantly alter fluid properties and flow behaviour. Fluid density, settling velocity, viscosity, flow velocity and transport capacity might all change. Such changes are generally not considered in present day soil erosion models. Sediment concentrations in runoff on the Loess Plateau are among the highest on earth. The Yellow River even derives its name from the transported loess and is rightly called the world's muddiest river (Douglas, 1989). Therefore, if erosion models are to be applied to Loess Plateau conditions the effects of high concentrations must be considered. Sediment concentrations on the Loess Plateau increase with increasing discharge to a certain limit and remain constant after that limit has been reached (Gong Shiyang & Jiang Deqi, 1979). According to their data, the 'stable concentration' is about 800 g/l. They studied catchments ranging in size from 0.49 to 3,890 km<sup>2</sup> and found that in small catchments the stable concentration is reached at lower discharge than in large catchments. Other authors, however, report concentrations of 1000 g/l (Jiang Deqi et al, 1981, Zhang et al, 1990, Zhaohui Wan & Zhaoyin Wang, 1994) and even 1600 g/l (Long Yuqian & Xiong Guishu, 1981) and 1700 g/l have been reported (Zhaohui Wan & Zhaoyin Wang, 1994) for river flow in Yellow River tributaries.

Bradley & McCutcheon (1987) gave an overview of the effects of high suspended sediment concentrations in rivers. They showed that different authors have classified flow in different ways as a function of sediment content. A useful classification is that used by Scott (1988) and Costa (1988). They distinguished normal streamflow, hyperconcentrated streamflow and debris flow. Table 5.1 shows some characteristics of these different types of flow. In nature, a continuum of flow conditions and concentrations occurs, so that changes from one type of flow to another can be gradual. Each flow type, however, has its own specific characteristics and processes.

Normal stream-flow is a Newtonian fluid. In a Newtonian fluid the shear stress is given by:

$$\tau = \mu \cdot \frac{du}{dy} \quad (5.1)$$

Where:  $\tau$  = shear stress  
 $\mu$  = dynamic viscosity  
 $u$  = velocity  
 $y$  = level above bed  
 $du/dy$  = shear rate

Hence, for Newtonian fluids a chart of shear stress as function of shear rate will be a straight line passing through the origin. Turbulence is probably the most important process in supporting the sediment in the flow.

Table 5.1 Characteristics of different types of flow (based on Costa, 1988)

	Normal Streamflow	Hyperconcentrated Flow	Debris Flow
Fluid density (kg/m <sup>3</sup> )	1010-1330	1330-1800	1800-2300
Dirty water concentration (g/l)	16-530	530-1285	1285-2088
Fluid type	Newtonian	non-Newtonian? (likely Bingham)	Visco-plastic?
Flow type	turbulent	turbulent/laminar	laminar
Sediment support mechanism	electrostatic forces turbulence	buoyancy dispersive stress turbulence	cohesion buoyancy dispersive stress structural support

For flow that contains large amounts of sediment the flow might transform in a Bingham fluid. For Bingham fluids the shear stress can be given by (Costa, 1988; Selby, 1993; Zhaohui wan & Zhaoyin Wang, 1994):

$$\tau = \tau_b + \mu \cdot \frac{du}{dy} \quad (5.2)$$

Where:  $\tau_b$  = yield stress

Hence, for Bingham fluids a chart of shear stress as function of shear rate will be a straight line with intercept  $\tau_b$  on the shear stress axis. In other words, a certain amount of stress can be exerted without any resulting strain rate. The existence of yield stress is one of the factors that can help explain why the behaviour of hyperconcentrated flows is different from that of normal streamflow. Yield stress increases with increasing sediment concentrations. Sediment in the flow is mainly supported by buoyancy, dispersive stress and turbulence. Hyperconcentrated flows are turbulent, solid-liquid two-phase flows (Xu Jiongxin, 1999a,b). The fluid phase is formed by water with the sediment particles below 0.01 mm uniformly distributed within it. The solid phase is formed by large (larger than 0.05 mm) suspended particles.

At very high sediment concentrations, flows might transform into debris flows. At such concentrations the flow has large yield stress (or cohesion) and also internal friction.

According to Costa (1988) the shear stress for such flow may be calculated with a Coulomb-viscous model:

$$\tau = c + \sigma \cdot \tan \varphi + \mu \cdot \frac{du}{dy} \quad (5.3)$$

Where:  $c$  = cohesion  
 $\sigma$  = normal stress  
 $\varphi$  = angle of internal friction

For debris flows turbulence is usually greatly suppressed and the most important sediment supporting processes are buoyancy, dispersive stress, structural support and cohesion. Solids and water move together as a single viscoplastic body from which there is hardly any sedimentation (Selby, 1993).

Scott (1988) placed the boundaries between these three types of flow at dirty water concentrations of 530 and 1590 g/l respectively. Other authors (e.g. Xu Jiongxin, 1999b) placed the boundary between 'normal' flow and hyperconcentrated flow at the transition from Newtonian fluid to Non-Newtonian (usually Bingham) fluid. According to Xu Jiongxin this boundary is at about 300 to 400 g/l. Many of the floods on the Loess Plateau have concentrations above 400 g/l and can therefore be called hyperconcentrated flows.

Despite the different concentrations that different authors used to distinguish between the different flow types it is clear that hyperconcentrated flow occurs regularly on the Chinese Loess Plateau. Debris flows, however, are rare. Nevertheless, the high concentrations encountered in hyperconcentrated flow can have large influence on fluid properties, flow behaviour and transport capacity of the flow. The aims of this chapter are:

- To find out what the effects of very high sediment concentrations are on fluid properties and flow behaviour.
- To determine if these effects require adaptations in process based erosion models, and if so, what kinds of changes are needed.
- To find out what concentration-related corrections are necessary to compare simulation results with measured values of discharge and sediment concentration in the Danangou catchment.

## **5.2 Causes of high concentrations**

### *5.2.1 Steep slopes with loose materials*

The concentrations in runoff on the Loess Plateau are exceptionally high. Such high concentrations have not been reported from other loess areas in the world. Instead, these concentrations are comparable to those reported from some badland areas and from lahars in volcanic regions. During extreme rainfall events in mountainous regions high concentrations can also be reached (e.g. Batalla et al., 1999).

Olivier & Pebay Peyroula (1995) and Mathys (1995) reported sediment concentrations of about 500 g/l for the Terres Noires marles near Draix, southern France. These concentrations were measured after the flow passed a sedimentation pool, so that concentrations before the pool must have been higher. Mudflows with concentrations of 1500 g/l were observed in the same region. Cantón et al. (2001) reported maximum concentrations of 800 g/l for the Tabernas badlands in southern Spain.

Scott (1988) reported concentrations in lahar-runout flows of over 1000 g/l. He showed that lahars (volcanic debris flows) can be formed rapidly from normal streamflow on the steep slopes of Mount St. Helens. These steep slopes are underlain by fragmental pyroclastic debris. Further downstream, such lahars can transform to lahar-runout flows (hyperconcentrated streamflow) because of dilution by clearer water. He also found that fine-material load in hyperconcentrated flows can be highly persistent.

In the case of both badlands and lahars, erodible materials are present on steep slopes. The presence of erodible loess on the steep slopes of the Loess Plateau might therefore be one of the most important causes for the high concentrations. Slope angles in other loess regions in the world are generally less. Steep slope angles mean that the water will have high energy, since the flow of water is driven by the potential energy. Further, for loose material, the slope angle might be close to the angle of internal friction, so that such material will already almost move under the influence of gravity alone. There are indications that though steep slopes might be needed to initiate hyperconcentrated flow they are not needed to maintain this type of flow. This is due to certain feedback mechanisms that operate in these kinds of flow. These mechanisms will be discussed in chapter 5.3.

### 5.2.2 *Loess characteristics*

Another explanation for the very high concentrations observed on the Chinese Loess Plateau could be that the loess of the Loess Plateau differs from loess elsewhere. The Plateau is located in an area with a pronounced semi-arid climate. As a result there is not much water available for weathering of the loess. Table 4.10 showed that even the upper loess layers in the Danangou catchment are still very calcareous, which demonstrates that the loess is hardly weathered. Unweathered loess has a very open structure in which the silt particles are bonded to each other by calcium, soluble salts and clay minerals (Tan, 1988). These soluble salts and clay minerals are very sensitive to changes in water content, so that wetting might result in collapse of the loess structure. Furthermore, Billard et al. (2000) reported that the dissolution of soluble salts can give rise to very basic pH values, which promote the dispersion of aggregates. They reported maximum pH values of 9.1-9.3 from the western part of the Loess Plateau (Gansu Province). Messing et al. (in press a) showed that soil pH in the Danangou catchment (Shaanxi Province) is generally above 8.5. The major loess deposits of Europe and North America, however, are mostly located in temperate climates. As a result, the loess in those regions is usually weathered and decalcified in the upper part (Table 4.10), while pH is also much lower. This could explain differences in behaviour between Chinese loess and e.g. European Loess. For ploughed soils, such structural differences are probably less



important than for undisturbed soils. Still, for ploughed soils these differences in structure might cause a more rapid disintegration of aggregates in the case of the Chinese Loess Plateau.

### 5.2.3 *Climate*

The harsh climatic conditions on the Loess Plateau result in poor vegetation covers, so that the soil is not well protected. The occurrence of heavy rainstorms in summer might therefore also be an important factor in causing the development of hyperconcentrated flow. Horton (1945) mentioned two factors that might explain why this can be especially important in semiarid areas. First, in semiarid areas the soils are likely to be very dry when a storm occurs. Such soils are more susceptible to erosion because capillary forces in the soil are weak and because very dry aggregates might explode when suddenly wetted. Second, high intensity storms (characteristic of semiarid areas) tend to produce the highest rainfall intensities early on in the storm, so that the soil is still dry when this happens. According to Horton, the soil might be beaten into a semifluid mass because of this.

From these three possible causes for very high sediment concentrations in runoff, the presence of steep slopes is probably the most important one, but loess characteristics and climate are likely to play a role too. A combination of these factors therefore seems the most likely cause of the very high sediment concentrations on the Chinese Loess Plateau.

## 5.3 **Consequences of high concentrations**

High sediment concentrations can have multiple effects on the behaviour of flow and its sediment transport capacity. These effects cannot really be separated since they occur simultaneously, but for the sake of clarity they will be discussed one by one.

### 5.3.1 *Fluid density*

Fluid density increases markedly with increasing sediment concentrations. The density of fluids with different concentrations can be calculated with:

$$\rho_f = \left(1 - \frac{C_f}{\rho_s}\right) \cdot \rho_w + C_f \quad (5.4)$$

Where:  $\rho_f$  = density of fluid (kg/m<sup>3</sup>)  
 $\rho_s$  = density of solid (kg/m<sup>3</sup>)  
 $\rho_w$  = density of clear water (kg/m<sup>3</sup>)  
 $C_f$  = dirty water concentration (g/l)

Assuming that the density of water is 1000 kg/m<sup>3</sup> and the density of sediment is 2650 kg/m<sup>3</sup> a concentration of 1000g/l will result in density of 1623 kg/m<sup>3</sup>. Such high-density

flows have larger potential energy and larger momentum than clear water flow. If all other properties of the fluid would remain the same, this should result in an increase in flow velocity in comparison to clear water flow. In addition, the shear stress exerted by the flow will be larger.

### 5.3.2 Viscosity

For clear water, viscosity is a function of temperature only. According to Van Rijn (1993) dynamic viscosity can be approximated by:

$$\mu_0 = \frac{\rho_w \cdot (1.14 - 0.031 \cdot (T - 15) + 0.00068 \cdot (T - 15)^2)}{10^6} \quad (5.5)$$

Where:  $\mu_0$  = clear water dynamic viscosity (Ns/m<sup>2</sup>)  
 $\rho_w$  = clear water density (kg/m<sup>3</sup>)  
 $T$  = temperature (°C)

According to equation 5.5 the viscosity of clear water of 15°C will be 1.14\*10<sup>-3</sup> Ns m<sup>-2</sup>. Viscosity of a fluid will increase with increasing sediment concentration. Many authors have developed equations to calculate viscosity from volumetric sediment concentration. Several equations calculate viscosity from volumetric sediment content alone, but some authors (e.g. Zhaohui Wan & Zhaoyin Wang, 1994) showed that clay particles have more influence than other particles, so that both grain-size distribution and clay mineralogy should be taken into account as well. Van Rijn (1993), Hsieh Wen Shen & Julien (1993) and Zhaohui Wan & Zhaoyin Wang (1994) all reported empirical equations to calculate viscosity for sediment-laden flows. Some of the equations are reproduced here:

*Bagnold, 1954*

$$\frac{\mu}{\mu_0} = (1 + p) \cdot (1 + 0.5p)$$

$$p = \frac{1}{(0.74 / C_{vf})^{0.33} - 1} \quad (5.6)$$

*Do Ik Lee, 1969*

$$\frac{\mu}{\mu_0} = (1 - C_{vf})^{-(2.5 + 1.9 \cdot C_{vf} + 7.7 \cdot C_{vf}^2)} \quad (5.7)$$

*Krone, 1963*

$$\frac{\mu}{\mu_0} = e^{(2.5 \cdot C_{vf})} \quad (5.8)$$

Fei Xiangjun, 1982

$$\frac{\mu}{\mu_0} = (1 - 1.35 \cdot C_{vf})^{-2.5} \quad (5.9)$$

Moliboxino, 1956

$$\frac{\mu}{\mu_0} = 1 + \frac{3}{\frac{1}{C_{vf}} - \frac{1}{0.52}} \quad (5.10)$$

Where:  $\mu$  = dynamic fluid viscosity (Ns/m<sup>2</sup>)  
 $\mu_0$  = dynamic viscosity of clear water (Ns/m<sup>2</sup>)  
 $C_{vf}$  = volumetric dirty water concentration (-)  
 $p$  = concentration parameter Bagnold equation

Figure 5.1 shows viscosities calculated with these different equations for different sediment concentrations. The viscosity is expressed as the fluid viscosity divided by the clear water viscosity. Viscosities calculated with the Bagnold equation are much higher than those calculated with the other equations. The other equations give more or less the same result, except for very high concentrations, where the Krone equation starts to deviate. For concentrations of 1000 g/l viscosity is about 5 times higher than for clear water. For concentrations of 400 g/l, which on the Loess Plateau would be called moderate, the increase in viscosity is about 60%. If all other fluid properties were to remain constant an increase in viscosity should result in a decrease of flow velocity. Zhaohui Wan & Zhaoyin Wang (1994) even reported that flow in some of the Yellow River tributaries actually stops sometimes because of the increase in viscosity.

### 5.3.3 Settling velocity

Traditionally settling velocity is calculated with the Stokes equation, which can be written as:

$$\omega = \frac{2gr^2(\rho_s - \rho_f)}{9\mu} \quad (5.11)$$

Where:  $\omega$  = settling velocity (m/s)  
 $g$  = gravitational acceleration (m/s<sup>2</sup>)  
 $r$  = grain radius (m)  
 $\rho_f$  = density of fluid (kg/m<sup>3</sup>)  
 $\rho_s$  = density of solid (kg/m<sup>3</sup>)  
 $\mu$  = dynamic fluid viscosity (Ns/m<sup>2</sup>)

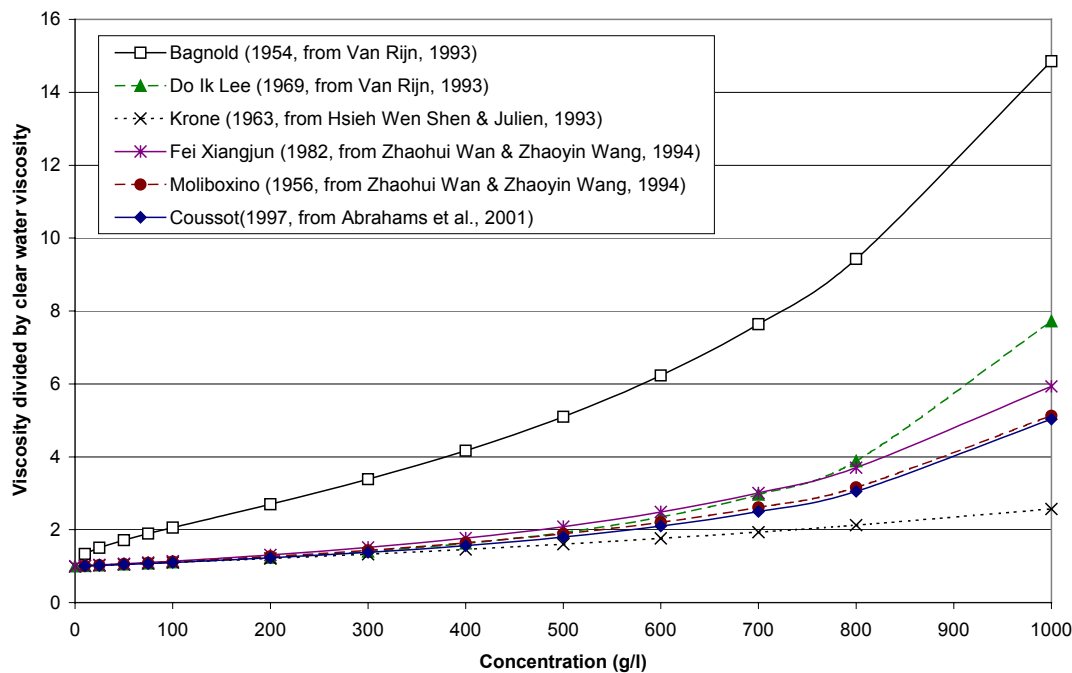


Figure 5.1 Dynamic viscosity as function of sediment concentration. Viscosity is expressed as the fluid viscosity divided by clear water viscosity. Values are for 15 degree centigrade fluid. Note that for the Bagnold and Moliboxino equations no solution is possible for zero concentration.

A for the Loess Plateau typical grainsize of 35  $\mu$  than has a settling velocity in clear water of about 1 mm/s. For water containing sediment  $\rho_f$  can be calculated with equation 5.4 and  $\mu$  with equations 5.6 – 5.10. In this way the effects of decreased submerged weight and increased viscosity can be incorporated in the Stokes equation. Increasing sediment concentrations, however, have more effects on settling velocity. With an increase in concentration settling velocity will decrease due to several effects (Zhaohui Wan & Zhaoyin Wang, 1994):

- The downward movement of particles will induce an upward movement of water, which causes a drag force on the particles
- The submerged weight of the particle decreases since the density of the fluid increases.
- The viscosity increases.
- If the fluid has become a Bingham fluid there will be yield stress.
- There is interference between the settling particles
- When there is enough clay in suspension flocculation occurs. In extremis the clay particles can form a flocculent structure that prevents the coarser particles from settling as well. Instead the settling proceeds at an extremely low pace and should be regarded as a consolidation process. Turbulence might (partially) destroy the flocculent structure, so that some particles might not settle in standing water, but will settle in flowing water.

The overall result is that for hyperconcentrated flow there is practically no settling of sediment (Gong Shiyang & Jiang Deqi, 1979, Long Yuqian & Xiong Guishu, 1981, Xu Jiongxin, 1999a,b).

Many authors have developed equations to calculate settling velocity from volumetric sediment concentration. Van Rijn (1993), Hsieh Wen Shen & Julien (1993) and Zhaohui Wan & Zhaoyin Wang (1994) all reported equations to calculate settling velocity. Some of the equations are reproduced here:

*Wan & Sheng, 1978*

$$\frac{\omega}{\omega_0} = \frac{(1 - C_{vf})^2}{1 + \frac{3}{\frac{1}{C_{vf}} - \frac{1}{0.52}}} \quad (5.12)$$

*Hawksley, 1951*

$$\frac{\omega}{\omega_0} = \xi(1 - C_{vf})^2 e^{\left(\frac{-k_1 C_{vf}}{1 - k_2 C_{vf}}\right)} \quad (5.13)$$

*Oliver, 1961*

$$\frac{\omega}{\omega_0} = (1 - 2.15 \cdot C_{vf}) \cdot (1 - 0.75 \cdot C_{vf}^{0.33}) \quad (5.14)$$

*Chien & Wan, 1983*

$$\frac{\omega}{\omega_0} = (1 - C_{vf})^b \quad (5.15)$$

Where:  $\omega$  = settling velocity in fluid (m/s)  
 $\omega_0$  = settling velocity in clear water (m/s)  
 $C_{vf}$  = volumetric dirty water concentration  
 $\xi$  = 1 without flocculation, 2/3 with flocculation  
 $k_1$  = 5/2 for spheres  
 $k_2$  = 39/64  
 $b$  = coefficient between 2.35 and 4.65

The Wan & Sheng equation makes use of the Moliboxino equation for viscosity.

Figure 5.2 shows settling velocities calculated with different equations for different sediment concentrations. The settling velocity is expressed as fraction of what the settling velocity would be in clear water. For the Hawksley equation, it was assumed that there was no flocculation, while for the Chien & Wan equation 4.65 was used as exponent. The figure shows that even for moderate concentrations (in Loess Plateau terms) of 400 g/l, and under the assumption that there is not enough clay to form a significant flocculation

structure, settling velocity already decreases to some 40%-50% of its clear water value. All equations give comparable results, only the Oliver equation deviates somewhat for low concentrations.

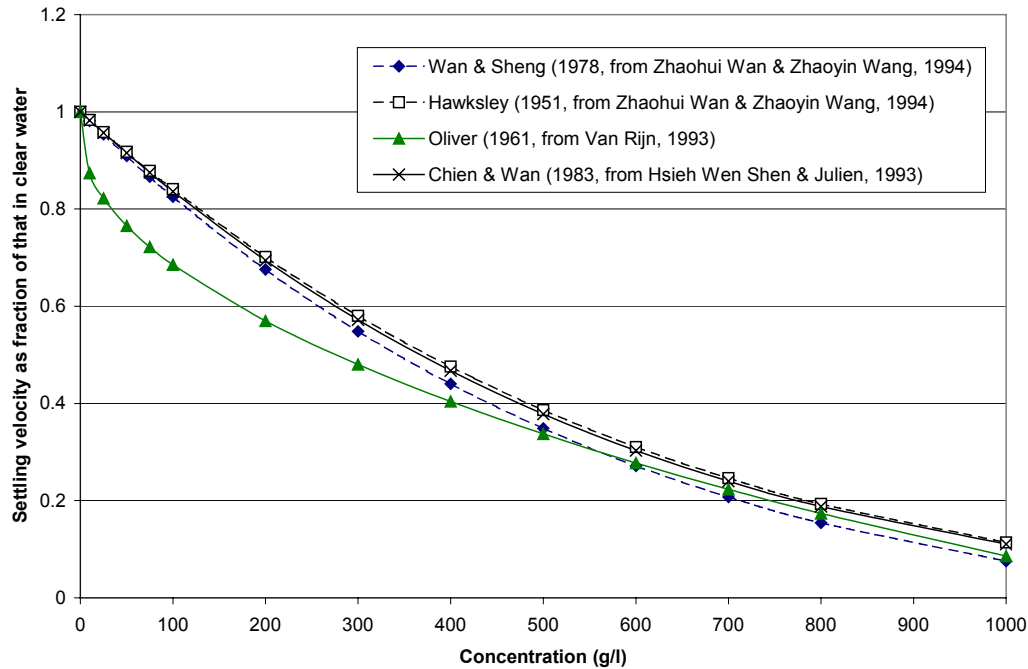


Figure 5.2 Settling velocity as a function of sediment concentration. Settling velocity is expressed as fraction of the clear water settling velocity. For the Wan & Sheng equation no solution is possible for zero concentration.

The effect of very low settling velocities should be that once sediment has been entrained by the flow there would be hardly any sedimentation out of the flow. This can be expected to result in an increase of transport rate and sediment yield. The energy needed to support the suspended sediment load is provided by turbulence. This means that the turbulence will decrease with increasing sediment load. More energy is thus used for sediment transport and less for turbulence. The net energy loss is small.

When the fluid is a Bingham fluid it has yield stress. Suspended particles exert a stress on the fluid because of gravity. If this stress is below the yield stress of the fluid the sediment will not settle at all. This load is called the neutrally buoyant load.

#### 5.3.4 Transport capacity

Xu Jiongxin (1999a) showed how, for hyperconcentrated flows, the transport capacity increases with increasing concentration. As the sediment concentration increases the fluid density increases. This results in a lower submerged density of the particles. Less energy is therefore needed to maintain this concentration and energy will be available to entrain more sediment. Zhaohui Wan & Zhaoyin Wang (1994) combined data from different Chinese sources and found that for high concentrations (above about 200 g/l) more

sediment can be carried by flows of weaker intensity. This can be attributed to a decrease in the settling velocity.

This shows that a positive-feedback mechanism is operating. Because of this feedback, there is a positive relationship between sediment concentration and suspended sediment size (expressed as D50, Xu Jiongxin 1999b, Gong Shiyang & Jiang Deqi, 1979). Another result of this feedback is that concentrations are likely to increase in the downstream direction. Zhaohui Wan & Zhaoyin Wang (1994) showed for the Chaba ravine, Dali catchment, how maximum sediment concentrations in runoff increase in the downstream direction from about 700 g/l at plot level to about 1200 g/l for the main river. In the Yellow River itself the suspended sediment concentrations can be about 600-700 g/l during the flood season. These slightly lower values might be the result of mixing with clearer waters, for example with baseflow. Hyperconcentrated flows on the Loess Plateau only occur during the flood season.

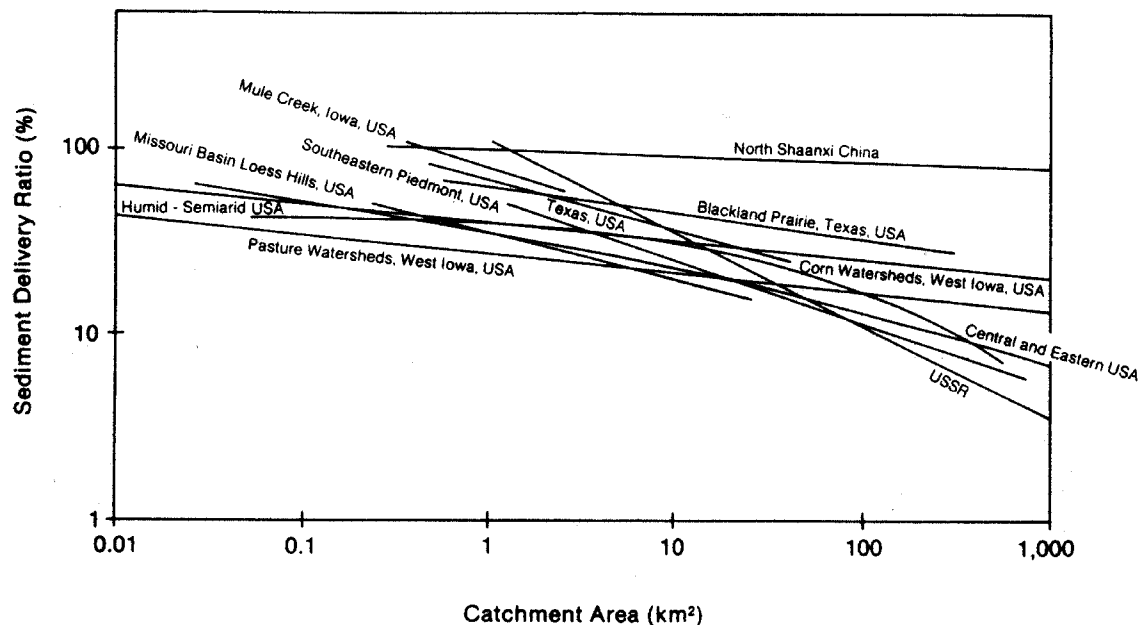


Figure 5.3 Sediment delivery ratio as a function of catchment size. Adapted from Graf (1988)

These high transport capacities result in very high sediment delivery ratios for Loess Plateau catchments. Figure 5.3 shows sediment delivery ratios for different regions as a function of catchment size. It shows that for the larger sized catchments the sediment delivery ratio for northern Shaanxi is much larger than for the other regions. According to Xu Jiongxin (1999a) the sediment delivery ratio is still almost 100% for areas as large as 10000 km<sup>2</sup>. The lower order channels on the Loess Plateau are essentially sediment-transporting channels and under natural conditions there is very little opportunity for sedimentation.

### 5.3.5 *Flow velocity and flow resistance*

High sediment contents should also have an influence on water velocity. On the one hand one would expect velocity to decrease because of increased viscosity. On the other hand the added sediment will add momentum to the flow.

Govers (1990) found a significant increase in flow velocity with an increase in sediment content for overland flow for sands with  $d_{50}$  of 218 and 1098  $\mu\text{m}$ . Flow with a volumetric sediment content of 0.32 had a velocity 40% higher than the clear water velocity. He attributed this to momentum added to the fluid by the sediment and to changes in the turbulence structure of the flow. According to Govers (1990) this phenomenon has also been long known to occur in rivers as well.

Einstein & Chien (1955) conducted a series of flume experiments with sands (median grainsize between 0.274 and 1.3 mm) and also found that average velocity increased with increasing sediment content. They suggested that this is the result of dampening of turbulence caused by the high concentrations. In their experiments, however, the sediment was concentrated in the lower part of the flow, while an increase in velocity was only found in the upper part of the flow. Their explanation, however, is probably valid, because turbulence will also be dampened in the upper part of the flow. Such dampened turbulence in the clear upper part of the flow might well result in higher velocity, but it might not give information about flows where high concentrations occur throughout the flow instead of just in the lower part.

Torri & Borselli (1991) showed that such an increase in velocity with increasing sediment content is only possible if less energy is dissipated in turbulence and friction. This means that flow resistance should decrease. Wan Zhaohui & Wang Zhaoyin (1994) discussed flow resistance and flow velocity for sediment-laden flows. According to them the flow resistance of sediment-laden flows consists of 3 parts:

- viscous resistance
- turbulent resistance
- resistance caused by bedload movement and bed configuration

They also distinguished between flows that carry only fines (pseudo one phase flow) and flows that carry fines as well as coarse material (sediment laden flow). For the flow carrying only fines, bedload is not important and resistance only consists of viscous resistance and turbulent resistance. As sediment content increases, viscous resistance increases, while turbulent resistance decreases. The net effect seems to depend on whether the bed is rough or smooth and whether the flow is laminar or turbulent. As a result, there need not be a decrease in resistance with increasing sediment content. According to Wan Zhaohui & Wang Zhaoyin (1994), there even usually is an increase in resistance with increasing concentration. In the case of sediment laden flow resistance caused by bedload transport and bed configuration can decrease with increasing sediment content if the higher concentration causes the flow to transport more coarse material as suspended load instead of bedload. The bed should then become smoother and the



resistance would be less. Wan Zhaohui & Wang Zhaoyin (1994), however, did not discuss what happens if bed material is so large that it cannot be transported as suspended load. In that case the bed would not become smoother and resistance might not decrease. Wan Zhaohui & Wang Zhaoyin (1994) also stated that as long as the flow remains fully turbulent the resistance to flow will be the same for Newtonian and Bingham fluids.

Thus, the effect of high concentrations on resistance remains unclear. The effect on flow velocity is therefore likewise unclear.

According to Bradley & McCutcheon (1987) the Manning and Chezy equations are only applicable when it can be assumed that the velocity distribution over depth is log-linear. According to them available data on the velocity distribution in hyperconcentrated flows contradict each other and the use of Manning's equation under such circumstances is therefore doubtful. Wan Zhaohui & Wang Zhaoyin (1994) showed how the velocity profile in hyperconcentrated flows depends on the flow being laminar or turbulent. In laminar flow of a Bingham fluid the shear stress will be lower than the yield stress for the upper part of the flow. There is therefore no velocity gradient and plug flow is developed. On the other hand, in turbulent flow the velocity profile generally remains logarithmic, even though the Von Karman constant might be different than for clear water.

#### 5.3.6 Discussion

From the preceding sections it is clear that large sediment concentrations in rivers may have considerable influence on a whole range of flow characteristics.

The effects can sometimes be unexpected and contradictory to accepted concepts in erosion modelling. For example, the observation that sometimes particles will not settle in standing water while they do settle in flowing water is unusual. Likewise, it was shown that transport capacity might increase with increasing sediment concentration. This obviously undermines the concept of transport capacity as normally used in erosion modelling. There, transport capacity is assumed to depend only on flow characteristics, while entrainment is usually modelled as a function of the difference between transport capacity and concentration.

The effects are also complex and hard to separate from each other. In addition, it seems likely that some effects will partly cancel each other out. For example, higher viscosity should decrease flow velocity, while higher density should increase it. Obviously, erosion models that want to deal with high concentrations should at least consider these effects.

### 5.4 Streamflow in the Danangou catchment

The maximum dirty water concentrations measured at the dam in the Danangou catchment were about 500 g/l (table 4.10), in the Yan River they were around 600 g/l. The concentrations are thus high, but in Loess Plateau terms not extremely high. This section will discuss how these high sediment contents were taken into account during

processing of measurement data and what the consequences are for modelling soil erosion in the catchment.

#### *5.4.1 Velocity and discharge*

The high sediment concentrations in the Danangou catchment could influence the discharge coefficient for the weir. As described in chapter 4 discharge at the weir in the Danangou catchment was measured with an equation based on the law of Bernoulli. The resulting equation (equation 4.7) also contains a correction factor that, among other things, depends on viscosity. The correction factor supposedly does not depend on fluid density. In the Danangou catchment viscosity is likely to be the most important factor to make the use of a correction factor necessary as high sediment contents will increase viscosity. Since bed material is so coarse that it cannot be transported as suspended material there is no reason to suppose that resistance caused by bed material will decrease with increasing sediment concentration. Sediment content in this region can be as high as 1000g/l and this can change viscosity considerably. Figure 5.1 shows that for such sediment concentrations viscosity could be about 5 times higher than for clear water. Data about the relationship between viscosity and discharge coefficient are however hard to find.

It seems, nevertheless, prudent to take viscosity into consideration, as the sediment contents encountered on the Loess Plateau could well be outside the range normally considered in the determination of the discharge coefficient. Increasing viscosity should decrease velocity. This would result in a lower discharge coefficient. A discharge coefficient of 0.9 is therefore used instead of the 0.95 that was suggested in chapter 4. Introducing a sediment content (hence viscosity) dependent coefficient instead of a constant (0.9) would be preferable, but insufficient data about the relationship between viscosity and discharge coefficient were available for this.

During the event of July 20<sup>th</sup>, 1999, surface velocity at the weir was measured. Plastic bottles partially filled with sediment were thrown into the stream upstream of the weir. The sediment was needed to be able to throw the bottles far enough, and also it was hoped that by using the sediment the bottles would flow more upright and be better visible. It was measured how long it took the bottles to travel a distance of 40 metres. Observations showed that most of the bottles were held up for some time along the way. Therefore, the fastest bottles were assumed to be most representative of flow velocity. The measurements gave a surface flow velocity of about 2 m/s. Since water levels were known from the ultrasonic sensor, discharge can be estimated as the product of wetted area and average velocity. The method is not very accurate, and moreover, average velocity is not equal to surface velocity, but the data nevertheless indicated that the discharges obtained from equation 4.7 with a correction factor of 0.9 were about right. Hence, a further viscosity correction was apparently not needed for velocity.

#### 5.4.2 Sediment content

As mentioned before sediment content of the discharge can become very high in the Danangou catchment. This not only influences viscosity, but also water level itself. Sediment contents up to 1000 g/l of fluid have been measured in the region. If a particle density of 2650 g/l is assumed this gives a sediment volume of 38%. Maximum concentrations measured at the dam are about 500 g/l. As this is suspended load, it can be expected that sediment velocity equals water velocity. In that case sediment volume can just be subtracted from fluid volume to give water volume. Note that this would not be possible if sediment velocity and water velocity are not equal (Govers, 1992a). Govers also summarized some results from studies on this subject, which were carried out for sheetflow. The quoted results were partially contradicting, which reflects the scantiness of our knowledge on this subject. Because of this Govers decided not to use a correction at all, so how to correct remains a question. For the discharge calculation in the Danangou catchment the discharge coefficient was first adapted (as described above) to calculate the fluid velocity and discharge. Calculated discharge was then corrected to clear water discharge by subtracting the sediment discharge. An alternative would be to first correct water level and then calculate discharge, as described by Steegen & Govers (2001). This approach was not used here because the discharge equation is highly sensitive to fluid level, so that using a corrected clear water level instead of the actual fluid level might well result in an underestimate of discharge. The following equation was used to correct discharge:

$$Q_w = \left(1 - \frac{C_f}{\rho_s}\right) \cdot Q_f \quad (5.16)$$

Where:  $Q_w$  = clear water discharge (m<sup>3</sup>/s)  
 $Q_f$  = fluid discharge (m<sup>3</sup>/s)  
 $C_f$  = dirty water concentration (g/l)  
 $\rho_s$  = particle density (2650 kg/m<sup>3</sup>)

The effects of this correction are shown in figure 5.4 for the event of July 20<sup>th</sup>, 1999. This correction is necessary to be able to evaluate the relationship between precipitation and discharge for areas with high sediment contents and also because the results from soil erosion models are expressed as clear water discharges. These erosion models also express concentration as gram per litre of clear water. Since measured concentrations are expressed as gram per litre dirty water a correction is necessary. Sediment discharge can be calculated with:

$$Q_{sed} = C_f \cdot Q_f = C_w \cdot Q_w \quad (5.17)$$

Where:  $Q_{sed}$  = sediment discharge (kg/s)  
 Corrected concentration can then be calculated with:

$$C_w = \frac{Q_{sed}}{Q_w} \quad (5.18)$$

or:

$$C_w = \frac{C_f}{\left(1 - \frac{C_f}{\rho_s}\right)} \quad (5.19)$$

When the correction proposed in equations 5.16 and 5.19 are applied simulation results can be compared to field measurements.

When the ultrasonic sensor did not function the data from the pressure transducer had to be used (see chapter 4). In that case equation 5.16 should also be applied, but before this is possible the water level should be calculated from the pressure transducer signal. The output of the pressure transducer is a level that is based on the assumption that the density of the fluid is  $\rho_w$  (density of clear water), while in fact it is  $\rho_f$  (density of the fluid with sediment). To correct for this the pressure has to be calculated from the level given by the sensor using  $\rho_w$ . Then the 'fluid level' can be calculated with  $\rho_f$ . The procedure is as follows:

$$P = \rho_w g H_w \quad (5.20)$$

And also:

$$P = \rho_f g H_f \quad (5.21)$$

Hence,

$$H_f = \frac{\rho_w}{\rho_f} \cdot H_w \quad (5.22)$$

Where:  $P$  = pressure (N/m<sup>2</sup>)  
 $H_w$  = water level from sensor (m)  
 $H_f$  = corrected level fluid (m)  
 $\rho_w$  = density of clear water (kg/m<sup>3</sup>)  
 $\rho_f$  = density of fluid (kg/m<sup>3</sup>, can be calculated with 5.4)

Then discharge can be calculated using  $h_c = H_f$  in equation 4.7. Finally, equation 5.16 can be applied.

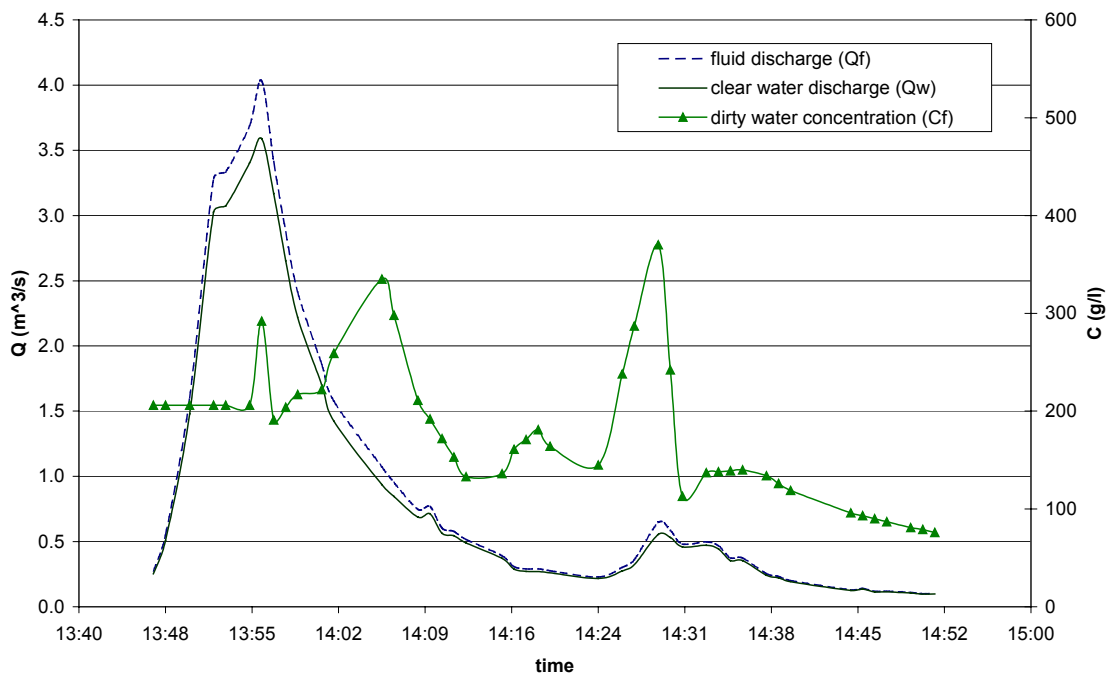


Figure 5.4 Measured discharge and concentration & sediment corrected discharge for the event of July 20<sup>th</sup>, 1999

#### 5.4.3 *Settling velocity*

Settling velocity as a function of concentration could not be measured. Since all reported equations (figure 5.2) yielded similar results it seems likely that these equations could also be applied for the Danangou catchment. Grainsize analysis of sediment samples taken at the dam indicated that the amount of clay-sized particles was not much more than 10%. It was therefore assumed that no flocculation structures developed, so that a settling velocity correction based on D50 sufficed. Literature data show that for the sediment concentrations measured in the catchment the settling velocity is significantly decreased. Concentrations of around 400 g/l have been measured repeatedly. Figure 5.2 shows that for such concentrations settling velocity is already half its clear water value. Therefore an equation relating settling velocity to sediment content should be implemented in erosion models.

### 5.5 **Overland flow in the Danangou catchment**

Both at the gully-flume and at the sediment plot high dirty water concentrations were measured, at the gully-flume 600 g/l (table 4.11), at the plot about 750 g/l (table 4.12). Both flumes are H-flumes that were constructed according to literature instructions (Bos, 1989).

### 5.5.1 *Velocity and discharge*

The discharge equations of H-flumes are based on previous calibrations. This should mean that if the flume is constructed according to the literature instructions the discharge equation is the same as given in the literature. Like for the weir, however, high viscosity might decrease the discharge in comparison to the calibration conditions, while on the other hand higher density and momentum might increase it. The net effect for the discharge equation could in principle be evaluated by comparing the calculated total discharge (from the sensor data) with the total discharge amounts that have been collected using the divisor system (see chapter 4). Assuming that all water was collected in the barrels a difference in total discharge as calculated from the barrel-data and from the water level data could be ascribed to the effect of viscosity. In practice, however, this will not be possible because of uncertainty about measured water level data, sediment levels in the flumes and concentration in the barrels. The discharge equations were therefore not changed.

### 5.5.2 *Sediment content*

After an event there is usually a layer of sediment present in the flumes, as shown in figure 5.5. Cantón et al. (2001) tried to solve similar problems by using tilted false floors in their flumes in the Tabernas badlands of southern Spain. This, however, was only partially successful and they were forced to correct the falling limbs of the measured hydrographs. In the Danangou catchment this was also necessary. To be able to determine discharge from the sensor signal one needs to know when the sediment layer developed. Because of the assumption that the discharge equations are correct the total discharge from the barrels can be used to guess at the build-up of sediment. The procedure is to estimate sediment levels during the event based on the levels observed in the flume after the event. By changing the timing of sediment-buildup the total amount of discharge changes and can be made to fit the observed barrel-totals as closely as possible. In this process two assumptions were adopted:

- 1) That sediment build-up always started after the runoff-peak
- 2) That the hydrograph should maintain a probable shape, i.e. that it will show an approximately exponential decrease after the peak.

Figure 5.6 shows the results of this procedure for the event of 990710. As can be seen from the figure the measured water level levelled off at about 0.018 m (1.8 cm). This was assumed to be due to a sediment layer of that thickness in the flume. Measurements of the sediment level on the day after the event gave an average sediment level of 1.35 cm in the flume, while at the sensor the sediment thickness was above average. To assume a sediment level of 1.8 cm was therefore acceptable.

Discharge was calculated by applying the discharge equation of the flume (equation 4.9) to the uncorrected measured water level and to the estimated sediment level. Discharge was then calculated as discharge from the uncorrected measured water level minus the hypothetical sediment discharge. This is necessary because of the v-shaped aperture of an



Figure 5.5 Thick sediment layer (about 10 cm) in the gully-flume after the event of 980712. At this time the barrels below the flume had not yet been installed. Picture by E. van de Giessen and J. Snepvangers

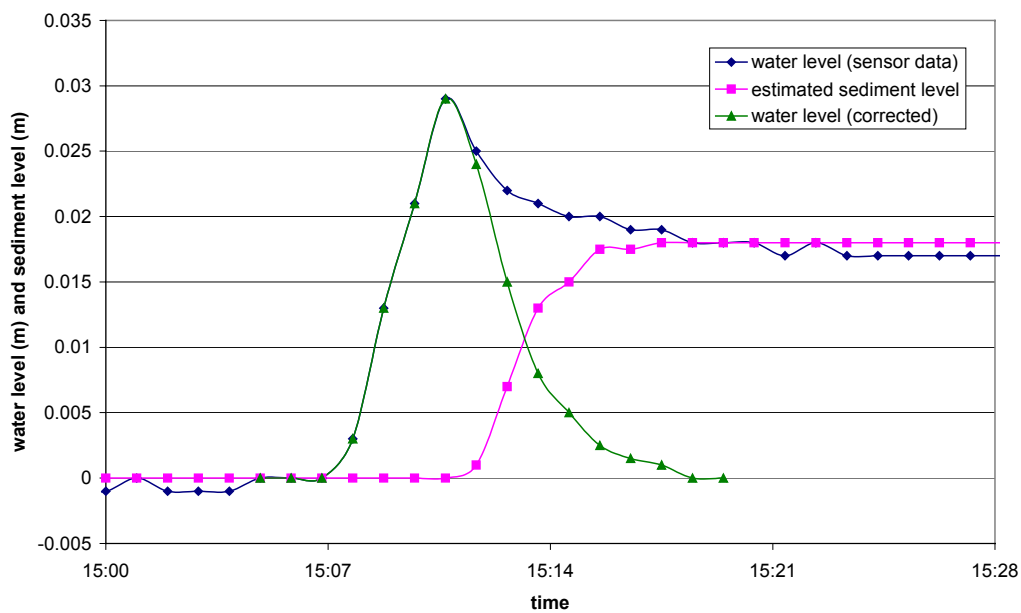


Figure 5.6 Measured water level, estimated sediment level and corrected water level for the event of 990710, sediment plot

H-flume (see figure 5.5). If the discharge equation were applied to the corrected water level discharge would be too low because the water is not flowing over the bottom of the flume, but over the sediment that deposited inside the flume. After the discharge was calculated with the discharge equation, it was corrected to clear water discharge using equation 5.16. Because no timeseries of sediment concentrations were available for the

sediment plot the average concentration as determined from the barrels was used. For the gully-flume the data collected with the turbidity sensor could not be used because concentrations were far outside the range of the sensor (chapter 4), so that for the gully-flume the barrel data should also be used. Finally, concentrations expressed in gram per litre clear water were calculated in the same way as described for the weir (equation 5.19).

### 5.5.3 *Settling velocity*

Application of the Stokes equation (equation 5.11) for the conditions of the Danangou catchment ( $d_{50}$  about 35  $\mu$ ) showed that settling velocity in clear water would be about 1 mm/s. Considering the concentrations measured at the flume real settling velocity could be about half that, i.e. 0.5 mm/s. This shows that settling velocity reduction is not likely to be important in shallow flows with depths of several millimetres only.

## 5.6 **Conclusions**

High sediment concentrations are a characteristic feature of the Loess Plateau. These high concentrations are probably caused by a combination of factors, in particular the occurrence of erodible materials on steep slopes, the structure and chemical constitution of the loess and the harsh climate that causes plant cover to be low.

When sediment concentration increases fluid density increases, viscosity increases and settling velocity decreases. The effect of this becomes increasingly important with increases in concentration and can result in flow behaviour that is quite different from that of normal streamflow. For large concentrations transport capacity might for example increase. The net effect of these changes on the flow is not always evident, for example the effect on flow velocity and flow resistance remains unclear. Despite this, erosion models that are dealing with high sediment concentrations cannot afford to neglect these effects altogether.

The data collected in the Danangou catchment indicate that even though sediment concentrations were considerable this did not change the fluid flow to such extent that special adaptations are needed to soil erosion models such as LISEM. A number of corrections are, however, necessary to be able to compare field measurements with results of soil erosion models. For the weir sediment volume should be subtracted from runoff volume and a density correction is needed to use data from the pressure transducer. For the flumes, the measured water level should be corrected by subtracting the sediment level in the flume from the water level, while the sediment volume should also be subtracted from the discharge. Finally, measured concentration should be corrected to give concentration expressed as gram per litre clear water.

Literature data show that for the sediment concentrations occurring in the catchment the settling velocity will be significantly reduced, so that soil erosion models should be adapted to incorporate a correction for settling velocity.



## 6 FLOW VELOCITY

*Based on: Hessel, R., Jetten, V. & Zhang Guanghui (in press) Estimating Manning's  $n$  for steep slopes. Catena*

### 6.1 Introduction

Hydrological and soil erosion models need to calculate the flow velocity to be able to simulate the flow of water over the land surface. These models generally use a separate water balance for each spatial element, in which the water depth available for runoff is calculated by subtracting interception, infiltration and surface storage from precipitation. Several equations are available to calculate overland flow velocity from this water depth. The most widely used of these equations are the Darcy-Weisbach and Manning equations.

Most field and laboratory studies on overland flow seem to use the Darcy-Weisbach  $f$ , whilst most studies of channel flow use Manning's  $n$ . This division, however, is not clear-cut, as the choice for either formula is also influenced by personal preference. Furthermore, there is no reason to assume major differences in results between the two methods. Both are calculated from the same variables and both suffer from the limitations of having to characterise flow patterns that are highly variable in space and time. On hill slopes, overland flow will occur as a shallow sheet of water, with faster flowing, diverging and converging flow threads around obstacles. Flow depth and velocity will therefore be highly variable in space. Abrahams et al. (1990) studied Darcy-Weisbach  $f$  for desert hill slopes and found that it varies with the rate of flow. Since the rate of flow is highly variable in space, so too is  $f$ . Resistance to flow will also be variable in time, as it depends on continuously changing flow conditions. This dependence is often expressed by developing relationships between the Darcy-Weisbach  $f$  and Reynolds number (e.g. Abrahams et al., 1990, Gilley et al., 1992). As Takken & Govers (2000) have noted, Manning's  $n$  is likely to behave in the same way as  $f$ . The flow will also tend to concentrate in the downslope direction, which is likely to decrease resistance to flow in that direction (Abrahams et al., 1990).

Contrary to field studies, most hydrological and soil erosion models use Manning's  $n$ , probably because the literature provides more data for  $n$  than for  $f$ . Another reason could be that the use of Manning's equation for overland flow is more or less accepted, while Darcy-Weisbach appears not to have been used for streamflow. It is obviously preferable to use only one equation for any one model application, and the choice for Manning's equation in modelling is therefore generally accepted. Table 6.1 shows some literature values for Manning's  $n$ . Morgan et al. (1998b) used the same values for Manning's  $n$  in the case of overland flow and channel flow. They stated, however, that the values for overland flow are likely to be relatively close to the 'high' value mentioned by them.

Table 6.1 Literature values of Manning's  $n$ 

Land use	Source <sup>a</sup>	Low	Mean	High
Mountain streams	1	0.030	0.040	0.050
Major rivers	1	0.035		0.100
Concrete or asphalt	3	0.010	0.011	0.013
Bare soil	2	0.010	0.020	0.030
Bare cropland	1	0.020	0.030	0.040
Fallow – no residue	3	0.006	0.050	0.160
Mature row crops	1	0.025	0.035	0.045
Mature field crops	1	0.030	0.040	0.050
Wheat	2	0.100	0.125	0.300
Sorghum	2	0.040	0.090	0.110
Short grass	1	0.025	0.030	0.035
Short Bermuda grass	2	0.030	0.046	0.060
Long Bermuda grass	2	0.040	0.100	0.150
Natural rangeland	3	0.100	0.130	0.320
Scattered brush	1	0.035	0.050	0.070
Dense brush (summer)	1	0.070	0.100	0.160

<sup>a</sup> 1: Ven Te Chow (1959), 2: Morgan et al. (1998b), 3: Engman (1986)

Engman (1986) summarised a number of studies on friction factors. The effects of rainfall, tillage and vegetation on friction factors have all been studied. Despite this, considerable uncertainty about the values of friction factors remains. An important subject of discussion is the applicability of the friction factors to different types of flow. Two distinctions in flow type deserve attention: laminar versus turbulent (defined with  $Re$ ) and sub-critical versus super-critical (defined with Froude number,  $Fr$ ). Ven Te Chow et al. (1988), for example, stated that Manning's equation is only valid for fully turbulent flow, when Darcy-Weisbach  $f$  is independent of Reynolds number. Abrahams et al. (1990), Gilley et al. (1992) and Nearing et al. (1997) found many different relationships between  $f$  and  $Re$  for overland flow, but apparently there was always some dependency. Similarly, the Manning and Darcy-Weisbach equations have been applied to laminar flow, and not always with different values for the friction factor than used for turbulent flow (Engman, 1986). The distinction between sub-critical and super-critical flow has received much less attention (if any). This is surprising since super-critical flow has both smaller water depth and larger velocity than sub-critical flow at the same discharge. This is contrary to the Manning and Darcy-Weisbach equations since both predict that if water depth is smaller velocity should be smaller. Thus, either  $n$  and  $f$  should be smaller for super-critical flow, or the equations would not be applicable at all. Nearing et al. (1997) performed a series of experiments in which both sub-critical and super-critical flow occurred. In some cases they found different relationships between  $f$  and  $Re$  for laminar and turbulent flow, but they paid no attention to the distinction

between sub-critical and super-critical flow. However, for their uniform sand experiments they found a clear increase of  $Fr$  with an increase of  $Re$  as well as a decrease of  $f$  with an increase of  $Re$ . Thus,  $f$  decreased with increasing  $Fr$ . Giménez & Govers (2001) did not question the applicability of Manning's equation for their super-critical flow. Their data for non-eroding rills show that  $Fr$  increased from sub-critical values to super-critical values with an increase in slope angle from 3 to 12 degrees, but that Manning's  $n$  was independent of slope angle. Thus,  $n$  was apparently independent of  $Fr$ . These different studies suggest that the Manning and Darcy-Weisbach equations can be applied to all types of flow, but that the values of the friction factors might be different for different flow conditions.

Ven Te Chow (1959) noted that Manning's  $n$ , which is often assumed to be constant, can actually vary for a number of reasons. The same will be true for Darcy-Weisbach  $f$ . The dependency of  $n$  and  $f$  on flow conditions has already been discussed above. Some other factors that can cause Manning's  $n$  to vary are (Ven Te Chow, 1959):

- Vegetation. The effect of vegetation on Manning's  $n$  depends on height, density, distribution and type of vegetation. Petryk & Bosmajian (1975) developed equations to calculate Manning's  $n$  as a function of flow depth and vegetation density for partially submerged vegetation. They found that if the vegetation density over height is constant Manning's  $n$  will increase with increasing flowdepth. Jin et al. (2000) tested these equations with flume experiments in which vegetation was simulated with propylene bristles. They found that the equations performed well. It should be noted that these equations only apply when flow depth is smaller than vegetation height. If this is not the case Manning's  $n$  usually decreases with increasing water level because of increasing submergence and because of bending plants (Petryk & Bosmajian, 1975).
- Silting and scouring. According to Ven Te Chow (1959) silting generally smoothens the channel so that Manning's  $n$  becomes lower, while scouring increases Manning's  $n$  because the channel becomes rougher.
- Stage and discharge. Manning's  $n$  usually decreases with increasing water level, at least if the roughness elements are fully submerged. In fact, the degree of submergence of obstacles determines whether roughness increases or decreases with increasing stage, as found by e.g. Abrahams et al. (1990), Gilley et al. (1992) and Takken & Govers (2000).
- Suspended material and bedload. Suspended material and bedload consume energy and cause head loss, so that Manning's  $n$  should be higher. Chapter 5, however, showed that there are also indications that the transport of suspended material does not cause head loss. Which is true probably depends on local flow conditions.

If friction factors are measured under natural conditions the values that are obtained are effective friction factors, since they include effects of raindrop impact, flow concentration, litter, crop ridges, rocks, tillage roughness, frictional drag and erosion and transport of sediment (Engman, 1986). However, from a viewpoint of simulating the hydrograph, such an effective friction factor is adequate. Determining Manning's  $n$  from field plots is complicated by the fact that assumptions about infiltration are needed.

Engman (1986) assumed a constant infiltration rate, while Mohamoud (1992) modelled infiltration with the Philips equation. Both used rainfall experiments on plots, so that even without infiltration discharge would not be constant along the plot. Runon-experiments, on the other hand, neglect the effect rainfall might have on the friction factor. These problems are almost unavoidable for field measurements. Values of friction factors obtained from laboratory experiments are, however, difficult to compare to field conditions. Emmett (1970), for example, found a tenfold increase in resistance on natural plots compared to laboratory plots. If the objective is to use erosion models, it is appropriate to use effective friction factors obtained for field conditions.

Research into the flow resistance on slopes as steep as in the Danangou catchment has been scant. Abrahams et al. (1990) measured  $f$  values on slopes of  $6 - 33^\circ$ , but they focussed on soil roughness effects and did not investigate the effect of slope itself.

The aims of the research project described in this chapter were the following. 1) To evaluate the use of Manning's equation for steep slopes. For this purpose, Manning's  $n$  was measured on slopes ranging from 6 to 64%. 2) To find out if Manning's equation can be used or if the Darcy-Weisbach equation is more suitable because of its relationship with the Reynolds number. 3) To obtain values of Manning's  $n$  or Darcy-Weisbach  $f$  for different types of land use in the Danangou catchment. The values obtained for different land uses and slopes were intended to be used as input for soil erosion models.

## 6.2 Experimental setup

Manning's  $n$  was measured using 2.5 by 0.4 m plots. The setup of the measurements is shown in Figure 6.1. Water was evenly applied to the top of the plot using a small, horizontally placed gutter. No rainfall was applied. Discharge could be regulated using the tap on the bucket above the gutter. The water level in the bucket (and hence the discharge) could be kept reasonably constant with the help of two Mariotte bottles with a volume of 25 litres each. Discharge was measured at the bottom of the plot by recording the water level in a bucket every 15 seconds. Low earthen walls were used as the boundaries of the plot, since these disturb the natural water flow less than metal sheets, which tend to result in concentrated flow along the boundaries of the plot. Water velocity was measured over a 2 m stretch, either every 30 seconds or every minute (depending on the velocity), using dye tracer. The leading edge of the dye cloud was used, so that the resulting measurement represented surface water velocity. Measuring over a stretch of 2 m was necessary to achieve sufficiently accurate time measurements. The actual flow width was measured with a ruler at several cross-sections along the length of the plot. The measurement required three people: one to check time and record the measurements, a second to inject the tracer and to keep track of its progress and a third to watch the water level in the bucket. The first person could generally also check the performance of the Mariotte bottles.

As one of the aims of the present study was to obtain input values of Manning's  $n$  for use in modelling, the plots were left intact as much as possible. No vegetation or litter was removed, as these would also be present in natural conditions during rainstorms.

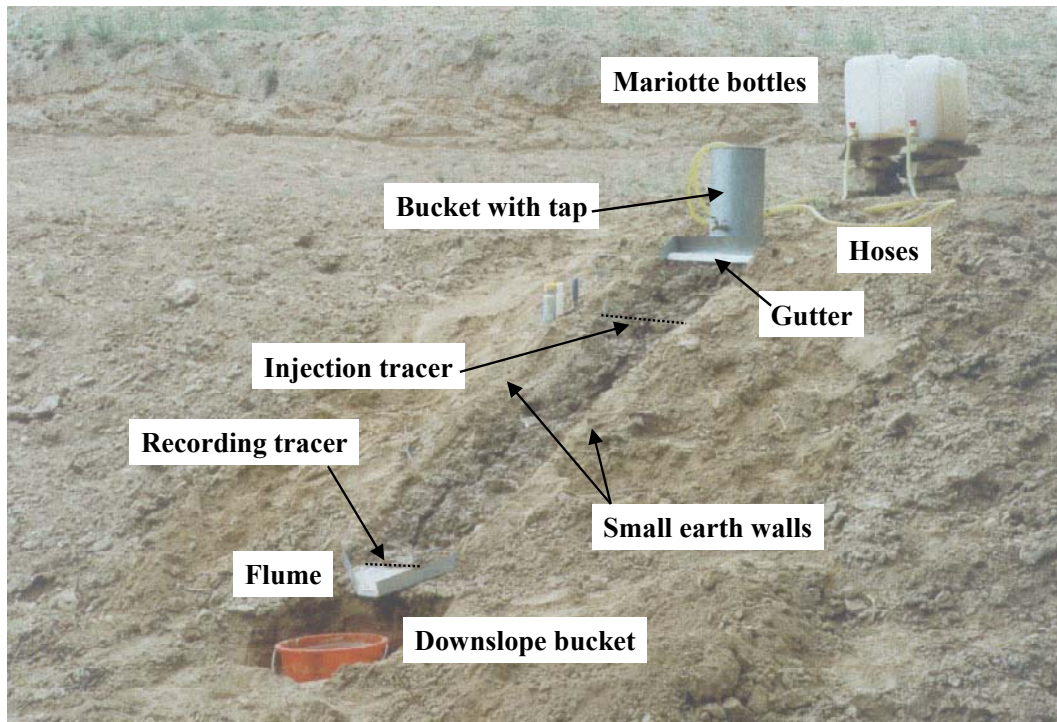


Figure 6.1 Setup of measurement 3 of the second series (2000). See Table 6.2 for plot characteristics

Before measurements started, the plot was prewetted until the wetted area of the plot no longer changed visibly. This was necessary to ensure a steady state flow during the measurement. Each measurement consisted of three runs, each lasting 10 minutes. About 40 litres of water were normally used in each run. As long as the water did not become too dirty from sediment and tracer, some of it was recycled for the next run. Nevertheless, the distance from available water sources limited the selection of possible locations for measurement. Total plot erosion could also be determined by measuring the sediment levels in the buckets at the lower end of the plot after the experiment had been completed.

Manning's  $n$  was calculated whenever the velocity was available, using running 1-minute averages of discharges. As the runs lasted 10 minutes each, only velocity measurements between 30 seconds after the start of the run and 30 seconds before the end of the run could be used. Manning's  $n$  was calculated in the following way:

$$n = \frac{R^{2/3} \cdot S^{1/2}}{v} \quad (6.1)$$

Where:  $R$  = hydraulic radius (area ( $A$ )/wetted perimeter ( $P$ )) in metres  
 $S$  = slope (sine of slope angle)  
 $v$  = average velocity (m/s)

Darcy-Weisbach  $f$  can be calculated from the following equation:

$$f = \frac{8 \cdot g \cdot R \cdot S}{v^2} \quad (6.2)$$

Where:  $g$  = acceleration due to gravity ( $\text{m/s}^2$ )

The area ( $A$ ) is given by discharge divided by mean velocity. Under the assumption of rectangular channels, dividing  $A$  by the measured width gives the water depth ( $h$ ).  $P$  is then equal to the sum of the width and twice the water depth. To calculate mean velocity, measured velocities are usually corrected as the dye measurements indicate surface velocity, rather than average velocity (Emmett, 1970, Abrahams et al., 1986, Li & Abrahams, 1997, Takken & Govers, 2000). Calculated Reynolds numbers suggested that the flow was laminar or transitional (see chapter 2). For laminar flow the correction factor would be 0.67, while for transitional flow it would be about 0.7 (Abrahams et al., 1986). All measured velocities were multiplied by 0.7 to obtain mean velocities. Thus, 7 - 18 values for Manning's  $n$  were usually obtained for each run. The differences between the runs were usually small, so the final Manning's  $n$  for the plot was calculated by taking the average of all values.

In 1999, Manning's  $n$  was measured on 28 plots, 16 of which were croplands. In most cases, two measurements were conducted in each field, using plots with different slope angles. This was done to investigate the effect of slope angle on flow resistance. In some cases, two plots of different lengths (2.5 and 1 m) but with the same slope angle were used. This was done for two reasons: to try and limit water use and to find out if flow concentration on the longer plots would result in lower values of Manning's  $n$ . In 2000, an additional series of measurements was conducted on 34 plots, 18 of which were croplands. Since the 1999 measurements had yielded no differences for different plot lengths, all experiments in 2000 were conducted on 2.5 m plots. The 1999 and 2000 measurements are referred to below as the first and second series, respectively. Table 6.2 summarises the plot characteristics.

Plant cover was estimated from a vertical viewpoint. It therefore included leaf cover for ground vegetation (but not for trees). Plant cover is not equal to cover at ground level, which is much lower because the cover of plant stems is lower than that of the leaves. The number of individual plants on the cropland plots (all  $1 \text{ m}^2$ ) was generally below 10 and at these concentrations the presence of plants did not seem to impede flow. In both years, the soil surface of the cropland plots had been ploughed some weeks before measurement and a slight crust had formed in most cases. On a few plots, weeds had been recently removed (Table 6.2), and in these cases the crust had been broken locally. The orchard plot had been weeded, but not ploughed. The other plots had remained undisturbed. Litter cover was incorporated in the soil cover estimations.

Table 6.2 Plot characteristics. The soil surface for the cropland plots showed slight crusting, unless otherwise stated

Land use	First series (1999)					Second series (2000)				
	Crop type	Plot Number	Slope (%)	Cover (%)	Comments	Crop type	Plot Number	Slope (%)	Cover (%)	Comments
Cropland	Maize & bean	3a	19	30		Pearl millet	3	44	0	thin crust
Cropland	Maize & bean	3b	40	30		Pearl millet	4	9	1	thin crust
Cropland	Sunflower & bean	5a	25	6		Maize	6	19	1	
Cropland	Sunflower & bean	5b	13	10		Maize	8	56	1.5	
Cropland	Foxtail millet	6a	14	4	weeding	Maize	9	32	5	
Cropland	Foxtail millet	6b	30	8	weeding	Maize	12	40	5.5	
Cropland	Potato	7a	55	4		Maize	13	46	5.5	
Cropland	Potato	7b	28	5		Pearl millet & bean	14	25	32	weeding
Cropland	Soy bean	8a	27	10		Pearl millet & bean	15	13	7	weeding
Cropland	Soy bean	8b	13	5		Pearl millet	16	51	4.5	
Cropland	Pearl millet	10a	38	10	weeding	Pearl millet	25	11	4	
Cropland	Pearl millet	10b	46	10	weeding	Pearl millet	26	9	7.5	
Cropland	Potato	11a	36	8	weeding	Maize	29	15	5.5	
Cropland	Potato	11b	47	5	weeding	Maize	30	29	8.5	
Cropland	Foxtail millet	12a	6	3	weeding	Potato	31	36	15.5	
Cropland	Foxtail millet	12b	7	5	weeding	Potato	32	62	15	
Cropland						Potato	33	7	5.5	weeding
Cropland						Pearl millet	34	7	1	
Fallow		9a	27	2			19	33	5.5	
Fallow		9b	44	1			20	42	6	
Fallow							22	16	61	
Fallow							23	8	32	
Orchard		2a	34	5			21	52	3	
Orchard		2b	34	4						
Wasteland		4a	62	25			18	44	26	
Wasteland		4b	62	20			27	57	21	
Wasteland		14a	54	25			28	61	30.5	
Wasteland		14b	54	35						
Woodland		1a	34	42			1	64	15.5	
Woodland		1b	34	44			2	52	5	
Woodland		13a	22	86			5	38	46	
Woodland		13b	23	44			7	18	27.8	
Woodland							10	22	36.2	
Woodland							11	30	7	
Woodland							17	55	1.5	
Woodland							24	62	31	

The second series of experiments, carried out in 2000, was conducted in much the same way as the first series had been in 1999. The only differences were that in 2000 flow width was measured more accurately and more attention was paid to erosion on the plot. The second series of results therefore gives a little more information than the first series.

### 6.3 Results

The data collected on the plots were used to calculate Manning's  $n$ , Darcy-Weisbach  $f$ , Reynolds number and Froude number (Appendix 6.1). Froude number was almost always below one, so that flow was sub-critical. As shown in Figure 6.2, both  $n$  and  $f$  increased with increasing Reynolds number ( $Re$ ). Nearing et al. (1997) also observed such a trend for loess-derived Miami soil from Indiana, USA. They attributed the increase of  $f$  with increase of  $Re$  to strong physical form roughness caused by rill erosion. Nearing et al. (1997) also concluded that in the case of eroding rills Reynolds number is not a good predictor for  $f$  because erosion and hydraulics are interactive. Linear regression on our data, however, showed that R-squared for both the  $n-Re$  relationship and the  $f-Re$  relationship was fairly high (0.52 and 0.42 respectively). This shows that  $f$  and  $n$  could both be predicted from  $Re$ , so that the approach of developing relationships to calculate  $f$  from  $Re$  is just as valid for  $n$ . In the remainder of this chapter, only Manning's  $n$  is used.

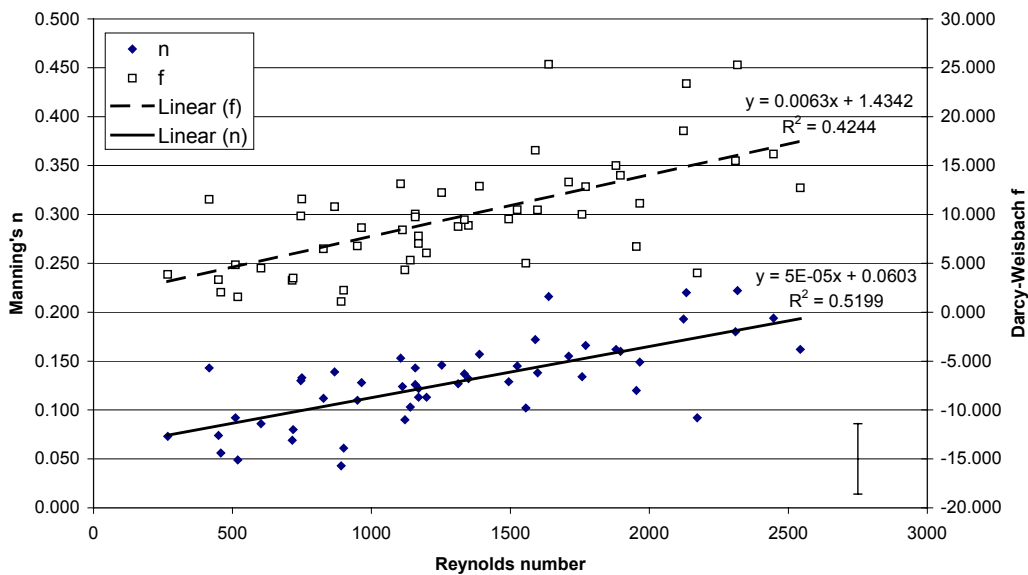


Figure 6.2 Manning's  $n$  and Darcy-Weisbach  $f$  as functions of Reynolds number. Data for all cropland runs of the second series. The bar in the lower right-hand corner shows the average error about the mean of two standard deviations

The calculated values of Manning's  $n$ , averaged for the various types of land use, are given in Table 6.3, which is based on the first data series (1999). Appendix 6.1 gives the measured data for all runs. The value of Manning's  $n$  found for woodland was much higher than for all other land uses. This was caused by the presence in some places of



dense undergrowth of herbs, together with litter. Fallow land included both short-term fallow (which should be similar to cropland) and long-term fallow (which can be expected to resemble wasteland). All cropland plots were combined because no

Table 6.3 Average values of Manning's  $n$  for the first (1999) series

Land use	Manning's $n$	Standard Deviation	N	Number of plots
Cropland	0.104	0.052	375	16
Fallow	0.076	0.016	49	2
Orchard	0.090	0.023	50	2
Woodland	0.211	0.083	58	4
Wasteland	0.084	0.025	92	4

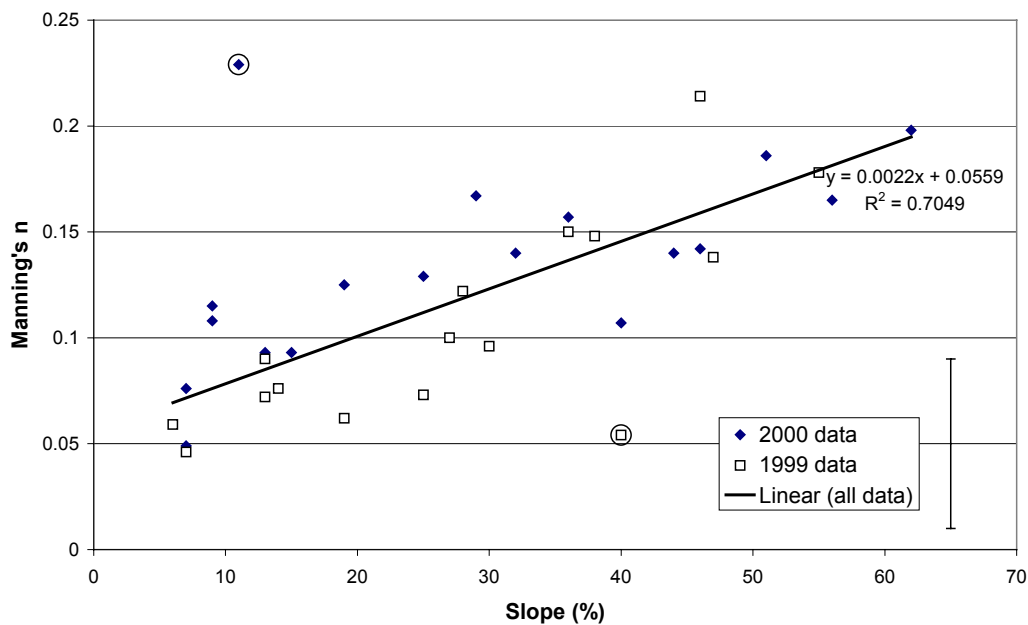


Figure 6.3 Cropland Manning's  $n$  as a function of slope, data per plot. Data for 1999 and 2000 combined. The circled points have been omitted from the regression. The bar in the lower right-hand corner shows the average error about the mean of two standard deviations

differences were found between the various crops listed in table 6.2. Instead, the Manning's  $n$  values calculated for cropland showed a clear relationship with slope angle. This is shown in Figure 6.3, which shows combined data for 1999 and 2000. Figure 6.3 also suggests that for the lower slope angles, the values found for Manning's  $n$  were lower in 1999 than in 2000. This might be caused by a more accurate measurement of flow width in 2000. In 2000 only water that actually flowed was measured, while in 1999 standing water was also measured. Since there is only standing water at low slope angles, this might explain the above observation. Despite the small difference in method between

1999 and 2000, the data for the 2 years are very similar and a single regression equation could therefore be used. The fitted linear regression line has the equation:

$$n = 0.0559 + 0.0022 \cdot S \quad (6.3)$$

where  $S$  is slope in percent. The value for  $R^2$  is 0.70.

The circled data points in figure 6.3 were omitted from the regression for the following reasons. The data point at slope 11% and Manning's  $n$  0.230 (measurement 25 in 2000) was on a very gentle slope with pronounced furrows across the slope. Many pools (six) with standing water were formed and the velocity was therefore much lower than is normally the case. Since the experiment forced the water across the plough ridges one can argue that it was not representative, as it did not reflect the natural flow direction. Obviously, plough ridges and furrows can play an important role in determining the direction of water flow on gentle slopes. Before applying equation 6.3 to a gentle slope one should therefore make sure that the flow is indeed in the direction of the steepest plot level gradient. The point at slope 40% and Manning's  $n$  0.06 (measurement 3b of 1999) differed from all other plots because no erosion was observed, despite the considerable slope. This plot was located very close to (and downslope of) a zone of water seepage, and it seems possible that this seepage had resulted in stabilisation of the loess through hydroconsolidation. Appendix 6.1 shows that both points also had Froude numbers that deviated from those of the other measurements.

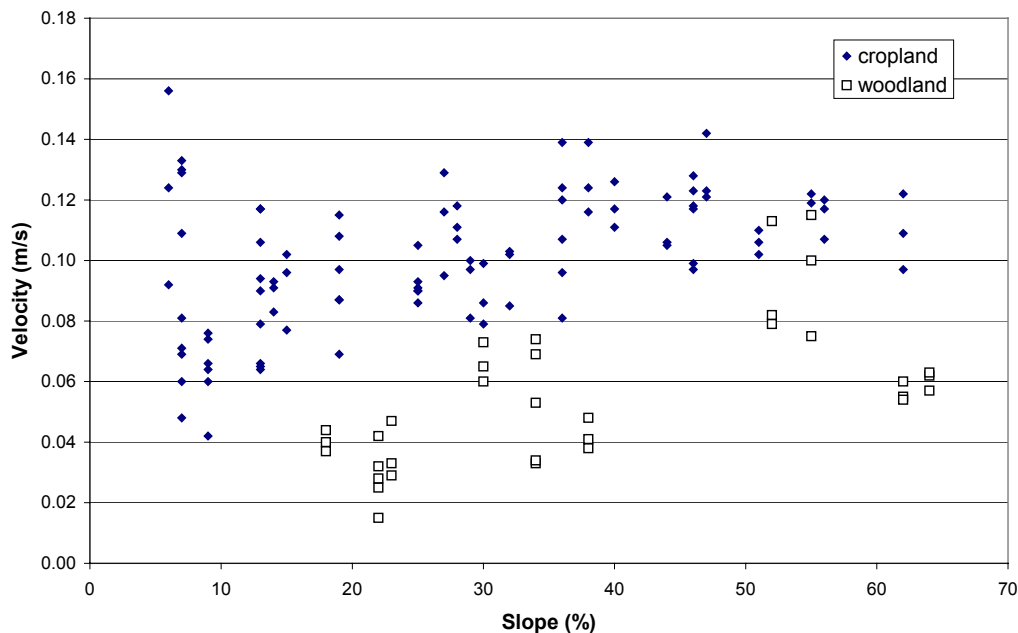


Figure 6.4 Velocity as a function of slope for cropland and woodland, all data

Using the data for all runs instead of those for all plots (Figure 6.3) reduced  $R^2$  to 0.57. These results show that slope was a slightly better predictor of Manning's  $n$  for cropland

in the Danangou catchment than Reynolds number, since Figure 6.2 shows that the Manning's  $n$  – Reynolds number relationship had a slightly lower  $R^2$ .

Because of the relationship with slope, the cropland values given in Table 6.3 should be interpreted with caution.

Contrary to cropland, no relationship between Manning's  $n$  and slope was found for woodland. On the other hand, the woodland plots showed a clearer relationship between velocity and slope than the cropland plots. Figure 6.4 shows velocity as a function of slope. Since discharge was different from run to run and velocity is related to discharge, Figure 6.4 shows a considerable spread in velocity. Nevertheless, it can be seen that there was no clear increase in velocity with increasing slope for cropland, while a more pronounced increase was found for woodland. For woodland, a relationship was found between Manning's  $n$  and plant cover. Such a relationship did not exist for cropland (which mostly had low covers) and could not be shown for the other land uses because there were too few data available.

## 6.4 Discussion

### 6.4.1 Slope versus Reynolds number

The data showed that slope was a slightly better predictor of Manning's  $n$  for croplands in the Danangou catchment than Reynolds number, since the  $R^2$  values for these relationships were 0.57 and 0.51 respectively. Although slope is much easier to determine than Reynolds number, predicting Manning's  $n$  from a combination of slope and Reynolds number could be a worthwhile approach, because slope only results in a spatial variation in Manning's  $n$ , while Reynolds number results in a temporal variation when used in simulations (since Reynolds number depends on changing flow conditions). Further research into this is needed.

### 6.4.2 Effects of steep slopes

Manning's  $n$  is usually considered a constant, so the question arises what caused this apparent increase of Manning's  $n$  with slope. For  $n$  to remain constant at increasing slopes, either  $R$  has to decrease or velocity has to increase according to equation 6.1. Observations during the experiments showed that on steeper slopes, the flow concentrated and rill erosion occurred. At the range of discharges used in the experiments, this resulted in an increased value of  $R$  because of flow concentration, as shown in figure 6.5. The lines in figure 6.5 were calculated by assuming a constant  $A$  equal to the average  $A$  of the measurements ( $287 \text{ mm}^2$ ). This assumption is reasonable in view of the fact that velocity is observed to be almost constant, irrespective of slope (figure 6.4). Since  $A$  is given by  $Q/v$ ,  $A$  would thus be constant for constant  $Q$ . The lines in the chart show that if  $A$  is kept constant  $h$  will tend to infinity and  $R$  to zero with decreasing  $w$ . This is a logical consequence of assuming a constant  $A$ , but what is interesting is that no measurements showed flow widths that would result in a decrease in  $R$  (which would occur for flow

widths of less than about 0.025 m, figure 6.5). This might indicate that flow concentration and accompanying erosion in rills tends to maximise  $R$ , which would also put a lower limit on flow width. For higher  $Q$ , both  $A$  and the lower limit on flow width would increase.

Figure 6.5 also shows that  $R$  is always smaller than  $h$ , and that for flow widths of less than 8-10 cm the difference is so large that  $h$  cannot be used in the Manning equation instead of  $R$ .

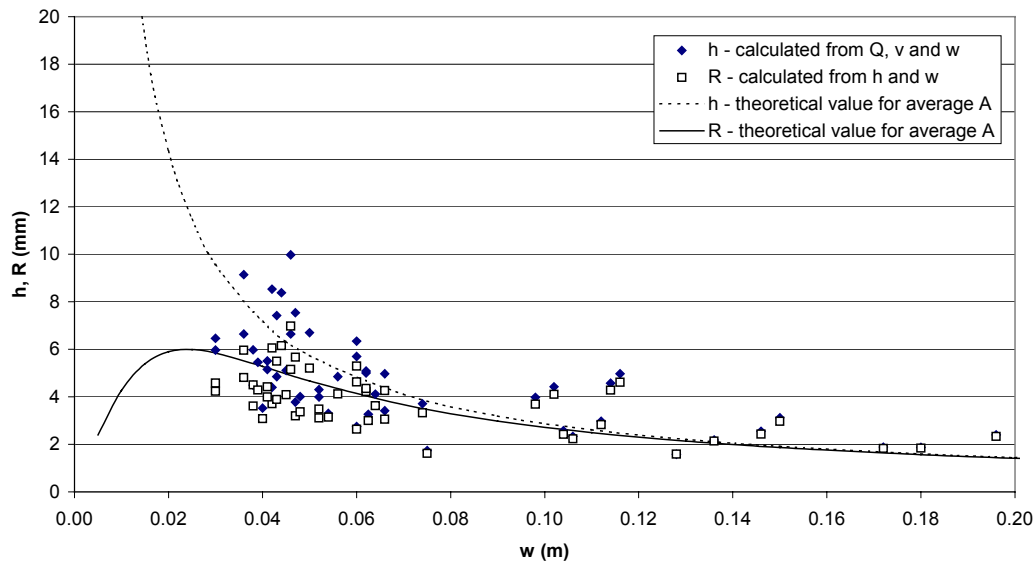


Figure 6.5  $R$  and  $h$  as function of flowwidth

The erosion rates clearly increased with increasing slope angles. Furthermore, it was observed that flow velocity hardly increased with increasing slope angles (Figure 6.4). This has already been observed for eroding rills by several other authors (e.g. Govers, 1992b, Nearing et al., 1997, Takken et al., 1998, Giménez & Govers, 2001). One could think of several possible causes:

#### *Increased roughness*

This is the most commonly proposed explanation for the observed lack of velocity increase with slope angle. According to Govers (1992b), roughness can play an important role in this situation because of two effects:

- Rill beds in cohesive materials are very irregular and are hydraulically rough. The effect of slope might be reduced for hydraulically rough surfaces.
- An increased erosion rate with increasing slope might result in increased bed roughness.

In subsequent research, Giménez & Govers (2001) used laser measurements to show that, for eroding rills, both roughness amplitude and frequency of roughness elements on rill beds increase with increasing slope angle. There is thus a real increase in roughness with

increasing slope angles, but their experiments did not show whether or not this increase is sufficient to explain the lack of increase in velocity with slope angle.

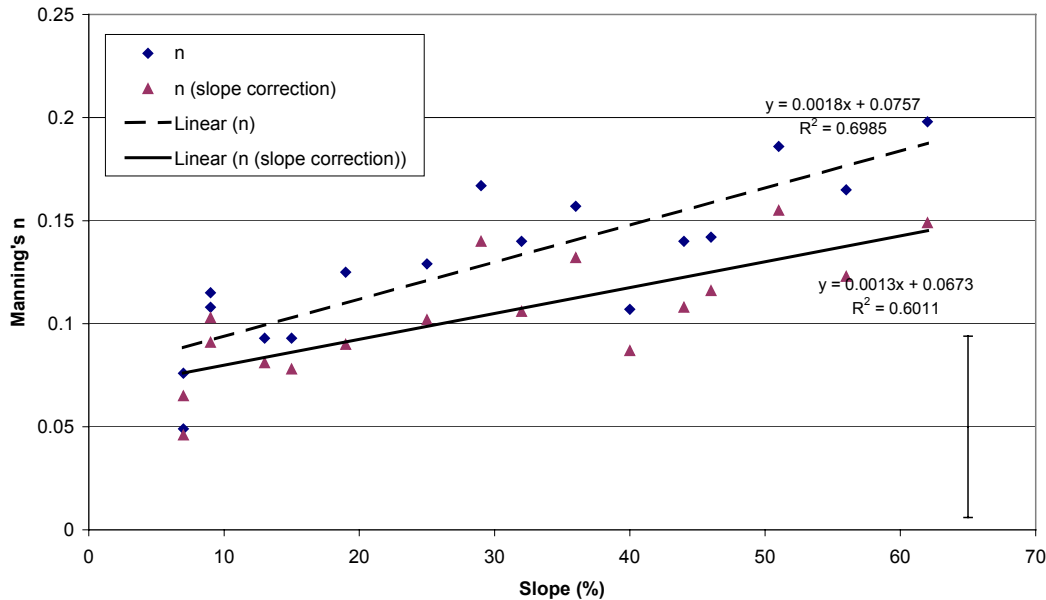


Figure 6.6 Manning's  $n$  as a function of slope for croplands, data of second series. The squares represent the original data, the triangles the data with slope correction. The bar in the lower right-hand corner shows the average error about the mean of two standard deviations

### *Slope decrease*

Our experiments found that erosion rates were higher for greater slope angles and that small vertical headcuts developed. The number and size of these headcuts can be expected to increase with increasing erosion rates, and thus with the slope angle. The effect of these headcuts will be to decrease the effective slope angle and thus the flow velocity. During the second year of measurements, these small headcuts were measured at the end of each run and the slope angle corrected. The lower line in Figure 6.6 shows that the dependence of Manning's  $n$  on slope has decreased, but not disappeared. The slope dependence in the equation has decreased by about 25%. The headcuts could therefore be a partial explanation of the observed relationship between  $n$  and slope.

### *Energy-based approach*

The third explanation for the lack of velocity increase with slope is the result of what might be called an energy-based approach. It was observed that rill erosion rates increased with increasing slope angle. This implies that more energy is used for erosion and transport of sediment than on more gentle slopes and this energy cannot therefore be used for increasing velocity. Both water flow and sediment transport are driven by the one available energy source: potential energy (ignoring raindrop impact energy). This potential energy drives the flow of water, which in turn plays a large role in erosion. With increasing slope angle, potential energy increases but, as was observed, so do erosion and

transport of soil, and the net effect might be that no more energy is available for water flow than on gentler slopes. Summer & Wei Zhang (1998) used more or less the same line of argumentation to explain the inverse relationship between turbulence and sediment concentration.

Such an energy-based approach is further complicated by the fact that eroded material entering the flow also has potential energy. Erosion therefore not only uses energy from the flow, but also adds energy to the flow. As a result, part of the energy used for erosion will return to the flow. Sediment entering the flow will also alter flow properties like density and viscosity. With increasing sediment content, internal friction will increase and more energy will be needed to overcome this friction. It is therefore perhaps more appropriate to argue that fluid velocity does not increase even though more energy might be used for it. Such a shift in the use of available energy could explain the lack of increase in velocity at greater slope angles. This, in turn, inevitably leads to an increase in apparent Manning's  $n$  with increasing slope angle (equation 6.1).

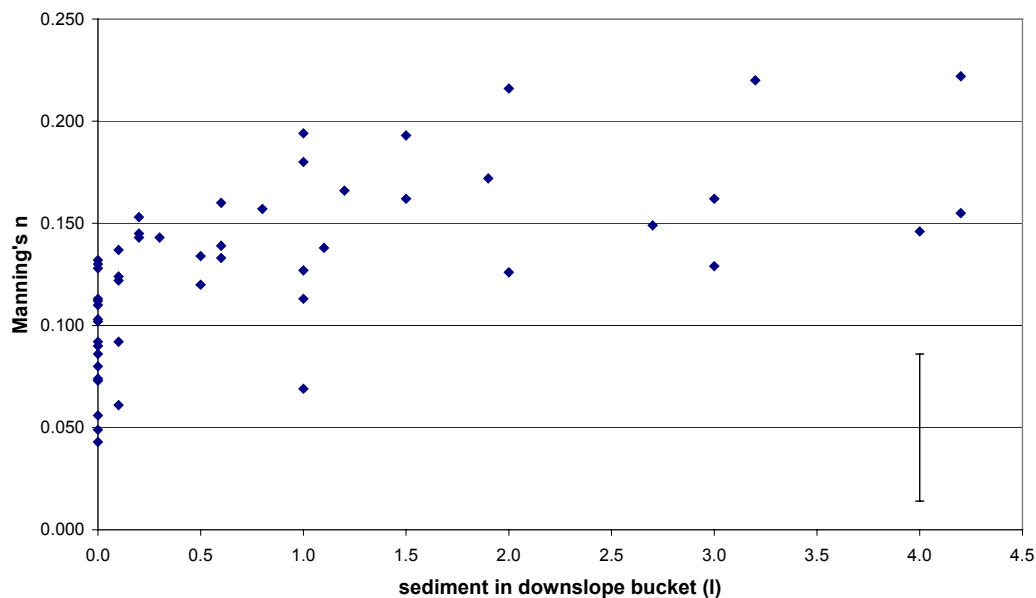


Figure 6.7 Manning's  $n$  versus sediment volume in the bucket at the downstream end of the plot. Data for the second series are shown. The bar in the lower right-hand corner shows the average error about the mean of two standard deviations

Although the exact mechanisms and energy uses of all these erosion-related effects cannot be studied with the present field experiments, some indication might be obtained from the quantities of sediment in the bucket at the lower end of the plot. These amounts were recorded in 2000 and if the hypothesis explained above were correct, one would expect an increase in Manning's  $n$  with increasing sediment volume in the bucket. Figure 6.7 shows the results obtained. Figure 6.7 shows a weak positive correlation between sediment volume and Manning's  $n$ , but the data are inconclusive. One has to bear in mind that the field observations showed that erosion rates increased with slope angle. It is

therefore difficult to ascertain if an observed relationship between sediment volume and Manning's  $n$  is a causal relationship or just the consequence of both depending on slope. Also, sediment volume might be significantly influenced by other parameters such as discharge and cohesion. Finally, it was observed that when two consecutive runs with comparable discharge were conducted, the second one generally produced less sediment, but not a reduction in the calculated Manning's  $n$ . The data therefore do not seem to support the hypothesis of a shift in energy use. Clearly, more research is needed.

#### 6.4.3 Consequences for modelling

In hydrological and soil erosion modelling, there are several ways to overcome the problem posed by the dependence of Manning's  $n$  on slope. The most radical method would be to use a different equation altogether. Another solution would be to allow Manning's  $n$  to change with slope. These methods will now be discussed briefly.

Govers (1992b) developed an empirical equation to calculate mean velocity in eroding rills from discharge alone. The equation is:

$$v = 3.52 \cdot Q^{0.294} \quad (6.4)$$

Where  $Q$  is given in  $\text{m}^3/\text{s}$  and  $v$  in  $\text{m}/\text{s}$ . Takken et al. (1998) found that this equation could be used in circumstances where the rills can freely change their shape (i.e., in bare, unconsolidated, stone-free soils). They suggest using equation 6.4 instead of Manning's equation to calculate flow velocity in eroding rills. Flow in cropland rills in the Danangou catchment can be assumed to meet these requirements. Vegetation cover is low, the soil consists of unconsolidated loess and contains no stones in its upper layers. Fitting a power equation like that of Govers to our cropland data gave:

$$v = 3.65 \cdot Q^{0.34} \quad (6.5)$$

Where  $Q$  and  $v$  are also in  $\text{m}^3/\text{s}$  and  $\text{m}/\text{s}$  respectively. This equation had a  $R^2$  of 0.33. The conditions mentioned by Takken et al. (1998) are, however, not met for most other land uses in the Danangou catchment. In woodland, for example, the soil is usually not bare and it is also much more consolidated than in cropland, making it impossible to apply equation 6.4 or 6.5. Figure 6.8 shows the results of the cropland measurements described in the present chapter, together with the equation developed by Govers (1992b) and equation 6.5. The Govers equation clearly over predicts velocity in this case. It should be noted that Figure 6.8 shows all measurements, not only those that had eroding rills. To be able to calculate a relationship of the same form as that given by Govers, these data points would have to be removed first, at least according to theory. It should be noted that the discharges used in the present study are much lower than those used by Govers. It is tempting to conclude from Figure 6.8 that Govers' (1992b) equation is not universally applicable in the case of eroding rills. However, if no velocity correction for the dye tracer is applied, our measured data match the equation developed by Govers reasonably well (Figure 6.8). Since equations 6.4 and 6.5 can only be used for channels freely able to

change their shape, it is less well suited for catchment-wide modelling. Using either equation in erosion models would involve the use of several velocity equations within the model area. Since the position of eroding rills is not likely to remain constant during a storm, the use of different equations would also have to change in time, with the expansion and contraction of the eroding rill network.

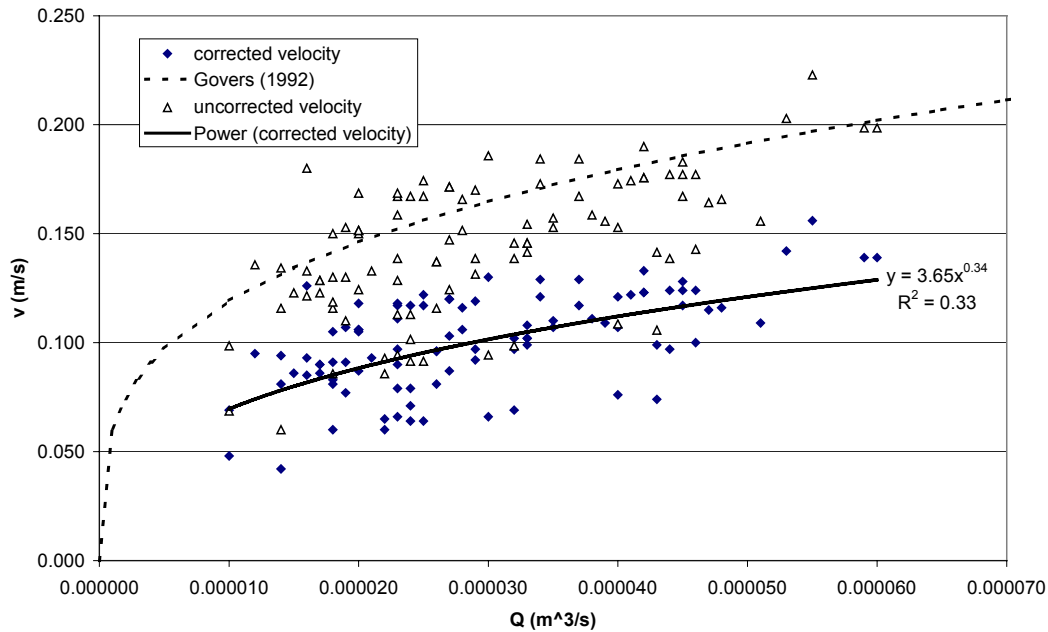


Figure 6.8 Velocity as a function of discharge. Measurements are compared with the relationship developed by Govers (1992b) and given in equation 6.4 and with equation 6.5. Data for all cropland runs of 1999 and 2000 are shown

Another option to overcome the modelling problems posed by a variable Manning's  $n$  is to use Manning's equation with a slope-dependent value of Manning's  $n$ . Nearing et al. (1999) also considered this option but they argued that developing such an equation is redundant because in that case a slope dependent equation is developed to overcome the slope dependency of the Manning equation. It would seem better to use a slope-independent equation in the first place. They therefore preferred predicting velocity directly from discharge with an equation similar to equation 6.4. For use in catchment models, however, the easiest and most practical solution is to allow Manning's  $n$  to change with slope. This avoids the problem of having to use different velocity equations in different parts of the model area. Besides, in this study, the relationship that was found between slope and Manning's  $n$  has a much higher  $R^2$  than that found between discharge and velocity. It can be assumed that equation 6.3 can be used for other Loess Plateau catchments as well as those catchments have similar characteristics of steep slopes, low cover croplands and erodible materials. For other regions, different equations might be necessary.



#### 6.4.4 Velocity correction factor

If dye tracing is used a correction factor has to be applied to derive the mean velocity from the measured dye velocity. This is needed because velocity is not constant over depth; there is a velocity profile, so that velocity is at a maximum at the surface. Since the leading edge of the dye cloud is used the surface velocity is measured. The value of the correction factor depends on flow conditions. According to theory (Emmett, 1970, Abrahams et al., 1986, Dunkerly, 2001) the correction factor should be 0.67 for laminar flow and 0.8 for turbulent flow. For transitional flow it should be about 0.7. A correction factor of 0.7 was therefore applied. Experiments have shown that the theoretical values of the correction factor do not apply in case of rough surfaces. Emmett (1970), Li & Abrahams (1997) and Dunkerly (2001) found correction factors well below the theoretical value, while Li & Abrahams (1997) found that the correction factor also decreases with increasing saltating sediment load. In our study, however, there are several indications that the applied correction factor is too low. In chapter 6.4.3 it was shown that our data fitted the equation of Govers (1992b) much better if no correction was applied. In addition, comparison of the measured values of Manning's  $n$  with literature (Ven Te Chow et al., 1988, Morgan et al., 1998b, see table 6.1) suggested that the measured values might be too high. In the Lisem calibration (chapter 10) it proved necessary to decrease Manning's  $n$  for all storms. If no correction was applied, the calculated values of Manning's  $n$  decreased by about 40%, so a value of, for example, 0.1 was reduced to about 0.06 (see also appendix 6.1). The quality of the data maybe does not allow firm statements about the correction factor, but it nevertheless casts some doubt. Therefore, it is useful to assess the reliability of the velocity measurement made with the dye tracing. Several potential problems existed:

- The problem of reaction time. This problem has also been assessed by Dunkerly (2001). In his case it was probably not important since he tried to anticipate both injection and arrival of tracer. In our case reaction time played a role several times. First, the person who kept time reacted to the time displayed on the watch and called. Then the person who injected the tracers reacted to the call. Then, the same person reacted to the arrival of the tracer and called. Finally, the person who kept time reacted to the call and looked at the watch before writing down travel time. The combined effect of these factors might be an overestimation of travel time by about 1-2 seconds. Since the travel time was usually around 12 seconds this could result in an underestimation of velocity by 8-17 percent.
- The watch that was used had second-accuracy. This could result in errors of maybe 1 second, or 8% if travel time is 12 seconds.
- In field conditions it is not always easy to see the leading edge of the dye-cloud. The problem is even more pronounced when there is a lot of sediment in the flow. This was often the case in our measurements on cropland.
- On most plots the flowpath was slightly meandering, so that the actual flow distance was longer than used in the calculation of velocity. This could result in an underestimation of velocity.

If all four factors are considered together, it seems likely that the measured travel times were too long. Hence, the measured velocities would have been too low. Therefore, the correction factor should increase. Since it is difficult to assess by how much the correction factor should increase the theoretical correction factor of 0.7 was maintained in the calculations. The results nevertheless raise some doubts about the value of the velocity correction factor, at least for field measurements on highly erodible soils.

#### 6.4.5 *Experimental setup*

Despite the potential problems with the velocity correction factor (section 6.4.4) the results from our experiments were consistent. The difference between the data obtained in 1999 and in 2000 was small. There were, however, some potential problems with the experimental setup that should be discussed.

During our experiments almost always a single flowpath developed. If, however, two or more flowpaths developed it became very difficult to obtain accurate values for Manning's  $n$ . In the case of several flowpaths, the combined discharge from these flowpaths would be measured in the bucket, but the velocity that was measured applied to only one flowpath. If the velocity in all flowpaths was similar that is no problem, but when this was not the case it might distort the results. In the calculation procedure the discharge, velocity and flowwidth should all apply to the same amount of water. Hence, if the total discharge is used, the total flowwidth should be used and a representative value for velocity. A representative value for velocity should be a discharge-weighted average. The result would then be an average value for Manning's  $n$ . Alternatively, if the velocity measured in one flowpath is used, the flowwidth and discharge for this particular flowpath should be used. The result would then be a value of Manning's  $n$  for that particular flowpath. In both cases the discharge from individual flowpaths is needed. This discharge cannot be measured with the present measurement setup. To avoid these difficulties it might be necessary to prevent the flow from forming several flowpaths. Such an approach was suggested by Rouhipour et al. (1999), but they could use pre-formed rills since they were interested in non-eroding conditions. The alternative is to adapt the method so that discharge from individual flowpaths can be measured, but that might be difficult.

Another issue is the measurement of discharge. Discharge has been measured using buckets at the downstream end of the plot. Because of infiltration, however, discharge will decrease in the downstream direction. In 2000, the water levels in the Mariotte bottles and in the bucket with tap were measured before and after each run. These measurements indicated that the amount of water reaching the bucket is on average only 55% of that entering the plot (see also appendix 6.1). A correction for this water loss can only be made if it is assumed that the loss is equally distributed over the plot. This, however, is often not the case as significant amounts of water sometimes infiltrated below the gutter, or locally into the earthen walls that bound the plot. Thus, no correction was applied. If a correction were applied, Manning's  $n$  would increase since in that case discharge would be larger, while velocity remains the same. The error in the measurement of discharge is thus in the opposite direction of that in the measurement of

velocity. What the net error would be, and whether or not a velocity correction is needed, cannot be determined with the measurements reported here.

## 6.5 Conclusions

Manning's  $n$  measurements in a small Loess Plateau catchment showed that Manning's  $n$  could, just like Darcy-Weisbach  $f$ , be estimated from Reynolds number. For croplands, Manning's  $n$  was found to increase with slope angle. This was caused by the fact that flow velocity hardly increased with increasing slope, while hydraulic radius increased somewhat because the flow became more concentrated at increasing slope, leading to rill erosion. Several factors can help explain why there was little increase in velocity with slope angle. All of these factors only apply to surfaces that can be eroded by the flow. The first is that Giménez and Govers (2001) have shown that, for eroding rills, there is an increase in roughness with increasing slope angle. The second is that the observed increase in erosion rates for steeper slopes resulted in the development of more vertical headcuts, which effectively decreased the slope angle. The measurement results confirmed that this may be a partial explanation. The third explanation is that velocity can be hypothesised not to increase with slope because more energy will be used for erosion and transportation of sediment. Our findings did not seem to support this hypothesis, but did not firmly indicate that it should be rejected either. An increase in Manning's  $n$  with slope angle was only observed for cropland. Other land uses, like woodland, had virtually no erosion and the velocity then increased with the slope angle. The results imply that in soil erosion models using Manning's equation, the value of  $n$  should be a function of slope for surfaces that can be eroded by the flow. The results also raise doubts about the validity of the application of a correction factor to convert measured velocities to average velocities.

## Appendix 6.1 Data for all Manning's $n$ measurements

This appendix gives the measured data as well as a number of variables that were calculated from the measured data. The table below describes what the different columns in the data sheets mean.

Variable	Unit	Explanation
Q-down	% up	Q at downstream end plot as % of Q from bottles and bucket
Q-down	l/s	discharge in the bucket at downstream end plot
v-cor	m/s	flow velocity measured with dye tracer and multiplied by 0.7
v-nocor	m/s	flow velocity measured with dye tracer
w	m	flow width (average of 5 measurements down length plot)
h	mm	flow depth (calculated from Q, w, v-cor)
A	mm <sup>2</sup>	cross-section of flow (calculated from w and h)
R	mm	hydraulic radius (calculated from A, w, h)
S	%	slope measured with inclinometer
Scor	%	slope corrected for headcut height
n		Manning's $n$ (calculated with equation 6.1)
stdev n		standard deviation of $n$
f		Darcy-Weisbach $f$ (calculated with equation 6.2)
C	g/l	concentration in downstream bucket (used in chapter 7)
S*v	cm/s	unit stream power (used in chapter 7)
Re		Reynolds number (calculated with equation 2.1)
froude		Froude number (calculated with equation 2.2)

Cropland 2000

Run	Land use	Q-down (% up)	Q-down (l/s)	v-cor (m/s)	v-nocor (m/s)	w (m)	h (mm)	A (mm <sup>2</sup> )	R (mm)	S (%)	Scor (%)	n	stdev n	f	C (g/l)	S*v (cm/s)	Re	froude
3.1	crop	52.4	0.020	0.105	0.150	0.054	3.3	190	3.1	44	33	0.126	0.016	10.04	150.0	4.62	1158	0.58
3.2	crop	65.6	0.020	0.106	0.151	0.052	4.3	189	3.1	44	34	0.143	0.014	9.75	22.5	4.66	1158	0.52
3.3	crop	71.9	0.040	0.121	0.173	0.060	5.7	331	4.6	44	28	0.149	0.016	11.13	101.3	5.32	1966	0.51
4.1	crop	24.9	0.014	0.042	0.060	0.112	3.0	333	2.8	9	7	0.143	0.029	11.54	21.4	0.38	417	0.25
4.2	crop	61.9	0.025	0.064	0.091	0.098	4.0	391	3.7	9	6	0.112	0.011	6.48	0.0	0.58	828	0.32
4.3	crop	47.5	0.022	0.060	0.086	0.146	2.6	367	2.4	9	5	0.092	0.007	4.85	0.0	0.54	511	0.38
6.1	crop	32.6	0.010	0.069	0.099	0.040	3.5	145	3.1	19	12	0.130	0.019	9.84	0.0	1.31	746	0.37
6.2	crop	49.3	0.020	0.087	0.124	0.041	5.5	230	4.4	19	12	0.132	0.017	8.87	0.0	1.65	1349	0.37
6.3	crop	69.0	0.033	0.108	0.154	0.046	6.6	306	5.2	19	11	0.120	0.013	6.72	22.7	2.05	1953	0.42
8.1	crop	54.6	0.023	0.117	0.167	0.030	6.5	197	4.6	56	39	0.162	0.032	14.99	195.7	6.55	1880	0.47
8.2	crop	46.2	0.019	0.107	0.153	0.030	6.0	178	4.2	56	36	0.172	0.029	16.57	150.0	5.99	1590	0.44
8.3	crop	55.2	0.027	0.120	0.171	0.038	6.0	225	4.5	56	39	0.160	0.017	14.01	33.3	6.72	1896	0.50
9.1	crop	35.6	0.016	0.085	0.121	0.042	4.4	188	3.7	32	26	0.153	0.020	13.13	18.8	2.72	1105	0.41
9.2	crop	51.4	0.027	0.103	0.147	0.064	4.1	262	3.6	32	21	0.127	0.013	8.76	55.6	3.30	1312	0.51
9.3	crop	57.5	0.033	0.102	0.146	0.066	5.0	324	4.3	32	19	0.145	0.016	10.48	9.1	3.26	1525	0.46
12.1	crop	33.4	0.016	0.126	0.180	0.075	1.7	127	1.6	40	30	0.069	0.018	3.26	93.8	5.04	715	0.96
12.2	crop	40.1	0.023	0.111	0.159	0.063	3.3	207	3.0	40	29	0.113	0.016	7.80	65.2	4.44	1169	0.62
12.3	crop	54.2	0.025	0.117	0.167	0.039	5.5	214	4.3	40	33	0.134	0.015	10.01	30.0	4.68	1758	0.51
13.1	crop	39.9	0.020	0.118	0.169	0.038	4.5	169	3.6	46	38	0.129	0.017	9.53	225.0	5.43	1494	0.56
13.2	crop	61.0	0.024	0.117	0.167	0.043	4.9	205	3.9	46	33	0.138	0.021	10.46	68.8	5.38	1598	0.54
13.3	crop	62.0	0.045	0.128	0.183	0.047	7.5	352	5.7	46	36	0.162	0.015	12.72	50.0	5.89	2543	0.47
14.1	crop	40.6	0.015	0.086	0.123	0.047	3.8	174	3.2	25	18	0.128	0.025	8.64	0.0	2.15	965	0.45
14.2	crop	56.9	0.021	0.093	0.133	0.045	5.1	226	4.1	25	18	0.137	0.007	9.46	7.1	2.33	1334	0.42
14.3	crop	50.3	0.019	0.091	0.130	0.052	4.0	209	3.5	25	19	0.124	0.018	8.41	7.9	2.28	1111	0.46
15.1	crop	55.8	0.024	0.079	0.113	0.062	5.0	304	4.2	13	11	0.122	0.023	7.03	6.3	1.03	1170	0.36
15.2	crop	65.9	0.028	0.106	0.151	0.104	2.6	264	2.4	13	10	0.061	0.005	2.24	5.4	1.38	900	0.67
15.3	crop	79.7	0.045	0.117	0.167	0.060	6.3	385	5.3	13	10	0.092	0.006	4.02	3.3	1.52	2172	0.47
16.1	crop	50.9	0.020	0.106	0.151	0.048	4.0	189	3.4	51	43	0.146	0.020	12.23	300.0	5.41	1253	0.53
16.2	crop	75.9	0.033	0.102	0.146	0.036	9.1	324	6.0	51	38	0.220	0.029	23.37	145.5	5.20	2133	0.34
16.3	crop	75.4	0.035	0.110	0.157	0.043	7.4	318	5.5	51	40	0.193	0.019	18.55	64.3	5.61	2123	0.41
25.1	crop	38.8	0.029	0.036	0.051	0.190	4.3	806	4.1	11	8	0.243	0.050	27.55	0.0	0.00	512	0.18
25.2	crop	46.6	0.030	0.038	0.054	0.156	5.2	789	4.7	11	9	0.264	0.069	28.90	0.0	0.00	632	0.17

## Cropland 2000 (continued)

Run	Land use	Q-down (% up)	Q-down (l/s)	v-cor (m/s)	v-nocor (m/s)	w (m)	h (mm)	A (mm <sup>2</sup> )	R (mm)	S (%)	Scor (%)	n	stdev n	f	C (g/l)	S*v (cm/s)	Re	froude
25.3	crop	59.7	0.039	0.051	0.073	0.138	5.5	765	5.1	11	8	0.192	0.020	17.37	0.0	0.01	919	0.22
26.1	crop	46.2	0.030	0.066	0.094	0.102	4.4	455	4.1	9	9	0.110	0.007	6.78	0.0	0.59	950	0.32
26.2	crop	65.6	0.043	0.074	0.106	0.116	5.0	581	4.6	9	8	0.113	0.010	6.07	0.0	0.67	1198	0.34
26.3	crop	67.0	0.040	0.076	0.109	0.114	4.6	526	4.3	9	8	0.103	0.008	5.33	0.0	0.68	1140	0.36
29.1	crop	34.8	0.019	0.077	0.110	0.106	2.3	247	2.2	15	13	0.086	0.010	4.51	0.0	1.16	602	0.51
29.2	crop	50.8	0.026	0.096	0.137	0.074	3.7	271	3.3	15	11	0.090	0.007	4.33	0.0	1.44	1120	0.50
29.3	crop	66.7	0.032	0.102	0.146	0.062	5.1	314	4.3	15	11	0.102	0.100	5.01	0.0	1.53	1556	0.46
30.1	crop	43.5	0.018	0.081	0.116	0.066	3.4	222	3.1	29	23	0.139	0.019	10.79	50.0	2.35	867	0.44
30.2	crop	71.1	0.032	0.097	0.139	0.050	6.7	330	5.2	29	24	0.166	0.016	12.83	56.3	2.81	1771	0.38
30.3	crop	75.7	0.046	0.100	0.143	0.046	10.0	460	7.0	29	22	0.194	0.019	16.18	32.6	2.90	2447	0.32
31.1	crop	59.8	0.026	0.096	0.137	0.056	4.9	271	4.1	36	29.6	0.157	0.010	12.88	46.2	3.46	1389	0.44
31.2	crop	37.2	0.014	0.081	0.116	0.060	2.8	173	2.6	36	29.6	0.133	0.016	11.58	64.3	2.92	750	0.49
31.3	crop	61.5	0.040	0.107	0.153	0.044	8.4	374	6.2	36	27.5	0.180	0.021	15.48	37.5	3.85	2310	0.37
32.1	crop	58.1	0.025	0.122	0.174	0.041	5.2	205	4.0	62	41.8	0.155	0.041	13.31	252.0	7.56	1710	0.54
32.2	crop	52.3	0.023	0.097	0.139	0.036	6.6	237	4.8	62	41.8	0.216	0.021	25.36	130.4	6.01	1638	0.38
32.3	crop	61.7	0.039	0.109	0.156	0.042	8.5	358	6.1	62	42.2	0.222	0.027	25.29	161.5	6.76	2317	0.38
33.1	crop	29.8	0.010	0.048	0.069	0.128	1.6	208	1.6	7	5.8	0.073	0.015	3.86	0.0	0.34	268	0.39
33.2	crop	42.2	0.018	0.060	0.086	0.136	2.2	300	2.1	7	5.2	0.074	0.008	3.32	0.0	0.42	450	0.41
33.3	crop	54.3	0.032	0.069	0.099	0.150	3.1	464	3.0	7	5.4	0.080	0.011	3.49	0.0	0.48	719	0.39
34.1	crop	54.4	0.024	0.071	0.101	0.180	1.9	338	1.8	7	6.2	0.056	0.006	2.04	0.0	0.50	458	0.52
34.2	crop	61.5	0.026	0.081	0.116	0.172	1.9	321	1.8	7	6.6	0.049	0.003	1.56	0.0	0.57	519	0.60
34.3	crop	76.4	0.051	0.109	0.156	0.196	2.4	468	2.3	7	6.2	0.043	0.003	1.10	0.0	0.76	891	0.71
<i>average</i>		<i>54.3</i>	<i>0.027</i>	<i>0.092</i>	<i>0.131</i>	<i>0.077</i>	<i>4.7</i>	<i>315</i>	<i>3.9</i>	<i>28.4</i>	<i>21.0</i>	<i>0.135</i>	<i>0.019</i>	<i>10.55</i>	<i>49.7</i>	<i>2.87</i>	<i>1277</i>	<i>0.45</i>

Other land uses 2000

Run	Land use	Q-down (% up)	Q-down (l/s)	v-cor (m/s)	v-nocor (m/s)	w (m)	h (mm)	A (mm <sup>2</sup> )	R (mm)	S (%)	Scor (%)	n	stdev n	f	C (g/l)	S*v (cm/s)	Re	froude
19.1	fallow	38.9	0.014	0.093	0.133	0.100	1.5	151	1.5	33	30	0.080	0.013	4.46	53.6	3.07	477	0.76
19.2	fallow	53.0	0.017	0.097	0.139	0.106	1.7	175	1.6	33	28	0.080	0.013	4.50	44.1	3.20	546	0.76
19.3	fallow	58.2	0.025	0.108	0.154	0.078	3.1	231	2.8	33	25	0.097	0.006	6.23	30.0	3.56	1043	0.62
20.1	fallow	58.9	0.023	0.107	0.153	0.090	2.4	215	2.3	42	37	0.102	0.013	6.65	32.6	4.49	851	0.69
20.2	fallow	69.3	0.031	0.110	0.157	0.080	3.5	282	3.2	42	35	0.124	0.009	8.99	72.6	4.62	1249	0.59
20.3	fallow	75.3	0.049	0.136	0.194	0.092	3.9	360	3.6	42	33	0.108	0.008	6.55	45.9	5.71	1721	0.69
22.1	fallow	44.7	0.024	0.081	0.116	0.136	2.1	296	2.1	16	15	0.080	0.006	4.12	0.0	1.30	600	0.56
22.2	fallow	32.4	0.011	0.065	0.093	0.128	1.4	169	1.3	16	13.6	0.075	0.017	3.92	0.0	1.04	295	0.56
22.3	fallow	47.4	0.022	0.074	0.106	0.118	2.5	297	2.4	16	15.2	0.097	0.012	5.65	0.0	1.18	627	0.47
23.1	fallow	27.5	0.014	0.064	0.091	0.102	2.2	219	2.1	8	8	0.073	0.016	3.21	0.0	0.51	462	0.43
23.2	fallow	42.0	0.016	0.066	0.094	0.130	1.9	242	1.8	8	8	0.065	0.006	2.66	0.0	0.53	419	0.48
23.3	fallow	37.0	0.015	0.063	0.090	0.114	2.0	238	2.0	8	8	0.069	0.008	3.25	0.0	0.50	446	0.45
21.1	orchard	35.2	0.016	0.091	0.130	0.113	1.5	176	1.5	52	48	0.098	0.019	7.61	93.8	4.73	484	0.74
21.2	orchard	37.9	0.015	0.099	0.141	0.067	2.2	152	2.1	52	45.7	0.110	0.007	9.01	50.0	5.15	737	0.68
21.3	orchard	76.2	0.061	0.188	0.269	0.062	5.3	324	4.5	52	43.9	0.100	0.015	5.26	66.4	9.78	2946	0.82
18.1	waste	59.4	0.013	0.074	0.106	0.176	1.0	176	1.0	44	44	0.086	0.013	6.34	0.0	3.26	256	0.75
18.2	waste	51.2	0.017	0.093	0.133	0.168	1.1	183	1.1	44	44	0.073	0.006	4.37	0.0	4.09	350	0.89
18.3	waste	65.3	0.029	0.104	0.149	0.131	2.1	279	2.1	44	44	0.099	0.011	6.71	0.0	4.58	752	0.72
27.1	waste	66.1	0.022	0.105	0.150	0.118	1.8	210	1.7	57	56	0.097	0.011	7.13	0.0	5.99	635	0.79
27.2	waste	75.8	0.019	0.093	0.133	0.116	1.8	204	1.7	57	56	0.111	0.020	9.01	0.0	5.30	557	0.70
27.3	waste	71.5	0.042	0.112	0.160	0.152	2.5	375	2.4	57	56	0.112	0.013	8.69	14.3	6.38	939	0.72
28.1	waste	46.2	0.012	0.063	0.090	0.114	1.7	190	1.6	61	60	0.159	0.007	19.96	37.5	3.84	359	0.49
28.2	waste	63.0	0.020	0.067	0.096	0.120	2.5	299	2.4	61	60	0.192	0.020	25.96	0.0	4.09	561	0.43
28.3	waste	75.7	0.034	0.080	0.114	0.142	3.0	425	2.9	61	59	0.182	0.015	21.89	17.6	4.88	806	0.47
1.1	wood	63.8	0.022	0.062	0.089	0.205	1.8	355	1.7	64	64	0.172	0.015	22.67	0.0	3.97	370	0.47
1.2	wood	61.3	0.023	0.057	0.081	0.153	2.6	404	2.5	64	64	0.240	0.029	40.18	0.0	3.65	510	0.36
1.3	wood	70.8	0.028	0.063	0.090	0.162	2.7	444	2.7	64	64	0.220	0.027	34.25	0.0	4.03	587	0.39
2.1	wood	57.9	0.020	0.082	0.117	0.260	0.9	244	0.9	52	52	0.079	0.011	5.76	0.0	4.26	268	0.85
2.2	wood	69.6	0.024	0.079	0.113	0.260	1.1	304	1.2	52	52	0.093	0.006	7.72	0.0	4.11	321	0.75
2.3	wood	78.0	0.052	0.113	0.161	0.305	1.5	460	1.5	52	52	0.081	0.018	4.87	0.0	5.88	592	0.93
5.1	wood	30.7	0.012	0.038	0.054	0.218	1.4	316	1.4	38	38	0.217	0.037	30.10	0.0	1.44	191	0.32
5.2	wood	57.6	0.028	0.041	0.059	0.216	3.1	683	3.1	38	38	0.301	0.026	55.58	0.0	1.56	442	0.24
5.3	wood	63.5	0.037	0.048	0.069	0.218	3.6	771	3.4	38	38	0.286	0.023	45.18	0.0	1.82	577	0.26

## Other land uses 2000 (continued)

Run	Land use	Q-down (% up)	Q-down (l/s)	v-cor (m/s)	v-nocor (m/s)	w (m)	h (mm)	A (mm <sup>2</sup> )	R (mm)	S (%)	Scor (%)	n	stdev n	f	C (g/l)	S*v (cm/s)	Re	froude
7.1	wood	32.9	0.018	0.040	0.057	0.245	1.8	450	1.8	18	18	0.154	0.013	16.29	0.0	0.72	254	0.30
7.2	wood	44.2	0.020	0.037	0.053	0.315	1.7	541	1.7	18	18	0.161	0.017	17.86	0.0	0.67	220	0.29
7.3	wood	53.3	0.029	0.044	0.063	0.274	2.4	659	2.4	18	18	0.156	0.008	17.58	0.0	0.79	365	0.29
10.1	wood	27.3	0.011	0.025	0.036	0.327	1.4	440	1.3	22	22	0.229	0.040	37.58	0.0	0.55	117	0.22
10.2	wood	58.2	0.021	0.032	0.046	0.320	2.0	656	2.0	22	22	0.232	0.026	34.80	0.0	0.70	227	0.23
10.3	wood	68.4	0.045	0.042	0.060	0.348	3.1	1071	3.0	22	22	0.234	0.021	30.18	0.0	0.92	446	0.24
11.1	wood	72.2	0.033	0.073	0.104	0.236	1.9	452	1.9	30	30	0.114	0.018	8.49	0.0	2.19	483	0.53
11.2	wood	68.9	0.029	0.060	0.086	0.214	2.3	483	2.2	30	30	0.155	0.029	14.75	0.0	1.80	466	0.40
11.3	wood	75.8	0.035	0.065	0.093	0.234	2.3	538	2.3	30	30	0.144	0.016	12.82	0.0	1.95	515	0.43
17.1	wood	55.0	0.014	0.075	0.107	0.190	1.0	187	1.0	55	55	0.090	0.011	7.61	0.0	4.13	256	0.77
17.2	wood	79.1	0.039	0.115	0.164	0.230	1.5	339	1.5	55	55	0.078	0.011	4.84	0.0	6.33	587	0.95
17.3	wood	76.1	0.034	0.100	0.143	0.216	1.6	340	1.6	55	55	0.095	0.014	6.82	0.0	5.50	544	0.80
24.1	wood	35.5	0.013	0.055	0.079	0.128	1.8	236	1.8	62	62	0.190	0.027	29.45	0.0	3.41	347	0.42
24.2	wood	38.7	0.014	0.054	0.077	0.108	2.4	259	2.3	62	62	0.238	0.024	39.07	0.0	3.35	435	0.35
24.3	wood	55.0	0.025	0.060	0.086	0.162	2.6	417	2.5	62	62	0.220	0.019	34.36	0.0	3.72	525	0.38
<i>average</i>		<i>56.3</i>	<i>0.025</i>	<i>0.077</i>	<i>0.110</i>	<i>0.173</i>	<i>2.2</i>	<i>352</i>	<i>2.1</i>	<i>40.9</i>	<i>39.5</i>	<i>0.139</i>	<i>0.016</i>	<i>15.64</i>	<i>11.6</i>	<i>3.32</i>	<i>578</i>	<i>0.55</i>

## Cropland 1999

Run	Land use	Q-down (% up)	Q-down (l/s)	v-cor (m/s)	v-nocor (m/s)	w (m)	h (mm)	A (mm <sup>2</sup> )	R (mm)	S (%)	Scor (%)	n	stdev n	f	C (g/l)	S*v (cm/s)	Re	froude
3a.1	crop		0.029	0.097	0.139	0.200	1.5	299	1.5	19		0.058	0.005	2.38		1.84	501	0.80
3a.2	crop		0.047	0.115	0.164	0.200	2.0	409	2.0	19		0.060	0.008	2.30		2.19	808	0.82
3a.3	crop		0.027	0.087	0.124	0.200	1.6	310	1.5	19		0.067	0.009	3.07		1.65	466	0.69
3b.1	crop		0.042	0.166	0.237	0.150	1.7	253	1.6	40		0.052	0.010	1.92		0.07	961	1.29
3b.2	crop		0.032	0.153	0.219	0.150	1.4	209	1.4	40		0.050	0.007	1.87		0.06	735	1.31
3b.3	crop		0.037	0.143	0.204	0.150	1.7	259	1.7	40		0.060	0.003	2.64		0.06	846	1.11
5a.1	crop		0.018	0.105	0.150	0.108	1.6	171	1.5	25		0.063	0.009	2.80		2.63	568	0.84
5a.2	crop		0.017	0.090	0.129	0.108	1.7	189	1.7	25		0.077	0.006	4.19		2.25	535	0.70
5a.3	crop		0.017	0.090	0.129	0.108	1.8	189	1.7	25		0.079	0.012	4.18		2.25	534	0.68



Cropland 1999 (continued)

Run	Land use	Q-down (% up)	Q-down (l/s)	v-cor (m/s)	v-nocor (m/s)	w (m)	h (mm)	A (mm <sup>2</sup> )	R (mm)	S (%)	Scor (%)	n	stdev n	f	C (g/l)	S*v (cm/s)	Re	froude
5b.1	crop		0.024	0.064	0.091	0.176	2.1	375	2.1	13		0.091	0.012	5.28		0.83	467	0.45
5b.2	crop		0.023	0.066	0.094	0.176	2.0	348	1.9	13		0.087	0.012	4.62		0.86	448	0.47
5b.3	crop		0.022	0.065	0.093	0.176	2.0	338	1.9	13		0.092	0.037	4.63		0.85	429	0.46
6a.1	crop		0.018	0.083	0.119	0.074	3.0	217	2.7	14		0.087	0.006	4.41		1.16	789	0.48
6a.2	crop		0.018	0.091	0.130	0.074	2.6	198	2.5	14		0.075	0.005	3.38		1.27	797	0.57
6a.3	crop		0.016	0.093	0.133	0.074	2.3	172	2.2	14		0.067	0.009	2.83		1.30	714	0.62
6b.1	crop		0.023	0.079	0.113	0.148	1.9	291	1.9	30		0.101	0.024	7.38		2.37	532	0.58
6b.2	crop		0.043	0.099	0.141	0.148	3.0	434	2.8	30		0.110	0.019	6.91		2.97	980	0.58
6b.3	crop		0.017	0.086	0.123	0.148	1.5	198	1.3	30		0.075	0.006	4.25		2.58	395	0.71
7a.1	crop		0.029	0.119	0.170	0.025	9.5	244	5.5	55		0.181	0.022	17.21		6.55	2313	0.39
7a.2	crop		0.041	0.122	0.174	0.056	6.0	336	4.9	55		0.165	0.008	14.61		6.71	2116	0.50
7b.1	crop		0.023	0.118	0.169	0.056	3.5	195	3.1	28		0.094	0.012	4.98		3.30	1281	0.64
7b.2	crop		0.038	0.111	0.159	0.056	6.2	342	5.0	28		0.140	0.023	9.10		3.11	1949	0.45
7b.3	crop		0.035	0.107	0.153	0.056	5.7	327	4.9	28		0.134	0.016	9.50		3.00	1822	0.45
8a.1	crop		0.037	0.129	0.184	0.056	5.1	287	4.3	27		0.105	0.012	5.62		3.48	1961	0.58
8a.2	crop		0.012	0.095	0.136	0.056	2.3	126	2.1	27		0.088	0.011	4.99		2.57	695	0.63
8a.3	crop		0.028	0.116	0.166	0.056	4.3	241	3.7	27		0.106	0.012	6.00		3.13	1521	0.57
8b.1	crop		0.023	0.090	0.129	0.074	3.3	256	3.2	13		0.084	0.007	4.07		1.17	1001	0.50
8b.2	crop		0.014	0.094	0.134	0.074	2.0	149	1.9	13		0.058	0.006	2.25		1.22	630	0.67
8b.3	crop		0.037	0.117	0.167	0.074	4.3	316	3.8	13		0.075	0.009	2.91		1.52	1572	0.57
10a.1	crop		0.042	0.123	0.176	0.044	7.8	341	5.7	46		0.171	0.022	13.94		5.66	2473	0.44
10a.2	crop		0.033	0.099	0.141	0.044	7.6	333	5.6	46		0.209	0.015	21.14		4.55	1956	0.36
10a.3	crop		0.044	0.097	0.139	0.044	10.4	454	7.0	46		0.247	0.013	27.38		4.46	2382	0.30
10b.1	crop		0.044	0.124	0.177	0.060	5.7	355	5.0	38		0.138	0.009	9.83		4.71	2162	0.52
10b.2	crop		0.048	0.116	0.166	0.061	6.7	414	5.6	38		0.160	0.021	12.57		4.41	2264	0.45
10b.3	crop		0.060	0.139	0.199	0.060	7.8	432	5.7	38		0.144	0.008	8.98		5.28	2785	0.50
11a.1	crop		0.059	0.139	0.199	0.040	11.7	424	6.7	36		0.156	0.018	9.98		5.00	3265	0.41
11a.2	crop		0.027	0.120	0.171	0.038	5.9	225	4.5	36		0.130	0.009	9.04		4.32	1902	0.50
11a.3	crop		0.046	0.124	0.177	0.040	10.3	371	6.1	36		0.165	0.019	11.47		4.46	2663	0.39
11b.1	crop		0.034	0.121	0.173	0.080	3.7	281	3.2	47		0.122	0.017	8.26		5.69	1365	0.64
11b.2	crop		0.042	0.123	0.176	0.064	5.3	341	4.6	47		0.147	0.023	11.38		5.78	1975	0.54
11b.3	crop		0.053	0.142	0.203	0.050	7.1	373	5.8	47		0.144	0.013	10.84		6.67	2897	0.54
12a.1	crop		0.029	0.092	0.131	0.070	4.5	315	4.0	6		0.068	0.007	2.26		0.55	1288	0.44

158 Cropland 1999 (continued)

Run	Land use	Q-down (% up)	Q-down (l/s)	v-cor (m/s)	v-nocor (m/s)	w (m)	h (mm)	A (mm <sup>2</sup> )	R (mm)	S (%)	Scor (%)	n	stdev n	f	C (g/l)	S*v (cm/s)	Re	froude
12a.2	crop		0.045	0.124	0.177	0.057	6.4	363	5.2	6		0.060	0.008	1.62		0.74	2262	0.50
12a.3	crop		0.055	0.156	0.223	0.050	7.5	353	5.4	6		0.050	0.006	1.07		0.94	2969	0.58
12b.1	crop		0.030	0.130	0.186	0.060	4.0	231	3.4	7		0.047	0.004	1.12		0.91	1548	0.66
12b.2	crop		0.042	0.133	0.190	0.076	4.2	316	3.7	7		0.048	0.004	1.18		0.93	1746	0.66
12b.3	crop		0.034	0.129	0.184	0.080	3.4	264	3.0	7		0.044	0.005	1.02		0.90	1374	0.71
<i>average</i>			<i>0.033</i>	<i>0.111</i>	<i>0.159</i>	<i>0.090</i>	<i>4.4</i>	<i>295</i>	<i>3.5</i>	<i>27.2</i>		<i>0.103</i>	<i>0.012</i>	<i>6.67</i>		<i>2.74</i>	<i>1439</i>	<i>0.60</i>

Other land uses 1999

Run	Land use	Q-down (% up)	Q-down (l/s)	v-cor (m/s)	v-nocor (m/s)	w (m)	h (mm)	A (mm <sup>2</sup> )	R (mm)	S (%)	Scor (%)	n	stdev n	f	C (g/l)	S*v (cm/s)	Re	froude
9a.1	fallow		0.033	0.095	0.136	0.215	1.6	347	1.6	44		0.090	0.009	6.21		4.18	531	0.76
9a.2	fallow		0.014	0.071	0.101	0.227	0.9	197	0.9	44		0.082	0.006	6.02		3.12	215	0.76
9a.3	fallow		0.025	0.092	0.131	0.190	1.4	272	1.4	44		0.088	0.014	5.86		4.05	455	0.79
9b.1	fallow		0.017	0.094	0.134	0.176	1.0	181	1.0	27		0.054	0.004	2.48		2.54	335	0.95
9b.2	fallow		0.038	0.120	0.171	0.158	2.0	317	2.0	27		0.066	0.004	2.93		3.24	823	0.86
9b.3	fallow		0.040	0.114	0.163	0.160	2.2	351	2.1	27		0.076	0.008	3.55		3.08	854	0.78
2a.1	orchard		0.048	0.108	0.154	0.200	2.3	444	2.2	34		0.092	0.025	5.07		3.67	823	0.72
2a.2	orchard		0.025	0.092	0.131	0.200	1.4	272	1.3	34		0.078	0.022	4.31		3.13	433	0.79
2a.3	orchard		0.025	0.088	0.126	0.200	1.5	284	1.4	34		0.089	0.032	4.92		2.99	432	0.73
2b.1	orchard		0.043	0.095	0.136	0.200	2.3	453	2.2	34		0.101	0.017	6.67		3.23	737	0.63
2b.2	orchard		0.019	0.081	0.116	0.200	1.2	235	1.2	34		0.080	0.016	4.80		2.75	329	0.75
2b.3	orchard		0.025	0.084	0.120	0.200	1.5	298	1.5	34		0.089	0.017	5.65		2.86	432	0.69
4a.1	waste		0.042	0.090	0.129	0.350	1.4	467	1.3	62		0.099	0.026	8.10		5.58	418	0.77
4a.2	waste		0.021	0.079	0.113	0.350	0.9	266	0.8	62		0.080	0.016	6.01		4.90	209	0.84
4a.3	waste		0.030	0.099	0.141	0.350	0.9	303	0.9	62		0.069	0.014	4.36		6.14	299	1.05
4b.1	waste		0.003	0.033	0.047	0.300	0.3	91	0.3	62		0.096	0.045	13.77		2.05	35	0.61
4b.2	waste		0.023	0.078	0.111	0.300	0.9	295	1.0	62		0.089	0.019	7.97		4.84	267	0.83
4b.3	waste		0.015	0.060	0.086	0.300	0.9	250	0.8	62		0.110	0.025	11.41		3.72	174	0.64
14a.1	waste		0.028	0.125	0.179	0.190	1.2	224	1.2	54		0.061	0.009	3.22		6.75	511	1.15
14a.2	waste		0.055	0.152	0.217	0.130	2.8	362	2.7	54		0.087	0.010	4.99		8.21	1423	0.92

Other land uses 1999 (continued)

Run	Land use	Q-down (% up)	Q-down (l/s)	v-cor (m/s)	v-nocor (m/s)	w (m)	h (mm)	A (mm <sup>2</sup> )	R (mm)	S (%)	Scor (%)	n	stdev n	f	C (g/l)	S*v (cm/s)	Re	froude
14a.3	waste		0.038	0.134	0.191	0.130	2.2	284	2.1	54		0.084	0.010	5.08		7.24	992	0.91
14b.1	waste		0.034	0.121	0.173	0.200	1.4	281	1.4	54		0.071	0.014	4.09		6.53	588	1.03
14b.2	waste		0.044	0.127	0.181	0.188	2.0	346	1.8	54		0.083	0.014	4.83		6.86	804	0.91
14b.3	waste		0.041	0.133	0.190	0.170	2.0	308	1.8	54		0.080	0.022	4.33		7.18	827	0.95
1a.1	wood		0.023	0.053	0.076	0.350	1.5	434	1.2	34		0.096	0.014	11.90		1.80	229	0.44
1a.2	wood		0.055	0.074	0.106	0.350	2.2	743	2.1	34		0.129	0.033	10.42		2.52	545	0.50
1a.3	wood		0.030	0.069	0.099	0.350	1.3	435	1.2	34		0.099	0.026	7.04		2.35	299	0.61
1b.1	wood		0.028	0.033	0.047	0.350	2.7	848	2.4	34		0.243	0.036	59.63		1.12	276	0.20
1b.2	wood		0.027	0.034	0.049	0.350	2.8	794	2.2	34		0.215	0.039	52.55		1.16	266	0.21
13a.1	wood		0.008	0.015	0.021	0.350	1.6	533	1.5	22		0.403	0.018	118.12		0.33	79	0.12
13a.2	wood		0.026	0.028	0.040	0.350	2.6	929	2.6	22		0.304	0.044	58.69		0.62	257	0.18
13b.3	wood		0.020	0.029	0.041	0.350	2.1	690	1.9	23		0.254	0.034	42.60		0.67	198	0.20
13b.1	wood		0.018	0.033	0.047	0.350	1.9	545	1.5	23		0.201	0.011	26.05		0.76	179	0.24
13b.2	wood		0.059	0.047	0.067	0.350	3.8	1255	3.5	23		0.231	0.011	29.24		1.08	579	0.24
<i>average</i>			<i>0.030</i>	<i>0.082</i>	<i>0.117</i>	<i>0.258</i>	<i>1.7</i>	<i>422</i>	<i>1.6</i>	<i>41.1</i>		<i>0.123</i>	<i>0.020</i>	<i>16.26</i>		<i>3.57</i>	<i>466</i>	<i>0.67</i>



## 7 TRANSPORT CAPACITY

*Partly based on: Hessel, R. (in press) Suitability of transport equations in modelling soil erosion for a small Loess Plateau catchment. Proceedings of the second international symposium on gully erosion under global change, Chengdu, China (May 22-25, 2002).*

### 7.1 Introduction

Sediment transport is an important process in catchment soil erosion because through this process eroded sediment is removed from the catchment. By far the most important transporting agent on most of the Chinese Loess Plateau is flowing water, which can also be a major cause of erosion. Water can transport sediment in several ways. The total sediment load of flowing water is usually subdivided into bedload and suspension load. Apart from this distinction water flow is also often subdivided in overland flow and channel flow (or streamflow). There are several differences between streamflow and overland flow:

- Overland flow is much shallower. Shallow flow exhibits undulation, so that flow conditions are changing continuously (Alonso et al., 1981, Singh, 1997).
- Overland flow is much more influenced by surface roughness and raindrop impact (Alonso et al., 1981, Singh, 1997, Abrahams et al., 2001).
- Saltation and even suspension might be limited in overland flow because of the small flow depth, so that bedload transport is likely to be the dominant mode of transport (Julien & Simons, 1985, Morgan, 1996, Singh, 1997).
- In upland areas soil surfaces are usually more cohesive than in alluvial channels (Singh, 1997).
- Streamflow is usually turbulent, while overland flow may be turbulent or laminar (Julien & Simons, 1985)
- Slopes are usually much steeper in the case of overland flow than in the case of streamflow (e.g. Govers, 1992a).

Slope steepness and runoff are probably the most important controlling factors in sediment transport. Both are very different for streamflow and overland flow.

Many empirical equations to predict transport capacity have been developed. Most equations predict transport from a combination of flow velocity, discharge, water depth, energy slope and particle characteristics. These equations can be subdivided in bedload equations and total load equations, but also in overland flow equations and channel flow equations. Flume experiments have often been used to derive the equations. As Beschta (1987) noted each equation has usually been developed for a limited range of conditions and when used in field application the estimated transport rates for the different equations may vary over several orders of magnitude. One should thus be very cautious in applying laboratory-derived flume transport capacities to field conditions since the resulting equations are usually only applicable to the conditions for which they were developed. As noted above, channel flow and overland flow differ in a number of ways. Thus it is hazardous to apply equations developed for channel flow to overland flow and vice versa.

In erosion studies of plots and fields, there is often no channel flow at all. Equations developed for streamflow have nevertheless been applied to flow on such plots. A reason for this is that the number of transport equations that has been developed for channel flow is much larger than that for overland flow. Some transport equations for interrill flow are available (e.g. Everaert, 1991, Huang, 1995), but these equations were developed using extremely small laboratory plots that might not be representative for field conditions either. Besides, for catchments, both overland flow and concentrated flow are likely to occur. Several authors have tested the performance of a number of different equations on their data set.

Low (1989) applied several transport equations to his flume data and found the Einstein-Brown formula performed well, but the Meyer-Peter Muller, Shields, Bagnold, Yalin and Smart equations were not satisfactory. An equation developed by Low, however, was found to perform better than any of the others.

Alonso et al. (1981) compared several transport equations and for streamflow recommended the use of the Yang equation (coarse sands), Laursen equation (fine sands) and Yalin equation (low density sediments). Alonso et al. (1981) also tested several transport equations developed for streamflow for their applicability to overland flow on concave slopes using literature data. They recommended the use of the Yalin equation for overland flow. The Meyer-Peter Muller equation also performed well, but the results from the Bagnold, Laursen and Yang equations were unacceptable. The Engelund-Hansen equation also performed badly.

Govers (1992a) evaluated several transport equations for their performance in the case of overland flow. Flume data collected by Govers (1990) were used for the evaluation. None of the used equations performed well over the range of conditions tested, but the Low (1989) equation gave the best results. Nevertheless it systematically underpredicted transport for small grainsizes. Govers found that simple equations based on shear stress or stream power gave better results. Govers also found that the Yang equation did not give good results for overland flow.

Julien & Simons (1985) reviewed a number of bedload equations for their applicability to overland flow. Only the equations by Engelund-Hansen and Barekyan were found to be relevant to overland flow. Julien & Simons (1985) also found that the Yalin equation can only be expected to perform reasonably well for overland flow if the shear stress is close to the critical shear stress.

Guy et al. (1992) tested six fluvial transport equations for their applicability to overland flow. They used laboratory flume measurements with sands and hollow ceramics. In their experiments, sediment was added with a sediment hopper and transport capacity was reached when the sediment flux from the flume equalled the injection rate of sediment. They concluded that fluvial sediment transport equations are generally unsuitable for overland flow, especially if the flow is impacted by rain. Sediment transport thresholds used in the equations appeared inappropriate. Only the Schoklitsch equation could be

considered suitable for overland flow. The other tested equations (Yang, du Boys, Bagnold, Laursen and Yalin) were unsuitable.

Prosser & Rustomji (2000), like Julien & Simons (1985), reviewed a large number of available transport equations. They reason that discharge ( $q$ ) and slope ( $S$ ) are the basic controlling factors and that other parameters such as shear stress and stream power are derived from these two basic parameters. Therefore, expressing all equations in terms of  $q$  and  $S$  will make comparison possible. They found similar equations for lab-plots, plots and rivers. Only flume-studies gave slightly different results.

All studies mentioned here tested different sets of transport equations, using different methods, and reached different conclusions about what the most suitable transport equation is. The studies also reached different conclusions about the applicability of channel flow equations to overland flow. In several cases, the most suitable equation proved to be one developed by the author himself. This shows that the suitability of an equation depends on the local conditions. For certain equations there are some known limits of application, e.g. the Ackers-White equation is apparently unsuitable for fine sediments (Van den Berg & Van Gelder, 1993). In most cases such limits are not known beforehand and the applicability of any particular equation can only be evaluated by testing it for the local circumstances. Depending on local circumstances one equation might perform better than another, while in other circumstances it might be the other way round. This means that the choice for any particular equation is mainly pragmatic since it will be governed by the ability of the equation to deal with the local circumstances and is not so much based on theoretical considerations.

In theory, the equations discussed in this chapter are not transport capacity equations, but transport equations. In practice, this amounts to the same thing since most equations suppose cohesionless materials. Therefore, the transport rate is determined by fluid conditions instead of sediment availability. On the Loess Plateau the soils are cohesive. The actual transport rates are therefore likely to be lower than those predicted by the transport equations. Thus, the transport equations can safely be applied as if they were transport capacity equations.

In this study a number of transport equations was applied to a small catchment on the Chinese Loess Plateau. The aims of this study were:

- To evaluate the suitability of different transport equations for the extreme conditions of the Loess Plateau.
- To test these equations in the context of catchment erosion modelling, where overland flow and channel flow both occur.
- To test the applicability of an equation developed for overland flow, the Govers (1990) equation, for overland flow in the Danangou catchment.

## 7.2 Study area

With its steep slopes, erodible soils, low vegetation cover and heavy storms in summer the Danangou catchment is representative for the hilly part of the Chinese Loess Plateau. These conditions can have implications for the use of transport capacity equations.

Elevation in the catchment ranges from 1070 to 1370 metres and the catchment is deeply dissected by gullies, which, according to the digital elevation model (DEM), have slope angles of up to 250% ( $68^{\circ}$ ). Gullies occupy about 25% of the catchment area (table 3.2). The croplands are generally located near the drainage divides above these gullies, and often have slopes in excess of 50% ( $27^{\circ}$ ). Soil erosion models have not been applied to steep slopes very often. The cause for this is probably that they focus on predicting erosion from arable land. Since in the areas where most of the models were developed (Europe and the USA) arable land is not situated on steep slopes not much attention has been paid to slope angle. Slopes of 10% are usually considered 'steep', while in many other areas of the world, including China, cropland occurs on much steeper slopes. There, a 10% slope would be considered gentle. Equations used for sediment transport capacity were not developed for such steep slopes and their validity should therefore be evaluated.

Because of the characteristics mentioned above the Loess Plateau is also an area with extreme sediment concentrations (Chapter 5). Such concentrations will also influence sediment transport by flowing water.

## 7.3 Use of the LISEM model

As a distributed model LISEM uses thousands or tens of thousands of pixels for any particular catchment. In this chapter a pixel size of 10 metres was used, so that the total number of pixels is about 20,000 for the area upstream of the weir. Since the model simulates discharge and erosion for single storms, time step length is usually in the order of several tens of seconds, in this case 15 seconds. For every pixel a water balance is performed and a water layer depth at the soil surface is calculated. The water is then routed to the catchment outlet using Manning's equation and the kinematic wave. Sediment production and transport capacity are also calculated for every pixel. The sediment concentration in the runoff is then compared to the transport capacity. If concentration is larger than transport capacity sedimentation occurs, if it is smaller erosion occurs. At the end of the time step water and sediment are redistributed and concentration is recalculated. The total duration of the simulations was 100 minutes, or 400 time steps.

Chapter 10 shows that the LISEM model can be calibrated fairly well for the larger storms, at least if the discharge at the weir is considered. The calibrated data set used in this chapter predicted peak discharge correctly (0.1% error), but overpredicted total runoff by about 30%. The implication of this is that if sediment concentration is predicted correctly, total predicted soil loss will be 30% too high.



It is important to realize that the transport equations are tested by using them in the soil erosion model LISEM. The resulting LISEM version is LISEM TC, which also includes all the changes proposed in chapter 9. Testing the transport equations by using them in LISEM means that the results obtained are an integrated result for the entire catchment upstream of the weir (2 km<sup>2</sup>). This is a very different from the usual testing on flume data or river sections (e.g. Alonso et al., 1981, Guy et al. 1992), since in those cases many parameters are constant. For example, slope, fluid density, discharge and velocity are usually constant in such situations, at least for any one experiment. In such studies sediment transport for any single experiment can be calculated and plotted against sediment transport measured. By performing a number of tests a scatterplot of points is obtained. If these points plot close to the 1:1 line the tested equation is performing well. In a natural catchment, however, all parameters change in time and space. This makes comparison of the results more difficult in the sense that it is often difficult to trace what caused results to be different from other results. If for the weir a different sediment concentration is predicted by different equations the cause need not be located anywhere near the weir. On the other hand, such testing is obviously much more realistic for catchments.

#### 7.4 Transport equations

Before starting with the discussion of transport equations, it is useful to define some parameters that are often used in transport equations. All symbols are defined in Appendix 7.1. Flowing water exerts a force on its bed that, in terms of stress, can be expressed as:

$$\tau = \rho_f \cdot g \cdot R \cdot S \quad (7.1)$$

Another important parameter of the flow with respect to sediment transport is stream power. It can be expressed in many different ways (see Rhoads, 1987). The stream power per unit wetted area (or mean stream power, Rhoads (1987)) is given by:

$$\Omega = \rho_f \cdot g \cdot R \cdot S \cdot V = \tau \cdot V \quad (7.2)$$

The product of  $S$  and  $V$  is called unit stream power. It represents the power per unit weight of water. The energy slope  $S$  is equal to the sine of the slope angle (Rhoads, 1987, Ven Te Chow et al., 1988). The Shields parameter is often used in transport equations and is given by:

$$Y = \frac{U_*^2}{g \cdot D50 \cdot (s-1)} = \frac{R \cdot S}{D50 \cdot (s-1)} \quad (7.3)$$

Shear velocity is given by:

$$U_* = \sqrt{g \cdot R \cdot S} \quad (7.4)$$

Sediment concentration can be expressed in several ways: as volume of sediment per volume of fluid or as mass of sediment per volume of fluid. In both cases the fluid can be taken either as clear water or as the water-sediment mixture. For larger sediment contents the difference between clear water concentration and dirty water concentration becomes very large.

By applying the different transport equations to an entire catchment they will be used to model both overland flow and channel flow. Since the channel network is likely to extend and contract in the course of an event the use of a single transport equation for both conditions is to be preferred. Until now LISEM has used the Govers (1990) equation for both overland flow and channel flow. This equation was developed for overland flow, and rill-flow in particular (Govers, 1992a). It could therefore be expected that the equation is less suited to channel flow as it was not developed for channel flow conditions. Several other equations were therefore also tested. The tested equations are:

- Govers (1990): total load equation for overland flow
- A combination of Govers (1990) and an empirical relationship developed for the main stream in Danangou (discussed below).
- Low (1989): bedload equation for channel flow
- Rickenmann (1990, in Rickenmann, 1991): bedload equation for channel flow
- Yalin (1963): bedload equation for channel flow
- Yang (1973): total load equation for channel flow
- Bagnold (1980): bedload equation for channel flow
- Schoklitsch (1962, in Guy et al., 1992): bedload equation for channel flow

The equations are given in Tables 7.1 and 7.2, while Appendix 7.1 gives a list of symbols. Several criteria were used in selecting these equations. The chosen equations were either: 1) well known and widely used or 2) reported to be suitable for steep slopes, high concentrations or small grain sizes.

The Govers (1990) equation is at present being used by the soil erosion models EUROSEM and LISEM. Govers (1990) conducted flume experiments using materials that ranged from silt ( $D_{50} = 58 \mu\text{m}$ ) to coarse sand ( $D_{50} = 1098 \mu\text{m}$ ). The flume length was 6 meters to ensure that transport capacity would be reached. Slopes ranged from 1 to 12 degrees and unit discharges from 2 to 100  $\text{cm}^3 \text{cm}^{-1} \text{s}^{-1}$ . According to Govers (1992a) these discharges are more representative for rill flow than for overland flow. Instead of comparing the results with available transport equations Govers (1990) compared the results with simple hydraulic parameters such as shear stress and stream power. For the coarser sediment effective stream power (depth corrected stream power) gave the best results, while for the finest sediments a very good empirical relationship was found between transport capacity and unit stream power (equation 7.5). For high flow intensities maximum sediment concentrations of 1000 – 1200 g/l were observed (Govers, 1992a). A

Table 7.1 Selected transport equations: main equation and conversion to transport capacity

	Main equation		Conversion to Transport capacity	
Govers (1990)	$TC_f = c \cdot (S \cdot u - S \cdot u_{cr})^d \cdot \rho_s$	(7.5)	$TC = \frac{TC_f}{\left(1 - \frac{TC_f}{\rho_s}\right)}$	(7.13)
Power (this study)	$TC_{\min} = 180.21 \cdot Q_{cor}^{0.1381}$	(7.6)	-	
Low (1989)	$q_b = \frac{6.42}{(s-1)^{0.5}} \cdot (Y - Y_{cr}) \cdot D50 \cdot V \cdot S^{0.6}$	(7.7)	$TC = \frac{q_b \cdot w \cdot \rho_s}{Q}$	(7.14)
Rickenmann (1990)	$q_b = \frac{12.6}{(s-1)^{1.6}} \cdot \left(\frac{D90}{D30}\right)^{0.2} \cdot (q - q_{cr}) \cdot S^2$	(7.8)	$TC = \frac{q_b \cdot w \cdot \rho_s}{Q}$	(7.14)
Yalin (1963)	$q_s = (\rho_s - \rho_f) \cdot D50 \cdot U_* \cdot P$	(7.9)	$TC = \frac{q_s \cdot w}{Q}$	(7.15)
Yang (1973)	$\log C_p = I + J \cdot \log\left(\frac{V \cdot S}{\omega} - \frac{V_{cr} \cdot S}{\omega}\right)$	(7.10)	$TC = \frac{\rho_f \cdot \frac{C_p}{1E6}}{\left(1 - \frac{C_p}{1E6}\right)}$	(7.16)
Bagnold (1980)	$q_s = q_{s*} \cdot \left(\frac{\Omega - \Omega_{cr}}{(\Omega - \Omega_{cr})_*}\right)^{3/2} \cdot \left(\frac{h}{h_*}\right)^{-2/3} \cdot \left(\frac{D}{D_*}\right)^{-1/2}$	(7.11)	$TC = \frac{q_s \cdot w}{Q}$	(7.15)
Schoklitsch (1962)	$q_s = 2.5 \cdot \rho_f \cdot S^{1.5} \cdot (q - q_{cr})$	(7.12)	$TC = \frac{q_s \cdot w}{Q}$	(7.15)

Table 7.2 Selected transport equations: secondary equations and transport threshold

	Secondary equations	Transport threshold
Govers (1990)	$c = \left( \frac{d50 + 5}{0.32} \right)^{-0.6} \quad (7.17)$	$S \cdot u_{cr} = 0.4 \quad (7.23)$
	$d = \left( \frac{d50 + 5}{300} \right)^{0.25} \quad (7.18)$	
Power (this study)	-	$Q > 50, \text{ Power} > \text{Govers}$
Low (1989)	-	$Y_{cr} = 0.06 \quad (7.24)$
Rickenmann (1990)-		$q_{cr} = 0.065 \cdot (s-1)^{1.67} \cdot g^{0.5} \cdot D50^{1.5} \cdot S^{-1.12} \quad (7.25)$
Yalin (1963)	$P = 0.635 \cdot \left( \frac{Y}{Y_{cr}} - 1 \right) \cdot \left( 1 - \frac{\ln(1+as)}{as} \right) \quad (7.19)$	$Y_{cr} = 0.06 \quad (7.24)$
	$as = \frac{2.45}{s^{0.4}} \cdot \sqrt{Y_{cr}} \cdot \left( \frac{Y}{Y_{cr}} - 1 \right) \quad (7.20)$	
Yang (1973)	$I = 5.435 - 0.286 \cdot \log\left(\frac{\omega \cdot D50}{\nu}\right) - 0.457 \cdot \log\left(\frac{U_*}{\omega}\right) \quad (7.21)$	$\frac{V_{cr}}{\omega} = \max\left(\frac{2.5}{\log\left(\frac{U_* \cdot D50}{\nu}\right) - 0.06} + 0.66, 2.05\right) \quad (7.26)$
	$J = 1.799 - 0.409 \cdot \log\left(\frac{\omega \cdot D50}{\nu}\right) - 0.314 \cdot \log\left(\frac{U_*}{\omega}\right) \quad (7.22)$	
Bagnold (1980)	-	$\Omega_c = 0.004 \cdot \rho \cdot g \cdot R \quad (7.27)$
Schoklitsch (1962)	-	$q_{cr} = 0.26 \cdot (s-1)^{5/3} \cdot D40^{3/2} \cdot S^{-7/6} \quad (7.28)$

further increase in flow intensity did not result in higher concentrations. Experiments with concentrations above 1000 g/l were discarded from the analysis. Data obtained for the 12-degree slope were not used to derive equation 7.5, so that it is actually based on slope angles between 1 and 8 degrees. Morgan et al. (1998a,b) developed equations 7.17 and 7.18 using data reported by Govers.

The combination of the Govers equation and an empirical power equation (Govers & Power) was developed because it is conceivable that the Govers equation will predict transport capacities that are too low for gently sloping channels. Flow velocity in channels was estimated to be about 2 m/s (chapter 5). For a gentle slope of say 0.01 m/m stream power would then be only 2 cm/s. From the Govers equation follows that for 35- $\mu$ m material transport capacity would then only be about 200 g/l. Measured concentrations in the low gradient channels near the weir showed that real concentrations were much higher. Figure 7.1 shows the concentrations measured at the weir in the Danangou catchment for all 5 measured events combined. Both discharge and concentration were expressed as clear water values. Figure 7.1 can be used to derive a minimum transport capacity for the channel close to the weir if it is assumed that measured concentrations do not exceed transport capacity. Since there is no guarantee that transport capacity was reached the resulting value should be seen as a minimum value. To derive a minimum transport capacity an enveloping curve is used. A power function was used since several authors (e.g. Beschta, 1987, Graf, 1988) indicated that such a function is suitable for semi-arid conditions. Since there is no reason to assume that transport capacity is always reached at the weir it is not surprising that many measurement points plot well below the envelope. If one wants to calculate actual concentration from discharge the power equation fitted through the data should be used. The validity of such an approach is, however, doubtful since the actual concentration might depend on availability of sediment rather than discharge. Furthermore, the events for which concentration data are available for both rising and falling limb of the hydrograph show that hysteresis can be important. In general, concentrations are higher during the falling limb than during the rising limb of the hydrograph (chapter 8.5). Equation 7.6 is independent of slope angle and can therefore be used to avoid unrealistically low transport capacities for low slope angles. Since equation 7.6 is only meant for channel flow it should not be used for very low discharges. The equation was therefore only applied when discharge was more than 50 l/s. Equation 7.6 was used in combination with the Govers (1990) equation in such a way that the highest of the two predicted transport capacities is used. In practice this means that the equation of Govers is used for the steep slopes with low discharge and equation 7.6 for the gentler slopes with high discharge.

The Low equation was selected because Govers (1992a) found that, from available equations, this equation gave the best results. Low (1989) developed a bedload equation based on experiments with 3.5 mm cylindrical grains of different density. The experiments were performed in a 6 metre long flume. He used low slope angles of between 4.6 and  $14.9 \cdot 10^{-3}$  ( $0.3 - 0.9^\circ$ ) and rather high unit discharges between 4.5 and 30 l/s.

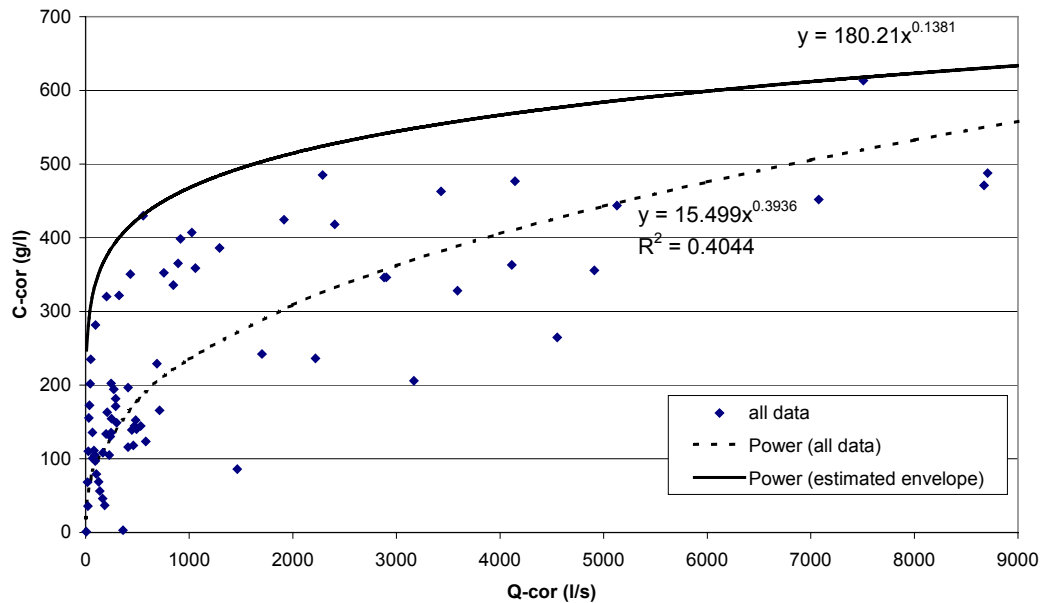


Figure 7.1 Clean water concentration as function of clean water discharge for all 5 events at the Danangou weir combined

The Rickenmann equation was selected because it was developed for flows with high sediment concentrations and slopes of up to 20%. Borges et al. (1995) studied sediment transport in a small badland catchment in the French Alps. Sediment concentrations of up to 500 g/l were measured in this area. Several transport equations that should be capable of dealing with such high sediment concentrations were tested. On theoretical grounds they concluded that the Rickenmann (1990) equation was the most suitable equation, but comparison with measurements did not seem to confirm this. Rickenmann (1991) conducted flume experiments on slopes from 7 to 20% and used hyperconcentrated flows with maximum densities of 1360 kg/m<sup>3</sup> to take into account the effects of density on bedload transport.

Adapted forms of the Yalin equation are used in e.g. the CREAMS and WEPP erosion models, but also in many other models (Singh, 1997). Yalin based his equation on theoretical and dimensional analysis of saltation. To derive the equation cohesionless movable beds consisting of grains of equal size and steady uniform flow were assumed. Note that in equation 7.9 the gravitational acceleration has been neglected to obtain units of kg/(m\*s) instead of N/(m\*s). This approach was also followed by Elliot (1988).

A frequently used total-load equation is the equation developed by Yang (1973). Yang's equation was developed for cohesionless natural sand with a median diameter between 62 and 2000  $\mu$ , specific gravity of 2.65 and a shape factor of about 0.7. The sediment is further assumed to be transported in alluvial channels under equilibrium conditions and at slopes angles small enough to neglect the downstream component of the gravitational force. The Yang equation is a non-dimensional equation based on unit stream power. The

Yang equation is interesting because it incorporates the effect of both settling velocity and viscosity, both of which depend on concentration. The equation to convert to clear water transport capacity (equation 7.16) was given by Govers (1992a).

Bagnold (1980) developed a bedload equation using literature data on both flumes and rivers. Although these data covered a large range in flow depth, grain size and stream power, the smallest grain size that was used was 0.3 mm. According to Bagnold (1980) the median grain size (D50) may be used instead of the mode if the bed sediment is unimodal. Govers (1990) gave a value of 0.4 cm/s for the critical unit stream power ( $S_u$ ). As can be seen from equation 7.11 sediment transport decreases with increasing flow depth. This is because bedload transport only occurs in a layer close to the bed. Suspended sediment is present through a larger part of the flow depth, so that equation 7.11 might potentially underpredict transport rates for suspended sediment.

The Schoklitsch equation was selected because it is a simple equation that has been reported to perform well for steep slopes (e.g. Guy et al., 1992).

Because of catchment conditions and to promote comparability of the results of the different equations a number of adaptations were necessary:

- 1) All of the selected equations were applied using the sine of slope angle. According to theory, shear stress and stream power based equations should use sine. The Shields parameter depends on shear velocity and should therefore also use the sine. The only equations that do not use either shear stress, Shields parameter or stream power are the Rickenmann and Schoklitsch equations. For the relatively gentle slopes (up to 20%) for which these equations were developed the difference between tangent and sine is small. Therefore, replacing tangent with sine will not affect the performance of the equations on their original data sets too much, while for the very steep slopes of the Danangou catchment using the sine is more prudent than using the tangent.
- 2) The effect of high concentrations was taken into account. All equations were tested with a correction equation for settling velocity (Chien & Wan, 1983, in Hsieh Wen Shen & Julien, 1993) because for high concentrations settling velocity will be much smaller than for clear water. Viscosity also depends on concentration and was corrected with the Fei Xiangjun (1982, in Zhaohui Wan & Zhaoyin Wang, 1994) equation. Fluid density is also concentration dependent (equation 5.4).
- 3) All predicted sediment transport rates were given as a clear water concentration (equations 7.13-7.16), i.e. mass of sediment per volume of water, not per volume of fluid. This was necessary because LISEM (like the other soil erosion models) does not adapt fluid levels or discharge for sediment content. Therefore, concentrations simulated by LISEM are clear water concentrations. Where necessary, measured fluid concentrations were converted to clear water concentrations to be able to compare model results with measurements.
- 4) All equations were converted to predict concentration in g/l, since this is the way in which erosion models deal with sediment load. Using this formulation transport capacity is explicitly dependent on fluid flow.

- 5) Particle density was assumed to be  $2650 \text{ kg/m}^3$  in all cases.
- 6) All equations were applied to an event that occurred on July 20<sup>th</sup>, 1999. This event was used because, from the events available, its dataset was the most complete. In this event 14.1 mm of high intensity rain fell. Catchment averaged maximum 1-minute intensity was 66.1 mm/h, while for individual rain gauges it was up to 120 mm/h. Peak discharge at the weir was 3,589 l/s, total discharge  $3,282 \text{ m}^3$  and total measured sediment yield 770 tonnes.

## 7.5 Catchment results

It was found that some equations predicted concentrations of several thousand g/l. For such concentrations the sediment can no longer be considered to be transported by water flow. Therefore, the maximum possible volumetric clear water concentration was assumed to be 0.4, which is slightly lower than the maximum concentrations that have been observed on the Loess Plateau. This concentration corresponds to a dirty water concentration of 757 g/l and a clear water concentration of 1060 g/l. All predicted transport capacities above this value were assumed physically impossible and were set to 1060 g/l. The results of the different equations can then be compared in two ways:

- 1) By comparing simulated sediment concentration to concentration measured at the weir.
- 2) By comparing the fraction of the catchment covered by transport capacities of 1060 g/l. This fraction indicates how often the respective methods exceed possible values. Therefore, the less often this happens the better the equation performs.

Figure 7.2 shows the predicted concentrations for the weir as well as the measured concentrations. It shows that the combination of Govers & Power as well as Yalin, Bagnold and especially Yang predicted concentrations that were too high. The results for the Yang equation clearly showed the effect of setting the 1060 g/l maximum. Schoklitsch predicted concentrations that were clearly too low. The results for the Low and Rickenmann equations were almost equal and their results were reasonable, though concentrations declined too rapidly after the discharge peak. Govers gave the best shape of the sedigraph, but slightly overpredicted sediment yield (table 7.4). Figure 7.3 shows the transport capacities calculated with the different equations for  $t = 10$  minutes, which was during heavy rain. Figure 7.3 shows that that all equations predicted low transport capacities in the northwest of the catchment as well as in some areas in the south. This is caused by the fact that according to the model there was no water at the surface at this time; in the northwest this was caused by lack of rain, while the areas in the south are woodland areas that had higher infiltration. The Govers equation and the Govers & Power equation gave almost the same transport capacity. The results for Low, Rickenmann, Yalin, Yang and Bagnold were similar to each other, though there were some minor differences between them. Figure 7.3 also shows that Low, Rickenmann, Yalin, Yang and Bagnold calculated transport capacities of 1060 g/l or higher for very large parts of the catchment. Govers and Govers & Power calculated transport capacities of 1060 g/l or higher in only a few places, while Schoklitsch occupied an intermediate position.



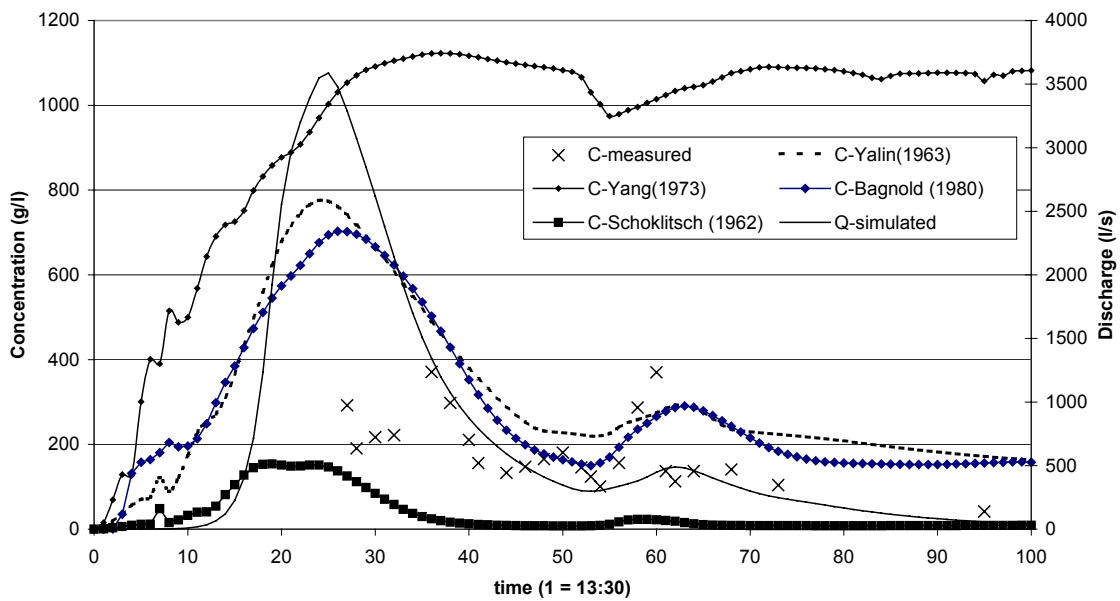
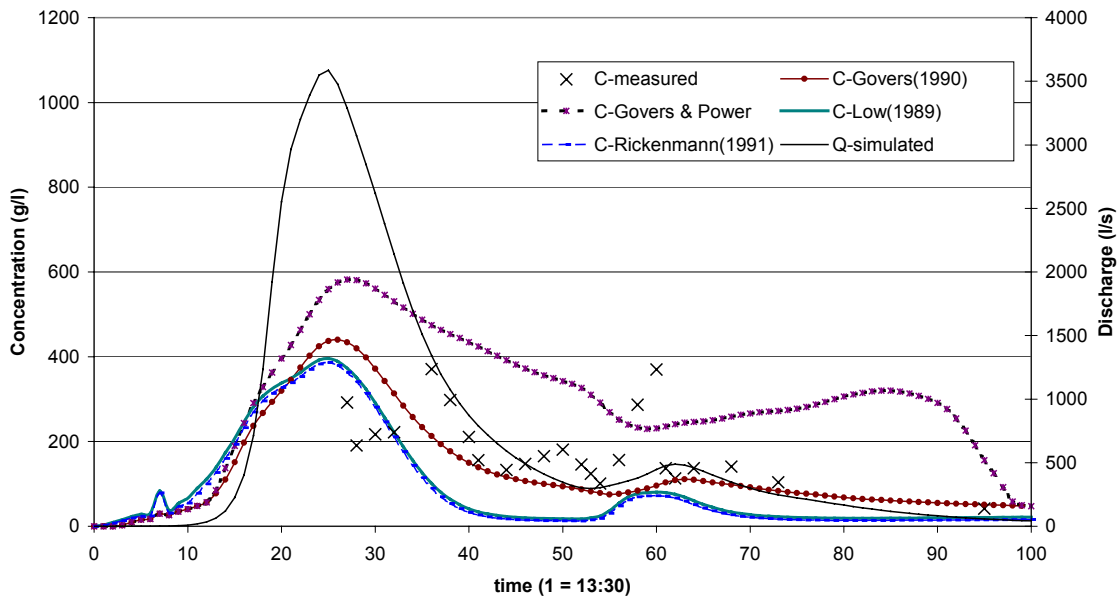
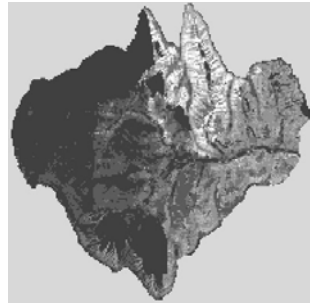
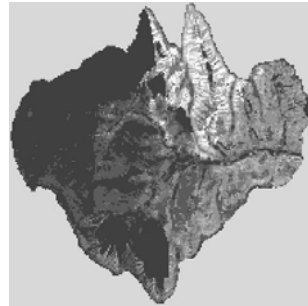


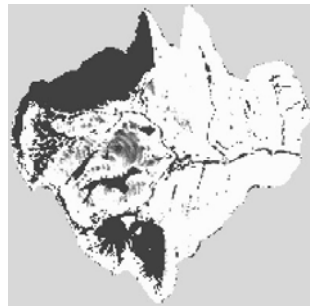
Figure 7.2 Results of different transport equations, event of 990720. Maximum possible clear water concentration was 1060 g/l



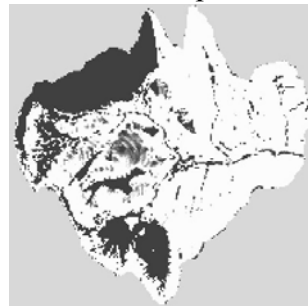
Govers (1990)



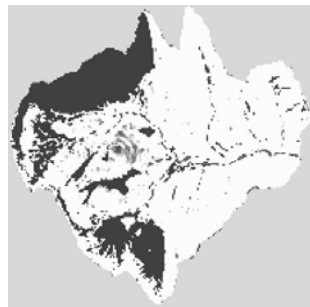
Govers (1990)  
& Power equation



Low (1989)



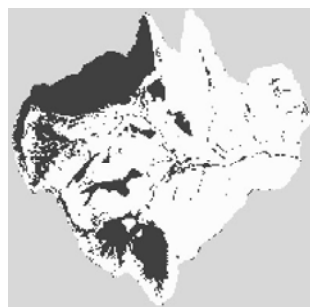
Rickenmann (1991)



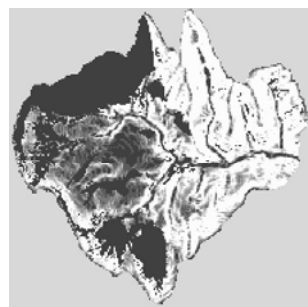
Yalin (1963)



Yang (1973)



Bagnold (1980)



Schoklitsch (1962)

Figure 7.3 Transport capacities predicted by different transport equations for  $t=10$  minutes (during heavy rain). Clear water transport capacities range from 0 (black) to 1060 (white) g/l

Table 7.3 shows simulated detachment and deposition for the different equations. A distinction was made between the hill slopes and the channel. Table 7.4 gives total sediment yield as a percentage of the measured value. Since total discharge was overpredicted by 30%, an overprediction of sediment yield by the same percentage would indicate a good performance of a particular equation. Tables 7.3 and 7.4 therefore confirm the results from figure 7.2: underprediction by Schoklitsch, reasonable prediction by Low and Rickenmann, slight overprediction by Govers and overprediction by Govers & Power, Yalin, Yang and Bagnold. The position of the channel was defined using the digital elevation model, and the total channel length was about 1300 m. As can be seen in Figures 3.1 and 3.2 the channel slope is generally low. Transport capacity in the channel will have a large influence on simulated sediment yield. Table 7.3 shows that the channel was an area of net deposition for all equations, except the combination of Govers & Power. Sediment yield ranged from 4% (Schoklitsch) to 54% (Yang) of detachment. The Yang equation had very large transport capacity for the channels and therefore simulated a far higher sediment yield than the other equations.

Table 7.3 Simulated detachment and deposition for different transport capacity equations. Maximum possible clear water concentration was 1060 g/l

	detach slope (tonne)	depo slope (tonne)	yield slope (tonne)	detach channel (tonne)	depo channel (tonne)	total loss (tonne)	yield (% of detach) <sup>a</sup>	yield (% of slope) <sup>b</sup>
Govers (1990)	6607	-5181	1426	382	-577	1229	17.6	86.2
Govers (1990) & Power	6459	-4649	1810	297	-170	1935	28.6	106.9
Low (1989)	8719	-7046	1673	223	-887	1007	11.3	60.2
Rickenmann (1990)	8839	-7203	1636	246	-913	967	10.6	59.1
Yalin (1963)	12543	-8887	3656	1548	-2769	2414	17.1	66.0
Yang (1973)	7937	-3462	4475	124	-157	4377	54.3	97.8
Bagnold (1980)	8485	-5847	2638	718	-1122	2228	24.2	84.5
Schoklitsch (1962)	8291	-7645	646	84	-364	365	4.4	56.5

<sup>a</sup> Sediment yield from the catchment (total loss) as percentage of total detachment (detach slope + detach channel)

<sup>b</sup> Sediment yield from the catchment (total loss) as percentage of the yield from the slopes (yield slope)

## 7.6 Discussion of catchment results

### 7.6.1 Govers and Govers & Power-equation

Figure 7.3 shows that the transport capacity predicted with the Govers equation and with the Govers & Power equation were almost equal, while figure 7.2 shows that the predicted concentrations at the weir were very different. The fact that predicted transport capacities were almost equal can be explained from several factors:

- Discharge can only be above 50 l/s in the main channels, and only during the main part of the event. Therefore, the Govers equation was used most of the time.

- From equation 7.6 follows that the transport capacity as calculated from that equation does not reach 1060 g/l until a discharge of about 373,000 l/s, so that equation 7.6 is extremely unlikely ever to produce transport capacities of 1060 g/l. A difference between Govers and Govers & Power would therefore not be clearly visible in the figure.

Nevertheless, the concentrations calculated with the method that uses equation 7.6 were much higher than those obtained by using the Govers equation alone. A comparison of total predicted erosion and deposition showed that the higher sediment yields for the Govers & Power equation were due to smaller deposition, not to higher erosion (Table 7.3). This must be caused by the fact that transport capacities for the main channels in the Danangou catchment are fluctuating much less when the power equation is used. Using the Govers equation alone rapid alternations in transport capacity occur because of large changes in slope from one pixel to the next. When the combination of Govers equation and the power equation is used these changes become less.

For grainsizes of 35  $\mu$  the  $d$ -exponent of the equation of Govers (1990) is about 0.6. This means that if critical stream power is much smaller than actual stream power transport capacity will depend on slope to the power 0.6 (but note that  $u$  also depends on  $S$  according to the Manning equation). Equation 7.6 does not depend on slope at all, but only on discharge. The effect of the use of equation 7.6 is, however, too large since the predicted concentrations were too high. The prediction might be improved by increasing the threshold used in the equation, but this is not much more than adding another calibration parameter to the model. Since Govers already predicted concentrations of the right magnitude this was not worthwhile.

### 7.6.2 Low

The Low equation was developed using flume experiments with 3.5 mm grains and slopes between  $4.6 \cdot 10^{-3}$  m/m ( $0.3^\circ$ ) and  $14.9 \cdot 10^{-3}$  m/m ( $0.9^\circ$ ), while unit discharge was rather high at 4.5 to 30 l/s. For the Danangou catchment characteristic values are: 35  $\mu$  grains and slopes of about 0.3 m/m ( $17^\circ$ ). The Low equation was thus developed for much coarser materials and much gentler slopes. In the Low equation the Shields parameter is used as calculated from equation 7.3. Using realistic values for streamflow at Danangou ( $R = 0.6$  m,  $S = 0.3$ ,  $D50 = 35 \cdot 10^{-6}$  m,  $s = 2$ ) gives a value for the Shields parameter  $Y$  of over 5000. Simulation results confirmed that the Shields parameter was usually very high in the case of the Danangou catchment. Therefore, transport capacities were also very high. If  $Y$  is very high,  $Y_{cr}$  can be neglected in the Low equation, which then turns into:

$$q_s = \frac{6.42 \cdot R \cdot V \cdot S^{1.6}}{(s-1)^{1.5}} \quad (7.29)$$

This equation is very sensitive to  $S$  and  $s$ . For maximum dirty water concentrations of 757 g/l the lower case  $s$  can vary between 1.8 and 2.65, while  $S$  can vary between 0.01 and 0.9, so that  $S$  is the more important variable. Note that  $V$  also depends on  $S$ . Figure 7.3

shows that on the steeper slopes in the Danangou catchment the predicted transport capacities were almost everywhere above 1060 g/l. The Low equation includes the effect of a decrease in density difference between particles and fluid through the  $s$  parameter, but only in its influence on bedload. Hence, for low slope angles with low  $s$  transport will still be negligible. In other words, the sediment needed to lower the value of  $s$  is not considered to be transported by the flow. This is not surprising given the fact that the equation is meant to predict bedload, while the sediment causing the decrease in  $s$  is suspended load. Nevertheless, it indicates that the equation might theoretically not be suitable to predict total load for conditions on the Chinese Loess Plateau. The reasonable predictions that were obtained are a consequence of using the 1060 g/l restriction on transport capacity. Without such a restriction the predicted concentrations would be too high for high-density flows on steep slopes.

### 7.6.3 Rickenmann

The Rickenmann and Low equations gave very similar results. The Rickenmann equation, however, does not use the Shields parameter. Instead it uses critical discharge as calculated from equation 7.25. From this equation can be seen that small grain size, high density and large slope angle all result in a decrease of critical discharge. Critical discharge therefore becomes negligible in comparison to discharge. The Rickenmann equation itself is like the Low equation very sensitive to changes in  $S$  and  $s$ . Here too, the sediment needed to lower the value of  $s$  is not considered to be transported by the flow, so that the equation might theoretically not be suitable to predict total load for conditions on the Chinese Loess Plateau. The reasonable predictions that were obtained are again a consequence of using the 1060 g/l restriction.

### 7.6.4 Yalin

The Yalin equation uses the Shields parameter, and like the Low and Rickenmann equations predicted transport capacities that are too high for the steeper slopes. The Yalin equation is, however, much more complex than Low and Rickenmann equations. If  $Y$  is very large,  $as$  (equation 7.20) will be very large.  $P$  will also be very large, but the net effect on  $q_s$  (equation 7.9) is more difficult to determine because on the one hand  $P$  and  $U_*$  will be large, while on the other hand  $(\rho_s - \rho_f)$  and  $D50$  will be small for the conditions at Danangou. The results indicated that the net effect was that predicted concentrations were too high (Figures 7.2 and 7.3). Julien & Simons (1985) suggested that Yalin only performs well for overland flow if the actual value of shear stress is close to the critical shear stress, which is not the case on steep slopes with fine sediment. Therefore, it appears that the Shields parameter is not suitable for the steep slopes and fine sediments of the Danangou catchment.

### 7.6.5 Yang

The Yang equation is difficult to assess because it is a complex equation in which the different consequences of high concentrations seem to have opposite effects in the equation. The  $(\omega D50/\nu)$  terms, for example, will become smaller, while the  $(U_*/\omega)$  terms

will become larger. The net result is hard to predict, also because several logarithms are used. In our simulation the logarithm of the  $(\omega D_{50}/\nu)$  terms was always negative, while that of the  $(U^*/\omega)$  terms was usually positive. The result was that  $I$  varied between 4.6 and 6.3, while  $J$  varied between 1.8 and 3.1. This, in turn, results in values for  $\log(C_p)$  that were almost always above 6 (sometimes as high as 12), so that predicted concentration was more than a million parts per million. Because of the used restriction in predicted transport capacities the predicted transport capacity was usually 1060 g/l, both for the slopes and the channel. The effect of this on simulated concentration at the weir is clearly visible in figure 7.2. When there is no water the predicted transport capacity is 0. Values between 0 and 1060 g/l hardly occur, so that the map shown in figure 7.3 is almost pure black and white. These results show that Yang should not be used for the Danangou catchment. Contrary to other equations the cause for this is not the slope dependency of the Yang equation. This dependency is difficult to determine since slope appears in the main equation as well as in  $I$  and  $J$  (equations 7.10, 7.21 and 7.22). It is, however, clearly low. Figure 7.3 confirms this since, contrary to all other equations, the low gradient channels do not stand out in the map. Instead, the cause is apparently a combination of small settling velocity, small grainsize and large viscosity. Alternatively, the constant of the Yang equation (5.435) is too high.

According to Alonso et al. (1981) Yang performs badly for low-density sediments. In the Danangou catchment the sediment is not low density, but the fluid density can become high. The effect could be the same as that of having low-density sediments, since in both cases the density difference between sediment and fluid is reduced. Alonso et al. (1981) proposed that this bad performance might be because the Yang equation only incorporates sediment density through settling velocity (instead of directly) and that it was only developed for sand. Note that this second criticism of Alonso et al. (1981) was not based on grainsize (Yang used sands with median grainsize as low as 62  $\mu$ ) but on the implicit assumption that small particles have low density. This is, however, not the case in the Danangou catchment. Govers (1992a) also found that Yang over predicts transport capacity for fine materials and he too ascribed this to the sensitivity of the equation to settling velocity. Guy et al. (1992) found that the Yang equation is unsuitable for overland flow. According to them, it seems particularly inadequate at specifying the transport threshold.

#### 7.6.6 *Bagnold*

The Bagnold equation predicted concentrations that are too high. The cause of this is that stream power was generally large, while grainsize was always small. The performance of the Bagnold equation might be improved by calibrating the reference values for stream power and grainsize to values that are more representative for the Danangou catchment than the 0.5 and 0.0011 that were used in the simulation (Appendix 7.1). Another potential problem with the Bagnold equation is that transport capacity decreases with increasing water depth. For suspended load that is not realistic. On the other hand, the predicted transport capacities for the channel were still higher than for most other equations.

### 7.6.7 Schoklitsch

The Schoklitsch equation calculates critical discharge in much the same way as the Rickenmann equation. Like was the case for the Rickenmann equation critical discharge will be very small for the Loess Plateau because small grainsize, high density and large slope angle all result in a decrease of critical discharge. Critical discharge therefore becomes negligible in comparison to discharge and the Schoklitsch equation reduces to:

$$TC = 2.5 \cdot \rho_f \cdot S^{1.5} \quad (7.30)$$

This equation is very sensitive to slope angle. As a result, the Schoklitsch map of figure 7.3 shows more slope influence than any of the other equations. Therefore, predicted concentrations were too high for the steep slopes, but far too low for gentle slopes. The net result in this case was that predicted concentrations at the weir were too low.

### 7.6.8 Choice of equation

The results indicate that the Shields parameter is not suitable for the Danangou catchment because the steep slopes, high density flows and small grainsize all contribute to very high values for the Shields parameter. Likewise, the same conditions cause critical discharge to be extremely small. Thus, the results of the simulations indicate that for the small grain sizes and steep slopes of the gully catchments on the Loess Plateau the transport threshold can usually be neglected in the equations. Most of the resulting equations are too sensitive to slope angle (Schoklitsch, Yalin, Bagnold, Low and Rickenmann), so that transport rates are overpredicted for steep slopes and underpredicted for gentle slopes. The net result of this for the catchment outlet is not always the same; most equations overpredicted concentration at the outlet, but the Schoklitsch equation underpredicted it. The Govers equation performed better than the other equations because it has lower slope dependency. The Yang equation appeared to be too sensitive to grainsize. Therefore, the use of the Govers equation is recommended for erosion models that deal with small grainsizes and steep slopes.

## 7.7 Discussion of catchment methods

### 7.7.1 Use of LISEM

The use of the different transport equations in the erosion model LISEM had certain implications. The most important was that the range of certain parameters had to be restricted to prevent that missing values were ever generated. Such values would cause the model to abort. In practice, this means that dirty water concentration could not be allowed to be equal to or larger than particle density ( $2650 \text{ kg/m}^3$ ) in the equations, since this would cause  $s$  to be 0 or negative, and clear water concentration to become infinite or negative. To be on the safe side, the maximum possible dirty water concentration was assumed to be equal to the maximum possible dirty water transport capacity (757 g/l), and the minimum  $s$  was set to 1.1. Such a choice of restrictive values can influence the

predicted concentrations, but tests with a maximum possible dirty water concentration of 2600 g/l suggested that the influence was not large for the catchment outlet.

### 7.7.2 Maximum transport capacity

In the simulations the maximum possible transport capacity was set to a clear water concentration of 1060 g/l. This value was rather arbitrarily chosen. To test the effect of setting the maximum possible concentration to 1060 g/l the simulations were also performed with a maximum possible concentration of 1767 g/l (an increase of 66%). This value corresponds to a dirty water volumetric concentration of 0.4, or a dirty water concentration of 1060 g/l. These runs showed that all equations predicted higher soil loss in that case (table 7.4). However, the difference with the 1060 g/l simulation varied considerably between equations. For the Govers and Govers & Power equations the difference was small (about 10%). These equations had transport capacities below 1060 g/l for most of the catchment anyway (Figure 7.2), so that changing the maximum

Table 7.4 Simulation results for different maximum possible clear water concentrations and different storms

	990720 max 1060		990720 max 1767			000829 max 1060	
	abs	% of meas	abs	% of meas	% of 1060	abs	% of meas
<i>water</i>							
Measured peak discharge (l/s)	3589	100	3589	100	100	8757	100
Simulated peak discharge (l/s)	3592	100	3592	100	100	8884	101
Measured total discharge (m <sup>3</sup> )	3282	100	3282	100	100	5893	100
Simulated total discharge (m <sup>3</sup> )	4277	130	4277	130	100	7191	122
<i>total soil loss (tonne)</i>							
Measured	770	100	770	100	100	2630	100
Govers (1990)	1229	160	1354	176	110	2082	79
Govers (1990) & Power	1935	251	2070	269	107	3095	118
Low (1989)	1007	131	2033	264	202	1640	62
Rickenmann (1990)	967	126	2010	261	208	1588	60
Yalin (1963)	2414	314	4267	554	177	4020	153
Yang (1973)	4377	568	6762	878	154	6561	249
Bagnold (1980)	2228	289	3888	505	175	4157	158
Schoklitsch (1962)	365	47	450	58	123	555	21

possible transport capacity affected only a small part of the catchment. The Schoklitsch equation also showed a relatively small change (23%). The other equations, however, showed an increase in simulated sediment yield of 54-108%. This shows the large effect that a choice for a certain maximum transport capacity can have for those equations for which the maximum transport capacities were reached in large parts of the catchment. The



distribution of physically impossible concentrations (now above 1767 g/l), however, did not change much. The shape of the sedigraphs was also similar to that obtained with 1060 g/l.

### 7.7.3 *Choice of storm*

The storm that was used in the simulations was a storm of medium size. In the 3-year measurement period several larger storms occurred, but also several smaller ones. The choice of storm can have an effect on the results of the simulation. It was shown here that the Govers equation predicted concentrations of the right magnitude for the storm of 990720. Calibration for the other storms, however, showed that this was not the case for an event that occurred on August 29<sup>th</sup>, 2000. This is the largest event for which data were available. Measured concentrations were considerably higher during that event than during the event of 990720, and the Govers equation (max clear water concentration 1060 g/l) underpredicted soil loss by more than 20% (table 7.4). Despite the fact that most of the other equations have been rejected for use in the Danangou catchment on grounds that are not event-specific, such as slope angle dependency and grain size, runs with the other equations were also conducted. The results confirmed that those equations predict transport capacities that are too high for large parts of the catchment. The shape of the simulated sedigraphs was also similar to the shapes shown in Figure 7.2. Most equations, however, clearly underpredicted measured concentrations (table 7.4). Only the Yalin, Bagnold and Yang equations still overpredicted yield for this event, but the percentage overprediction was much lower than for the 990720 event. The best prediction was obtained with the combination Govers & Power, which gave an overprediction of 18% compared to the overprediction of total discharge of 22%. This suggests that channel transport capacities predicted by the Govers equation can be too low for large events in this area.

### 7.7.4 *Choice of equation*

Many other transport equations exist. These could not all be tested, but it seems likely that the Loess Plateau characteristics of steep slopes, high concentrations and small grain size would cause most equations to behave in a way similar to that of the tested equations. This means that the transport threshold might be negligible, and that the equations might well be too sensitive to slope angle. Without testing these equations, however, it is not possible to give definite statements about their performance. As mentioned in chapter 2, one particular equation that would be worth testing is the equation developed by Abrahams et al. (2001). They used a very large data set obtained from flume experiments to develop a total load transport equation for interrill flow. This equation is interesting since it was developed using data obtained under a wide range of conditions with respect to: flow depth and velocity, Reynolds number, Froude number, slope, sediment size, sediment concentration, roughness concentration and diameter, flow density and viscosity. For application on the Loess Plateau especially maximum volumetric concentration (0.3), minimum grain size (98  $\mu$ m) and maximum slope (10 degrees) are relevant. These values compare favourably with those of some other transport equations, but grain size is still too large and slope angle too low for Loess Plateau conditions.

### 7.7.5 Limits of transport capacity

Abrahams et al. (2001) discussed the effect of steep slopes on transport and noted that cohesionless materials would move en masse if slope angle were larger than the angle of internal friction. They proposed to correct  $S$  for the downslope component of gravity:

$$S_{cor} = S \cdot \frac{\tan \varphi}{\cos \alpha (\tan \varphi - \tan \alpha)} \quad (7.31)$$

$S_{cor}$  will approach infinity when slope angle ( $\alpha$ ) approaches angle of internal friction ( $\varphi$ ), and should be taken as infinite when slope angle exceeds angle of internal friction. Thus, transport capacity would also be infinite. This shows that the concept of transport capacity has no physical meaning for slopes steeper than the angle of internal friction; any loose material would be transported through gravity anyway. However, in that case, we are no longer considering transport by flowing water, but mass wasting, since transport would be independent of fluid flow. On very steep slopes with cohesive soils there still is transport by fluid flow, but transport rate should become more dependent on detachment rate than on transport capacity. Since in the concept of transport capacity detachment depends on transport capacity (see equation 2.19) new approaches might be needed to model transport in those conditions.

The concept of transport capacity will also reach its limits when concentrations become extremely high. For such concentrations, flow properties progressively deviate from those of clear water (chapter 5). Hyperconcentrated flows can, up to a point, probably still be modelled using the transport capacity concept by taking into account the effects of sediment concentration on fluid density, settling velocity and viscosity. With increasing concentrations the behaviour of flows will become more and more like that of debris flows. Which concentration should be taken as upper limit is hard to say because the change from hyperconcentrated flow to debris flow is a gradual one. Costa (1988) placed the boundary between hyperconcentrated flow and debris flow at dirty water concentrations of 1285 g/l, but other authors have used different values.

By choosing to model transport based on the concept of transport capacity, only transport by flowing water can be modelled. The choice of a maximum possible concentration should reflect this, in that its value should not be so high that transport cannot be considered transport by flowing water. In this approach other methods of transport (debris flow, mass movements, soil fall etc) are neglected. As noted above these processes cannot be modelled with the concept of transport capacity. Where these processes are important, as on very steep slopes, or where concentrations are very high, the concept of transport capacity reaches its limits of applicability. Ultimately, however, these other processes will only deliver material to the valley bottoms in the catchment and all processes, except debris flow, are unlikely to transport material out of the catchment. Therefore, sediment yield from the catchment would still be determined by the transport capacity of flowing water.

## 7.8 Overland flow

LISEM at present uses the Govers (1990) equation for both overland flow and channel flow. In the previous sections its use for an entire catchment, in which overland flow and channel flow both occur, was evaluated. In this section its use for overland flow alone will be evaluated. The Govers equation was developed for overland flow, so that there is no a priori reason to suspect that it might not be applicable. The equation was, however, developed for slopes of only up to 8 degrees. In this section sediment data collected at the sediment plot (chapter 4.4) and from the measurements of Manning's  $n$  (chapter 6) will be evaluated and compared to the equations of Govers. In both cases, slope angles were much steeper than 8 degrees.

### 7.8.1 Sediment plot

The data collected at the sediment plot can be used to evaluate transport capacity. Since the plot was on a 34 m long cropland one can assume that:

- 1) There will be so much loose material available that transport will be transport limited.
- 2) That transport capacity will be reached before the downstream end of the plot.

The results from the sediment plot measurements have been reported in chapter 4.4. Table 4.2 showed that very high average sediment concentrations were observed at the sediment plot, especially in 1999. Chapter 4 also showed that the quality of the data collected at the sediment plot was not very high. From the 5 events measured only 3 can be used for modelling: the events of 990710, 000707 and 000829. Even the data collected on these storms have some problems. Nevertheless, they can be used to evaluate the performance of the Govers (1990) equation on a steep cropland. On the plot, flow will be either overland flow or rill flow. The Govers (1990) equation was developed for rill flow. This means that if it proves impossible to simulate the measured sediment concentrations the Govers equation is not suitable and another transport equation is needed. To be able to use the data collected at the plot some changes were needed:

- 1) LISEM was used to simulate the amount of water and erosion at the outlet of the plot, which is at the sensor. Since the total amount of water from the barrels was probably more reliable than the sensor data (as shown in chapter 4) the total amount of water collected in the barrels was corrected to the total amount of water passing the sensor. To do this event-rainfall downstream of the sensor was subtracted from the total collected amount of water. The sensor data were, however, the only data that could give any information about the shape of the hydrograph.
- 2) In reality significant sedimentation occurred in the gutters and flume upstream of the sensor, but downstream of the plot. Since it would be almost impossible to simulate this sedimentation correctly with LISEM the total amount of sediment coming from the plot was used.

- 3) The average concentration was then obtained by dividing the total amount of sediment by the total amount of water from upstream of the sensor. This is an artificial combination, but simulation-technically the best solution. It means that the calculated concentration was above the actual concentration of water passing the sensor (because of sedimentation upstream of the sensor), but below the actual concentration of water coming from the plot (because there was rain on gutters and flume upstream of the sensor).
- 4) To achieve the desired resulting combination LISEM was adapted in such a way that erosion and sedimentation were not allowed in the gutter and flume upstream of the outlet (sensor). To avoid problems with the mass balance it was necessary to equate the transport capacity with the sediment concentration for the gutters and flume.

Table 7.5 Available data and simulation results for the sediment plot events

Parameter	990710	000707	000829
<i>Plant and soil</i>			
Plant height (m)	0.10	0.06	0.65
Plant cover	0.02	0.03	0.20
Leaf area index	0.02	0.02	0.499
Random roughness (cm)	1.22	1.79	1.754
Cohesion (kPa)	7.55	n.a.	8.33
Aggregate stability	5	7	4
<i>Rain and discharge</i>			
Event rainfall (mm)	10.6	16.3	16.7
Max 1-minute intensity (mm/h)	59.1	71.6	189.1
Peak level flume (cm)	2.9	2.3	20.3
Peak discharge <sup>a</sup> (l/s)	0.18	0.12	8.1
Total discharge at sensor (l)	41.3	101.4	1622
Corrected average concentration (g/l)	600	275	406
Sediment yield (kg)	24.8	27.9	651
<i>Calibration settings LISEM</i>			
Saturated conductivity (cm/day)	16.37	13.63	6.49
Cohesion (kPa)	7.55	8.33	8.33
Aggregate stability	5	7	4
<i>Simulation results</i>			
Peak discharge (l/s)	0.21	0.22	7.82
Total discharge at sensor (l)	52.0	88.7	1643
Average concentration (g/l)	173	172	447
Sediment yield (kg)	9.0	15.3	735

<sup>a</sup> sediment volume subtracted, see chapter 5

The simulations for the sediment plot were performed with LISEM TC, using a grid size of 0.2 m and a time step of 1 second. The maximum possible dirty water transport capacity was set to 757 g/l in all cases, as was the case for the catchment simulations.

The simulated sedigraphs will not be shown because, as explained above, they included the sediment that would have been deposited upstream of the sensor. Since sedimentation can be expected to occur mainly during the falling limb of the hydrograph, the simulated concentrations would be too high during this period.

#### *LISEM input*

Slope angles of the sediment plot were measured and a digital elevation model was made. A small roughness was randomly added to the DEM to obtain a more realistic drainage direction map with slightly converging flowpaths. Since the plot is homogenous with respect to soil and land use, no soil map or land use maps were needed. Table 7.5 shows the available data for the events. Manning's  $n$  was calculated from slope angle as described in chapter 6.

#### *Results*

LISEM was calibrated for the plot in a way similar to that described in chapter 10 for the catchment upstream of the weir. An explanation of the calibration procedure at this point would go beyond the scope of the present chapter. The main calibration settings are, however, shown in table 7.5.

Figure 7.4 shows that simulated runoff did not match observed runoff for the events of 990710 and 000707. Total simulated runoff was similar to that measured, but shape of the hydrograph, peak discharge and timing of the peak were all different. In particular, the observed double runoff peak of the 000707 event was hardly predicted by the simulation at all. Table 7.5 shows that total soil loss was underpredicted for both events.

For the 000829 event the simulated discharge better matched the observed discharge than for the 990710 and 000707 events. As explained in chapter 4 there is some uncertainty about the falling limb of the measured hydrograph for the 000829 event. The simulated discharge peak, however, followed the measured one closely. The shape was similar and the main difference was a time shift of about 1.5 minutes between observed and predicted discharge. The cause of this could well be a time difference between the rain gauge and the Thalimedes sensor. The simulated peak discharge was slightly less than the measured one, but the simulated total discharge was almost equal to the observed total discharge (table 7.5). Therefore, the simulated hydrograph was considered acceptable. Table 7.5 also shows that the total amount of soil loss was slightly overpredicted.

#### *Discussion*

The LISEM simulation results for the sediment plot show that the shape of the hydrograph was reasonably well predicted for the large event of 000829. For the other two, smaller, events, however, the predicted hydrograph was less good. This indicates that larger events are easier to simulate than smaller events. The reason for this is probably that for larger events it matters less if the initial conditions (such as initial

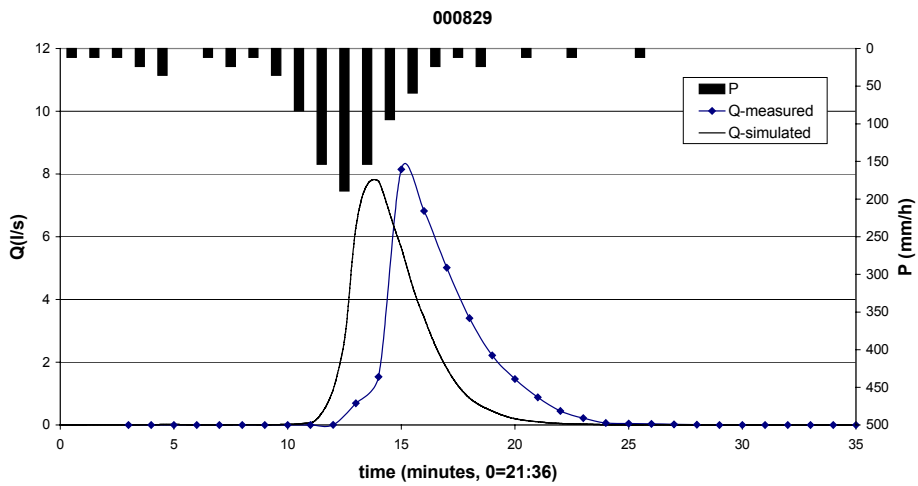
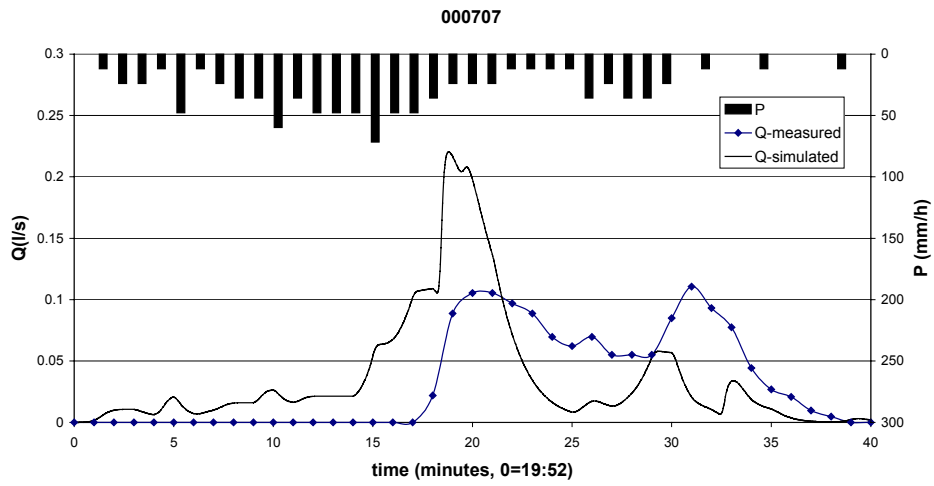
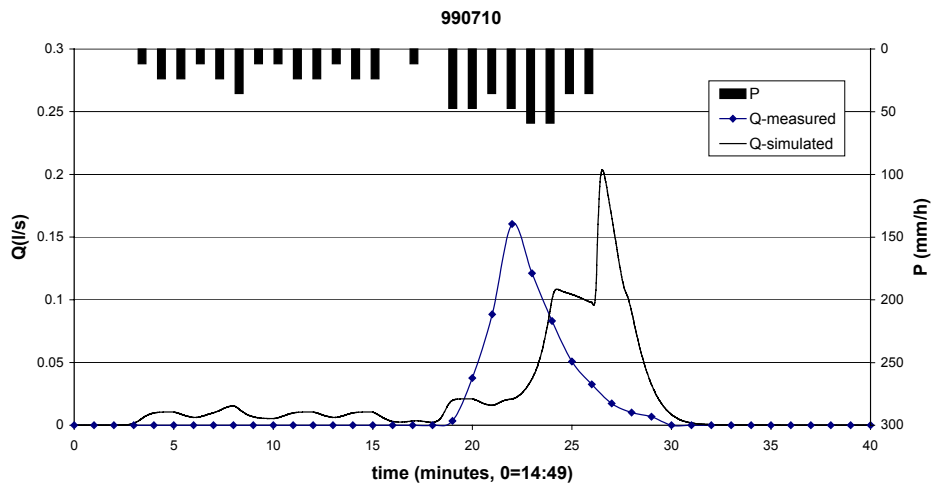


Figure 7.4 LISEM simulation results for the sediment plot, 990710, 000707 and 000829 events

moisture content) were accurately known or not, while for larger events spatial variability of input data is probably also less important.

The results from all 3 simulations showed time shifts between predicted and measured peak. However, there was some uncertainty about the timing of the measured discharge in relation to the timing of the rain. For the 000707 event, for example, the measured runoff peak occurred before the measured rainfall peak. This is highly unlikely to occur in reality. The cause is probably a time difference between the rain gauge and the Thalimedes sensor. Because the sediment plot was fairly small even a small time difference of a few minutes can make it impossible to fit simulated discharge with measured discharge. Therefore, time differences between simulated discharge and measured discharges were largely disregarded and more attention was paid to runoff amounts.

The simulation results show that the Govers (1990) equation can deal with the conditions at the erosion plot for the large event of 000829. For the smaller events, however, sediment yield was underpredicted. This could not be improved by calibrating cohesion or aggregate stability since that only resulted in more erosion as well as more deposition. Sediment yield remained the same, which suggests that transport occurred at transport capacity. Sediment yields for the 990710 event were also simulated with the Yalin and Low equations. This gave 37 kg and 36 kg respectively, compared to 9 kg obtained with the Govers equation and the 24 kg that were measured. However, as in the case of the entire catchment transport capacity was restricted by applying the 1060 g/l clear water maximum. This constriction was also applied to the Govers equation, but there it had no effect as that equation did not predict transport capacities that were above 1060 g/l in this case. The reasonable predictions that were obtained for Yalin and Low were probably a consequence of using the 1060 g/l restriction. Without such a restriction the predicted concentrations would likely be too high. The results from the plot therefore confirm those obtained for the entire catchment and also show that these results do not change significantly from one event to the next, since for the entire catchment the 990720 event was used. These results seem to indicate that the present transport equations cannot deal with high concentrations that were observed for small events. The cause might be that for such steep slopes gravity plays a very important role in transport, as noted in section 7.7.

### *7.8.2 Runoff experiments*

Chapter 6 mentioned that during the 34 measurements of Manning's  $n$  that were conducted in 2000 sediment levels in the bucket at the downstream end of the plots were recorded. After the experiment the clear water was poured out of the bucket and the remaining level of sediment was measured. Two samples taken from this sediment showed that the concentration was about 900 g/l. Using this value the erosion from the plots can be calculated. Only the data for cropland were used since the other land uses showed much smaller erosion and can thus not be used to determine transport capacity. Erosion for those land uses is detachment limited, not transport limited. On croplands rills developed for slopes of more than about 15%. Figure 7.5 shows the amount of sediment

in the bucket as a function of slope angle and of discharge. Prosser & Rustomji (2000) showed that sediment transport equations can be written as power functions incorporating a slope and a discharge term (section 2.3.3). Figure 7.5 shows that the sediment data did not have any relationship with discharge. The slope angle did have an influence, the data points can be interpreted as being bounded by an enveloping curve that would describe transport capacity. Points plotting below this hypothetical boundary thus indicate that transport capacity was not reached. However, there is no guarantee that the bounding envelope represents transport capacity; it just marks a lower limit to transport capacity. Real transport capacity could be much higher.

Concentrations calculated from the sediment amounts in the buckets are plotted against stream power in figure 7.6. The transport equation developed by Govers (1990) is also shown. A  $d_{50}$  of  $35 \mu\text{m}$  is used. Figure 7.6 shows that concentration increased with increasing stream power. Concentrations of several hundred grams per litre were reached for the higher stream powers. Nevertheless, all the points plotted far below the Govers equation. There was considerable spread in data points for higher stream powers. This was probably caused by the lack of relationship between erosion and discharge (figure 7.5). With a value of about  $2 \text{ cm/s}$  the threshold for transport was higher than the value of  $0.4 \text{ cm/s}$  mentioned by Govers (1990). For these low stream powers, detachment might be the limiting factor, so that it is not surprising that transport capacity was much higher than observed transport. Also, for higher stream powers the flow might not yet have reached transport capacity because the plot length was only  $2.5 \text{ metres}$ . There is, therefore, no reason to suspect that the Govers equation would not apply.

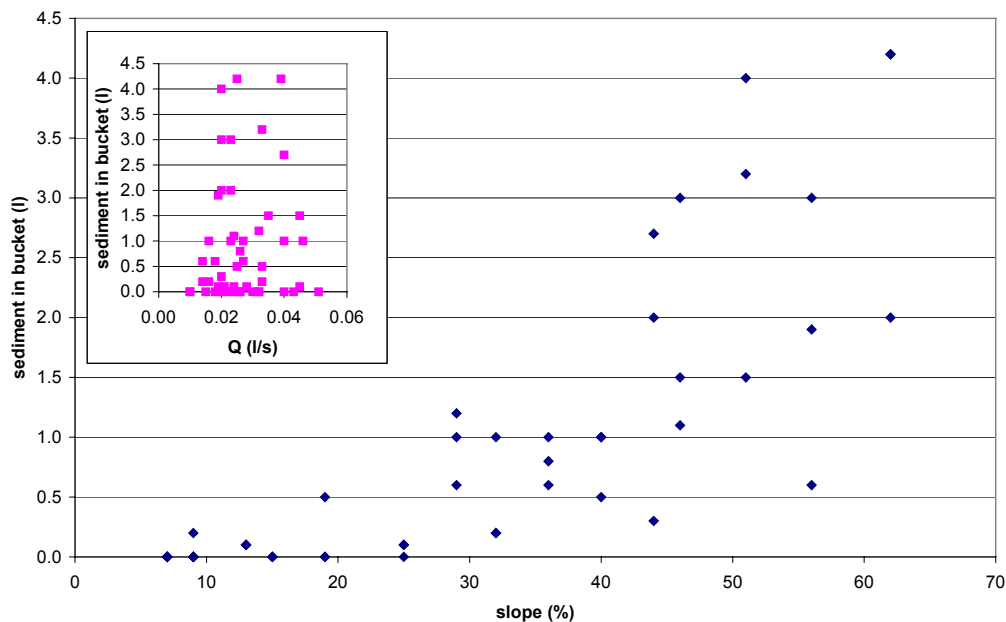


Figure 7.5 Amount of sediment in downslope buckets of Manning's  $n$  measurements as function of slope and discharge. Cropland plots only



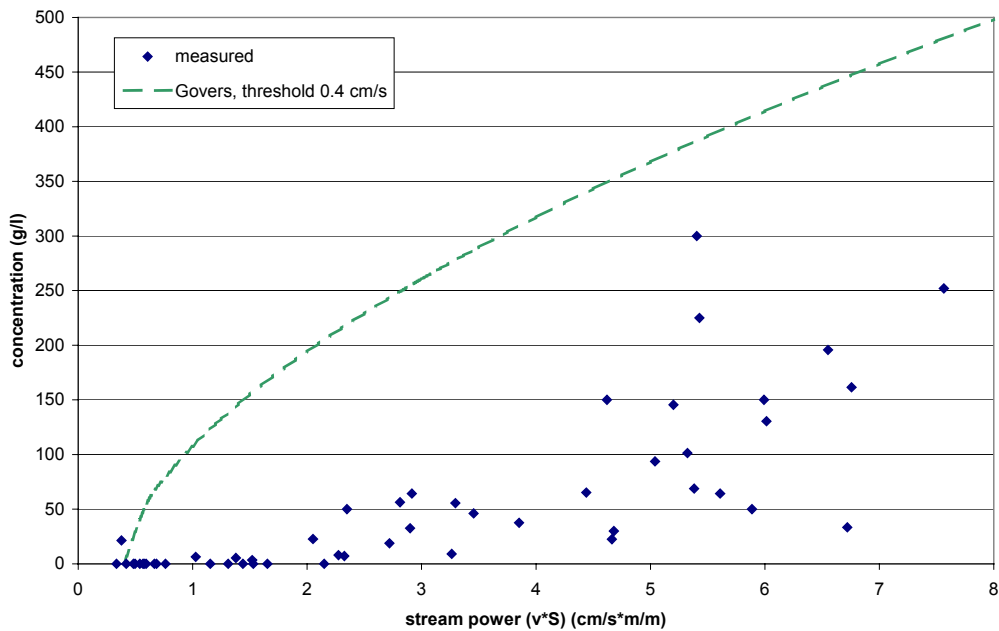


Figure 7.6 Concentration as a function of stream power. Data for cropland plot measurements only. Transport capacity ( $D_{50} = 35 \mu$ ) according to the Govers (1990) equations is also shown

## 7.9 Conclusions

Several transport equations were applied to a small catchment on the Chinese Loess Plateau by programming the equations into the LISEM model. The model was applied to an event that occurred on July 20<sup>th</sup>, 1999. A comparison of the results showed that the Govers (1990) equation performed better than the other equations because it correctly predicted average concentration at the weir and did not result in impossible transport rates inside the catchment as often as the other equations. It appears that for this storm the other transport equations predicted transport capacities that were too high due to several characteristics of the Danangou catchment:

- Steep slope angles
- Small grainsizes
- High density flow

The Shields parameter is not suitable for the Danangou catchment because the steep slopes, high-density flows and small grainsize all contribute to very high values for the Shields parameter. Thus, equations that use Shields overpredicted transport capacity, especially on steep slopes. Likewise, in equations using critical discharge, the critical discharge will be very low, so that transport capacity was also overpredicted. If the transport threshold is neglected, most equations appear to be too sensitive to slope angle. The Govers equation has relatively low slope dependency and was found to perform best. The Yang equation appeared to be too sensitive to grainsize.

Simulations for the sediment plot showed that the Govers (1990) equation also performed well for overland flow for the larger events, when there is sufficient water available, like during the large event of 000829. For small events, however, the transport capacity of overland flow was underpredicted by the Govers equation. Though other equations can yield better predictions in that case, they, like for the entire catchment, often predicted impossible concentrations. Nevertheless, the results might indicate that for steep slopes with small amounts of water the Govers equation is not really suitable. This can be due to the large effect gravity will have on transport for such slopes.

Runoff experiments on small plots showed that measured transport rates were always well below those predicted with the Govers equation.

These results show that the Govers equation is suitable for most flow conditions that occur in the Danangou catchment. Since, for modelling, it is preferable to use only one equation for the entire catchment, it is recommended to use the Govers equation. It will therefore be applied during calibration and also to evaluate the effects of different land use scenarios.

## Appendix 7.1 List of symbols used in chapter 7

Symbol	Unit	Meaning
<u>Greek</u>		
$\alpha$	$^{\circ}$	slope angle
$\nu$	$\text{m}^2 \text{s}^{-1}$	kinematic viscosity
$\rho_f$	$\text{kg m}^{-3}$	fluid density
$\rho_s$	$\text{kg m}^{-3}$	density solids
$\tau$	$\text{kg m}^{-1} \text{s}^{-2}$	shear stress
$\phi$	$^{\circ}$	angle of internal friction
$\omega$	$\text{m s}^{-1}$	settling velocity
$\Omega$	$\text{kg s}^{-3}$	stream power per unit bed area
$\Omega_{\text{cr}}$	$\text{kg s}^{-3}$	critical stream power per unit bed area
$(\Omega - \Omega_{\text{cr}})^*$	$\text{kg s}^{-3}$	reference excess stream power (0.5)
<u>Latin</u>		
$C_p$	ppm	concentration
$C_{\text{cor}}$	g/l	clear water concentration
$D$	m	mode of grainsize
$D_{30}$	m	characteristic grainsize, 30% by weight finer
$D_{40}$	m	characteristic grainsize, 40% by weight finer
$D_{50}$	m	median grain size
$d_{50}$	mu	median grain size
$D_{90}$	m	characteristic grainsize, 90% by weight finer
$D^*$	m	reference grain size (0.0011)
$g$	$\text{m s}^{-2}$	gravitational acceleration
$h$	m	water depth
$h^*$	m	reference water depth (0.1)
$q$	$\text{m}^2 \text{s}^{-1}$	fluid discharge per unit width
$q_b$	$\text{m}^2 \text{s}^{-1}$	volumetric bedload transport per unit width
$q_{\text{cr}}$	$\text{m}^2 \text{s}^{-1}$	discharge threshold for sediment transport
$q_s$	$\text{kg m}^{-1} \text{s}^{-1}$	sediment transport rate
$q_{s^*}$	$\text{kg m}^{-1} \text{s}^{-1}$	reference sediment transport rate (0.1)
$Q$	$\text{m}^3 \text{s}^{-1}$	clear water discharge
$Q_{\text{cor}}$	l/s	clear water discharge
$R$	m	hydraulic radius
$s$	-	ratio between grain and fluid density ( $\rho_s/\rho_f$ )
$S$	-	sine of slope angle
$S_{\text{cor}}$	-	S corrected for gravity
$Su_{\text{cr}}$	$\text{cm s}^{-1}$	critical unit stream power (assumed 0.4)
$TC$	g/l	clear water transport capacity
$TC_f$	g/l	dirty water transport capacity
$TC_{\text{min}}$	g/l	minimum clear water transport capacity
$u$	$\text{cm s}^{-1}$	mean velocity
$U^*$	$\text{m s}^{-1}$	shear velocity
$V$	$\text{m s}^{-1}$	flow velocity
$w$	m	flow width
$Y$	-	Shields parameter = dimensionless shear stress
$Y_{\text{cr}}$	-	critical Shields parameter (assumed 0.06)



## 8 GULLIES

*Partly based on: Hessel, R. & Van Asch, Th.W.J. (in press) Modelling gully erosion for a small catchment on the Chinese Loess Plateau. Catena*

### 8.1 Introduction

A striking feature of the hilly part of the Loess Plateau is the presence of many, large, permanent gullies. The Danangou catchment forms no exception. The loess deposits of the Chinese Loess Plateau can be subdivided into the Wucheng, Lishi and Malan formations. The Wucheng and Lishi formations are sometimes collectively called ancient loess, while the Malan formation is called new loess (e.g. Lin & Liang, 1982). Since the gullies in these two different loess types are different from each other it is important to study the properties of these types of loess. The ancient loess is an early Pleistocene loess deposit that has been altered by weathering. It has a higher clay-sized particle content than the overlying new loess of late Pleistocene age and also has greater bulk density and cohesion (Table 8.1). The weathering has also caused a change in colour from yellowish brown to reddish brown. For the purpose of distinguishing between the two loess types in the field, the ancient loess was called red loess while the new loess was called yellow loess in the present study (see section 3.3). Table 8.1 gives some characteristic properties of red and yellow loess as measured in the Danangou catchment. Table 8.1 shows that loess properties at Danangou (central Loess Plateau) and Gansu (western Loess Plateau) are similar. In the Danangou catchment, the red loess crops out in the deeper valleys, mainly north of the main valley and on the southern slope of the hill in the middle of the catchment (figure 8.1). Yellow loess is found on all hilltops. Its maximum thickness is slightly over 10m, while red loess makes up the rest of the total loess thickness of up to 200 m.

The presence of many large, permanent gullies is one of the main differences between the Chinese Loess Plateau and areas where soil erosion modelling has so far been used. The aims of the research described in this chapter were:

- 1) To find out if a storm based soil erosion model like LISEM can be adapted to model gully erosion in the Danangou catchment. This requires an evaluation of the gully processes that are operating.
- 2) To find other ways of modelling gully erosion if it proved impossible to model it with current soil erosion models.
- 3) To determine the importance of gully erosion in the Danangou catchment. This requires that a sediment balance for the Danangou catchment be made.

### 8.2 Gully types and processes

The heights of the most important gully heads were measured with tape whenever possible. Table 8.2 gives the heights of the 10 highest vertical headcuts found in red loess and yellow loess, as well as field estimates of the amount of loose soil material

Table 8.1 Properties of different types of loess. Gansu loess data were derived from Derbyshire et al. (2000), Derbyshire & Meng (2000) and Dijkstra et al. (2000)

Parameter	Gansu loess		This study	
	Wucheng/ Lishi loess	Malan loess	Red loess	Yellow loess
D50 (mu)	10-18	30-40	20	42
Clay (% below 2 mu)	18-25	8-14	10	6
Silt (% 2 - 64 mu)	70-77	63-69	82	73
Sand (% above 64 mu)	5	23	8	21
Cohesion (kN/m <sup>2</sup> ) <sup>a</sup>	75-100	50-75	100 <sup>b</sup>	45 <sup>b</sup>
Bulk density (kg/m <sup>3</sup> )	1520-1810	1380-1440		
Dry bulk density (kg/m <sup>3</sup> )			1570	1270
Wet bulk density (kg/m <sup>3</sup> )			2018	1777

<sup>a</sup> assuming a condition of structural strength, i.e., without any fissures or cracks

<sup>b</sup> derived through back-analysis by assuming that measured headcut heights are maximum possible headcut heights.

Table 8.2 Measured and estimated (*Italic*) headcut heights (m) of red loess and yellow loess gullies and estimated volume of loose soil material below the headcut, May 1999. The position of the headcuts is shown in figure 8.1

Red loess gullies			Yellow loess gullies		
Gully No.	Gully Height (m)	Soil fall volume (m <sup>3</sup> )	Gully No.	Gully height (m)	Soil fall volume (m <sup>3</sup> )
1	28.6	1	1	14.3	0
2	28.6	10	2	<i>12.0</i>	0.5
3	27.0	*	3	11.8	0
4	24.9	5	4	10.6	0.5
5	24.1	1	5	10.5	3
6	23.9	1	6	10.3	0.5
7	22.1	0.5	7	<i>10.0</i>	0.5
8	<i>20.0</i>	0	8	<i>10.0</i>	0.5
9	19.3	0.5	9	<i>10.0</i>	0
10	17.3	*	10	9.9	0.5
Mean	23.6	2.4		10.9	0.6

\* volume of loose soil material could not be estimated as the gully bottom was not visible

accumulated below the headcut. Figure 8.1 shows the position of the gullies included in table 8.2. Figure 8.2 shows pictures of some of the gullies listed in the table, indicating a clear difference in size and morphology between red loess and yellow loess gullies. Both table 8.2 and figure 8.2 show that red loess gullies are much larger. They are also more

directly linked to the stream network, as they are usually found at lower elevation than the yellow loess gullies. In all, more than 50 gullies with headcut heights of over 7 m were measured. The total number of gullies in the catchment is much higher. Table 8.2 also shows that loose sediment volumes were highly irregular; some gullies had large quantities of loose sediment, but most had little or none. Red loess gullies appeared to have more loose sediment than yellow loess gullies, but this is probably caused by the fact that they are larger and that one gully (No. 2) had a very large amount.

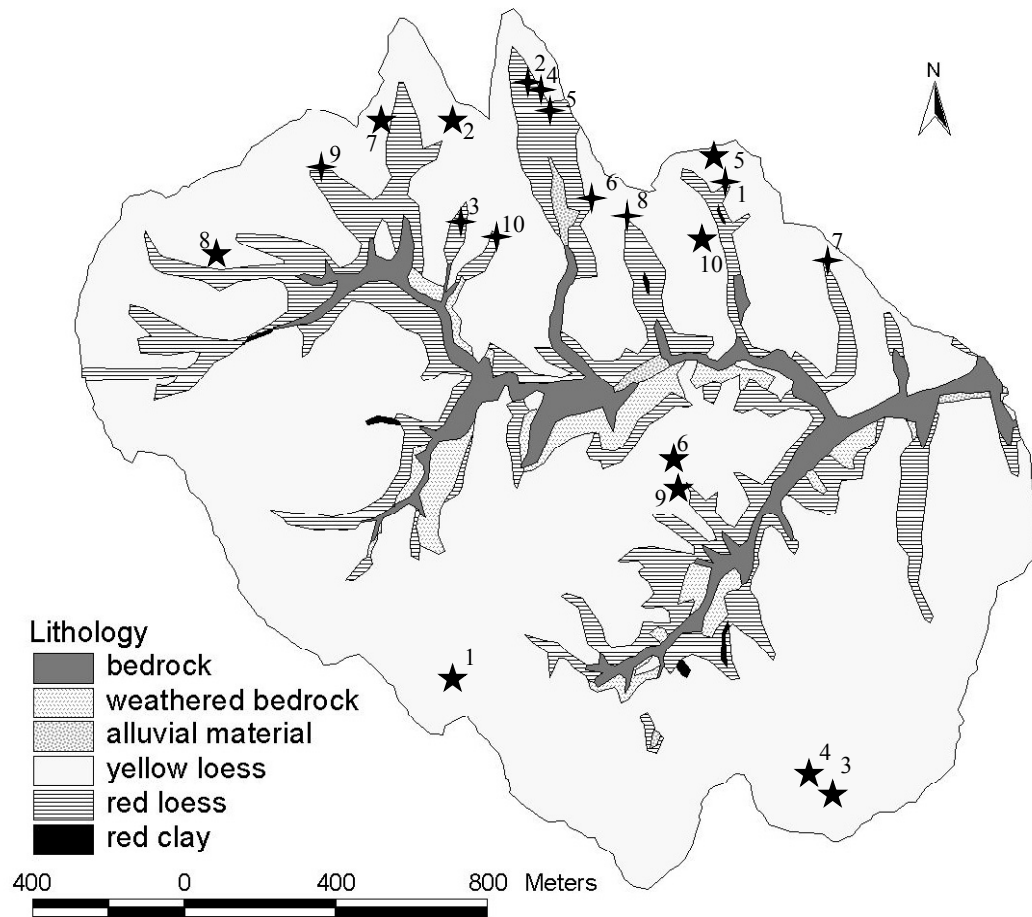


Figure 8.1 Lithological map of the Danangou catchment. The position of the gully headcuts from table 8.2 is also shown in the map; red loess gully headcuts are shown with a 4-point star, yellow loess gullies with a 5-point star

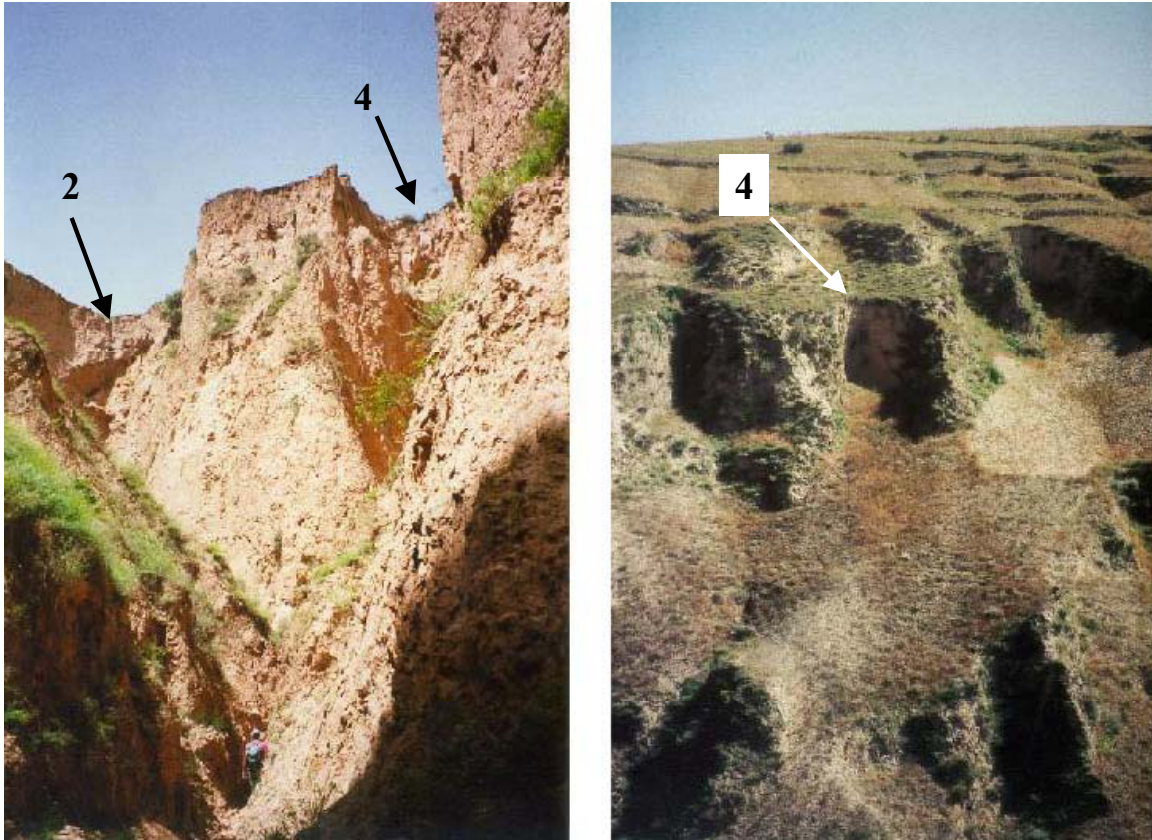


Figure 8.2 Left: red Loess gully complex containing red loess gully heads 2, 4 and 5 of table 8.2. The position of gully heads 2 and 4 is indicated with arrows; gully head 5 is not included in the picture. Note the person in lower middle portion for scale. Picture taken by R.Vergouwe. Right: yellow loess gully 4 of table 8.2 (indicated with arrow)

In principle, the difference in headcut height between red loess gullies and yellow loess gullies should reflect a difference in cohesion. It must, however, be realised that the yellow loess thickness is generally not much more than 10 m, so that the difference suggested by table 8.2 is in fact greater than would be the case if the yellow loess thickness did not limit the size of the gullies.

As described in chapter 4.5, over 200 erosion pins were installed in 12 gullies distributed evenly over the Danangou catchment. Pins were classified according to their position on headcut tops, headcut walls, sidewall tops, sidewall walls and gully bottoms. Pin lengths were measured 5 times between October 1998 and September 2000. Pins that had been disturbed (e.g. by children or goats) were not used in the analysis. The measuring results over the 2-year period are shown in table 8.3. The data suggest that there is erosion on gully walls, no change around the gully edge and deposition on gully bottoms. The large standard deviations are caused by individual pins being affected by soil fall. There are some uncertainties with regard to the measurements (e.g. the degree of disturbance), but the data nevertheless suggest that average gully headcut retreat rates are small and that soil fall on gully headcuts is an important process. It should be noted that the measurement period had below average rainfall.



Table 8.3 Pin length change over a 2-year period (October 1998 – September 2000). Negative sign indicates a decrease in pin length

Pin Position	Number of pins	Average change Pin length (cm)	Standard deviation (cm)
Gully bottom	28	-0.95	2.08
Headcut top	16	0.16	2.34
Headcut wall	37	0.89	2.62
Sidewall top	40	-0.00	1.08
Sidewall wall	80	0.41	1.45

Repeated observations (before and after runoff events) at gullies without erosion pins also showed that the gully heads in the Danangou catchment do not change shape perceptibly during runoff events. Nevertheless, gullies do produce sediment during runoff events. Since many gullies are very large (table 8.2), even a small retreat rate can still produce large amounts of sediment. Some flow erosion and wall collapse may occur during events, but much material coming from the gully during events was probably produced by soil falls in between and just after events. Field observations showed that in many gullies, soil falls occur from time to time in between events (chapter 3). The loess shows many almost vertical cracks, which may have formed by tectonic forces, stress release or desiccation. Because of the presence of these cracks, soil falls are mostly of a slab-like or column-like form. Most soil falls are fairly small, with heights and widths of a few metres and a thickness of about 0.2 – 0.4 m.

Vandekerkhove et al. (2001) measured headcut retreat rates of gullies in southern Spain and also found that soil fall as a result of tension crack development was one of the major causes of gully headcut retreat. Their average headcut retreat rates were much larger (10 cm per year), but their results were also dominated by soil falls in certain individual gullies. Another study in semi-arid southern Spain, Collison (2001), likewise identified tension crack development as a major cause of gully head instability. Oostwoud Wijdenes & Bryan (2001) studied gully headcut retreat in silt-loams near Lake Baringo, Kenya. They found that tension and desiccation cracks developed in between storms and that the depth of these cracks was a function of headcut height, soil properties and the length of the dry period since the last storm.

The material produced by these soil falls accumulates on the bottoms of the gullies, ready to be transported during the next runoff event. Figure 8.3 shows one of the yellow loess gullies in the catchment before and after a runoff event that occurred on July 20<sup>th</sup>, 1999. As can be seen from the picture on the left, there was a great deal of loose soil material available on the gully bottom before the event. Most of it was produced by a small soil fall on the left bank of the gully (to the right in the pictures). The picture (Figure 8.3) reveals that all this loose soil material was removed during the runoff event. Some erosion of the right bank (left in the pictures) probably occurred during the runoff event.

The runoff discharge passing through this gully has been estimated at several hundred litres per second, based on flow width and depth estimated after the event. The estimated flow width was about 1.3 m, while the estimated depth was 0.3 m. Surface velocity of the runoff was measured in the main stream during the event and was found to be about 2 m/s. A flow velocity of, e.g., 0.75 m/s for this much smaller stream is therefore reasonable. This gave a discharge of close to 300 l/s. The yellow loess gully shown in figure 8.3 was not a typical gully for this area (its position and activity were influenced by a large mass movement), but it clearly showed the process of soil accumulation between events and removal during events.



Figure 8.3 Loose soil material in one of the gullies of the Danangou catchment before (left) and after (right) the runoff event of July 20<sup>th</sup>, 1999

As noted in chapter 2 the LISEM model is a storm-based erosion model. Since gully headcut retreat as a result of storms is negligible in the Danangou catchment, it can be ignored in storm-based modelling. Gullies can, however, produce major sediment volumes during runoff events because of the removal of loose soil material accumulated on the gully bottom due to soil fall. The process of soil fall is, however, one that cannot be modelled on a storm basis. Instead, it should be modelled on a daily basis. As the number of gullies is large, it is not easy to simulate soil falls using process based stability models. Such models would require detailed information about soil cohesion and shear strength, as well as about soil moisture content. In addition, the location of cracks should be known. All this information would be required for all gullies in order to perform a thorough analysis. The only possibility is to use a pragmatic approach by assuming certain values for the soil physical parameters. Such a daily-based model should produce a map showing the locations and amounts of loose soil material available in the gullies at the time of a particular event. The LISEM model could then be adapted to incorporate

such a map in the calculations for the event. Since the accumulated soil fall material is loose, it will show very little cohesion, and the transport capacity will be the only factor controlling sediment removal.

### 8.3 Stability model

As the number of gullies is very large and their positions are not always easy to map, the first aim of the stability model to be developed is to determine gully headcut positions based on the DEM (Digital Elevation Model). If such an approach proves successful, the method could also be applied to catchments for which no headcut mapping was done. The DEM was produced from a 1:10,000 topographical map with a 5 m interval between contour lines. The resulting DEM had a pixel size of 5 m. The index developed by Montgomery & Dietrich (1992) is used to extract the location of gully heads from the DEM. This index relates the position of the channel head to the local slope and upstream area:

$$Index = \frac{A}{b} \cdot S^2 \quad (8.1)$$

Where:  $A$  = upstream area (m<sup>2</sup>)  
 $b$  = pixel size in the direction perpendicular to the flow (m)  
 $S$  = slope (m/m)

$b$  has been reformulated for use with pixel data. In practice, this means that  $b$  is equal to either pixel size (when flow is perpendicular to the pixel boundary) or the square root of 2 times the pixel size (when water leaves the pixel in a diagonal direction). Montgomery & Dietrich found that almost all channel heads were located between index values of 25 and 200, but these values might be grid size dependent. As gully heads and channel heads differ, some adaptations are necessary. First, as gully heads can also occur downstream of the channel head, only the minimum value of the index (25) is used. Finding the upper gully head along a channel is not straightforward either, as there are some differences between gully heads and channel heads that have to be taken into account. Channel heads are defined as the upstream end of where flow between definable banks occurs (Dietrich & Dunne, 1993), while gully heads have additional characteristics, e.g. in terms of size, shape and slope. Three further conditions are therefore introduced to allow the detection of gully heads. Since gully heads always have steep gradients, the first additional condition is that gully heads have gradients of more than 1.2 m/m (50°). If this is not the case, a channel head might exist, but a gully head cannot. The second condition is that it is assumed that gully heads can only occur in loess, not in bedrock, weathered bedrock or alluvial material. A lithological map of the catchment has been made and is used to implement this condition (Figure 8.1). The third and last condition is that gully heads were assumed to be concave in plan view. This condition is necessary to prevent landslide scarps from being classified as gully heads. Landslide scarps are often also concave in plan form, but not at a 5-m pixel size.

After the location of the gully head has been determined, its height can be calculated by assuming that gully headcuts are vertical. Since the gradient is given by the elevation difference between pixels, divided by the horizontal distance between pixel centres, the headcut height can be obtained by multiplying the gradient with the distance between adjacent pixel centres. This distance is equal to  $b$  in equation 8.1. When gully heads in adjacent pixels in a flowpath are found they are combined into a single headcut.

Since field observations have shown that headcuts are almost vertical and that failures often occur as slabs, the Rankine earth pressure theory applies (Lohnes & Handy, 1968). This theory can be used to calculate the critical vertical headcut height with the help of the following equation (for derivation see Lohnes & Handy, 1968):

$$H_c = \frac{4 \cdot c}{\gamma \cdot (\cos \varphi - 2 \cdot \cos^2(45 + \varphi / 2) \cdot \tan \varphi)} - y \quad (8.2)$$

Where:  $H_c$  = critical headcut height (m)  
 $c$  = cohesion ( $\text{kg/m}^2$ )  
 $\gamma$  = bulk density ( $\text{kg/m}^3$ )  
 $\varphi$  = angle of internal friction ( $^\circ$ )  
 $y$  = depth of cracks (m)

Values for bulk density ( $\gamma$ ) have been measured for red and yellow loess (Table 8.1), while the angle of internal friction ( $\varphi$ ) for red and yellow loess has been derived from Dijkstra et al. (2000). Since table 8.1 shows that Gansu loess and Danangou loess are similar, this means that values of  $\varphi$  determined for Gansu loess can also be applied to Danangou loess. Dijkstra et al. (1994, 2000) performed several kinds of shearing test on Gansu loess to determine the soil physical parameters  $c$  and  $\varphi$  for the different loess types of the Loess Plateau. They made a distinction between undisturbed and disturbed loess. Undisturbed loess has no cracks and therefore has structural strength, while disturbed loess has cracks and is at residual strength. Their results show that for undisturbed loess  $c$  is by far the most important factor, so that  $\varphi=0$  can be used for undisturbed loess. Under these circumstances, equation 8.2 reduces to:

$$H_c = \frac{4 \cdot c}{\gamma} \quad (8.3)$$

Values for cohesion can therefore easily be estimated if measured headcut height is assumed to be critical headcut height. Table 8.1 gives values for the cohesion ( $c$ ) of undisturbed loess estimated in this way. As explained above, this could result in an underestimation of cohesion in the case of yellow loess. Maps of bulk density, angle of internal friction and cohesion have been created by reclassification of the lithological map (Figure 8.1). For weathered loess,  $y$  is assumed to be 0.5 m based on field observations.

For disturbed (weathered) loess, both  $c$  and  $\varphi$  are important. Dijkstra et al. (1994, 2000) investigated the relationships between residual moisture content and  $c$  and  $\varphi$  for

remoulded loess. Residual moisture content is the moisture content at the end of the shearing test. The relationships between gravimetric residual moisture content and  $c$  are shown in figure 8.4.

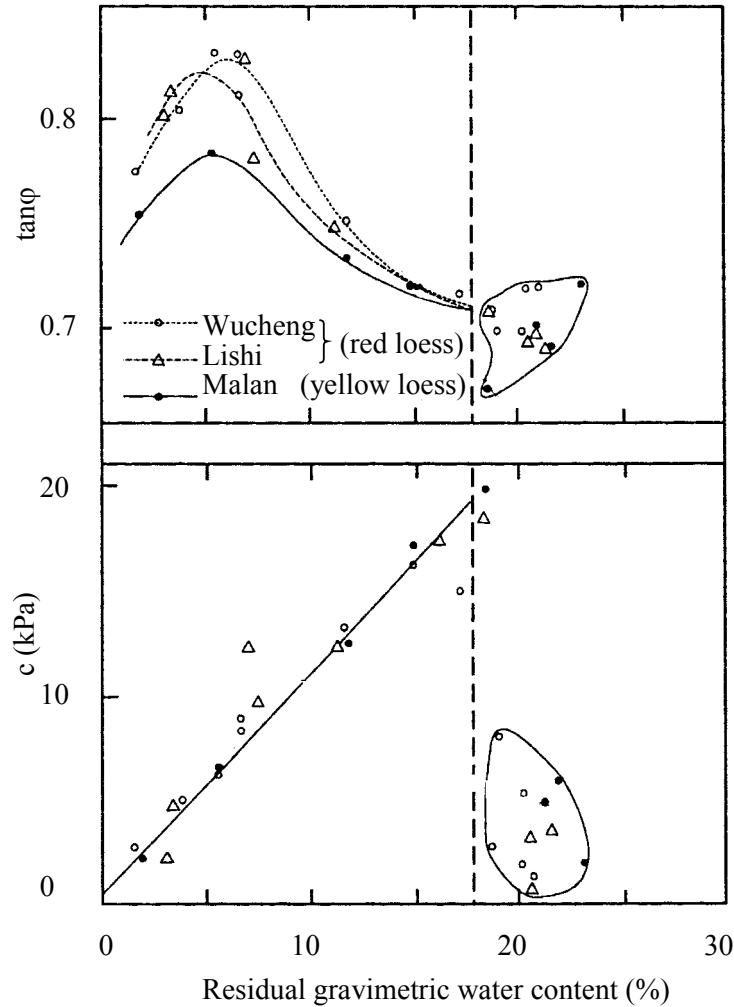


Figure 8.4 Relationship between residual gravimetric soil water content and  $c$ ,  $\phi$  for remoulded (weathered) loess. Adapted from Dijkstra et al. (2000). The dashed line is a threshold water content of 18% specified by Dijkstra et al. (2000), above which there is no longer a relationship between water content and  $c$  and  $\phi$ , as shown by the circled data points

Figure 8.4 shows that  $\phi$  can be assumed to be constant, as it is always between about 35 and 40 degrees ( $\tan \phi$  is between about 0.7 and 0.8).  $c$  shows a clear trend with moisture content, showing threshold behaviour as it increases above moisture contents of about 18%. For residual moisture contents of over 18%, cohesion has a constant value of about 3 kPa (Figure 8.4). It is assumed that the loess in cracks is weathered, allowing the data from figure 8.4 to be used. As there are no data available about the distribution or numbers of cracks, it is assumed that a certain percentage of the loess is weathered. A map with normally distributed random values is used to assign the properties of

weathered loess to about 0.1% of the catchment for every time step. Since the map with random values changes with every time step, so too does the distribution of weathered loess. Before the threshold value of 0.1% is applied to the map with random values, the random value is adapted using the headcut height to increase the probability of the loess being weathered at increasing headcut height. As a result, the highest headcuts are more often weathered, so that more soil falls occur with increasing headcut height. For unweathered conditions, the original parameter values are used, while for weathered conditions,  $c$  can be calculated using figure 8.4;  $\phi$  is also estimated from figure 8.4 as  $36^\circ$  for yellow (Malan) loess and  $38^\circ$  for red (Lishi and Wucheng) loess.

In the present study, soil moisture contents are calculated with a simple water balance using daily precipitation and daily potential evapotranspiration, calculated with the Penman formula. Precipitation has been measured in the Danangou catchment using 6 tipping bucket rain gauges. The data needed for the Penman calculation were collected by the Ansai Research Station of Soil and Water Conservation, which is located at a distance of about 5 km from the catchment. The upper 50 cm of the soil is used for the water balance. Storage capacity is calculated from porosity. Rainfall (with simulated runoff subtracted) is added to actual storage, and evapotranspiration is subtracted from storage. If actual storage exceeds storage capacity, the surplus is added to runoff. This simple hydrological model results in gravimetric soil moisture contents that can be used to determine  $c$  according to figure 8.4.

Field observations have shown that failed slabs are always smaller than 5 m in height and that their average thickness is 0.2 m. Randomly distributed values of existing slab heights are therefore assumed for the headcuts, using 5 m as a maximum. The slab height is independent of headcut height, but the frequency of soil falls will be larger on larger headcuts. Whether or not a soil fall occurs can now be determined by comparing the critical headcut height calculated with equation 8.2 with the assumed slab height. Failure occurs when the critical height is smaller than the slab height. This can only occur when the loess is weathered. The width of the failed slab is assumed to be half the pixel size. The mass of the soil fall is then determined as:

$$M = \gamma_d \cdot H \cdot d \cdot 0.5 \cdot DX \quad (8.4)$$

Where:  $M$  = mass of soil fall (kg)  
 $\gamma_d$  = dry bulk density ( $\text{kg/m}^3$ )  
 $H$  = height of failed slab (m)  
 $d$  = slab thickness (m)  
 $DX$  = pixel size (m)

A map of total loose sediment deposits in the gullies is produced by adding up the mass of fallen material during each time step.

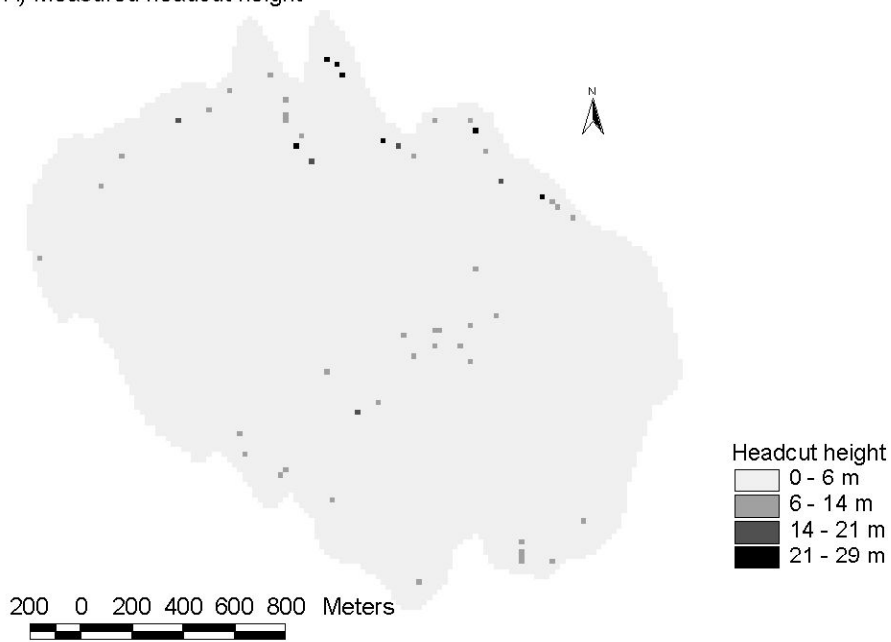
The stability model has been implemented in the PCRaster dynamic modelling language (Wesseling et al., 1996).

## 8.4 Model results and discussion

Meteorological data were available for May – October 1998, a period of 155 days. The model was therefore run over this period. Figure 8.5 shows maps indicating the mapped position of gullies and the location of gully heads as determined with the model. The maps clearly show that the simulated number of gullies was much larger than the number actually measured. This was to be expected, as the gully measurements could, for practical reasons, not be complete. No small gully heads were measured and many parts of the catchment are simply inaccessible. The real number of gullies is therefore much higher than the number measured, and the DEM-derived number did not seem unrealistically high. No air photos with sufficient detail were available to verify the predicted number of gullies. Figure 8.5 also shows that the DEM-derived gully head positions did not exactly match the mapped positions. When comparing the location of gully headcuts determined in these two different ways, one has to keep in mind that the difference may have been caused by both mapping inaccuracy and limited DEM resolution. One cannot expect field mapping in a 3.5 km<sup>2</sup> area to be accurate to within 5 m. Nevertheless, the main cause of the difference was probably that the DEM has insufficient resolution to extract the position of individual headcuts. Despite this, the general distribution of headcuts as derived from the DEM seemed reasonable. Surprisingly, the highest simulated headcut had exactly the same height as the largest headcut measured (28.6 m). The number of gullies identified by the model could easily be changed by changing some of the threshold conditions used in the model, should field observations indicate that this is necessary.

Figure 8.6 shows measured, non-weighted average daily rainfall (with modelled runoff subtracted) as well as simulated daily soil fall amounts (average of 10 runs). As both weathering status and actual slab height were modelled as random processes in the simulation, each model run will produce a different pattern of soil falls. Using the average of a number of runs should therefore show the trend more clearly. Figure 8.6 shows that according to the model, soil falls were concentrated in a few periods; between day 13 and 28, between day 42 and 60 and after day 125. Comparison with the rainfall data shows that the first period occurred after heavy rain, while the other two occurred under drier conditions. This is caused by the fact that, according to Figure 8.4, cohesion is low for both very dry and very wet soils. As the soil becomes drier, its cohesion decreases gradually. Daily soil fall mass during soil fall periods caused by dry soil conditions will therefore gradually increase with increasing drought. Under very wet conditions, however, the soil water content might exceed 18% for large parts of the catchment, so that, according to Figure 8.4, cohesion will drop dramatically. Daily soil fall mass during soil fall periods caused by wet soil conditions will therefore start abruptly. Figure 8.6 also shows that the effect of a particular amount of rain depended very much on the moisture content before the rain; in some cases, rain increased the moisture content enough to stop soil falls (e.g. at day 60), while in others it had no effect (e.g. day 82) and in still others it increased the moisture content to above 18%, thus increasing the number of soil falls (e.g. day 13).

A) Measured headcut height



B) Simulated headcut height

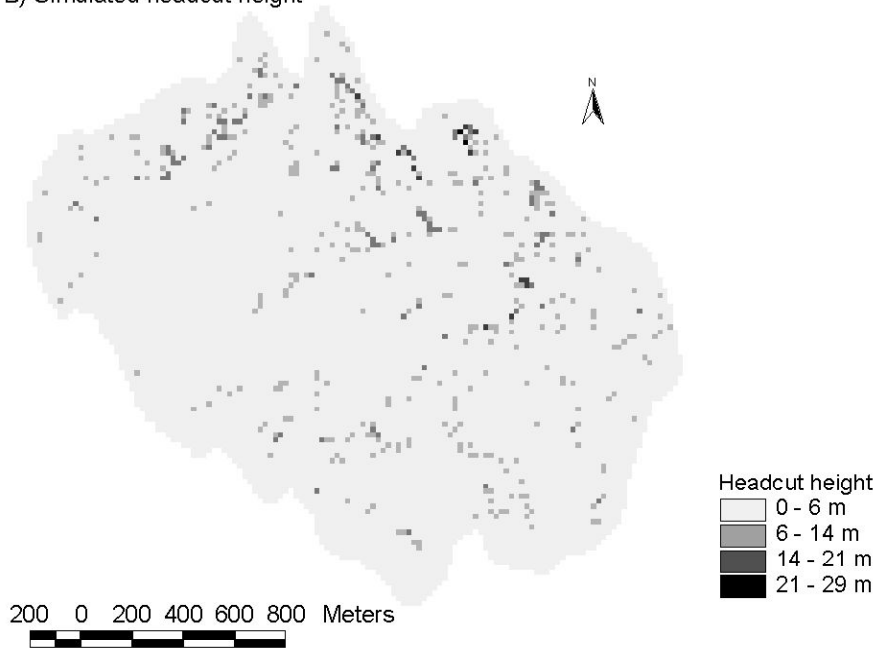


Figure 8.5 Measured headcut heights (A) and simulated headcut heights (B) for the Danangou catchment. Simulation pixel size 5 m, display pixel size 20 m



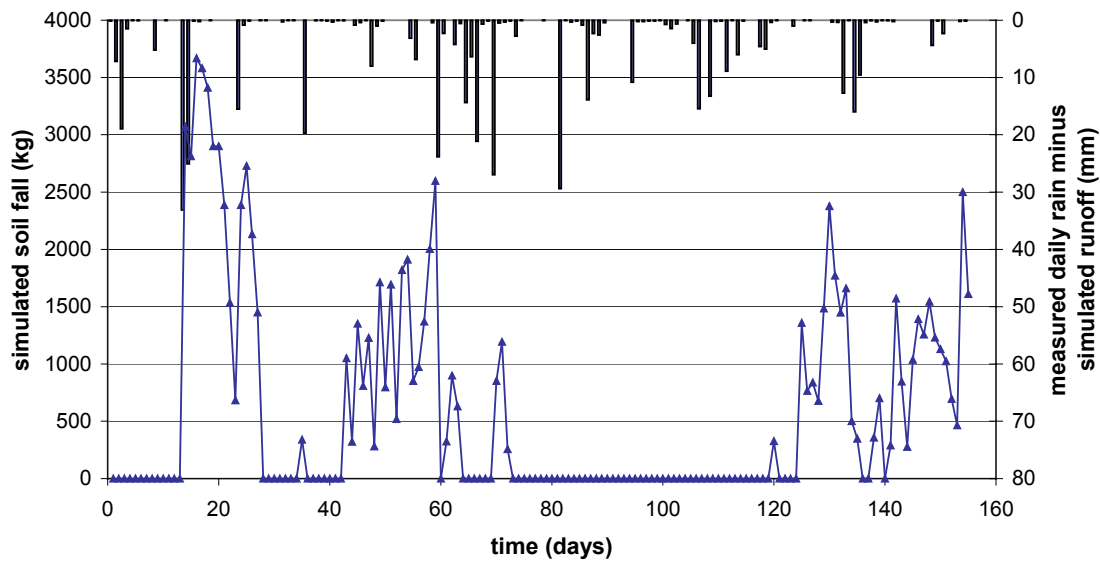


Figure 8.6 Simulated 10-run average daily soil fall amount (line with triangles) and average measured rainfall minus simulated runoff (bars), May to October 1998

The 10-run average total simulated mass of soil that fell over the period May – October 1998 was 93 tonnes, with a standard deviation of 11 tonnes. A field estimate in May 1999 indicated 53 cubic meters or about 77 tonnes, accumulated over an unknown period, but presumably since August 1998. These data indicate that the amount of loose soil material simulated was reasonable.

The method presented here has several potential shortcomings. First, the number of gullies surveyed was smaller than the actual number. It can therefore be expected that the actual amount of loose soil material is also larger than estimated in the field. It is impossible to say by how much, but the simulated amount of 93 tonnes seems plausible when compared to the observed amount of 77 tonnes.

Second, the simulations cover the summer period of 1998, while the observations cover the winter of 1998/1999 and the spring of 1999. Because of limited availability of meteorological data, only the summer period of 1998 could be modelled. In reality, however, soil falls might also occur in winter, e.g. because of frost, or because of thaw in spring. Modelling the effect of such processes requires a more sophisticated hydrological model. Also, one needs to know what effect soil temperature (especially below 0°C) has on geotechnical parameters such as soil cohesion. Such a more sophisticated model can be developed, but will require more input data as well.

Third, a comparison of the simulation results with the field data (as summarised in table 8.2) shows that the process of soil fall in the field is more irregular. Some gullies had large volumes of loose sediment, but many had none. Vandekerckhove et al. (2001) monitored gully retreat rates in southern Spain and also observed that soil fall volumes varied widely between gullies. The simulations, however, do not show any gullies with

unusual amounts of loose sediment. It is likely that the large amounts of loose sediment in some gullies were caused by local circumstances (like position of cracks and headcut geometry) that can never be reproduced in a catchment scale model such as that used here. The model should therefore be evaluated on total simulated amounts rather than on individual gullies.

Finally, one can seriously question to what extent the very simple water balance used here is relevant to moisture contents inside fissures around a gully head. Careful field observations will be needed to gather more information on the moisture conditions prevailing during failure.

At present, there is too much uncertainty to really judge the validity of an approach like that outlined here. Clearly, there is a need for more field data. Field monitoring of soil fall volumes and dimensions (height of slab, thickness of slab, width of soil fall) as well as of soil moisture conditions is required, as well as more geotechnical data. Only when such data become available, will some sort of calibration be possible. However, as mentioned above, a catchment scale model can never reproduce the soil fall mass of every single gully, since it is impossible to incorporate all the local conditions. From a catchment modelling point of view, the focus of further research should be on accurately representing the average gully.

The model presented here not only has potential shortcomings, it also has a limited scope. The model only simulates the occurrence of fairly small soil falls on headcuts, while large soil falls or small slumps might occasionally occur as well. Besides, it is important to realise that the loose soil material accumulated below gully heads is just one source of sediment during runoff events. Where gully banks are steep, loose soil material can also accumulate along the length of the gully. Another potential source of loose soil material is that of lobes of old mass movements. These sources of loose soil material could be mapped or modelled and added to the loose material map that serves as input for storm-based erosion models. Other major potential sources of sediment during runoff events include runoff erosion on the arable land above the gullies, piping and, in some cases, active erosion of gully heads or banks. Since these processes actually operate during the runoff event, they should be modelled by the storm-based erosion model itself.

## **8.5 Sediment balance**

### *8.5.1 Introduction*

In order to combat erosion effectively it is important to know why, where and when erosion occurs. This requires insight into the erosion processes that are operating. The sediment balance of the Danangou catchment can be written as:

$$S_{\text{out}} = S_{\text{gullies}} + S_{\text{crop}} + S_{\text{other}} - \text{Storage} \quad (8.5)$$

Where  $S_{out}$  is the sediment leaving the catchment,  $S_{gullies}$  is sediment derived from gullies,  $S_{crop}$  is sediment coming from croplands,  $S_{other}$  is sediment coming from other land uses and Storage is the change in storage. It is positive when storage increases. Most storage will be in the valley bottoms of the main gorge and in some of the large gullies.

Gong Shiyang & Jiang Deqi (1979) studied sediment sources in several gully catchments of the Loess Plateau. Their results are given in table 8.4. Table 8.4 shows that erosion was about equally distributed between gullied land and intergully land. Per unit area, erosion on gullied land was higher. Erosion per unit area was lower for cropland than for other land uses, but because of the large cropland area total erosion from cropland was more than 50% of the catchment total.

Table 8.4 Sediment sources of gully catchments on the Loess Plateau (based on Gong Shiyang & Jiang Deqi, 1979)

	Wangjia		Jiuyuan	
<i>Catchment characteristics</i>				
Catchment area (km <sup>2</sup> )	9.1		70.1	
Annual soil loss (tonnes/km <sup>2</sup> )	13,800		18,100	
<i>Land use</i>	<i>area (%)</i>	<i>loss(%)</i>	<i>area(%)</i>	<i>loss(%)</i>
Farmland	61.8	52.5	66.7	59.3
Wild grazing land	20.0	18.0	8.1	8.7
Steep slopes and cliffs	15.1	23.2	20.8	25.1
Village, road, gully bottom	3.1	6.3	4.4	6.9
<i>Geomorphology</i>	<i>area (%)</i>	<i>loss(%)</i>	<i>area(%)</i>	<i>loss(%)</i>
Interfluves	59.5	47.1	56.6	50.1
Gullied land	40.5	52.9	43.4	49.9

Jiang Deqi et al. (1981) summarised studies on the contribution of different sediment sources for several catchments in the Wuding catchment. The data presented by them were at least partly based on those of Gong Shiyang & Jiang Deqi (1979) and are given in table 8.5. Their data show that relative contributions from interfluves and gullied land were variable, but that on average their contribution was about equal. Farmland will be the dominant sediment source for interfluves, so that farmland erosion and gully erosion were the two dominant sediment sources for the catchments. These results, however, cannot be extrapolated to the Danangou catchment directly for several reasons:

- Table 3.2 shows that gullied land occupies 24% of the Danangou catchment, which is much less than reported in Tables 8.4 and 8.5. This is, however, probably caused by a difference in definition of gullied land. In our mapping only those areas that actually had gullies were mapped as gullied land, while Tables 8.4 and 8.5 probably call all land downslope of the gully boundary edge (figure 3.5) gullied. Using that definition gullied land is likely to include some cropland and other land uses as well.

- Table 3.3 shows that farmland in the Danangou catchment is around 25%, which is much lower than reported in Tables 8.4 and 8.5. The tables, however, do not include fallow land, which occupies about 20% of the Danangou catchment. It is possible that fallow land is included in farmland in Tables 8.4 and 8.5, but it is also possible that no fallow land existed.
- Table 8.6 shows that for 1998-2000 annual erosion rates in the Danangou catchment were much lower than those reported in Tables 8.4 and 8.5. Only 1998, however, can be considered a year with normal precipitation.

Thus, the Danangou catchment has less farmland, less erosion and might have fewer gullies. It is not clear what effect this will have on the relative contribution of the different sediment sources.

Table 8.5 Sources of soil erosion in small catchments (0.18 – 70.7 km<sup>2</sup>) in the gullied hilly part of the Loess Plateau (based on Jiang Deqi et al., 1981)

	Area (% catchment)	soil loss (% total)	annual erosion (tonnes/km <sup>2</sup> )
<i>Land use</i>			
Farmland	57-67	44-59	15,800-19,900
Wild grazing land	8-25	9-23	13,400-16,100
Steep slopes and cliffs	13-21	20-25	21,800-26,500
Village, road, gully bottom	4-7	7-13	28,400-36,200
<i>Geomorphology</i>			
Interfluves	44-74	30-62	11,600-26,300
Gullied land	26-56	38-70	14,200-34,500
Gully slopes	25-52	32-62	16,600-26,100
Gully bed	1-4	6-8	38,500-70,800

In a more recent study, Zhang et al. (1997) found that gullied land occupied 47% of the area of their catchment but delivered 77% of the sediment in 1993. They also used the gully boundary edge to define gullied land. Using reservoir deposits and cesium-137 they found that over the period 1973-1977 the average contribution of gully erosion to total erosion had been 79%. Their study area was morphologically similar to the Danangou catchment and was only about 50 km northeast of Ansai.

Observations during, after and in between runoff events have shown that the major sources of sediment in the Danangou catchment also are croplands and gullies. Erosion rates for other land uses are much lower. Even the very steep wastelands generally do not produce much sediment. Storage mainly occurs in the channel bed. In some places there is sedimentation because of former check dams built by farmers. It might well be that deposition in those places causes erosion further downstream. It therefore seems reasonable to neglect both  $S_{\text{other}}$  and Storage, so that total sediment yield equals the sum of cropland erosion and gully erosion.

For each year total erosion can be calculated from the data measured at the dam and is given by:

$$S_{out} = \sum_{i=1}^{i=n} Q_i \cdot C_i \quad (8.6)$$

Where:  $S_{out}$  = total sediment yield (kg)  
 $Q_i$  = total discharge of event number  $i$  ( $m^3$ )  
 $C_i$  = average concentration during event  $i$  (g/l)  
 $i$  = event number  
 $n$  = number of events during a year

Total erosion can be calculated in this way since there is only sediment leaving the catchment during events.  $S_{out}$  is likely to be dominated by a few large events each year. Thus, to develop a mass balance for the Danangou catchment two of the three unknown parameters ( $S_{out}$ ,  $S_{gullies}$  and  $S_{crop}$ ) should be determined. The purpose of this section is to determine two of the three unknown parameters, and to develop a sediment balance for the catchment.

### 8.5.2 Method

To develop a sediment balance several methods can be used. Some of these methods aim to determine  $S_{gullies}$  or  $S_{crop}$  directly, while others aim at determining  $S_{gullies}$  and  $S_{crop}$  indirectly, namely through analysis of sediment samples taken at the catchment outlet. In that way, the relative contribution of gullies and cropland might be determined from samples taken at the weir if the gullies and croplands have some characteristic soil property. A number of techniques might be used to determine sediment source for the Danangou catchment:

1) Cropland erosion mapping. Cropland erosion can be estimated from catchment wide rill mapping, supplemented with data from the sediment plot (chapter 4.5). The results of these mapping exercises give an estimate of total cropland erosion. Sediment plot data are necessary to obtain an estimate for sheet erosion rate. As shown in chapter 10.4 the erosion rate measured at the sediment plot cannot be equated with sheet erosion rate directly. A sediment delivery ratio should be applied because not all sediment eroded on the erosion plot would actually leave the field. Thus, the choice of delivery ratio influences the estimate of sheet erosion, which influences the estimate of cropland erosion. Note that this only applies to 1999 and 2000 since in 1998 the sheet erosion estimate was not based on a sediment delivery ratio.

2) Direct estimation of gully erosion through observation or simulation. Gully erosion is very difficult to estimate. The estimation method described in this chapter can be used to obtain an indication of the total amount of loose material in gullies. However, such field observations require that most, if not all, gullies be visited. If these observations lack the total amount of loose material in gullies could be modelled in the way described in this chapter. This simulation result is, however, likely to be an underestimate since not only

gully heads provide sediment, gully walls will also provide sediment. In addition, erosion of gully headcuts and walls during storms is not taken into account with this method. Another option would be to measure all sediment coming from a gully, but this will give an aggregated result of the total area upstream of the gully outlet. This total area usually includes cropland areas upstream of the gully headcuts.

3) Caesium-137 content. Caesium has been applied to estimate the contribution of gully erosion before (e.g. Zhang et al, 1997). Caesium-137 is a fission product of thermonuclear weapon tests and has accumulated in the topsoil due to atmospheric fallout, mainly in the 1950's and 60's (Loughran, 1989). Caesium-137 is quickly and firmly adsorbed to the fines in a soil, which means that it is not translocated chemically, but only through transport of soil. The principle of the method is to compare caesium-137 concentrations of disturbed sites with a site that is known to be undisturbed since the 1950's. Low amounts of caesium then indicate erosion, while high amounts indicate deposition. The caesium content of sediment coming from croplands could be expected to be higher than that coming from gullies, especially if the gullies were formed after the 1960's, since in that case, the present gully surface was not exposed to the caesium fallout. If these contents are known, measurements of caesium-137 at the catchment outlet can indicate how much sediment came from where. The caesium technique was, however, not available in this study.

4) Mineralogy. If the mineralogy of cropland soils and gully soils were different, mineralogical analysis of material at the outlet could show which part of the sediment came from the gullies. The problem with this approach is that the distinction red loess – yellow loess is not the same as gullies – croplands. Most gully-derived material that reaches the weir will be red loess, but not all. Besides, table 4.2 shows that there are hardly any mineralogical differences between red loess and yellow loess.

5) The main difference between red loess and yellow loess is grain size distribution (chapter 4.3). One can therefore attempt to determine the relative importance of the different sediment sources (red loess versus yellow loess) by performing a grain size analysis on water samples taken at the dam. Since all red loess erosion occurs in gullies (there are almost no red loess croplands) all red loess comes from gullies, but not all yellow loess comes from croplands. Nevertheless, being able to distinguish between red loess and yellow loess sediment source would help developing a mass balance.

6) In principle, the timing of the sediment discharge peak could give information about the sediment sources. An early sediment peak would indicate a source close to the outlet, e.g. from the channel bed and red loess gully beds. Hysteresis would then be clockwise, since concentrations would be higher for the same discharge during the rising stage than during the falling stage. DiCenzo & Luk (1997) found a predominantly clockwise hysteresis loop for a small catchment in southern China. They also found that in this catchment, gully erosion accounted for 85% of total erosion. A late sediment peak would indicate that erosion is taking place on the croplands above the gullies. Hysteresis would then be counterclockwise. In reality, however, many other factors play a role in determining the occurrence of sediment discharge peaks. DiCenzo & Luk (1997), for

example, mentioned storm characteristics, antecedent moisture conditions and sediment availability.

7) Another option would be to estimate the maximum possible cropland erosion using a soil erosion model such as LISEM. This requires that a calibrated version of the model be used because this method assumes that the LISEM results match reality. Since this is not necessarily the case, the simulation result could give no more than an indication. The procedure would be to create an output map that shows the cumulative maximum possible transport. The maximum possible transport for any time step would be transport capacity times discharge times time step length ( $TC \cdot Q \cdot dt$ ). Concentration can sometimes be higher than transport capacity (see equation 3.25), but this is not likely to introduce large errors in the estimate of maximum possible transport. From this map all pixels draining from cropland to another land use can be selected and their maximum possible transport can be added to give an estimate of catchment wide maximum possible cropland erosion. The same procedure could be used to estimate maximum possible gully erosion.

Table 8.6 measured and simulated (in italics) total event erosion (tonnes) in the Danangou catchment.

Year	Event erosion <sup>a</sup> (tonnes)					yearly sum (tonnes)	annual erosion (tonnes/km <sup>2</sup> )
	1	2	3	4	5		
1998	<i>18.4</i>	572	2880	1280	96	4846	2341
1999	<i>3.3</i>	770	53			826	399
2000	<i>2.6</i>	16	2630			2649	1280

<sup>a</sup> event numbers are defined as follows: 1998: 1=980705, 2=980712, 3=980715, 4=980801, 5=980823. 1999: 1=990710, 2=990720, 3=990721. 2000: 1=000807, 2=000811, 3=000829.

### 8.5.3 Results

#### *Total soil loss from catchment*

Total erosion from the Danangou catchment can be obtained by summing the total soil loss for the individual events that occurred during each year. All 11 events that were used for simulations (chapters 4 and 10) were used to estimate total yearly erosion. Table 8.4 shows that the total erosion from the catchment was dominated by the largest events that occurred. This was to be expected since larger events not only have more discharge, but also higher sediment concentration (chapters 4 and 10). Table 8.6 shows that the estimate of total erosion for 1998 was less certain than that for the other two years. For 1998 more than 70% of the total was based on simulations, while chapter 10 shows that such simulation results are not very reliable for uncalibrated storms.

### *Croplands*

The results of cropland erosion mapping were presented in chapter 4.5. Using the erosion rates for the different erosion classes that were presented in table 4.13 it is possible to calculate total cropland erosion by multiplying the rate with the area occupied by that particular erosion class. The results are shown in table 8.7. It seems likely that real cropland erosion were higher since:

- Part of the rills formed during events will be obliterated by management practices of farmers in between events.
- In some parts of the catchment, single large rills or ephemeral gullies occur on the lower slopes. These single large rills are difficult to map with the method applied and have usually been neglected. Since these rills have large cross-sectional surface areas they might deliver large amounts of sediment
- The mapping was only performed for cropland. For some of the other land uses, e.g. fallow land and orchard, there might also be rill erosion during events. These rills cannot be incorporated in the mapping since they might well be more than a year old.
- It is not possible to investigate every separate field. When mapping from even a short distance vegetation might obscure rills.

Table 8.7 measured and estimated erosion rates (tonnes) in the Danangou catchment, 1998-2000

	1998	1999	2000
<i>Absolute values (tonnes)</i>			
Total sediment yield	4846	826	2649
Gully erosion	77	77	77
Cropland erosion	875	171	666
<i>Relative values (%)</i>			
Total sediment yield	100	100	100
Gully erosion	1.6	9.3	2.9
Cropland erosion	18.1	20.7	25.1

The effect of the choice of sediment delivery ratio on the estimate of cropland erosion was evaluated by using values of 0 and 1 for the delivery ratio. It was found that the contribution of cropland erosion to total erosion varied between 6 and 57% for 1999, and between 5 and 45% for 2000. The choice of a transport delivery ratio therefore has considerable influence.

### *Gullies*

As reported in chapter 8.4 field observations of loose material in gullies resulted in an estimate of 77 tonnes. Since there are no other data available this value is assumed to apply to all years. Table 8.7 shows that the sum of estimated gully erosion and mapped cropland erosion was far less than total erosion for all years. It seems also likely that the gully erosion estimate was, like the cropland erosion estimate, an underprediction. In reality cropland and gullies will not be the only sediment sources, since there will also be



some erosion from other land uses as well as changes in storage in the channels. As stated before, field observations indicate that relatively small amounts of sediment are involved in that, so that a plausible guess would be that 10% of sediment yield could originate from those sources. Considering the quality of the available data the real relative importance of cropland erosion and gully erosion cannot be determined. If the cropland mapping is assumed more reliable than the gully estimate a plausible guess would be cropland erosion 20-50% and gully erosion 40-70%.

#### *Grain size*

Field observations during the event of August 11<sup>th</sup>, 2000 suggested that the colour of the discharge changed from yellow to red during the course of the event. If the contribution of red loess increased during the event this should be reflected in the grain size distribution of sediment load at the weir. Sediment samples were taken at the weir during 5 events. Since one of the clearest differences between yellow loess and red loess is a difference in grain size distribution, some of the samples taken at the weir were analysed with laser diffractometry (see chapter 4). It was hoped that the grain size distribution of the samples taken at the weir would give information about the relative contribution of yellow loess and red loess. Figure 8.7 shows the results for the event of August 11<sup>th</sup>, 2000. It shows that all samples were finer than the red loess. It is possible that the coarser material was deposited before reaching the weir. It is also possible that the grain size distribution was not constant over flow depth. In any case, the resulting grain size distributions cannot be used to obtain information about sediment source. Analysis of the D50's for all 5 events revealed a relationship between sediment concentration and D50 (figure 8.8). As shown in chapter 7 (figure 7.1), there was also a relationship between discharge and concentration. It is hard to draw any firm conclusions from figure 8.8 for several reasons:

- The observed trend might be a result from different sediment source, i.e. the higher the concentration the higher D50. This can be explained by the fact that the yellow loess areas are generally further removed from the stream than the red loess areas. It is probable that the yellow loess areas would deliver more sediment with an increase in event size. Thus, the larger the event, the higher the discharge. And the higher the discharge the more material originates from the yellow loess areas. If this were the only cause of the relationship shown in figure 8.8 it would be possible to estimate the relative contributions of red and yellow loess.
- Since concentration shows a relationship with discharge the larger D50 for the higher concentrations might just be because higher discharge has larger transport capacity and is able to transport coarser sediments. Thus, D50 would not give information about sediment source.
- As discussed in chapter 5 one of the effects of high concentrations should be that D50 increases. Since concentration increases with increasing discharge (figure 7.1), D50 would also increase with increasing discharge, as is shown in figure 10.7. Thus, D50 would not give information about sediment source.

Therefore, neither grain size distribution nor D50 can be used to determine the relative contribution of red loess and yellow loess.

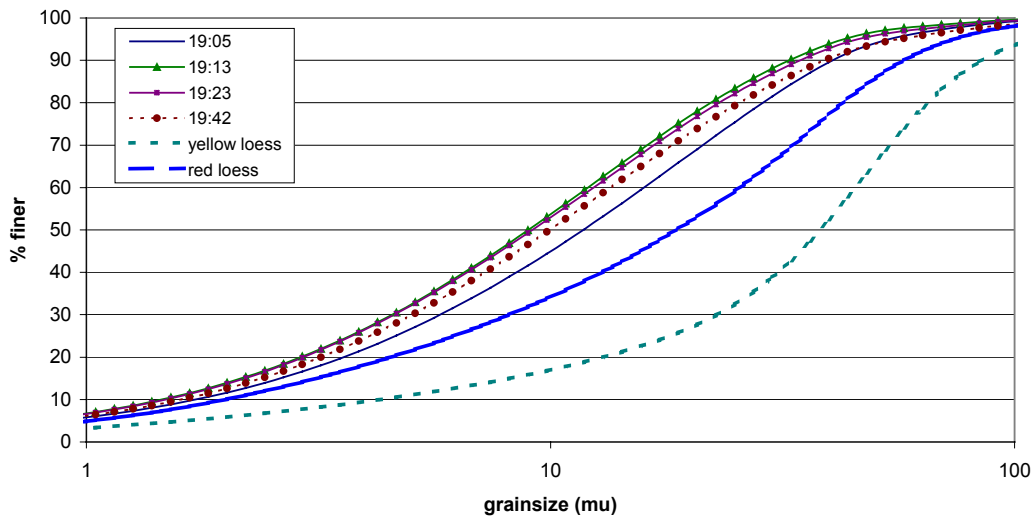


Figure 8.7 Grainsize distribution of samples taken at the weir during the event of August 11<sup>th</sup>, 2000

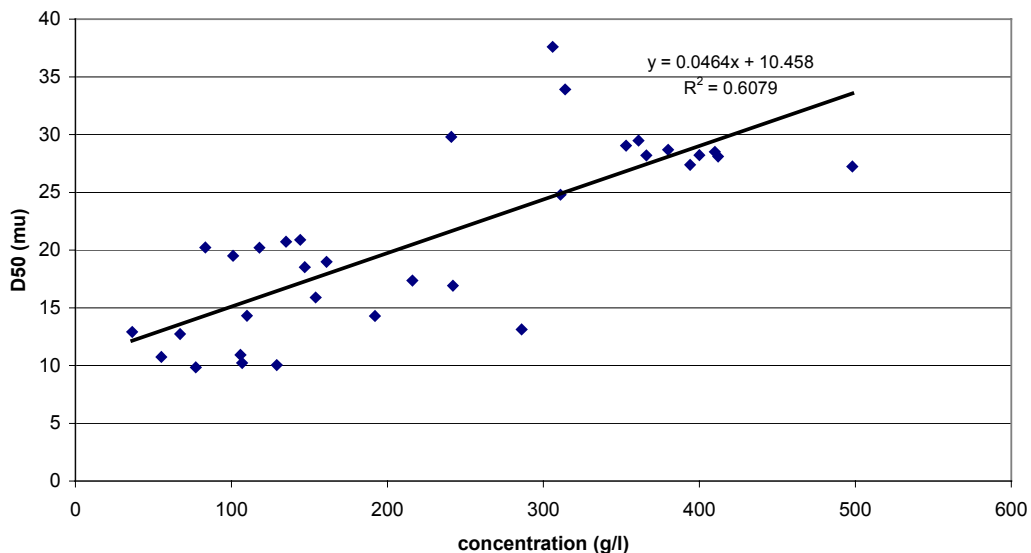


Figure 8.8 D50 as a function of concentration, all 5 events combined

*Timing sediment peak*

At least some sediment samples were taken during 5 events: 980801, 980823, 990720, 000811 and 000829. The measured concentrations are shown in figure 4.6. In the data, the falling limb of the hydrograph is much better represented than the rising limb.

For the 990720 event the first samples taken by the automatic sampler were lost due to problems with the sampler. The remaining samples showed strong fluctuations in sediment concentration. These fluctuations might well be due to the functioning of the sampler instead of to real fluctuations in concentration (chapter 4). Manual samples were

only taken during the falling limb and showed a gradual decrease in concentration, with a small peak during the secondary discharge peak of the event. During the 000811 event samples were only taken during the falling limb. Concentration steadily rose until it reached a peak 20 minutes after the discharge peak. For the 000829 event there was uncertainty about the sampling time (chapter 4.4). The samples that were certainly taken during the falling limb show a gradual decrease in concentration.

The best available data on sediment concentration as a function of discharge were collected during the 980801 and 980823 events. These data are shown in figures 8.9 and 8.10, which show that during both events the hysteresis loop was predominantly counter clockwise. The partial data of the other 3 events also seem to indicate that concentrations were generally higher during the falling stage than during the rising stage. Figure 8.9 also shows that high concentrations can be maintained even for small discharge during the falling stage of the hydrograph. However, both figures 8.9 and 8.10 show an involuted loop, because during both events two sediment peaks occurred, one slightly before the discharge peak, and a larger one after the discharge peak. This suggests that the first peak was due to sediment derived close to the weir, e.g. in the channel bed, and the other from further away from the weir. This distinction can, however, not be equated to the distinction between gullies and croplands for several reasons:

- Gullies and cropland are present both close to the weir and far away. Field observations after the 000811 event, for example, showed that the water during this event mainly came from the red loess gullies along the northern boundary of the catchment. Though these gullies are directly linked to the channel network they are still far away from the weir and are linked through a long and tortuous channel. An early peak is more likely to result from entrainment in the main channel.
- It seems likely that sediment source depends on the magnitude of an event. Very small events, like that of 990710 mainly produce discharge in the main valley bottom. Somewhat larger events might produce discharge in the main valley, in the main gullies and on fields close to the main channels. Only for large events would water (and sediment) from the furthest parts of the catchment (such as hilltop croplands) reach the outlet. Thus, one would expect that the larger an event is the larger its cropland contribution would be.
- One cannot neglect the fact that sediment data were rather scarce. Even though both figure 8.9 and 8.10 show an involuted loop, the total number of measurements on which this is based was only three. Thus, more attention should be paid to the observation that the loops are counter-clockwise than on the observation that both loops were involuted. Comparison of the 980801, 980823 and 000811 events would suggest that the smaller an event is, the more the sediment peak lags behind the discharge peak. In addition, it is clear that the larger an event is, the higher the concentration will be, as for example shown in figure 7.1.

Thus, the timing of the sediment peak does not give clear indications about the sediment source, but the counter clockwise loop suggests that the source is not close to the weir.

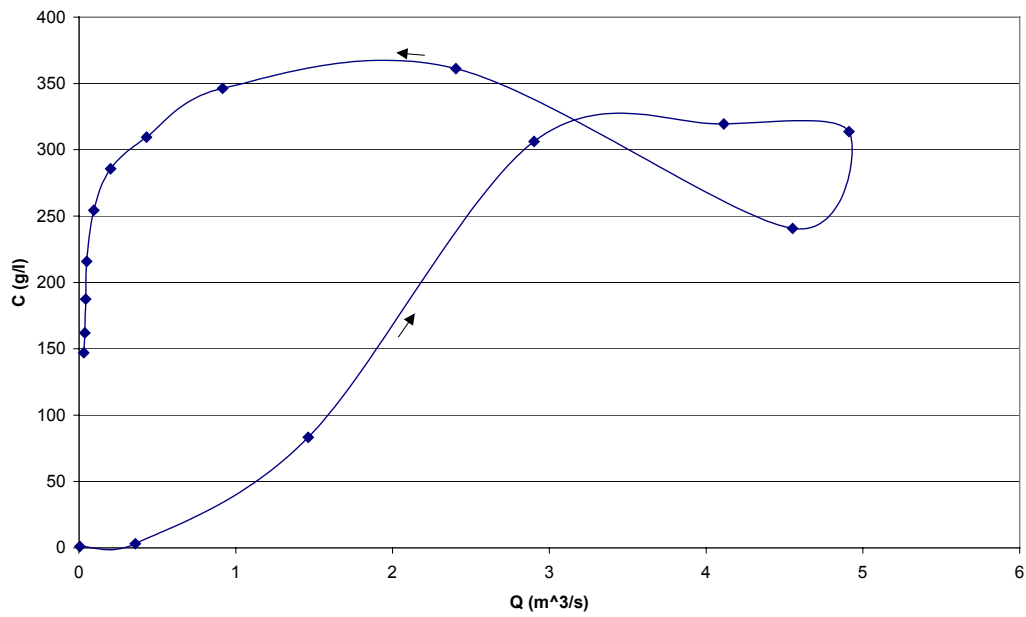


Figure 8.9 Sediment concentration as a function of discharge, 980801 event

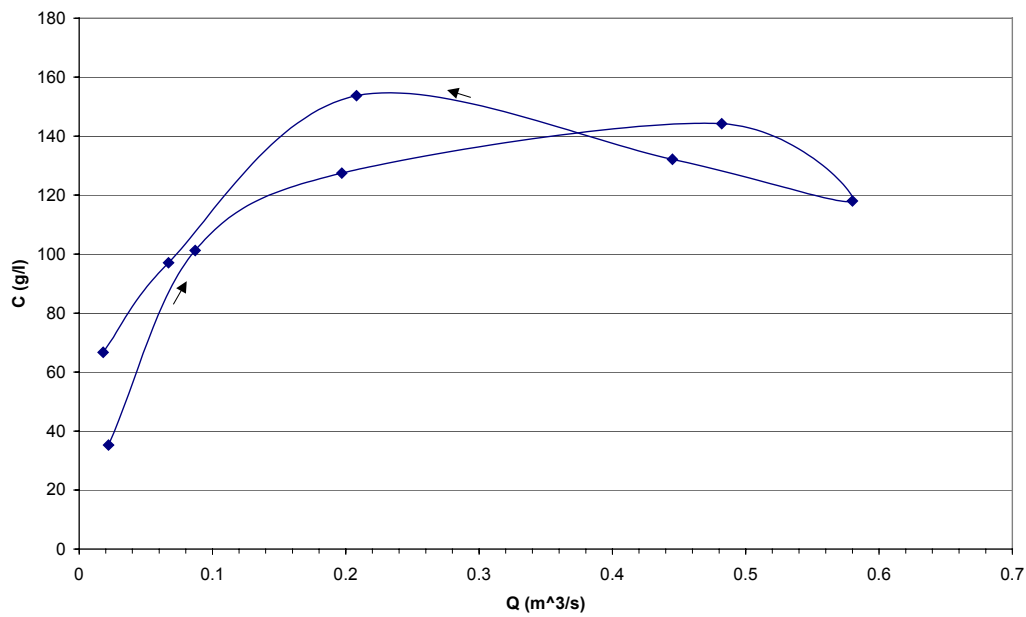


Figure 8.10 Sediment concentration as function of discharge, 980823 event

### *LISEM simulations*

To be able to estimate maximum total erosion for a particular land use or area with LISEM a map giving a time-summation of  $TC \cdot Q \cdot dt$  was created during the simulations. Here, the simulation results for the entire Danangou catchment will be used for a calibrated run of the 990720 event. The results for this simulation are given in chapter 10.4.2. A map of all croplands was derived from the land use map (figure 3.14) and a

map of all gullied areas was derived from the geomorphological map (figure 3.5). The procedure followed was equal in both cases and will here be discussed for the cropland map only. With the cropland map the map of local drainage direction (LDD) was adapted, so that a LDD map of the cropland only was obtained. This map was then used to determine which pixels drain from the cropland to another land use. Only for those pixels the value on the maximum potential transport map were added to give a catchment total. This resulted in the following maximum possible transport amounts: cropland 16976 tonnes, gullies 9022 tonnes and catchment outlet 12530 tonnes.

Table 10.13 shows that according to the simulation sediment yield from all croplands equalled 1991 tonnes, which is only 12% of the maximum possible amount of 16976 tonnes estimated above. Total soil loss from the catchment was found to be 3358 tonnes, or 27% of the maximum possible amount. The values reported above and in table 10.13 clearly show that it is not straightforward to determine how important cropland erosion is. From table 10.13 cropland erosion would appear to be  $1991/3358 = 59\%$  of total erosion. Other land uses would than have negative contribution to erosion. In reality, erosion occurs in all land uses and deposition occurs in all land uses. There is no way of telling how much of the 1991 tonnes of net cropland erosion actually reached the outlet of the catchment. Using the values obtained with the maximum possible transport would even indicate that all erosion could potentially take place on croplands.

Another problem with table 10.13 is that large amounts of erosion are predicted for the steeper wasteland and fallow lands, while field observations indicate that such erosion does not occur in reality. The most likely cause is that some of the soil characteristics (such as cohesion) do not differ enough from one land use to the next in the simulations. As a result, the predicted amounts of erosion are mainly determined by slope angle. Maximum possible cropland erosion is calculated as  $TC \cdot Q \cdot dt$  and therefore does not consider soil characteristics at all (except for D50). This procedure is, in principle, correct, but in practice, will result in maximum possible erosion that is unrealistically high. The distribution of cropland and gullies over the catchment also influences the results. Firstly, because maximum possible transport is closely related to slope angle, which means that if a pixel draining onto another land use happens to be steep the maximum possible transport will automatically be high. Secondly, scattered small patches of land use (cropland) might well give a different result than larger areas (gullies), since they will have many more pixels draining into another land use. Finally, water leaving a land use might re-enter the same land use further downstream, which would cause double counting of transport capacity.

#### 8.5.4 Discussion

The results presented in this section show that it is difficult to develop a sediment balance for the Danangou catchment with the data available. It was found that no mineralogical differences between soils from different source areas could be used. Grainsize distribution was found to be too much affected by either transport or the sampling techniques. Timing of the sediment peak could not be used either. Nevertheless, both grain size data and timing of the sediment peak suggest that with increasing event size the

cropland contribution to sediment yield might increase, although alternative explanations are available. LISEM simulations could not be used to estimate a maximum possible erosion for different source areas. Comparison of measured/estimated total erosion at the weir with estimates of gully erosion and mapped/estimated amounts of cropland erosion showed that the sum of cropland erosion and gully erosion appears to be much smaller than total catchment sediment yield. Therefore, no reliable mass balance can be developed for sediment, and the best possible guess is 20-50% cropland erosion and 40-70% gully erosion. These values are comparable to those reported by Gong Shiyang & Jiang Deqi (1979), Jiang Deqi et al. (1981) and Zhang et al. (1997), which is not surprising given the large uncertainty in the estimate.

To improve on this estimate the cesium-137 technique might be useful, since it was successfully applied on the Loess Plateau before (e.g. Zhang et al., 1997). Another possibility would be to perform more accurate measurement and mapping of cropland erosion and of accumulation of loose material in gullies. Cropland erosion is probably easier to map than accumulation in gullies, because it is less dependent on site-specific circumstances and suffers less from accessibility problems. Finally, a more rigorous measurement campaign could be used to obtain separate data for erosion in gullies and on croplands. This would involve measuring discharge and sediment concentration for areas that have either cropland or gullies, but not a combination of both.

## **8.6 Conclusions**

In the Danangou catchment, soil falls on gully headcuts are an important sediment-producing process. This process does not operate on a storm-basis, so it cannot be modelled with storm-based erosion models. Instead, a simple slope stability model with a daily time step can be used to simulate the accumulation of loose sediment on gully floors. Very detailed digital elevation models would be needed to accurately extract the position of the present gully heads from such DEMs. The DEM used in the present study is insufficiently accurate for this purpose, but can nevertheless be used to produce a reasonable distribution of gullies. Sediment accumulation due to soil fall has been calculated with a simple stability model in which failure frequency is a function of headcut height and soil moisture content. Other processes could be incorporated as well if necessary. Such a daily-based stability model can provide storm-based erosion models such as LISEM with a map showing the distribution of loose soil material at the start of the storm. Such a map could also be supplemented with loose material derived from other soil erosion processes.

A satisfactory sediment balance could not be produced and it remains unclear which part of sediment comes from gullies and which from croplands. Both appear to be important, but based on the collected data a guess of cropland 20-50% and gullies 40-70% seems to be the most accurate guess possible. There are some indications that for larger events the cropland contribution will be larger than for small events.

## 9 LISEM CHANGES AND SETTINGS

### 9.1 Introduction

In previous chapters, a number of changes have been proposed that are theoretically necessary to implement a process based erosion model to a catchment on the Chinese Loess Plateau. This chapter will discuss how these changes have been incorporated in the LISEM model and what the effect of these changes was on the simulation results. All changes were evaluated one by one by programming them into LISEM 163. LISEM LP incorporates all these changes and is used in chapters 10 and 11.

This chapter will also discuss the influence of grid size and time step on simulation results obtained with LISEM LP. From previous studies (e.g. Doe & Harmon, 2001; Jetten et al., in press) it appears that the choice of grid size and time step length might influence simulation results considerably. Therefore, the effect of these choices should be evaluated.

### 9.2 Effects of LISEM changes

The changes to LISEM proposed in chapters 5 to 8 were implemented one by one to evaluate the effect of each. These changes can be summarized as:

- 1) Slope angle correction (discussed below)
- 2) Use of a slope dependent Manning's  $n$  (chapter 6)
- 3) Introduction of a concentration dependent settling velocity (chapter 5)
- 4) Introduction of a map with loose material derived from gullies (chapter 8)
- 5) Use of alternative transport equations (effects already discussed in chapter 7)
- 6) Use of the sine of slope angle instead of the tangent (chapter 2)

Where 1) and 2) affect runoff simulation as well as sediment yield and 3) to 6) affect only sediment yield. To evaluate these changes a calibrated dataset for the 990720 event was used. This event was chosen because it had the most complete dataset. The effect of using different transport equations was discussed in chapter 7 using LISEM TC. In this chapter the Govers (1990) equation was used because it was found to give the best results for this event. The calibration method will be discussed in chapter 10.

All the proposed changes are in theory an improvement of LISEM. For some changes it is, however, difficult to assess whether or not a change also results in an improvement of simulation result. If one starts with a calibrated model and then implements a theoretical improvement, it can be expected that the adapted model gives less good predictions. To evaluate if the implemented change is an improvement in terms of simulation accuracy one has to recalibrate the model. If this results in either a better fit with observations or the use of more realistic calibrated parameter values, the change can be considered an improvement. This method most easily applies to changing Manning's  $n$  and to slope

correction because these changes affect the hydrograph. Therefore, the hydrographs can be compared to the predicted hydrographs of the original LISEM version and to the measured hydrographs. The other changes affect only sediment transport and are more difficult to test since the measurements of sediment transport are less frequent and probably less reliable, so that there is also uncertainty about the accuracy of the measurements.

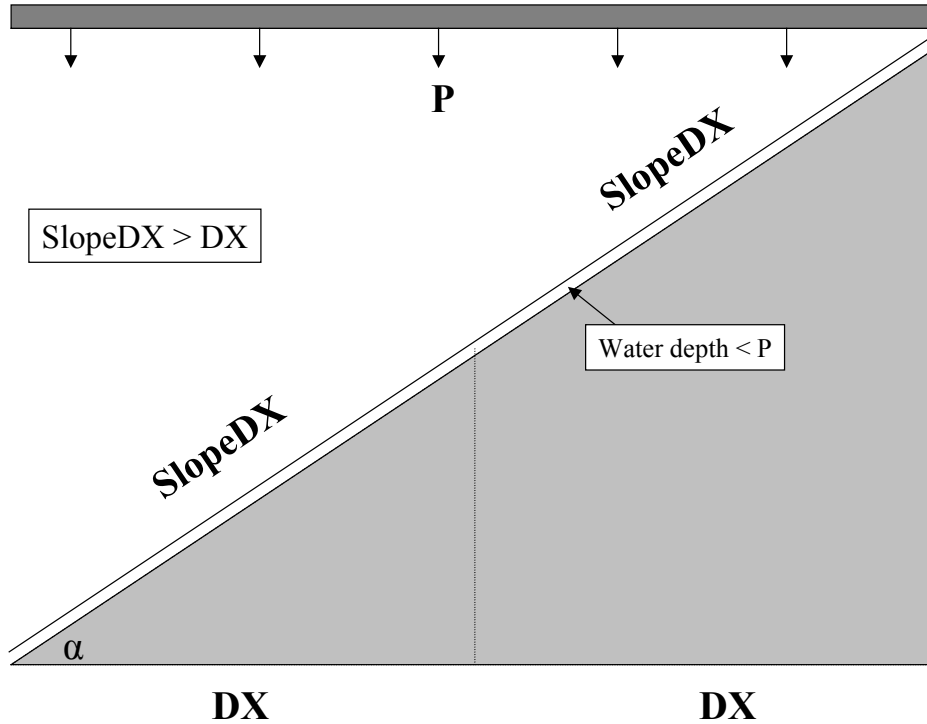


Figure 9.1 Effect of slope correction: smaller water depth and longer flow distance

### 9.2.1 Flow distance

So far, LISEM used the distance between pixel centres as flow distance. The grid is, however, essentially a horizontal grid. For steep slopes, the overland flow distance is not equal to the distance between pixel centres. Figure 9.1 shows the concept. The distance over the surface is *SlopeDX*, while the horizontal distance is *DX*. *SlopeDX* can be calculated as:

$$SlopeDX = \frac{DX}{\cos \alpha} \quad (9.1)$$

For example, if the slope is 45 degrees and the distance according to the grid (*DX*) is 10 metres the actual distance over the surface (*SlopeDX*) is 14.1 metres. In this procedure, it is necessary to make an assumption about the direction of sub-grid partitions like roads, wheel tracks, grass strips etc that are incorporated in LISEM. It was assumed that all these features are located in the direction of the slope. This assumption was also made in



the original version of LISEM (LISEM 163), but there it remained hidden since pixel width and pixel length were equal ( $DX$ ). In the new version pixels are assumed to be of dimensions  $DX * SlopeDX$ . Another slope-related difference between the original version of LISEM and the new version is that in the new version the Manning equation uses sine instead of tangent. It was shown in chapters 2 and 6 that this is theoretically better since the slope in the Manning equation is the energy slope. The sine of the slope angle gives the actual distance over which friction is exerted on the flow.

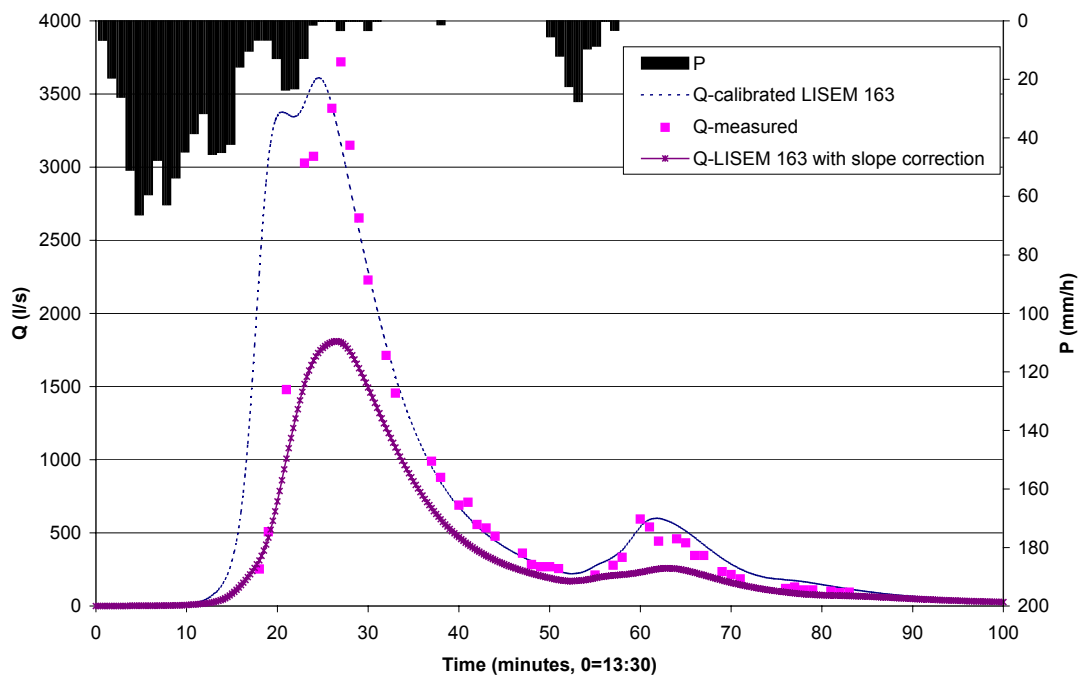


Figure 9.2 Predicted discharge with LISEM 163 and using a slope correction

The combined effect of the two slope corrections is shown in figure 9.2. Figure 9.2 shows that the difference was large; peak discharge decreased by about 50%. A decrease in discharge was to be expected since:

- On steep slopes the pixel areas have increased. The amount of rainfall per pixel is unaffected because it is assumed that the rain is falling vertically. The same amount of water is therefore spread out over a larger area, so that the water layer will be thinner. The hydraulic radius will also be smaller, so that flow will be slower according to the Manning equation.
- The flow distance between pixels is larger since it is now  $SlopeDX$  instead of  $DX$ . Only for zero slope angles  $SlopeDX$  and  $DX$  are equal.
- Since on steep slopes the pixel area is larger ( $SlopeDX$  times  $DX$ ) infiltration will be larger as well.
- For large slope angles sine is significantly smaller than tangent, hence the flow velocity as calculated by the Manning equation will be smaller too. Figure 9.5 shows the difference between tangent and sine for the Danangou catchment.

Note that factors that affect flow distance and flow velocity will also affect discharge because longer flow distance and lower flow velocity allow more time for infiltration.

### 9.2.2 Manning's n

Manning's n can either be calculated as a land use average, or it can be calculated as function of slope angle for those land uses that have erodible soils. Chapter 6 showed that only the cropland soils should be considered erodible. For the other land uses the values of Manning's n were the same for both methods. In LISEM 163, Manning's n was already calculated from slope for cropland. Therefore, it was investigated here what the effect would be of not using a slope dependent Manning's n. Thus, the evaluation of Manning's n is the reverse of the other changes to LISEM, since for the other changes it was investigated what the effect of introducing the change would be. Table 9.1 shows the results of a run for the event of 990720. It shows that the difference between the results obtained with both methods was fairly small. In principle, the result depends not only on the average value of Manning's n (reported in the table), but also on its distribution. However, all the results were logical in view of the difference in average Manning's n. The slope independent map had lower average Manning's n as well as an earlier peak, higher peak discharge, total discharge and total soil loss. The fit between simulation result and observed values was slightly better for the slope dependent map, but that was to be expected because that map was used during calibration.

Table 9.1 Effect of using a slope dependent Manning's n

	Slope independent	Slope dependent
Peak time (min)	24	24.75
Peak discharge (l/s)	3844	3592
Total discharge (m <sup>3</sup> )	4473	4277
Total soil loss (tonnes)	1098	1065
Average Manning's n	0.069	0.083

### 9.2.3 Settling velocity

As shown in chapter 5 the concentrations measured in the Danangou catchment make the use of a settling velocity correction necessary. The Chien & Wan (1983) equation (equation 5.15) was implemented because it was developed for Chinese conditions. The effect of using other equations is likely to be similar because figure 5.2 indicated that there is not much difference between the results of the equations. Figure 9.3 shows that by using the settling velocity correction the predicted sediment concentrations increased during the runoff peaks, but remained equal otherwise. The result is slightly unexpected since the settling correction could be expected to slow down settling after the sediment peak. This would result in higher concentrations after the sediment peak. Instead, concentrations rose faster and declined faster. This might be caused by the fact that the chart shows the integrated result for the entire catchment. However, the increase of total soil loss that was caused by the settling correction seems reasonable.

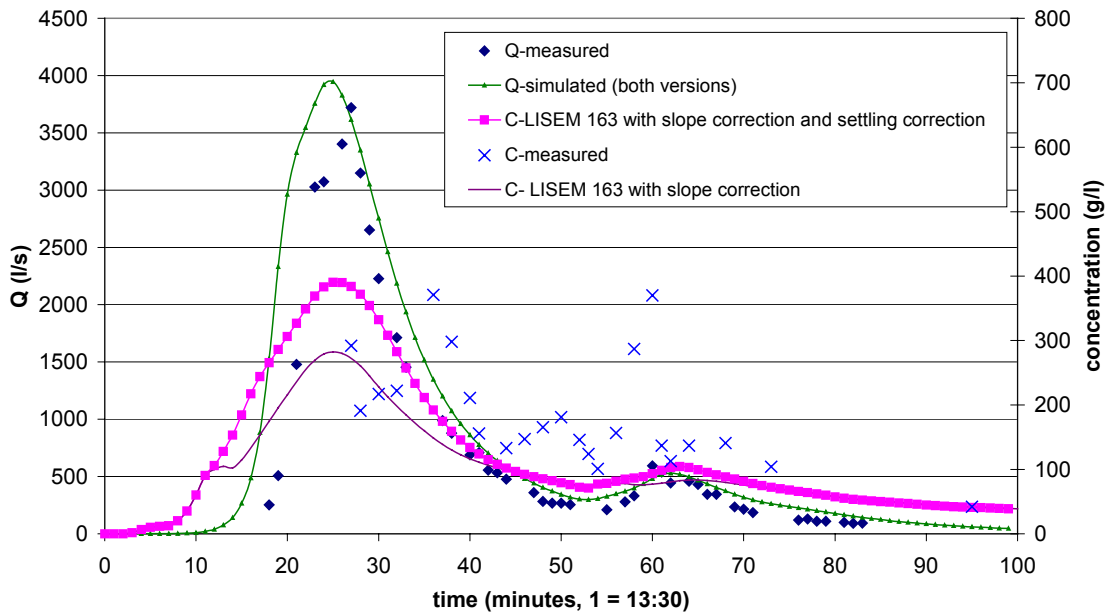


Figure 9.3 Comparison of sediment concentration predicted with a version of LISEM 163 that incorporated the slope correction, without and with settling correction added. Event of 990720. Since this LISEM version was an intermediate version the model was only approximately calibrated

#### 9.2.4 Loose material map

The daily-based gully model described in chapter 8 provides a map showing the position and amount of loose material available for transport at the gully heads during an event. In chapter 8, the model was only applied to gully heads because only for gully heads observations of loose material were available. To create an input map for the LISEM simulation the plan curvature requirement (section 8.3) was dropped because this requirement was used to distinguish gully heads from other very steep slopes. Gully heads would be concave in plan view, while other steep slopes would not. Since loose material will not only accumulate below the gully head, but everywhere where there are near vertical slopes, the requirement needed to be dropped. The model was then rerun. The resulting maps had an average amount of loose material at the end of the simulation of about 400 tonnes. Before the plan curvature requirement was dropped this was about 100 tonnes. The run that was used for the LISEM simulation had 372 tonnes. The resulting loose material map could be supplemented with mapping results of landslide lobes, or even with the position of croplands with zero-cohesion (freshly ploughed fields). The advantage of the map over the cohesion map is that a volume of material is specified, so that if this volume is removed erosion will stop. In the simulation only the map produced by the stability model of chapter 8 was used. During the LISEM run the only factor determining whether or not the material is removed is the availability of transport capacity. The remaining available material will be recalculated during each time step and erosion will stop when there is no material remaining.

The results using the model developed in chapter 8 are shown in figure 9.4. Figure 9.4 shows the amount of loose material for a small part of the Danangou catchment before and after the LISEM simulation. As can be seen the maps are very similar. Nevertheless, there are several pixels where a considerable amount of material has been removed. The arrow points at one such pixel; in this pixel loose material was 4700 kg before simulation and 0 after simulation. For the entire catchment the amount of loose material has declined from 372 to 265 tonnes. Nevertheless, the total amount of sediment leaving the catchment only increased by 1 - 2 tonnes.

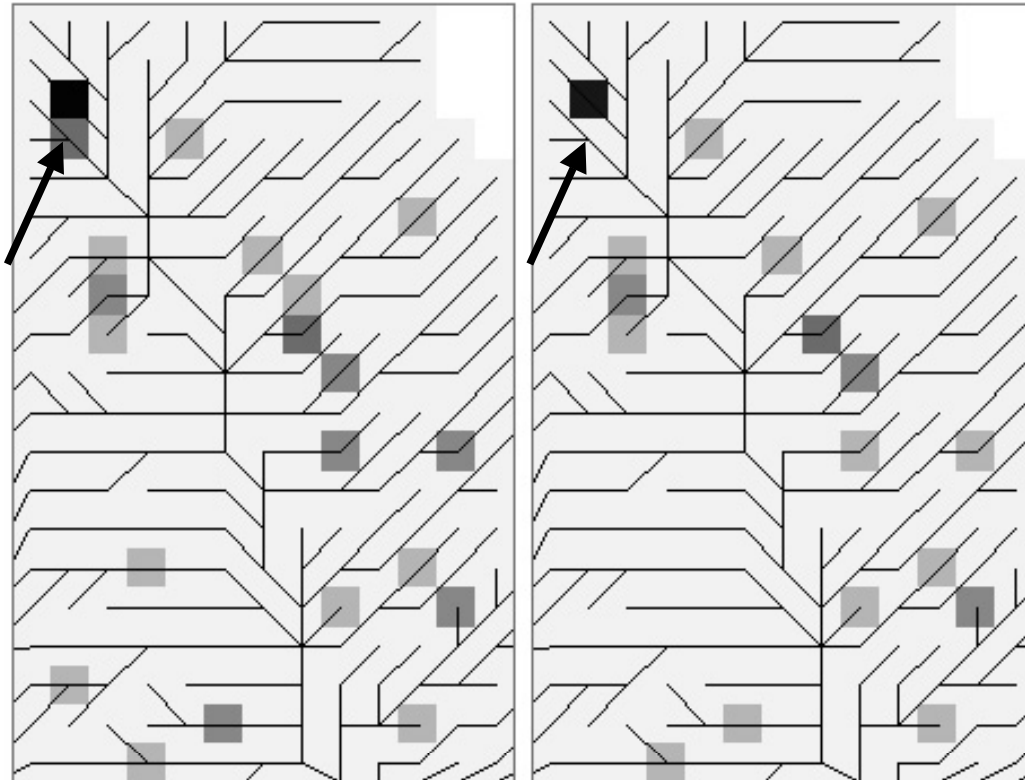


Figure 9.4 Loose material map of a small part of the Danangou catchment before (left) and after (right) LISEM simulation. Loose material amounts range from 0 (light grey background) to 10000 (black) kg. Black lines show the drainage network

Apparently, the extra eroded sediment was deposited before reaching the outlet. The deposition map confirmed that this happens. The fact that many pixels showed only a small decline in loose material can be explained by the position of these pixels on the drainage network. Many of these pixels did not experience much runoff because they had small upstream areas. The results indicated that including a loose material map is likely to have more effect when the loose material is present close to the outlet of the catchment. If no loose material is available, the result is exactly the same as for the original version of LISEM.

### 9.2.5 Sine versus tangent

The effect of using sine instead of tangent has already been discussed in section 9.2.1 for the simulation of discharge. It will, however, also influence sediment transport. The effect on sediment is evaluated separately from that on simulated discharge. It should be kept in mind that the slope correction for discharge also influences the amount of sediment transport. As shown in chapter 2 the equations for shear stress and stream power incorporate the sine of the slope angle. For gentle slopes the tangent is almost equal to the sine. The LISEM model has so far used the tangent of slope angle. For steep slopes, however, the tangent becomes much larger than sine. Therefore, shear stress and stream power will be larger for steep slopes when tangent is used instead of sine. Figure 9.5 shows the slope of the Danangou expressed as tangent and as sine of slope angle. The maximum slope in the catchment (at 10 m grid size) is 65 degrees, which corresponds to a tangent of 2.16 and a sine of 0.91. The figure shows that the map using sine has a larger area with intermediate slopes and a smaller area with steep slopes. Obviously, sine cannot be above 1. The effect of using sine instead of tangent is small for simulations for the entire catchment. Simulated total soil loss from the catchment decreased from 1065 tonnes to 1024 tonnes. Simulated soil loss from the sediment plot was also only slightly affected.

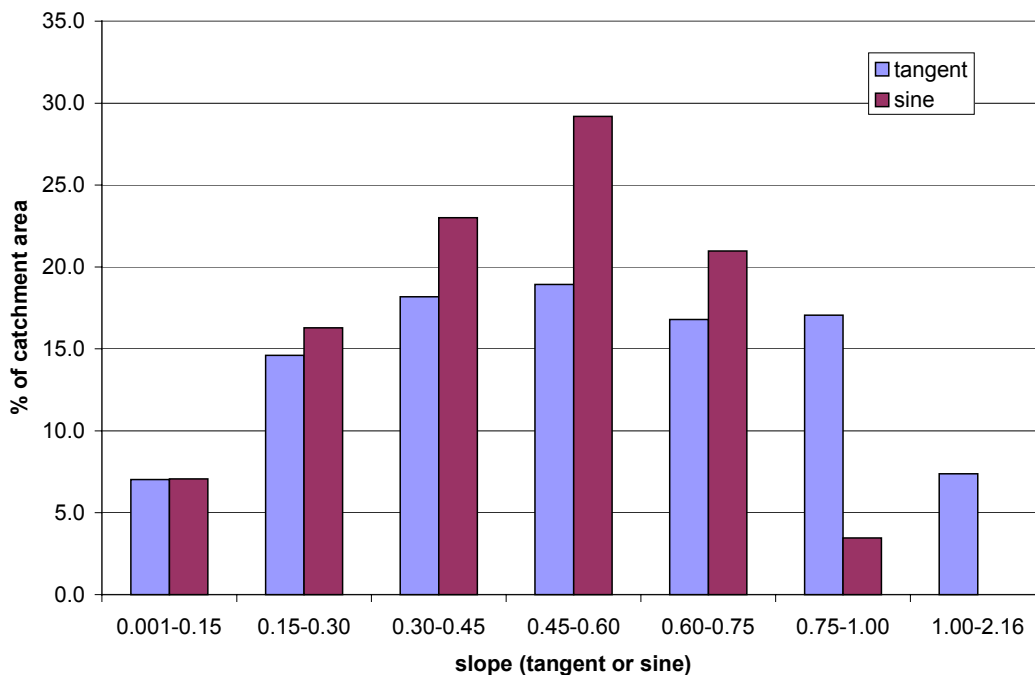


Figure 9.5 Areas occupied by different slope classes in the Danangou catchment. Based on maps with 10 m grid size

### 9.3 Cell size and time step length

One of the problems with LISEM is that the obtained results depend on both cell size and time step length. Practical considerations often limit the choice of time step length and grid size. Halving the grid size, for example, quadruples the number of pixels and the calculation time. Besides, cell size and time step length are linked to each other. If the cell size is small, the time step should be small too. A condition that should be met for the kinematic wave solution to be stable is the Courant condition (Ven Te Chow et al., 1988). According to this condition, the time step should be smaller than the grid cell size divided by the kinematic wave celerity. However, as a rule of thumb it can be stated that time step length in seconds should not be larger than cell size in metres. This condition, however, is not always met in reality and is also not enough to ensure that the solution will always be numerically stable.

The effects of grid size and time step were studied by simulating the 990720 calibrated dataset with LISEM LP.

#### 9.3.1 Cell size

As Doe & Harmon (2001) noted different model outputs can be computed if the same system is modelled with different grid cell size. Zhi-Yong Yin & Xinhao Wang (1999) studied the effect of grid size on drainage basin parameters. They used maps having 30-metre and 92-metre resolution to determine a number of basin characteristics and found that the change in resolution was most prominently reflected in the slope parameters mean slope and maximum slope. Both decreased significantly with an increase in grid size. Garbrecht & Martz (1994) found that channel length decreases with increasing grid size, especially if the channels are tortuous.

Schoorl et al. (2000) studied the effect of DEM resolution on the processes of erosion and sedimentation. They used artificial DEMs with different cell size (1,3,9,27 and 81 m), but with equal spatial extent (a slope of 81\*81 m) and a single slope angle. Transport capacity, detachment and deposition were calculated as a function of discharge. Total discharge from the slope was equal for all cell sizes. Schoorl et al. (2000) found a clear increase of soil loss with an increase in cell size, which was caused by the number of calculations in the downslope direction. Though they do not explain their routing method, it is obvious that pixels higher up on the slope will have less discharge and less soil loss than those lower down. Thus, if only 1 pixel is used the discharge at the lower boundary of the slope is assigned to the entire slope, so that sediment transport is overpredicted. It would seem that the smaller the cell size is, the more reliable the result will be. To obtain more reliable results for coarser grids some of the model parameters should be changed. Vázquez et al. (2002) found that effective parameter values are scale dependent for the process based MIKE-SHE model. Braun et al. (1997) stated that either relevant principles or characteristic parameters should be changed when changing from a small to a large scale. They propose the use of scaling functions to calculate effective parameters at a certain scale from those at another scale.

To study the effect of cell size on the simulation result the original 5-metre resolution dataset was converted into 10 (which was used for calibration), 20, 50 and 100 metre resolution grids. The procedure used to produce the different resolution data sets was as follows:

- 1) The 3 basic maps were converted from the original grid size (5 m) to the appropriate cell size using PCRaster. The 3 basic maps are the DEM, the land use map and the lithology map.
- 2) The rest of the data set was then produced by using the same PCRaster script files for all grid sizes. This ensured that the only difference between the datasets was the grid size. Since the channel width was also specified in one of these scripts it was also constant for all grid sizes. Because channel width should always be smaller than grid size it was set to 4.95 metres.

Time step length was 15 seconds for all grid sizes.

### Results

The results are presented in figure 9.6 and table 9.2. Table 9.2 shows some changes that occurred with an increase in grid size:

- The larger the cell size the smaller the maximum slope and the average slope were. This is an inevitable consequence of averaging the DEM.
- Channel length decreased somewhat with an increase of grid size.
- The larger the cell size the higher the average channel slope was, while maximum channel slope first decreased and then increased.
- The larger the cell size the larger the catchment area was.

Table 9.2 Effects of different grid sizes (m) on catchment characteristics and simulation results

	5	10	20	50	100
<i>Catchment characteristics</i>					
Catchment area (ha)	207	210	214	228	253
Average slope (tangent) <sup>b</sup>	0.59	0.55	0.51	0.41	0.30
Maximum slope (tangent)	3.73	2.16	1.44	0.96	0.91
Channel length (m)	1165	1130	1120	1150	1100
Average channel slope (tangent)	0.052	0.056	0.052	0.061	0.078
Maximum channel slope (tangent)	0.57	0.27	0.17	0.21	0.30
<i>Simulation results</i>					
Time to peak (min)	24.5	24.75	25.25	26.5	27.5
Peak discharge (l/s)	3695	3592	3305	2536	2075
Total discharge (m <sup>3</sup> )	4470	4277	3990	3598	3419
Total erosion (tonnes)	5396	5616	5900	5950	5189
Total deposition (tonnes)	4517	4590	5171	5435	4710
Net erosion outside channels (tonnes)	1146	1167	727	356	157
Net erosion in channels (tonnes) <sup>a</sup>	-267	-141	2	159	322
Sediment yield (tonnes)	877	1024	726	512	474

<sup>a</sup> negative sign indicates net deposition

<sup>b</sup> tangent is shown here for clarity, in LISEM sine is used

Figure 9.6 and table 9.2 show that both peak discharge and total discharge (area below curves) decreased with increasing grid size. Figure 9.7 shows the simulated concentrations for the different grid sizes, while table 9.2 gives simulated values for erosion, deposition and sediment yield. Table 9.2 shows that sediment yields generally decreased with an increase in grid size, thus following the trend for water. It also shows

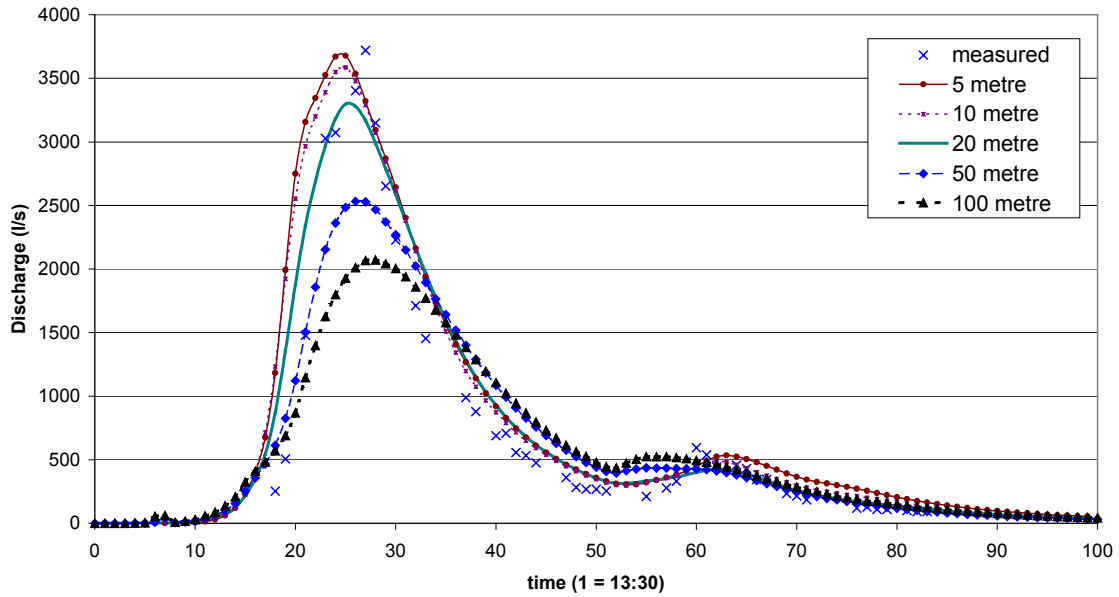


Figure 9.6 Effect of grid size on simulated discharge, 15-second time step, 990720 event

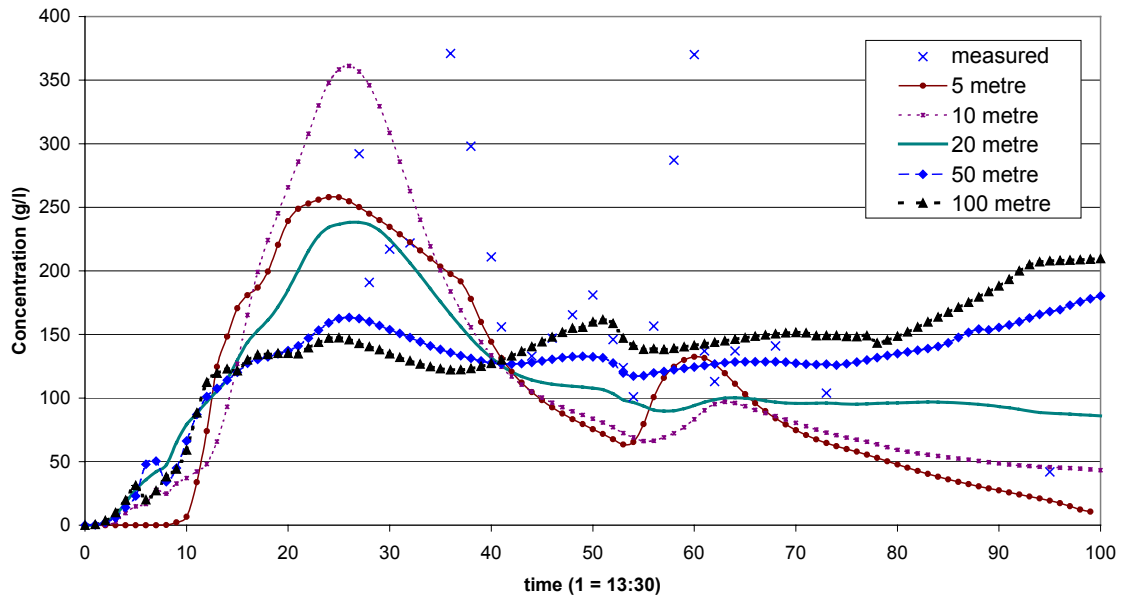


Figure 9.7 Effect of grid size on simulated concentration, 15-second time step, 990720 event



that for total erosion and total deposition the 100-metre grid deviated from the trend of the other grid sizes. For net erosion, however, this was not the case. Other trends were the change of the channel from sediment sink for small grid sizes to sediment source for large grid sizes, and the rapid decrease of net erosion outside the channels for grid sizes larger than 10 metres.

Figure 9.7 shows that the results of the 10-metre grid partly deviated from the results of the other grid sizes, especially during the main concentration peak. During the runoff peak (compare with figure 9.6) simulated concentrations decreased with an increase in grid size, except for the 10-metre grid, which had the highest simulated concentrations. Consequently, the 10-metre grid also resulted in the highest total soil loss (table 9.2). By contrast, during low discharge, predicted concentrations increased with increasing grid size. During those periods the 10 metre grid results were in line with the other grid sizes.

### *Discussion*

The observed decrease in discharge with increasing grid size was probably due to a combination of two causes. The first cause is the kinematic wave calculation. Ven Te Chow et al. (1988) and Fread (1985) showed that the numerical solution of the kinematic wave inevitably results in numerical errors that cause the flood wave to disperse. According to Ven Te Chow et al. (1988) this dispersion increases with increasing distance steps. This can explain why peak discharge decreased with an increase in grid size. Dispersion of the flood wave, however, also implies that it would take longer before all water leaves the catchment. Hence, there would be more time for infiltration. The second cause is that with the decrease in slope for an increase in grid size flow will also slow down, so that there is more opportunity for infiltration to occur.

The general trend in predicted sediment yield might be explained from the changes of slope with increasing grid size. The larger the grid size, the smaller the maximum slope as well as the average slope. Therefore, the transport capacity on the steep slopes will be lower if grid size is larger. This would result in a decrease of simulated concentration, so that soil loss will also decrease with increasing grid size. Soil loss was found to decrease from 877 tonnes for the 5-metre grid to 474 tonnes for the 100-metre grid; only the 10-metre grid deviated from the decreasing trend. Comparison of figures 9.6 and 9.7 shows that during low discharge the trend in concentration was reversed. During such periods the behaviour of the channel was much more important, because flow from the slopes had virtually ceased. Since the average channel slope increased with increasing grid size (table 9.2) the channel transport capacity should also increase. This explains why simulated concentrations increased with grid size during these periods. Since the amount of water involved was small, the effect on soil loss was small too.

The deviating behaviour of the 10-metre grid is more difficult to explain. Table 9.2 shows that it only deviated from the trend shown by the other grid sizes by having a slightly higher average channel slope than the 5 and 20 metre grids. This would mean slightly larger channel transport capacities, but this small difference seems insufficient to explain the large difference in predicted concentration (figure 9.7). Soil loss was 1024 tonnes, which was also much higher than for the 5 metre and 20 metre grids that had 877 and 726

tonnes respectively. Table 9.2 suggests that the cause was a larger net erosion outside the channels than might have been expected. The cause for this is unclear. Jetten et al. (in press), however, also found that the variation of net soil loss with grid cell size was fairly unpredictable, which they attributed to the large influence individual pixels had on deposition.

In conclusion, it can be said that clear differences have been found for simulations using the same data set but different grid size. Most of the differences could be explained from changes in slope angle that inevitably result from changing grid size. Based on figures 9.6 and 9.7 grid sizes of over 20 metres seem inadequate for the Danangou catchment.

### 9.3.2 Time step length

To study the effect of time step length on the simulation results the 10 metre dataset was used with different time step lengths of 2, 5, 10, 15 (used for calibration), 20, 30, 60, 90 and 120 seconds.

#### Results

The results are shown in figure 9.8 and tables 9.3 and 9.4. Table 9.3 shows that both predicted peak discharge and predicted total discharge start to decreased when time step length was longer than 20 to 30 seconds. For shorter time step lengths the differences between the different time step lengths were small. Mass balance errors for discharge were 0.002 % or lower for all simulations and they did not show a relationship with time step length.

Table 9.3 Effect of time step length (seconds) on LISEM simulations. Calibrated dataset of the event of 990720 is used

	Discharge			Sediment		
	Tp (min)	Qp (l/s)	Qtot (m <sup>3</sup> )	Soil loss (tonnes)	MB-er cor (10 <sup>-5</sup> %)	MB-er nocor (%)
2	24.7	3674	4287	1644	-200	53.8
5	24.8	3667	4294	1473	50	32.6
10	24.7	3628	4285	1177	20	13.7
15	24.8	3592	4277	1024	10	4.73
20	24.7	3560	4265	935	100	0.71
30	25.0	3512	4245	841	-30	-1.77
60	25.0	3376	4202	718	30	-1.16
90	25.5	3164	4093	669	-20	0.02
120	26.0	2746	3634	592	-3	1.86

By contrast, soil loss showed a large decrease with increasing time step length for the smaller time step lengths. Furthermore, the largest differences in predicted concentration

occurred when there were only small changes in predicted discharge, which indicates that the cause is not directly related to discharge. Figure 9.8 shows that for longer time step lengths the predicted concentration became more constant over time. LISEM normally uses a mass balance correction for the sediment prediction. The results in table 9.4 were obtained with this correction. When this correction was switched off, mass balance errors for the sediment prediction became very large for small time step lengths (table 9.3).

Table 9.4 Summary of time step length results. Negative sign indicates net deposition

Time step length (seconds)	Total erosion (tonnes)	Total deposition (tonnes)	Net erosion non-channels (tonnes)	Net erosion channels (tonnes)	Total net erosion (tonnes)
2	8093	6448	2101	-456	1645
5	7144	5670	1863	-389	1474
10	6178	5000	1426	-248	1178
15	5616	4590	1167	-141	1026
20	5266	4328	1007	-69	938
30	4901	4058	832	11	843
60	4923	4201	616	106	722
90	6478	5804	524	150	674
120	6770	6172	436	162	598

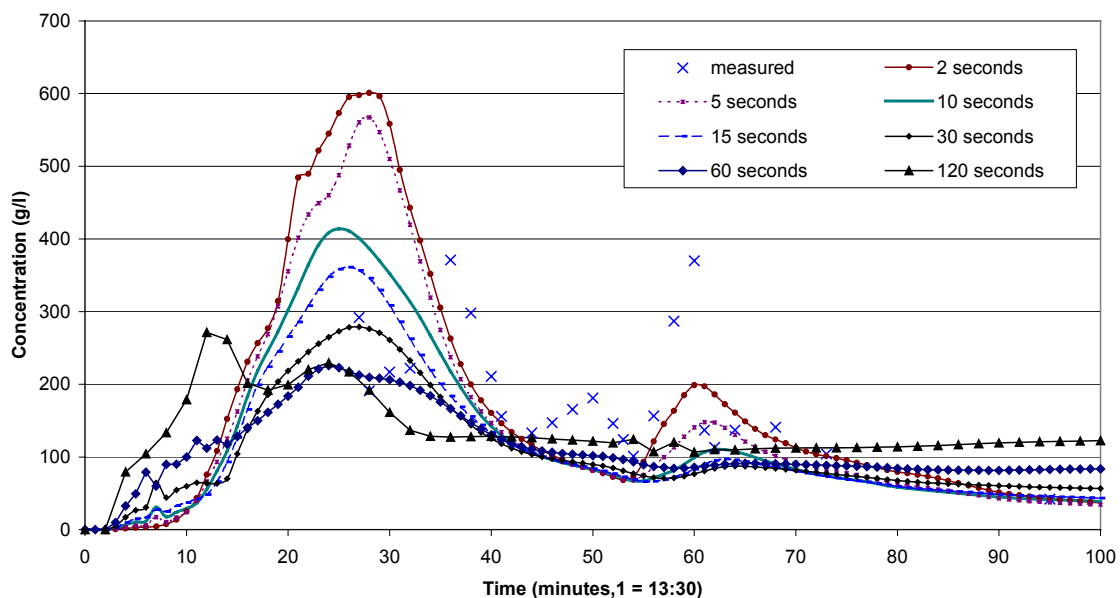


Figure 9.8 Predicted sediment concentration for different time step lengths, calibrated dataset of 990720, 10-metre grid

Table 9.4 shows that total erosion and total deposition decreased from time step lengths of 2 seconds to 30 seconds. For larger time step lengths they increased again, even though the amount of water available was clearly less (table 9.3). Net erosion outside the channels and net total erosion continuously decreased with increasing time step length. Net erosion in the channels switched from negative (= net deposition) to positive at time step length of 30 seconds. Because of this trend in net channel erosion, total net erosion decreased less than the net erosion outside the channels.

### *Discussion*

The most likely causes for the observed differences between discharges simulated with different time step lengths are the kinematic wave and the water balance.

The kinematic wave redistributes the water in the direction of the catchment outlet. According to Ven Te Chow et al. (1988) and Fread (1985) numerical errors are unavoidable in the calculation of the kinematic wave by means of finite differences. These errors should increase with an increase in time step length, so that small time steps should be chosen. The result of these errors would be to disperse the flood peak, so that peak discharge will become lower with longer time step lengths. Total discharge is not directly affected, so that the effect of dispersion is not included in the mass balance error given by LISEM. Because of dispersion, peak discharge continuously decreased with an increase in time step length.

Time step length also has several effects on the water balance:

- During each time step, the amount of rain that fell during the time step is added to the water layer present in a pixel. Since the amount of rain falling during a time step is equal to rain intensity multiplied by time step length, larger time step lengths mean that more water is added at once. In other words: the larger the time step length the coarser the water balance is. What effect this had on simulated discharge is not clear, but a smaller time step length should in principle give a more reliable result.
- After the kinematic wave is performed, the discharge in a pixel is converted back to wetted area (and back to water level) using the alpha (equation 2.3) of the previous time step. Alpha depends on the wetted perimeter and might have changed due to the kinematic wave. For longer time step length the difference between old alpha and new alpha is likely to be larger than for shorter time step length. Thus, for longer time step length larger errors can occur. These errors, however, are not likely to be systematic and can therefore probably not explain a systematic decrease in discharge with an increase in time step length.
- Another effect of time step length occurs when the simulation time step length becomes longer than the time step length that is used in the rainfall file. LISEM will then calculate average rainfall intensity, which will be lower than peak intensity in the rainfall file. The total amount of rainfall does not change. Nevertheless, the decrease in maximum intensity might result in an increase in infiltration. In the simulations presented here the time step length of the rainfall data was 60 seconds. Hence, this effect could have influenced the simulation results for time step lengths of 90 and 120 seconds.

A combination of these effects adequately explains the decrease in peak discharge and total discharge that can be seen in table 9.5.

The results for the discharge simulation were satisfactory and indicated that as long as time step length is 30 seconds or less the differences in predicted discharge will be small.

The simulated concentrations also showed a trend with time step length. As with the prediction of water, the most likely cause would seem to be a combination of the sediment balance and the kinematic wave. A complicating factor is that LISEM contains a correction on the sediment balance. This correction is applied after the kinematic wave and distributes any mass balance error caused by the kinematic wave for a particular time step over the catchment using the sediment that is already present in the pixels as weighting factor. Without such a mass balance correction, mass balance error of the sediment was a function of time step length. For a time step length of 2 seconds the error was as high as 54% of total erosion (table 9.3). This suggests that the error was a function of the number of time steps. What causes the error is unknown, but the magnitude of the error shows that as long as the error has not been removed from LISEM a mass balance correction is needed to obtain reliable results. However, since the same error still occurs in the kinematic wave, large amounts of sediment that are lost without the correction are put back into the flow with the correction. This can explain why predicted soil loss increased with decreasing time step length. However, the sediment that is redistributed also causes erosion to be smaller and deposition to be larger than would be the case without correction. Thus, without mass balance correction total erosion varied even more with time step length, though total soil loss was more constant. It therefore seems that the mass balance correction cannot explain why erosion should decrease with increasing time step length until time step lengths of 30 seconds. Nevertheless, it might still partly cause the observed results. Since the high erosion rates caused deposition to be high, the high erosion rates should be explained. Table 9.4 shows that the differences between different time step lengths were moderated by differences in deposition in the channel. Therefore, the cause for the difference in results should be sought outside the channels, i.e. on the steep slopes of the catchment.

In LISEM, detachment and deposition linearly increase with time step length (equation 2.19). Considering the case of detachment, total detachment would, over a given period, be larger for long time step lengths than for short time step lengths because detachment is a function of the initial difference between transport capacity and concentration. For small time step lengths this initial difference would decrease every time step, so that detachment decreases every time step. Therefore, one could expect detachment to increase with time step length. Thus, for a larger time step length the amount of sediment in the flow will be larger, which should also result in a larger sediment outflow per unit of time. This should cause an increase in erosion with an increase of time step length, as observed for time step lengths larger than 30 seconds. The effect for deposition could be larger than for detachment since  $y$  (equation 2.19) is larger for deposition. However, there are several limitations to this reasoning:

- 1) It depends on the assumption that there is no redistribution between the time steps. In reality, there will be some redistribution in every time step. Thus part (or all) of

the sediment that is detached in a time step is removed from the grid cell before the next time step, so the initial difference between transport capacity and concentration is modified every time step. For longer time steps this occurs less often. Cells not only loose sediment in this way, but can also receive sediment from upslope.

- 2) Without redistribution the effect might be different for the next time step, because the short time step length now has lower concentration (as explained above) and therefore a larger transport deficit and more detachment than the long time step length.
- 3) The increase of detachment and deposition with increasing time step length may be limited by the fact that not more sediment can be detached than is needed to fill transport capacity, while not more sediment can be deposited than there is in the flow. For longer time step lengths this limit is more likely to be reached.

The simulation results show that for pixels that have no upstream area detachment increased from time step lengths of 2 seconds to time step lengths of 120 seconds. This could be expected based on the considerations above. However, the same results also show that somewhat further down the drainage network such clear relationships between time step length and erosion or deposition no longer existed. This is probably due to the redistribution by the kinematic wave. The effect apparently is that with longer time steps less and less sediment reached the channels, so that they can change from sediment sink to sediment source (table 9.4).

As figure 9.8 shows, simulated concentrations initially increased more rapidly for the larger time step lengths. This is in line with an expected increase of detachment with increasing time step length. Later on, however, simulated concentrations became increasingly stable in time, while simulations with short time step lengths showed much more fluctuation in concentration. During those periods the slopes apparently did not deliver much sediment to the channel for the longer time step lengths. Generally, during periods when channel flow dominated, simulated concentrations followed the expected trend of larger concentration with longer time step. During the discharge peaks, however, the trend was reversed. No adequate explanation for the large differences between the different time step lengths was found.

From the results it is clear that because of the dependency of predicted sediment on time step length the time step length should be chosen before calibration starts. Based on the results for discharge time step lengths of longer than 30 seconds seem inadequate for the Danangou catchment. The results for the simulated concentration indicate that there are potential problems with mass balance errors (corrected or not) for short time step lengths. Thus, intermediate time step lengths (15-30 seconds) seem most appropriate at present. If the problems with the sediment prediction would be solved shorter time step lengths would be preferable because for shorter time step lengths the mass balance should be more accurate. These considerations are mostly theoretical since reasonable predictions can probably be obtained for all time step lengths by using other values for the LISEM calibration parameters.

## 9.4 Conclusions

The changes to LISEM that were proposed in chapters 4 to 8 were found to have effects of different magnitude on the LISEM predictions. Some of the changes were found to have a large effect, but the effect of others was small. Predicted discharge decreased by about 50% from applying a slope correction for the calculation of overland flow, but was only marginally affected by using a slope dependent value of Manning's  $n$ . Predicted concentration increased by applying a concentration dependent settling velocity, but was hardly changed by introducing a map with loose material or by using sine instead of tangent in the transport equations. Chapter 7 showed that the predicted sediment concentration is also very dependent on the choice of transport equation.

The analysis of the effect of time step length and cell size showed that both grid size and time step have large influence on the prediction by LISEM. In both cases, the difference in runoff prediction could be explained. The behaviour of the sediment prediction, however, proved much more difficult to explain. Several possible reasons for this can be mentioned:

- 1) The sediment prediction depends on the water prediction, but with additional complicating factors. Therefore, sediment prediction is bound to be more complicated than water prediction.
- 2) Sediment prediction depends on the difference between concentration and transport capacity. The equations for detachment and deposition include both grid size and time step. Thus, there might be alternation of detachment and deposition in time and space. Water movement, on the other hand, is more continuous (even though influenced by rainfall and infiltration). The amount of rainfall, for example, is independent of the amount of water present in a pixel.
- 3) The kinematic wave causes redistribution of sediment for every time step. This makes it very difficult to explore what the effect of grid size and time step alone would be on detachment and deposition.
- 4) Individual pixels can have large influence on the total amounts of detachment and deposition. Especially deposition can be concentrated in the gentler parts of the channels.

Thus, the resulting sediment prediction is probably the result of a complex interplay of available water, transport capacity and the kinematic wave. Though this behaviour has not been fully explained, it is clear that a certain cell size and time step length should be chosen before calibration starts. For the Danangou catchment grid size should not be larger than 20 metres and time step length should not be longer than 30 seconds.





## 10 LISEM CALIBRATION AND VALIDATION

*Partly based on: Hessel, R., Jetten, V., Liu Baoyuan, Zhang Yan & Stolte, J. (in press). Calibration of the LISEM model for a small Loess Plateau catchment. Catena*

### 10.1 Introduction

Although theoretically fully physically based models should not have to be calibrated, reality is different. Models are never fully physically based and many authors have demonstrated the need to calibrate process based erosion models to obtain an acceptable predictive quality (e.g. Jetten et al., 1999). In the case of hydrological/erosion models calibration has mostly been done using measured data at the outlet of the plot or catchment. Recently, however, several authors have pointed to the necessity of calibrating process based, distributed models in a spatial way (e.g. Jetten et al., 1996; Takken et al., 1999; Beven, 2002; Jetten et al., in press). Such a calibration is a logical step since the main advantage of distributed models over lumped models should be that they are able to predict spatial patterns. Also, there are circumstances where the location of erosion or deposition in a catchment is more important than the precise amount of water/sediment passing the outlet, for example to design effective anti-erosion measures. Takken et al. (1999) applied the LISEM (Limburg Soil Erosion Model, De Roo et al., 1996a, Jetten & De Roo, 2001) model to a small catchment in eastern Belgium. Their catchment was not far from the Limburg catchments that were used to develop the LISEM model. Topography, soils and climate are similar in Limburg and eastern Belgium. Hence, there should be no doubt about the applicability of LISEM in their case. Takken et al. (1999) showed that although the net soil loss at the catchment outlet was well predicted, the erosion/deposition rates on the individual fields were considerably different from the measured values. Similar conclusions were reached by Jetten et al. (1996), who used a theoretical LISEM modelling approach for conditions representative of northern France.

The aim of the study presented in this chapter was to evaluate the applicability of the LISEM model for a catchment on the Chinese Loess Plateau. The prediction of both catchment soil loss and spatial erosion patterns was evaluated. To do this a 2-step approach was used. First, the LISEM model was calibrated on runoff and sediment yield measured at the catchment outlet (sections 10.3 and 10.4). Then, the simulation results of the calibrated model were evaluated in a spatial way using field observations on erosion patterns (section 10.5). Both the original version of LISEM (LISEM 163) and the version containing the changes described in chapter 9 (LISEM LP) were calibrated and the results of both versions were compared with each other.

## 10.2 Catchment outlet calibration

### 10.2.1 Materials and method

In accordance with chapter 9, pixel size and time step length were chosen before calibration started. For all simulations, LISEM was used with a pixel size of 10 meters and a time step length of 15 seconds. Since the upper few decimetres of the soil are crucial for infiltration during a storm, 10 calculation layers were used in the finite difference solution of the Richards equation, with node spacing increasing with depth. A single median grainsize (D50) of 35 micrometer is used in all cases in the sediment transport equations of LISEM. As a process based distributed model LISEM needs a large amount of input data (table 2.1). During the study period (1998-2000) most of the input parameters needed for the LISEM model were measured repeatedly in the Danangou catchment (chapter 4). Plant and soil characteristics were measured on a fortnightly basis, except for Manning's n, which was measured in two separate campaigns using small runoff plots (chapter 6). Soil physical characteristics such as saturated hydraulic conductivity, soil moisture retention curves and the water content-conductivity relationships were determined using samples taken in the catchment. All these measurements are discussed elsewhere (Wu Yongqiu et al., in press, Liu Guobin et al., in press, Stolte et al., in press). The field data were converted to input maps for LISEM using the land use map as basis, so that, for a given storm, these variables were constant within a land use, but differed between land uses. For variables that clearly also depend on soil type (e.g. cohesion) a combination of land use and soil type was used to extrapolate the measurements. Initial moisture content was predicted with multiple regression equations based on aspect and slope (table 10.1) and was therefore spatially variable. The equations predicted moisture content from slope and aspect for different soil depths. The resulting moisture contents were yearly averages, but these could be corrected for particular events using TDR (time domain reflectometry) measurements that were performed close to the date of the event.

Table 10.1 Multiple regression equations used for predicting initial moisture content (equations provided by Qiu Yang, Research Center for Eco-Environmental Sciences, Beijing, China)

Depth (cm)	Equation
5	$SW = 0.0712 + 0.0054*As + 0.0003*S$
15	$SW = 0.0883 + 0.0046*As + 0.0001*S$
25	$SW = 0.0996 + 0.0051*As - 0.00005*S$
45	$SW = 0.1172 + 0.0042*As - 0.0002*S$
75	$SW = 0.1264 + 0.0051*As - 0.0004*S$

Explanation: SW = soil water content (volume fraction)  
 As = classified aspect (8 directions), from 0 (north) - 360 degrees  
 in 45 degree steps respectively 8,6,4,2,1,3,5,7  
 S = slope angle (degrees)

Crusting was often observed on croplands, but also sometimes on other land uses. This might be the reason why the measurements of saturated conductivity yielded the lowest

conductivities for cropland (table 4.5). This study did not focus on the effect of crusting, but to take crusting into account to a certain degree the cropland saturated conductivity was used when crusting was observed.

Rainfall was measured using 6 tipping bucket rain gauges (1998-2000) and 4 simple rain gauges that measure total rainfall only (1999-2000). The rain gauges were distributed throughout the catchment (Figure 4.1). Thus, the number of rain gauges used in LISEM is between 6 and 10. Which rain gauge was used for any particular pixel was a function of distance and elevation difference between the pixel and the different rain gauges. Discharge and sediment concentration were measured at a v-shaped weir built in 1998 (chapter 4). The area upstream of the weir is slightly over 2 km<sup>2</sup>, but the total area of the catchment is 3.5 km<sup>2</sup>. The position of the weir is indicated in figure 4.1. In the 3-year study period only 6 events could be measured, one of which was not used for calibration because no sediment concentration data were available.

Model calibration had several objectives: to correctly simulate peak discharge, total discharge and total soil loss. The LISEM model was calibrated first on peak discharge (including time to peak and hydrograph shape) to obtain the correct shape of the hydrograph and after that an adjustment was made to obtain the correct total discharge. Once the discharge prediction cannot be improved any more the model can be calibrated on sediment yield. Several parameters were used to calibrate on peak discharge:

1. Saturated conductivity. Values for saturated conductivity were obtained in two ways: by constant head measurement on soil samples ( $K_{sat_m}$ ) and by using the so-called Wind evaporation method (Halbertsma & Veerman, 1997). The latter method gives relationships between moisture content and conductivity that use the Mualem-van Genuchten equations (see Stolte et al., in press). These relationships can be extrapolated to saturated conditions to give a fitted value of  $K_{sat_f}$ . In LISEM, a saturated conductivity estimated from  $K_{sat_m}$  and  $K_{sat_f}$  was used:

$$K_{sat} = a \cdot K_{sat_f} + (1 - a) \cdot K_{sat_m} \quad (10.1)$$

This procedure ensured that  $K_{sat}$  was always between  $K_{sat_f}$  and  $K_{sat_m}$ . The rationale behind this approach is that  $K_{sat_f}$  might be too low because it is an extrapolation of unsaturated conductivity, while  $K_{sat_m}$  is probably too high since during sampling some disturbance is likely and dead-end pores might be cut through. Calibration on saturated conductivity was performed by changing the value of  $a$ .

2. Initial suction. Initial suction determines the unsaturated conductivity (and thus infiltration) during the start of a rainfall event. Initial suction was only used for calibration if calibrating on saturated conductivity proved insufficient.
3. Manning's n. Manning's n influences the velocity of runoff and therefore affects the shape and timing of the hydrograph.
4. Channel length. In LISEM pixels can be defined that contain a channel characterised by a separate Manning's n. The width of these channels can be defined by the user, but must be smaller than the pixel size. Flow velocity in the channel will generally be higher as a result of different hydraulic radius. Changing

the channel length therefore influences timing and shape of the simulated hydrograph.

All these parameters were changed within reasonable boundaries; that is within boundaries that could be argued to be realistic given the available amount of data and its uncertainty. Ksat, for example, was only allowed to vary between the values measured on the samples and the values determined with the Wind evaporation method. Manning's n was not allowed to be lower than 0.03 or higher than 0.3. Because of the limited number of storms a normal calibration/validation procedure in which a number of events is used for calibration and a number of events for validation was not possible. Instead, each event was calibrated separately. This resulted in five different calibration sets. Each calibration set was validated by applying it to the other four events.

Peak discharge calibrations are most suited to evaluate the performance of LISEM because they use time to peak, peak discharge and shape of the hydrograph. The use of a goodness of fit (e.g. Nash-Sutcliffe) coefficient was less appropriate because these coefficients are very sensitive to a time shift in runoff. Therefore the fitting was done by eye, and the Nash-Sutcliffe coefficient was only calculated to compare the final calibrated versions of LISEM 163 and the adapted version of LISEM (LISEM LP). The total runoff volume calibrations were necessary as sediment loss is calculated as the product of runoff volume and concentration. The total runoff volume calibrations used the peak discharge calibration as a starting point. For the total runoff calibrations only saturated conductivity was changed.

Where the fit between predicted soil loss and measured soil loss was unsatisfactory, the LISEM model was calibrated on sediment yield. To do this cohesion, aggregate stability and median grain size can be used because these parameters affect only sediment yield and have no influence on predicted discharge.

### *10.2.2 Data*

There were only 6 events that could be measured at the weir: August 1<sup>st</sup> 1998, August 23<sup>rd</sup> 1998, July 20<sup>th</sup> 1999, July 21<sup>st</sup> 1999, August 11<sup>th</sup> 2000 and August 29<sup>th</sup> 2000. The data collected during these events were discussed in chapter 4. Table 10.2 repeats some of the data given in table 4.10. Table 10.2 suggests that discharge in the Danangou catchment is a rainfall intensity-driven phenomenon: average rainfall amounts between the events are not that different, but the lower intensities of the 980823 and 000811 events clearly result in much lower discharges. This is also shown by the fact that a 17-hour event on May 20/21, 1998, which produced 73 mm of rain, did not produce runoff at all. Maximum intensities for that event were 36.2 mm/hour for single rain gauges. Thus, it seems that runoff from the catchment only occurs if more than about 11.5 mm of high intensity rain fell. Only the event of 990721 deviated from this trend. This is probably because it occurred shortly after the 990720 event, so that the soil was still very wet. Since the hydrograph of the 980801 event was not complete total discharge had to be estimated. The 990720 event was special in that the rainfall amounts in the eastern and

western part of the Danangou catchment were very different: at the eastern border about 30 mm of rain fell, while at the western border (about 2 km away) only 3 mm fell.

Table 10.2 Event characteristics

	980801	980823	990720	990721	000811	000829
Average rainfall (mm)	15.1	13.0	14.1	3.5	11.6	17.8
Max 1-min intensity (mm/h) <sup>a</sup>	69.9	47.2	66.2	35.8	49.5	84.9
Time to peak (minutes) <sup>e</sup>	15	34	19	32	31	15
Peak discharge (l/s)	5125	701	3589	453 <sup>d</sup>	214	8757
Tot discharge (m <sup>3</sup> )	3982 <sup>b</sup>	735	3282	488 <sup>d</sup>	199	5893
Tot sediment yield (tonnes) <sup>c</sup>	1280	96	770	n.a.	16	2630

- a. The given value is a weighed average of the entire catchment. Intensities at individual rain gauges can be much higher (up to about 120 mm/h for 1-minute intervals in the case of both the 980801 and 990720 events, and up to 190 mm/h for the 000829 event).
- b. The hydrograph was incomplete, so this value is estimated by assuming a linear reservoir
- c. Calculated from total discharge and measured sediment concentration
- d. Not corrected for sediment content because no concentration data were available.
- e. Time difference between maximum rainfall intensity and peak discharge

Table 10.3 correction factors for prediction of initial moisture content

Event	Depth (cm)				
	5	15	25	45	70
980801	1.33	1.29	1.13	1.02	0.95
980823	0.62	0.75	0.83	0.89	0.85
990720	1.31	1.25	1.11	0.98	0.79
000811	1.31	1.25	1.11	0.98	0.79
000829	0.62	0.75	0.83	0.89	0.85

The initial moisture contents as predicted with the equations given in table 10.1 were corrected for the individual events by using measurements of soil moisture that were conducted close to the date of the event. Table 10.3 shows the correction factors that were used for the five events that were used for calibration. Since no moisture measurements were performed in 2000, data from other storms were used based on a comparison of rainfall amounts prior to the event.

Table 10.4 shows the LISEM input dataset as used for the 990720 event. Datasets for the other events were similar. The availability of input data made it necessary to limit the number of land use based units to 10.

Table 10.4 Measured LISEM input dataset (plant and soil characteristics) for the 990720 event

	Crop <sup>a</sup>	Fallow	Orchard	Shrub	Waste	Forest
Aggregate Stability (median drop no)	6	5	6	6	8	7.25
Cohesion (kg/cm <sup>2</sup> )	0.08	0.10	0.10	0.09	0.11	0.11
Random roughness (cm)	1.75	1.11	1.28	1.03	1.66	0.88
Manning's n	SD <sup>b</sup>	0.079	0.092	0.153 <sup>c</sup>	0.091	0.214
Leaf Area Index	0.06	0.12	1.46	1.25	0.54	1.63
Plant cover (fraction)	0.06	0.10	0.18	0.40	0.23	0.35
Plant height (m)	0.28	0.11	3.1	0.97	0.25	13.6
Ksat-meas (cm/day)	55.9	82.2	96.9	164	153	122
Ksat-fitted (cm/day)	1	1	25	10	5	13
Theta-init	-----equations from table 10.1 used-----					

a. Cropland was subdivided in 5 types. Here the values for foxtail millet are given. The other types are pearl millet, potato, tall crops (maize, sorghum) and beans.

b. SD = slope dependent, Manning's n is calculated from slope angle based on a series of 16 experiments, see chapter 6.

c. Average of wasteland and forest

### 10.2.3 Results peak discharge calibration

Table 10.5 shows the calibrated values of LISEM input parameters for all 5 events, both for LISEM 163 and for LISEM LP. It shows that the calibration gave different results for the different storms. Figure 10.1 shows the measured discharge as well as the calibrated discharge for each of the events, while table 10.9 gives a summary of the simulation results. These calibration results show a number of features that are common to most events, as well as some features that were event-specific.

#### *Saturated conductivity*

Calibrated saturated conductivity was always much lower than the measured values. A possible explanation for this would be disturbance during sampling. Soil sealing/crusting could also be important. The effect of sealing/crusting is hard to measure on samples taken from the field. It is also possible that in the field complete saturation was not reached. Since for very wet soils the difference in conductivity is very large for a very small change in water content, this could also be an important factor in explaining the much lower conductivities that need to be used during simulation. Another complicating factor is that saturated conductivity appears to increase with an increase in rainfall intensity (e.g. Morgan, 1996, Van Dijck, 2000), which might help explain differences between the events.

#### *Manning's n*

The calibrated values of Manning's n were always lower than measured. The reason for this is not certain, but it seems possible that measured values were too high (chapter 6).

Table 10.5 Peak discharge calibrated values for all events

	980801	980823	990720	000811	000829
<i>LISEM 163</i>					
Ksat <i>a</i> LISEM <sup>a</sup>	0.90	0.96	0.85	0.85	0.81
Initial suction (*ori) <sup>b</sup>	1	0.45	1	1	1
Manning's n <sup>c</sup>	m-0.2*s	m-1*s	m-1*s	m-1*s	m-1*s
Tot chan length (m)	2576	2114	1319	1319	2114
Manning's n channel	0.04	0.06	0.05	0.05	0.05
<i>LISEM LP</i>					
Ksat <i>a</i> LISEM <sup>a</sup>	0.95	0.98	0.90	0.92	0.89
Initial suction (*ori) <sup>b</sup>	1	0.45	1	1	1
Manning's n <sup>c</sup>	m-0.2*s	m-1*s	m-1*s	m-1*s	m-1*s
Tot chan length (m)	2576	2114	1319	1319	2114
Manning's n channel	0.04	0.05	0.05	0.05	0.04

a. See equation 10.1 for explanation

b. Original initial suction is the suction that results from the predicted water content, see table 10.1. The original value is multiplied by the value in the table. Hence, for the 980823 event the suction becomes smaller and the soil is wetter.

c. m = mean of measured data, s = standard deviation of measured data. Values of Manning's n below 0.03 were set to 0.03.

### *Peak time*

The graphs (figure 10.1) of simulated discharge show that the discharge peak almost always occurred too early. Several possible explanations for this can be given. First, it could be caused by large macropores (such as fissures and sinkholes). The effect of macropores is not simulated with LISEM, since the Richards equation is only valid for matrixflow. In reality the first runoff on hillslopes might well infiltrate by way of fissures or sinkholes. Another possible cause would be slope angle. For grid maps, slope angle can be easily calculated when a DEM is available, but the fact that steep slopes increase the actual surface area (or overland distance) is not used. Thus, for steep terrain such as in Danangou it is conceivable that the actual distance travelled by the water is larger than calculated from the maps. This could cause a too early arrival of the discharge peak in the case of LISEM 163. LISEM LP, however, corrects for this effect (chapter 9). A third possibility would be storage in the channels or infiltration into the channel bed. Since the streams in the catchment are usually dry, depressions in the channel bed have to be filled before the water can advance further. Furthermore, it seems likely that in that case infiltration of channel flow could be important. This process is not simulated in either of the LISEM versions used here.

### *Total discharge*

Simulated total discharge was always too high when LISEM was calibrated on peak discharge (table 10.7). Figure 10.1 shows that LISEM was generally unable to accurately predict the very rapid rise and fall of water level that occurred in reality. This was especially the case for the smaller events.

### *LISEM version*

In LISEM LP, calibrated saturated conductivity was always lower than it was for LISEM 163. As shown in chapter 9 this is mainly due to the slope correction that has been applied. Comparison of the calibrated hydrographs of LISEM 163 and LISEM LP shows that for most events the runoff peak arrived a little later, though still before the measured peak. The overall fit was usually similar, because the predicted water level also tended to decline a little less rapidly. This shows that using a model that is theoretically better does not guarantee that the prediction will also be better. Nevertheless, the Nash-Sutcliffe coefficient was higher for 4 out of 5 events (Table 10.6). This was mainly due to the fact that the time shift between the rise of the measured and simulated hydrographs has decreased somewhat.

### *Event specific observations*

The 980823 event showed very low saturated conductivities as well as much wetter soils (table 10.5) than predicted from the used regression equations. One of the causes of this is likely to be data-inaccuracy. The data suggest that a low intensity storm on relatively dry soil did produce discharge. In particular, the moisture content of the upper part of the soil profile can change rapidly, and the 2-week measurement interval that was used for practical reasons might not be able to reflect these changes accurately. Thus, it is possible that in reality the initial moisture contents were higher than the data indicate, especially since the rainfall data show that about 17 mm of low intensity rain fell two days before the event.

Table 10.6 Nash-Sutcliffe coefficients for LISEM 163 and LISEM LP for the 5 events used for LISEM calibration

	980801	980823	990720	000811	000829	average
LISEM 163	0.74	-0.28	0.64	-0.50	0.94	0.31
LISEM LP	0.86	0.24	0.91	0.33	0.85	0.64

For the 990720 storm the ‘calibration’ channel length was much shorter than for most other events. This can be explained by the fact that this storm only produced high intensity rain in the areas close to the catchment outlet. The most striking difference between the simulation with LISEM 163 and LISEM LP is that LISEM LP no longer simulated a double peak. The double peak was probably caused by water from different parts of the catchment that arrived at the weir slightly out of phase. The hydrograph predicted with LISEM LP suggests that the first peak has been retarded by the adaptations to LISEM, so that both peaks are now in phase.

Calibration for the event of 000811 did not give good results. The predicted peak occurred too early for LISEM 163. For LISEM LP this did not happen. Total discharge for LISEM LP was, however, far too high. Time lapse between rainfall peak and measured discharge peak is large, which suggests that the water originated far from the weir.



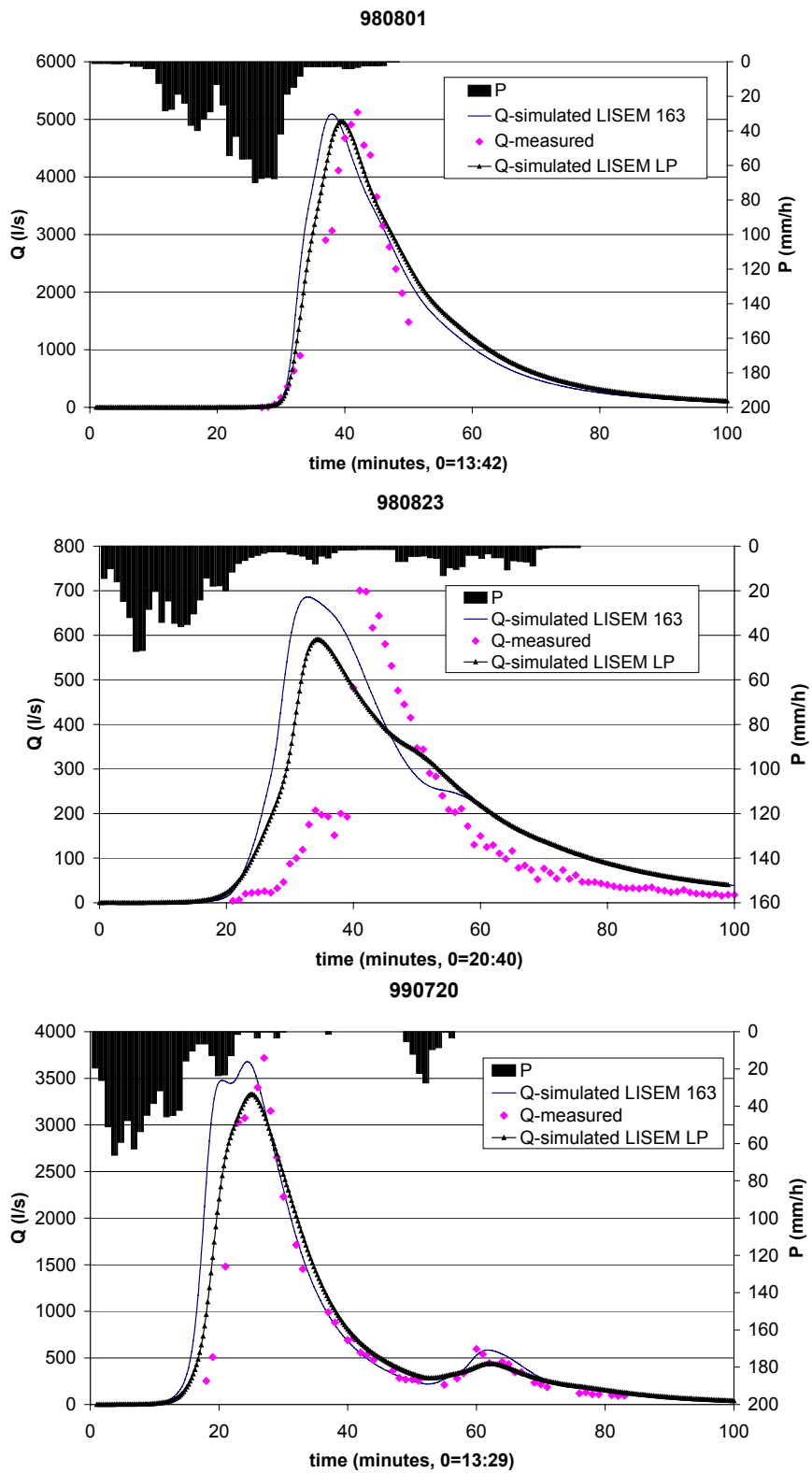


Figure 10.1 Calibration results for the five events that were measured at the weir

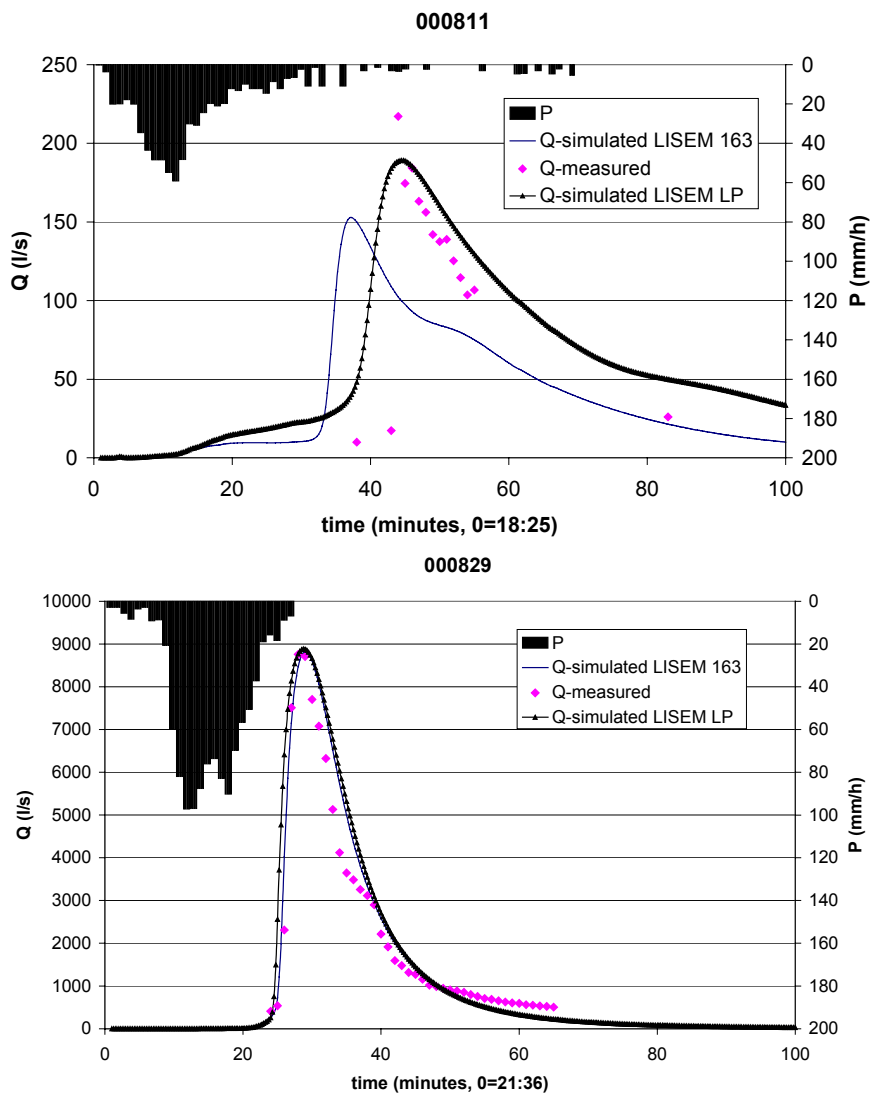


Figure 10.1 (continued)

Calibration of the 000829 event does not show an early peak (figure 10.1). The rising limb of the hydrograph was reproduced almost perfectly, especially by LISEM 163, but the falling limb of the hydrograph went down a little too slowly. Three possible causes for the early peaks have been mentioned earlier. Because of the very abrupt nature of the 000829 storm, where very high intensity rain suddenly occurred it is possible that the mentioned effects of infiltration in macropores (such as fissures and pipes) and the channel bed did not play a large role in this case. The effect of overland flow distance should still occur. The simulated hydrograph fell below the measured hydrograph at the end of the simulation. This is probably caused by the fact that the measured hydrograph was based on the pressure transducer signal. Figures 4.4 and 4.5 show that the pressure transducer is likely to give water level values that are too high during the later stages of the runoff peak (when water levels are low). Overall, the simulated hydrograph matches the measured one very well. Contrary to the other events the result for LISEM 163 was

slightly better than for LISEM LP, as was also indicated by the Nash-Sutcliffe coefficient (Table 10.6).

#### 10.2.4 Results peak discharge validation

To validate LISEM LP the calibrated data sets for each storm were applied to the other 4 events. Using the calibration data set of one event for the other four events usually gave worse fits than those presented in figure 10.1. The results of this validation are shown in figures 10.2 and 10.3 for the 990720 and 000829 events respectively. Table 10.7 gives a summary of the results for peak discharge. Figures 10.2 and 10.3 show that applying calibration settings of another event almost always gave results that differed much from those obtained by calibrating on that particular event. There are, however, a few cases in which applying another calibration setting gave results that were almost as good. Figure 10.2, for example shows that application of the 000829 calibration settings to the 990720 event gave a hydrograph that was very close to the one simulated using the 990720 calibration. Interestingly, applying the 990720 calibration to the 000829 event gave results that were very different than those obtained with the 000829 calibration settings (figure 10.3). This shows the complexity of the issue. Figures 10.2 and 10.3 also show that the 980801 tended to deviate from the other events. This is probably due to the fact that for this event one additional calibration parameter was used, namely the Manning's  $n$  in valley bottoms upstream of the channel head. Table 10.7 shows that using different calibration settings for a particular event almost always gave results that were worse than those obtained using the appropriate calibration settings. This is especially the case for the 980823 event; applying its calibration settings to other events always resulted in a large overprediction of discharge, while applying calibration settings of other events to

Table 10.7 Simulated peak discharge using the calibrated data sets for the different events

Event	Calibration data set					Measured
	980801	980823	990720	000811	000829	
980801	4967	12004	3617	4346	3873	5125
980823	35	591	13	13	24	701
990720	4649	10536	3330	4151	3301	3589
000811	612	4573	83	189	95	214
000829	9608	21329	14331	15471	8886	8757

the 980823 event always gave simulated discharge that was far too low. The most important parameter that causes the differences in simulated discharge between calibration settings is saturated conductivity. This indicates that developing a relationship between rainfall intensity (event magnitude) and saturated conductivity could be worthwhile, since such a relationship could potentially decrease the difference between calibration sets. At present, however, such a relationship is not available. Furthermore, saturated conductivity is apparently not the only cause, since the 990720 and 000829 calibration settings have slightly different saturated conductivity but still yield almost the same result for the 990720 event. It is therefore concluded that a separate calibration is

necessary for events of different magnitudes, and probably even for each event separately.

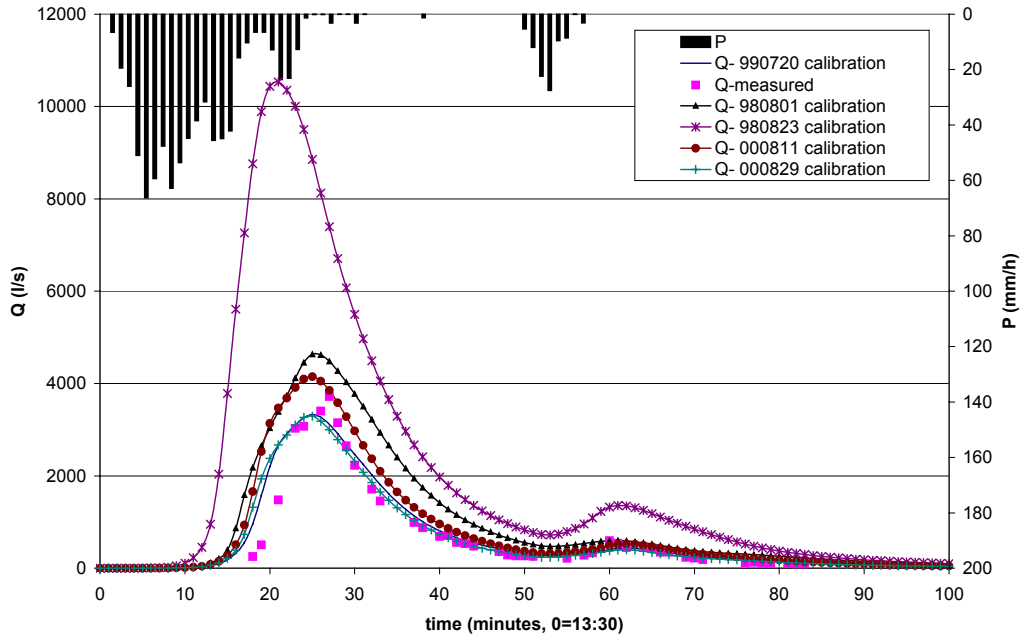


Figure 10.2 Validation results for the 990720 event. Data shown correspond to the third row of table 10.6

#### 10.2.5 Results total discharge calibration

A total discharge calibration was performed for the events of 980801, 990720 and 000829. The 980823 and 000811 events were not used because their peak calibration results were not satisfactory. The only difference with the peak discharge calibration is that the  $K_{sat} a$  (see equation 10.1) has been changed: from 0.95 to 0.91 for the 980801 event, from 0.90 to 0.89 for the 990720 event and from 0.89 to 0.86 for the 000829 event. Table 10.8 shows the results for the total discharge calibrations. For the 990720 event the total discharge calibration gave good predictions of both total discharge and total sediment yield. Sediment yield was, however, underpredicted for the 980801 and 000829 events. For all three events the total discharge calibrations underpredicted peak discharge. This shows that one has to perform a slightly different calibration depending on which objective one has with the model.

Table 10.8 Summary of the total discharge calibration results

Event	Q <sub>peak</sub> (l/s)		Q <sub>tot</sub> (m <sup>3</sup> )		Sediment yield (tonnes)	
	Sim.	Obs.	Sim.	Obs.	Sim.	Obs.
980801	3370	5125	4078	3982	746	1280
990720	2930	3589	3478	3282	762	770
000829	6733	8757	5735	5893	1269	2630

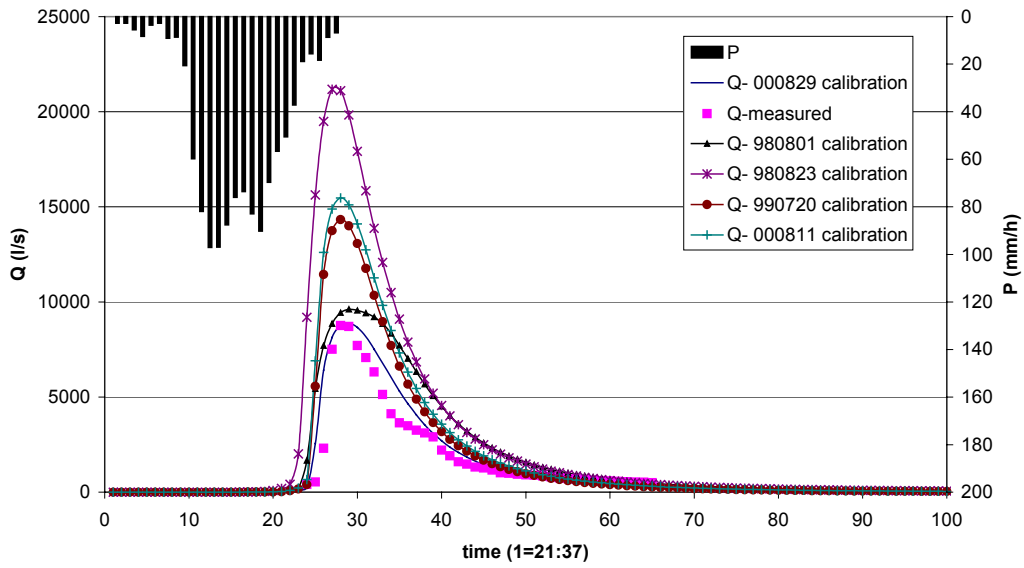


Figure 10.3 Validation results for the 000829 event. Data shown correspond to the fifth row of table 10.6

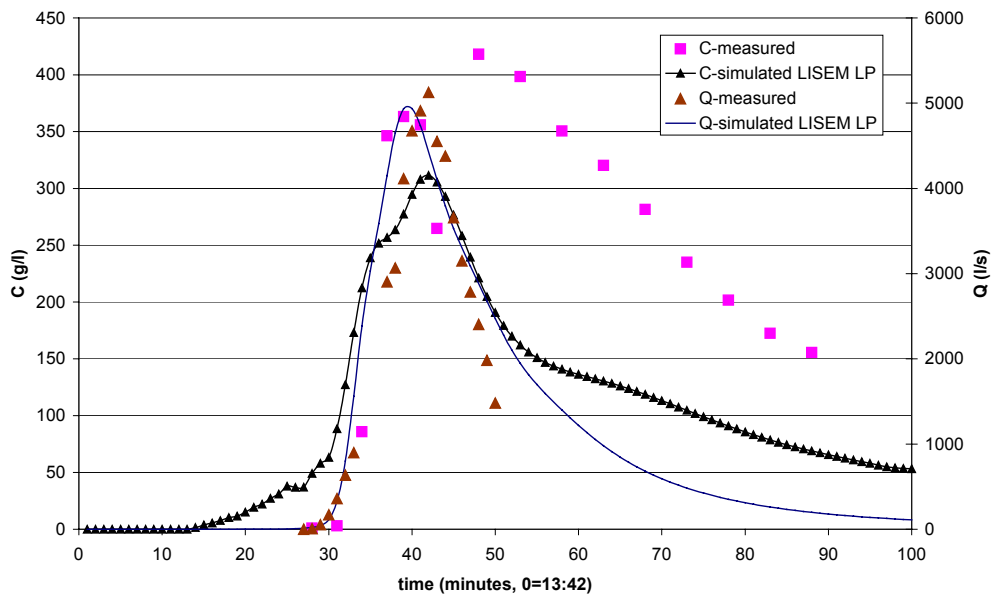


Figure 10.4 Simulated and measured concentration for the 980801 event

Table 10.9 Simulation summary

	980801	980823	990720	000811	000829
<i>Measured (table 10.2)</i>					
Peak discharge (l/s)	5125	701	3589	214	8757
Tot discharge (m <sup>3</sup> )	3982	735	3282	199	5893
Tot sediment yield (tonnes)	1280	96	770	16	2630
<i>Simulated (LISEM LP)</i>					
Peak discharge (l/s)	4967	591	3330	189	8886
Tot discharge (m <sup>3</sup> )	5918	1054	3931	361	7191
Tot sediment yield (tonnes)	1285	76	898	18	1784

### 10.2.6 Results soil loss calibration

Table 10.9 shows that even though total discharge was overpredicted for all events, soil loss was generally predicted reasonably well. Only for the 000829 event predicted soil loss was clearly too low. Since total discharge was overpredicted these results mean that concentration was underpredicted. Figure 10.4 shows that for the 980801 event simulated concentration was far too low during the later stages of the event, and slightly too low during the discharge peak. This results in a total soil loss that was almost correct, because during the later stages of the event predicted discharge was much higher than measured discharge. Together with the initial part of the runoff peak (where both predicted concentration and predicted discharge were higher than measured) this fully compensated for the lower soil loss simulated for the main part of the runoff peak. It would be better to simulate total runoff correctly and then calibrate on cohesion to obtain the correct concentration.

Cohesion, aggregate stability and median grainsize (D50) can be used to calibrate simulated soil loss once simulated discharge is satisfactory. These LISEM parameters only influence soil loss, not discharge. Cohesion influences flow detachment, aggregate stability splash detachment and D50 transport capacity and flow erosion. On catchment scale, splash erosion can usually be neglected, so that no calibration on aggregate stability was attempted.

To calibrate on cohesion two additional model runs were performed for the 000829 event: one with half cohesion and one with minimum cohesion. In the minimum cohesion run cohesion was set to 0.2 kPa, because LISEM requires that cohesion is larger than 0.196 kPa. The results for the 000829 event are shown in figure 10.5. It shows that simulated concentration only increased for discharges of over about 1500 l/s. This suggests that for lower discharges transport occurred at transport capacity anyway, while for higher discharges this was not the case. Furthermore, even for the minimum cohesion run simulated concentration was still too low on average. As a result the simulated soil loss was 2046 tonnes, compared to the 2630 tonnes that were observed. This relatively small effect was the sum of erosion and deposition amounts that both increased significantly.

These results show that calibrating on cohesion is not an effective way to change predicted sediment yield.

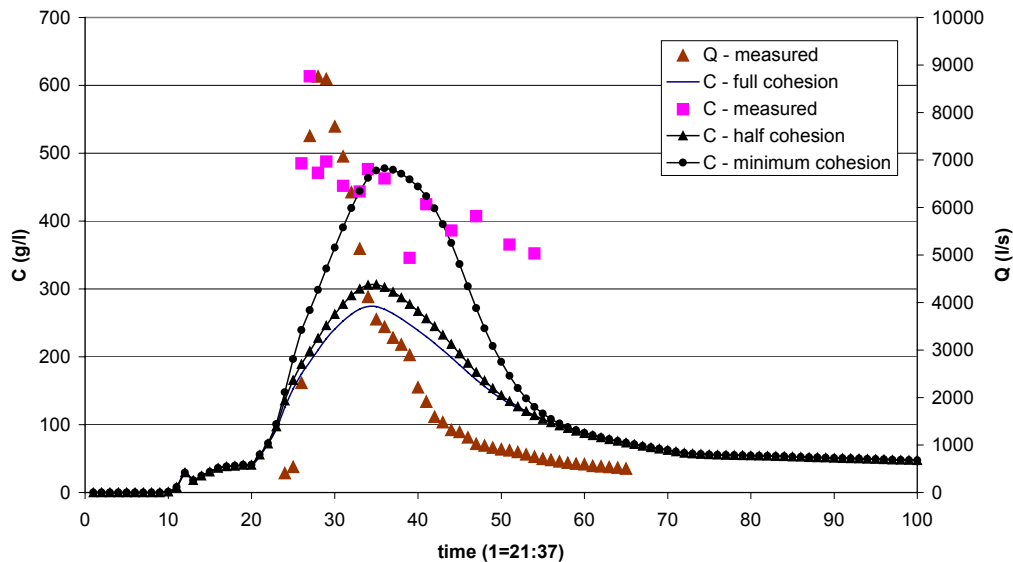


Figure 10.5 Simulated concentration for the 000829 event as function of cohesion

In LISEM, D50 influences both transport capacity (which decreases with increasing D50) and settling velocity (which increases with increasing D50). Several simulation runs were performed using different values of D50 for the 990720 event. The results (figure 10.6) show that LISEM is very sensitive to D50. Total simulated soil loss decreased from 1621 tonnes for D50 = 20  $\mu$ m to 695 tonnes for D50 = 50  $\mu$ m, while measured soil loss for this event was 770 tonnes (table 10.2). D50 would be a useful calibration parameter because the true value of D50 of the suspension is difficult to determine for several reasons:

- D50 of the material that is being transported is likely to be smaller than D50 of the parent material because the coarsest particles would settle first.
- D50 of the suspension is not easy to determine because it is likely to vary over water depth. Since most water samples were taken from the water surface (chapter 4) it can be expected that average D50 of the suspension is higher than that of the sediment sampled.
- D50 can vary in time. Figure 10.7, for example, shows that in the Danangou catchment there is a clear relationship between D50 and discharge. D50 was determined by laserdiffraction on surface samples taken at the weir during all 5 events that occurred.
- D50 of the suspension is likely to vary spatially since the different lithologies of the Danangou catchment have different D50s (chapter 4). Therefore, figure 10.7 is only valid for the weir.

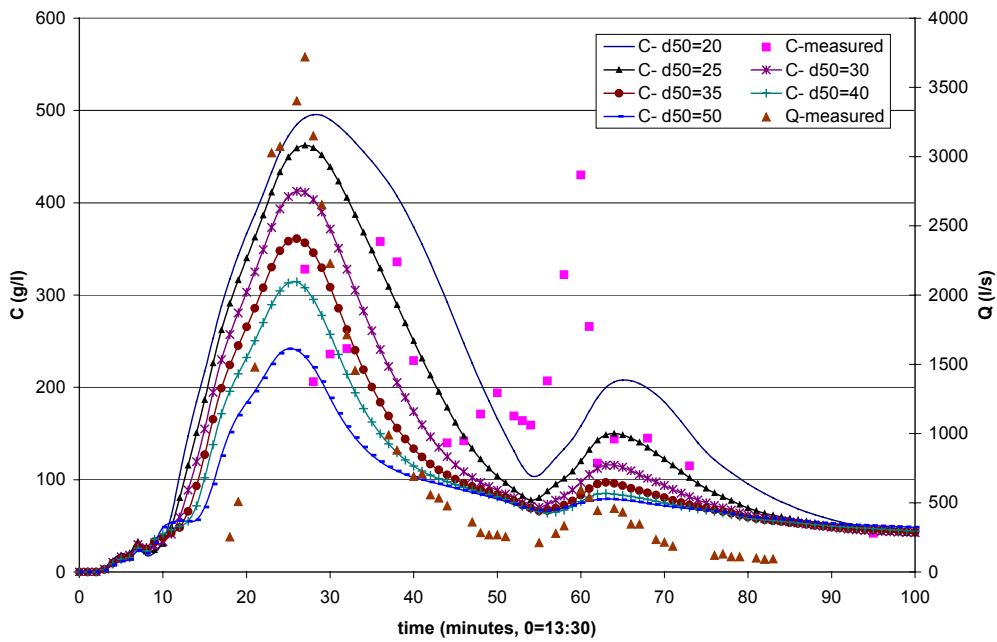


Figure 10.6 simulated concentration for different values of D50, 990720 event

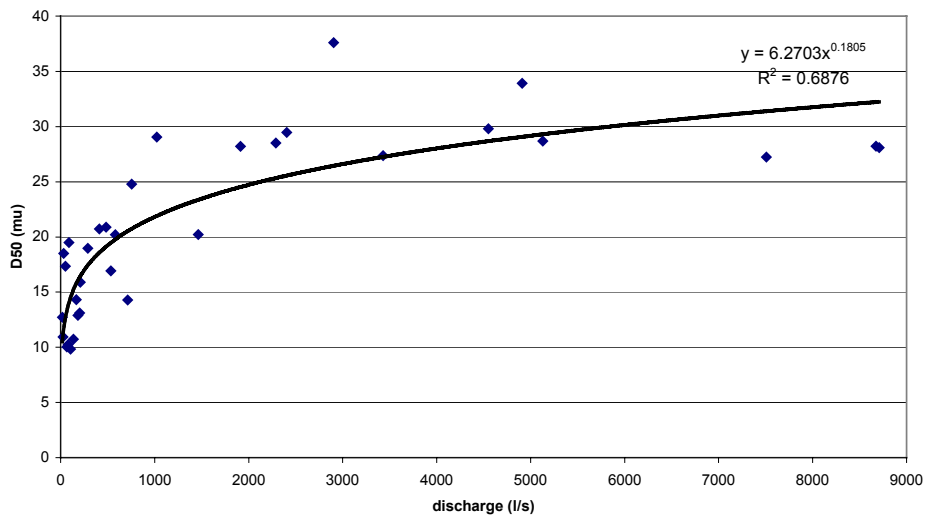


Figure 10.7 Relationship between D50 of the suspension and clear water discharge, all 5 events combined

The effect of calibrating on cohesion was found to be much smaller than that of calibrating on D50. It must be noted, however, that the effect of choice of transport equation (chapter 7) on simulated soil loss is also large. For the 000829 event correct sediment yield could not be simulated by calibrating on cohesion. Table 7.4, however, shows that the measured sediment yield could be reached without any cohesion



calibration by choosing another transport equation, e.g. the Govers & Power equation. Likewise, by using a D50 of 25 instead of 35 simulated total soil loss increased to 2318 tonnes.

### *10.2.7 Discussion*

The results presented for the peak discharge calibration show that LISEM cannot be calibrated for small storms, but that it can be calibrated for large storms. Several authors (e.g. Nearing, 1998, Jetten et al., in press) also found that erosion models have difficulty predicting small events. They ascribed this to spatial variability and uncertainty in the input data. In this study, it was found that different calibrations for all events are preferable. The problem with small storms in the Danangou catchment is probably caused by several factors:

- 1) For smaller storms it is much more important to get the initial conditions right. For large storms, a smaller or larger initial loss probably does not matter much for the total amount of runoff, while for small storms it might be a large percentage of total runoff.
- 2) The rainfall data suggest that during both the 980823 and 000811 events there was localized heavy rain in the catchment. One or two rain gauges received a lot of rain, while most received little. Thus, there was large spatial variability of rainfall. This caused the large difference in catchment-averaged maximum rainfall intensity and maximum intensity at a single gauge (table 4.2). Thus, the water reaching the dam came from a restricted part of the catchment. The time difference between measured rainfall peak and measured discharge peak suggests that the water originated far from the weir. In principle, LISEM should be able to deal with this. However, since the runoff-causing rain was very localized there is no guarantee that the maximum rainfall intensities and amounts were measured, nor is it likely that the spatial rainfall distribution used in LISEM represented the actual distribution. Chapter 4 showed that for discharge generation in the Danangou catchment rainfall intensity is crucial. Thus, if the rain gauges missed the maximum intensity it is likely that the LISEM model cannot reproduce the measured discharge.
- 3) If the runoff was caused by heavy rainfall occurring in part of the catchment only, it is also crucial to get the other input data, including initial conditions, for this region right. For both the events of 980823 and 000811, this region was the heavily gullied northern part of the catchment. Most LISEM parameters were not measured there, but were extrapolated from elsewhere. Thus, it is possible that some of these extrapolated values were not representative for this area because of large-scale spatial variations of soil characteristics.
- 4) Finally, the largest valley in the northern part of the catchment drains into the main stream through a long and tortuous channel with many storage possibilities (pools) on the way. Not only might there be storage, but also the flow length could be larger than determined from the DEM, while besides small errors in e.g. Manning's  $n$  of the stream could result in changed arrival times of discharge at the weir.

A combination of these factors might explain why the peak discharge occurs so long after the rainfall peak for the smaller events (table 10.2). Our finding that a separate calibration is necessary for small and for large events means that one should be cautious when applying the LISEM model to predict runoff for future events. Such predictions might be possible when these events would be similar in size to the ones used here. Even then, initial conditions might well be different, so that it would probably be necessary to do simulations with different initial moisture contents. The bigger an event is, the smaller the effect of these initial conditions should be. At present LISEM might be more suited to evaluate certain land use and management scenarios for their effects on erosion, since in that case all scenarios will use the same rainfall data and the same initial conditions.

The validation results showed that in certain cases different calibration settings gave almost equal results, which is called equifinality. Furthermore, the calibration results showed that a slightly different calibration was needed for peak discharge simulation and for total discharge simulation. Calibration of peak discharge, calibration of total discharge and calibration of soil loss can be seen as different objectives of the calibration process. As Madsen et al. (2002) stated it is important to recognise that calibration results might be non-unique, i.e. that different sets of calibration parameters might give equally good predictions for a certain calibration objective, and that different equally good trade-offs might exist between the different calibration objectives. In their view, this makes it necessary to attach priorities to certain objectives of the calibration process, such as the correct simulation of peak discharge or the correct simulation of total discharge and erosion. How these priorities should be set up will depend on the model application being considered.

### **10.3 Additional events**

In section 10.2, LISEM was validated by applying calibrated versions of the model to other events for which runoff data were available. LISEM was also applied to six storms for which no quantitative runoff data were available. This was done for two reasons:

- 1) To find out if LISEM can simulate probable discharge when a single calibration set is applied to different events. Since only qualitative runoff data are available for these storms simulated discharge will be somewhat speculative.
- 2) To obtain estimates of sediment yield for these 6 events. These estimates were needed to develop a sediment balance for the catchment (section 8.5).

A large event occurred on 980715, but no runoff data were available because of malfunction of equipment. A small event is known to have occurred on 990721. The rainfall data also suggest that additional runoff events might have occurred on 980705 and 980712. Finally, two rainfall events (990710 and 000807) that are known not to have produced runoff were also simulated. In both cases observations at the weir showed that water level remained well below the detection limit of the ultrasonic water level sensor. This limit corresponds to about 100 l/s. Table 4.2 shows the rainfall data for all these events. Table 10.10 shows the correction factors that were applied to the initial moisture content predicted with the equations given in table 10.1.

The 1998 storms were simulated with the calibrated LISEM LP model of the 980801 event. The only difference is that a value of  $a$  (equation 10.1) of 0.90 was used instead of 0.95. The 980801 event was chosen because it occurred in the same year (hence the land use map is the same), the use of 0.90 instead of 0.95 makes the simulations a little more conservative. In practice this means that the actual discharge might have been higher, but almost certainly not lower. Therefore, if discharge is predicted for these events it is almost certain that discharge actually occurred, though the discharge amount might have been higher in reality. The 1999 and 2000 storms also simulated with  $a = 0.90$ , but used calibration settings of the event of July 20<sup>th</sup>, 1999. The results of the simulations are shown in figure 10.8 and are also summarised in table 10.11.

Table 10.10 correction factors for prediction of initial moisture content

Event	Depth (cm)				
	5	15	25	45	70
980705	0.82	0.71	0.76	0.88	0.98
980712	1.33	1.29	1.13	1.02	0.95
980715	1.33	1.29	1.13	1.02	0.95
990710	1.44	1.38	1.03	0.82	0.68
990721	2.00	2.00	2.00	1.00	1.00
000807	1.44	1.38	1.03	0.82	0.68

Table 10.11 Result for additional storms

	980705	980712	980715	990710	990721	000807
Average P (mm)	20.7	23.2	30.5	9.6	4.2	18.4
Max 1-min intensity (mm/h)	41.3	59.4	66.2	67.7	35.8	18.2
Qp simulated (l/s)	112	2165	8277	25.7	2.1	7.2
Qtot simulated (m3)	366	4320	13927	104	2.7	90.0
Soil loss simulated (tonnes)	18.4	572	2880	3.3	0.02	2.6

From figure 10.8 a number of observations can be made. First, it confirms that runoff events occurred on July 5<sup>th</sup>, July 12<sup>th</sup> and July 15<sup>th</sup> 1998. The amount of runoff was probably small on July 5<sup>th</sup>, since the predicted peak discharge is only 112 l/s. On the other hand, when a different value of  $a$  is used runoff might be much larger. Table 10.7, for example, shows that simulating the storm of August 23<sup>rd</sup>, 1998 with an  $a$  of 0.90 (990720 calibration) gave only 13 l/s, while observed discharge was 701 l/s. The predicted hydrograph clearly had 2 peaks for the 980705 event, even though rainfall did not. Apparently water originating from different parts of the catchment did not arrive at the

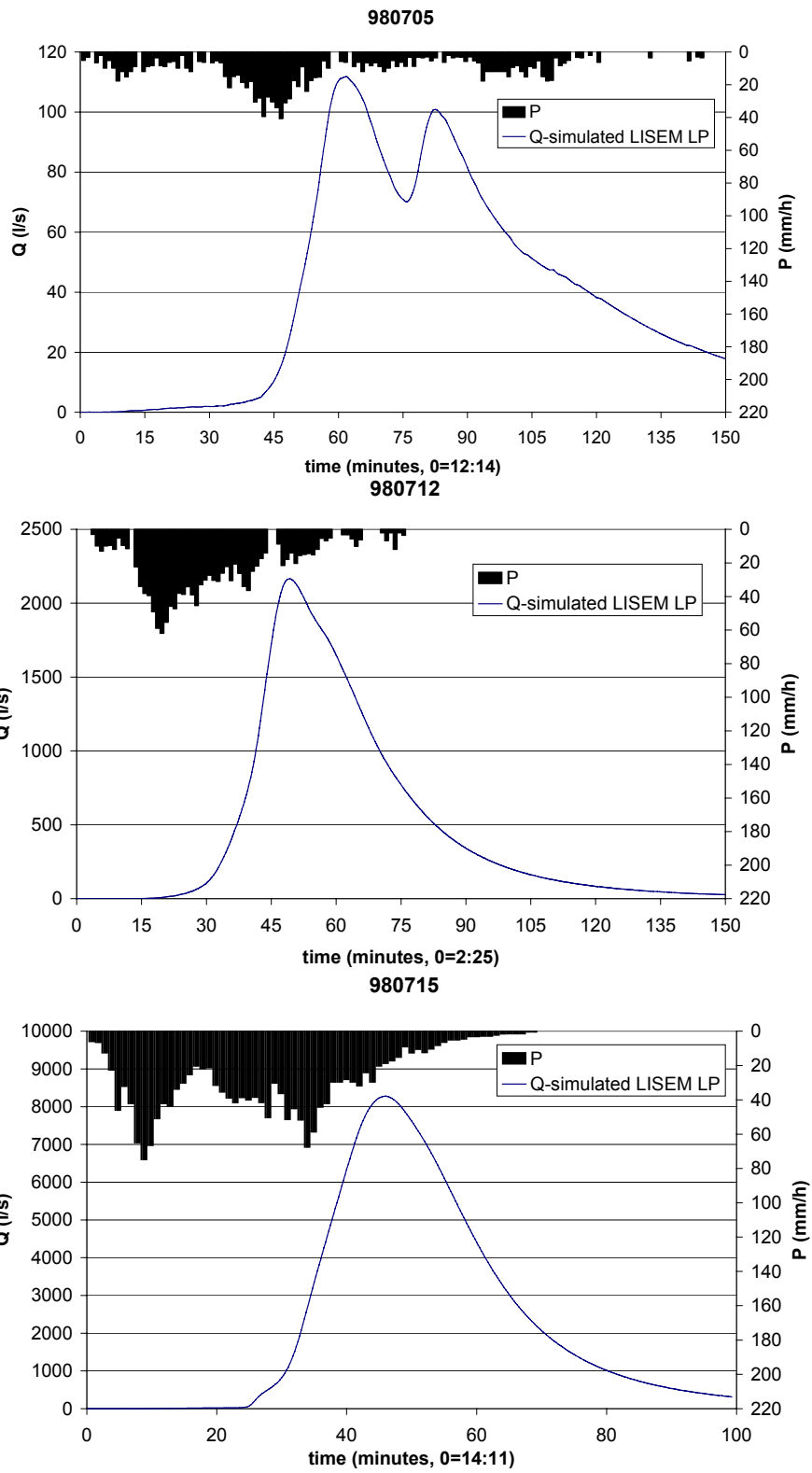


Figure 10.8 Observed rainfall and simulated discharge for six events

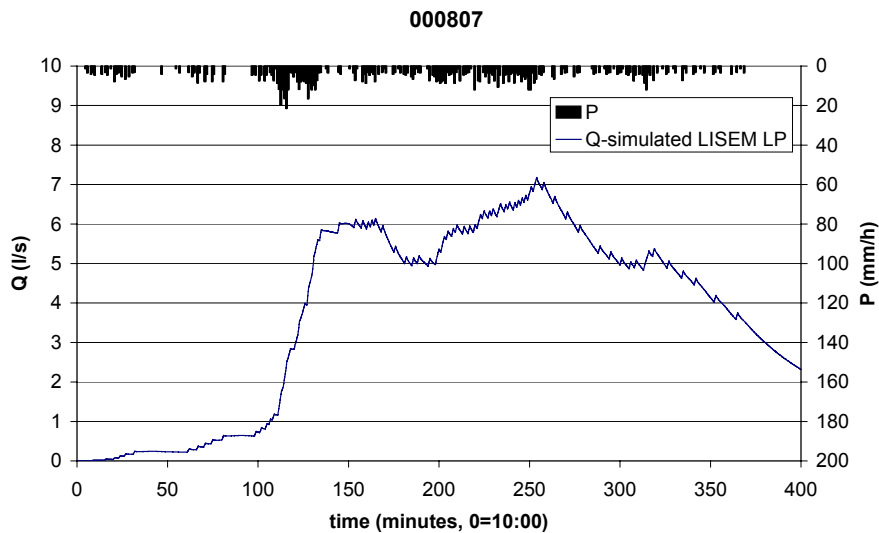
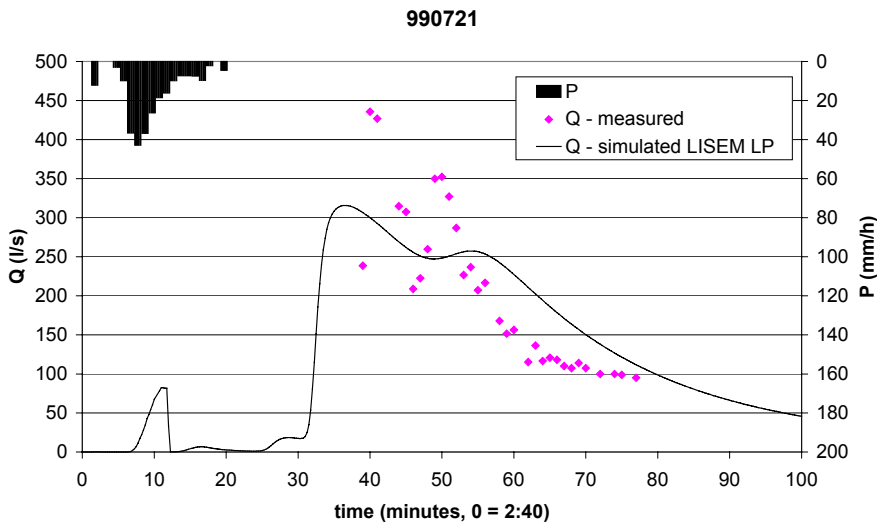
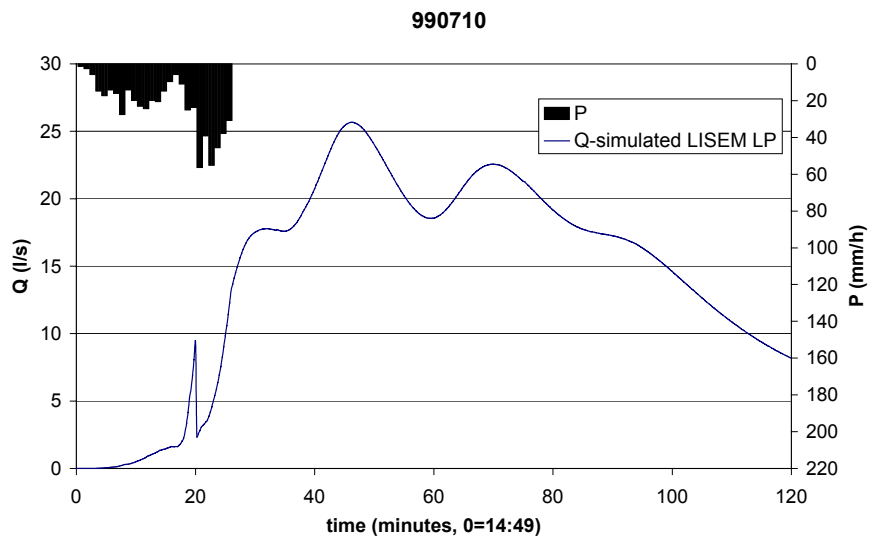


Figure 10.8 (continued)

weir simultaneously. The simulated discharge peak for the event of July 15<sup>th</sup>, 1998 was over 8000 l/s. During this event the initial supporting construction for the ultrasonic sensor was destroyed, while the dam was also undermined and had to be restored afterwards. After the event the maximum water level was estimated to have been approximately 1.4 metres. Using equation 4.7 this would give a peak discharge of 15000 l/s. Assuming a concentration of 400 g/l and using equation 5.16 the clear water discharge would have been about 13000 l/s. In view of the large uncertainties in estimated clear water discharge the prediction of 8277 l/s is very reasonable. The peak discharge was thus comparable to that of the 000829 event, which had much higher rainfall intensities but much shorter duration. The total runoff during the 980715 event was, however, much larger (tables 10.11 and 10.2). It is also interesting to see that LISEM predicted a single discharge peak for this 2-peaked rainfall event.

A second observation is that for those events for which qualitative field data showed that there was no significant runoff, no significant runoff was predicted by LISEM either. The predicted maximum runoff rate for the high-intensity event of July 10<sup>th</sup>, 1999 was about 26 l/s. Field observations during the event showed that there was some discharge at the weir, but that it remained well below the lower limit of the ultrasonic water level sensor (about 100 l/s). The predicted runoff was therefore reasonable. Hardly any runoff was simulated for the prolonged low-intensity rain of August 7<sup>th</sup>, 2000. Observations in the field indicated that there was some discharge at the dam, but that it remained far below the minimum level that can be recorded by the ultrasonic water level sensor. The simulation therefore gave reasonable results. The importance of rainfall intensity in runoff production was shown by the fact that the 990710 event had a clearly higher peak discharge than the 000807 event.

Finally, for the event of 990721 hardly any runoff was predicted (table 10.11), despite the fact that the correction factors (Table 10.10) were chosen to take into account the very wet soil conditions during the event. After calibration (initial suction = 0.45 times original,  $K_{sat} a = 0.97$ ) simulated discharge better matched measured discharge (figure 10.8).

### *Discussion*

LISEM produced results that were consistent with the qualitative data available for 5 out of 6 storms that were not used for calibration. Thus, LISEM produced reasonable results for events for which no runoff data were available, so that no calibration was possible. As shown in section 10.2 it is unlikely that the simulation results for these rainfall events match real runoff that occurred. The results for the 990721 event confirmed this.

Nevertheless, LISEM is able to indicate whether or not an event occurred and also if it was a large event or not, at least if the soil was not extremely wet prior to the event. Thus, the model might also be used to predict whether or not a runoff event will occur given a certain rainfall event.

## 10.4 Erosion pattern evaluation

### 10.4.1 Materials and method

At the end of each rainy season (September) the occurrence and intensity of rilling was mapped throughout the 3.5 km<sup>2</sup> catchment. Rill intensity was classified in 3 classes: slight rill erosion, moderate rill erosion and severe rill erosion. Quantification of the amount of erosion for each class was possible due to a number of measurements of rill frequency, width and depth that were conducted for each rill erosion class (see section 4.5). For most years such mapping will give an aggregated result for all events, but in 1999 only a single rill-producing event occurred so that the rill erosion map made in that year can be used directly to evaluate the performance of LISEM for the 990720 event. The 990721 event can be neglected since it was too small to produce rills.

A single erosion plot (Figure 4.9) was installed in 1999 to determine the amount of erosion occurring in arable fields. The plot is assumed to be representative for the cropland area in the Danangou catchment. Its dimensions were about 34\*6.5 meters, while slope angles ranged from 15% at the top to 55% at the bottom. At the plot, the total amount of water and sediment was measured on an event basis using a divisor and barrels. All runoff from the plot was collected in a gutter that drained into the first barrel. If the first barrel was full, 1/11 of the surplus water flowed into the second barrel. Water levels in the barrels were always measured on the day after the rain event, and samples were taken from the barrels to determine sediment concentration. Sediment accumulated in gutter and flume was also taken into account. Since rill measurements were also conducted on the plot it was possible to calculate the total sheet erosion by subtracting rill erosion from total plot erosion. Often the fields that are located on the hilltops are convex with a slight concavity in the lower part of the field. For practical reasons the erosion plot could not end at the lower boundary of the field. It can therefore be assumed that part of the material collected at the plot outlet would redeposit before leaving the field, so that introduction of a sediment delivery ratio for the sheet erosion was necessary.

Using the data from the sediment plot an estimate of the sheet erosion was obtained. This estimate is expressed as an amount of erosion per unit area of cropland. The rill erosion mapping also gave an amount of erosion per unit area. Therefore, a field erosion intensity map could be made by combining the two maps. The resulting map was then compared with the erosion map produced by the LISEM model.

### 10.4.2 Results

A minor event that occurred at the sediment plot on July 21<sup>st</sup>, 1999 was used to derive a sheet erosion rate on event basis. The sediment plot is in the western part of the catchment, so that rainfall during the 990720 event was only 3 mm and no runoff occurred on that day. The minor storm of 990721 did not result in any rill-formation on the sediment plot. Nevertheless, the sediment concentration as determined from the barrels at the bottom of the plot was in excess of 700 g/l, resulting in a sheet erosion rate of 836 tonnes/km<sup>2</sup> (8.4 tonnes/ha). The sediment delivery ratio of the fields was assumed

0.3. This gives erosion rates (on event basis) of 251 tonnes/km<sup>2</sup> for croplands that do not show evidence of rill erosion.

Table 10.12 Average observed rill erosion rates (with sheet erosion rates added) and approximate boundaries between classes of rill erosion severity, 1999 data. The performance of LISEM for the different classes is also shown

Erosion class	Erosion rate (tonnes/km <sup>2</sup> )	Class boundaries (tonnes/km <sup>2</sup> )	Correctly predicted by LISEM (% of observed class area)
No rill erosion	251	0 – 800	51
Slight rill erosion	1450	800 – 3000	25
Moderate rill erosion	4822	3000 – 8000	21
Severe rill erosion	17195	above 8000	14

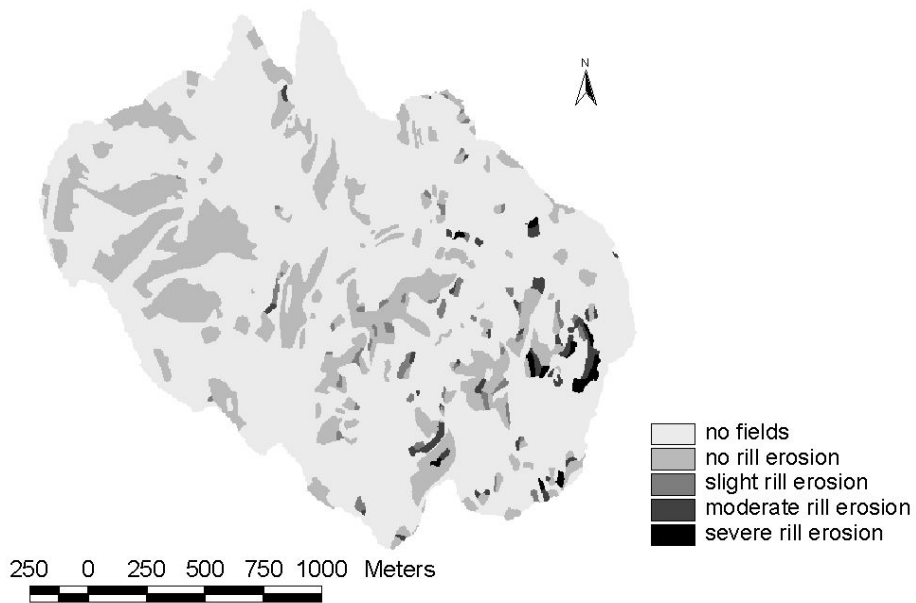
Table 10.12 shows the average erosion rates obtained from the erosion plot data as well as the rill measurements on the fields. The erosion rate for the ‘no rill erosion’ class is thus a single event estimate based on sediment plot data, while the other rates are based on rill mapping. The sheet erosion rate was also added to the rill-based measurements of the other classes. Since only one event produced rills in 1999, all these rills must have formed on July 20<sup>th</sup>. The resulting 1999 rill erosion map is shown in figure 10.9a.

LISEM produces maps of erosion and deposition rates in tonnes/ha. By using the range of measured rill erosion rates for each rill erosion class (table 10.12) one can classify the LISEM output map. Since the field mapping only involved erosion and not deposition, it would appear logical to use the LISEM erosion map only. Erosion and deposition, however, cannot be treated as separate entities in LISEM simulations; deposition and re-entrainment can occur during the simulation. Thus, the same sediment can be eroded several times and be deposited several times. This provides an explanation for the very large predicted erosion and deposition amounts (e.g. table 10.13) and also for the fact that such large amounts have not been observed in the field. Therefore, the net erosion map should be used to assess the performance of the LISEM model in a spatial way. The result should be judged more on patterns than on amounts because during mapping deposition was ignored. The net erosion map was also classified using the values given in table 10.12 and is shown in figure 10.9b. Since the rill erosion map (figure 10.9a) only shows erosion on fields, only the cropland areas were used for classification of the LISEM net erosion map.

Comparing the maps in figure 10.9 it is obvious that both maps have the highest erosion rates in the southeastern part of the catchment. This is also in agreement with the observed distribution of rainfall on 990720, since there was a strong spatial trend in rainfall from east (30mm) to west (3mm). This lack of heavy rain in the western part of the catchment is probably the reason why the LISEM prediction for the ‘no rill erosion’ class is much better than for the other classes (table 10.12). Closer inspection of figure 10.9 shows that though the overall pattern was similar, the pattern in detail was very



A) Rill erosion mapping



B) Lisem simulation

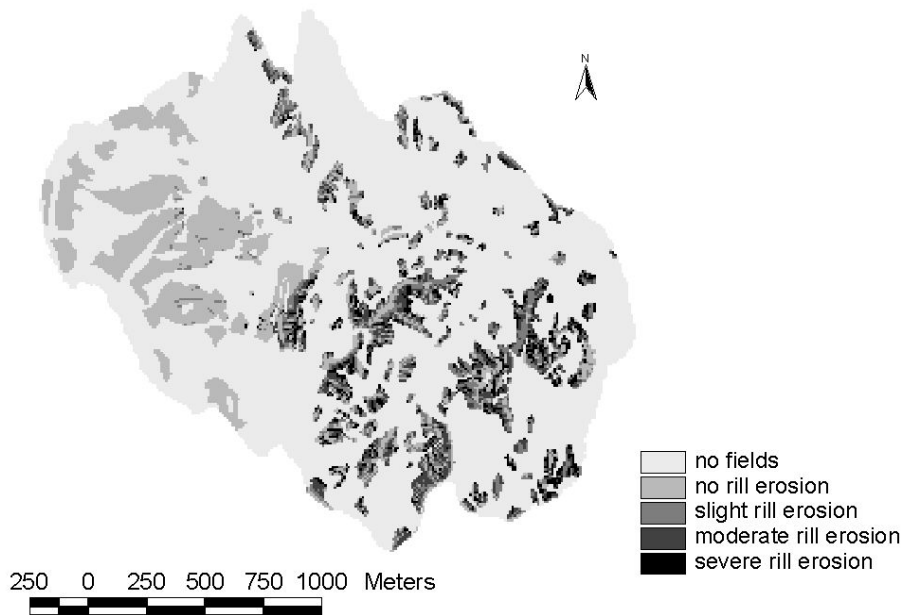


Figure 10.9 A) Mapped rill erosion of 1999. Pixel size is 5 meter. B) LISEM simulation results for the 990720 event. This map gives a classified map of the net erosion (erosion-deposition). Pixel size is 10 meter. For both maps the classification scheme given in table 10.12 was used

different. This is also reflected by the data given in table 10.12, which show that for the classes with more severe rill erosion, only about 20% of the observed area for that particular class is predicted correctly.

The simulated erosion and deposition for different land uses are given in table 10.13. Table 10.13 shows that according to the simulations the major sediment sources were cropland and fallow land, while the major sink was wasteland. According to the simulation sediment yield from cropland was 1991 tonnes, while according to the rill erosion mapping the total amount of field erosion was 805 tonnes. Field observations did not indicate large erosion amounts on fallow land. Table 10.13 also shows that 5263 tonnes of sediment were deposited in the valleys, which is over 60% of all sediment entering them. According to the table, most deposition occurred in valleys with wasteland. Such very high deposition rates have never been observed in the Danangou catchment, thus the erosion rates must also be too high (as the model is calibrated on total sediment yield). Both figure 10.9 and table 10.13 therefore suggest that LISEM did not simulate the sediment sources correctly. Summarizing, LISEM over-predicted the erosion for most land uses (including croplands) and compensated this with too much deposition in the valleys. It might be possible to change this by calibrating on cohesion in such a way that total sediment yield remains the same but the distribution of erosion changes.

Table 10.13 Distribution of erosion (tonnes) according to LISEM simulation. Negative sign indicates deposition. Here, all pixels with an upstream area of more than 1 ha are assumed valleys

Land use, % of catchment occupied	erosion	deposition	yield	yield to valleys	erosion/ depo. in valleys
Crop (28%)	3380	-1389	1991	1950	41
Orchard (1%)	24	-29	-5	-2	-3
Woodland (9%)	231	-921	-690	-308	-382
Wasteland (40%)	7301	-8632	-1331	3387	-4718
Vegetables (1%)	51	-21	30	17	13
Fallow (21 %)	4042	-679	3363	3577	-214
<b>Total</b>	<b>15028</b>	<b>-11670</b>	<b>3358</b>	<b>8621</b>	<b>-5263</b>

#### 10.4.3 Discussion

Many explanations are possible for the discrepancy between observed and simulated erosion rates and patterns inside the catchment (see e.g. the discussion by Takken et al. 1999). For the topographically complex Danangou catchment the following factors are likely to be important:

- DEM inaccuracy. This is one of the most obvious reasons and probably one of the most important ones since the flow direction as used in the model is derived from the DEM. The flow direction, in turn, determines where erosion will occur

according to the model. On relatively flat areas, the tillage direction can determine the direction of water flow (Ludwig et al., 1996, Takken et al., 1999 and Van Dijk, 2000), and slope determined from the DEM is than more or less irrelevant (except were furrows overflow). The tillage direction problem is unlikely to be important for steep terrain such as the Danangou catchment. Nevertheless, also in steep terrain, the flow direction is not determined by the average slope of a pixel-sized piece of land. The Danangou DEM (figure 3.1) was derived from a topographical map with contour line interval of 5 meter (total relief is 300 m) and the 10-meter pixel size that was used is therefore very 'reasonable' to accurately depict the variations in relief of a 3.5 km<sup>2</sup> catchment. Nevertheless, such a DEM can only provide average slope directions and cannot contain information about much smaller topographic features (like furrows, pathways, gullies, cut-off drains, local escarpments) with dimensions in the order of several metres or less, which determine the direction of water flow in reality. For topographically complex areas such as the Danangou catchment, it is in reality impossible to obtain a DEM with sufficient detail to extract flow directions accurately. For topographically less complex areas it might be possible by mapping topography and flow direction with the use of surveying techniques.

- Limitations of LISEM. The pixel-based approach used in LISEM has some consequences for the calculation process. The most important are related to inertia and to exceedance of thresholds. Both problems are generally more pronounced where there is more water, hence in the channels. Often the net erosion map shows an alternation of pixels with high erosion rates and pixels with high deposition rates. There is apparently not enough inertia in the model. An example: velocity and stream power are calculated for each pixel separately. This means that in the simulation much more abrupt changes of velocity and stream power can occur than in reality, because in reality the flow will keep part of its velocity and stream power when it for example enters a reach with lower gradient. In the model, this can result in high sedimentation rates, which in reality will not be the case. The effect of the sedimentation is that the water loses much of its sediment and can therefore cause large erosion rates just downstream. Another cause for this might be that erosion and deposition occur when a certain threshold was exceeded. The problem with this is that such a threshold might be exceeded continuously for certain pixels because the factors that cause the exceedance do not change during simulation, while in reality they do change. Both factors mainly influence the distribution of erosion and might have little influence on total sediment yield. These effects are more pronounced for topographically complex areas with strong alternations in slope angle and are at least partly caused by the grid-based approach itself. They can therefore be only partly solved by changing computation procedures.
- Incomplete or incorrect process descriptions. The issue of steep slopes, for example, was discussed in previous chapters. All currently available erosion models use sediment transport equations that have been developed for slopes of no more than 20%. Much steeper slopes are, however, very common in the

Danangou catchment. Similarly, other characteristics of the catchment might also be outside the range of conditions for which equations that are being used were developed. Besides, process knowledge is usually incomplete. When simulation errors appear to be systematic there might be incomplete process descriptions in LISEM. The fact that the discharge peak always seems to arrive too early might for example indicate this. Incomplete and incorrect process descriptions might affect both distribution and amount of erosion. As Beven (2001) points out, such errors in theory might be masked by calibration and can therefore be hard to find.

- **Data inaccuracy.** There can be inaccuracies in the data used to evaluate model performance as well as in the input data for the model. Morgan & Quinton (2001) suggested that such inaccuracies are a more important cause of incorrect model predictions than model flaws. Inaccuracies in the data used for evaluation can stem from two sources. The first is the estimation of sheet erosion by using the sediment plot data, for example by choosing a sediment delivery ratio. This might affect amount of erosion, but not pattern. The second is mapping inaccuracy and might affect mapped patterns, e.g. because mapping is done by classifying parts of fields and not on a pixel-by-pixel basis. Inaccuracies in input data can be caused by several factors. The first is incorrect measurements. For example, erosion in our simulation seems to be mainly determined by slope angle and less by differences in land use. This might reflect reality, but might also be caused by the fact that cohesion does not seem to change much from one land use to the next (table 10.4). Inaccuracies can also be caused by non-representative measurements. Input data for the LISEM model were collected on fields that were supposed to be representative of their respective land uses. Finally, some parameters (e.g. soil moisture content) are liable to rapid fluctuations, while others (e.g. saturated conductivity) are notoriously heterogeneous in space. Simulation results also indicated that the rainfall distribution has large influence on simulated runoff and erosion. This is a fundamental problem with distributed modelling; it is impossible to accurately represent existing spatial patterns for all variables. Nowadays, distributed models can contain several tens of thousands of pixels for which the different calculations are performed. Data on saturated conductivity, soil roughness, plant characteristics etc. are needed for all these pixels. Furthermore, even if such data were available one can for reasons of spatial variability and up-scaling seriously question if the used values are indeed representative for the given pixel. It seems likely that the actual amount of runoff and erosion occurring is controlled by many variations in parameters operating on sub-grid scale. One has to face reality: At present it is impossible to collect enough input data, nor is this likely to be possible in the foreseeable future.

Often, a combination of factors could be operating, so that it will be difficult to find out what exactly causes an observed discrepancy between simulation and measurement. For example, the data that are available are still not good enough to decide whether incorrect predictions are due to incorrect models or incorrect data. Obtaining data that are more accurate (such as a better cohesion map) could in principle solve some of the problems mentioned above. In practice, however, this can be very difficult. To evaluate the LISEM

model (or any other process based, distributed erosion model) in a spatial way, very detailed data both on model input and on erosion and deposition patterns distribution are needed. Such data-sets are very hard to obtain for catchment -size areas, especially when topography is complex. It seems therefore unrealistic to aim at a pixel-by-pixel comparison of simulated and measured erosion. Data for the catchment outlet are easier to obtain, so that calibration on the outlet alone will often be the only possibility. Our data, however, confirm the findings of Takken et al. (1999) that an erosion model calibrated on outlet-data might well predict spatial patterns incorrectly. Furthermore, even if the necessary data for spatial evaluation were available there is no guarantee that simulated erosion patterns will match observed erosion patterns. This is because errors in model theory or structure as well as problems caused by the grid-based approach itself can also result in incorrectly simulated erosion patterns. These problems can probably never be solved completely for complex catchments. For such areas, process-based distributed erosion models can help increase our understanding of erosion, but they might never be able to accurately predict erosion distribution.

## 10.5 Conclusions

Calibration of the LISEM soil erosion model for the Danangou catchment showed that the LISEM model can simulate runoff and soil loss from the catchment. However, it was not possible to find a general calibration set that could be used for all measured events. In fact, each storm had to be calibrated separately to obtain acceptable results. Validation indicated that it might be possible to find calibration sets for low-magnitude and high-magnitude events when more storms would be available. LISEM gave the worst results for small events with low average rainfall intensity. These events had large response times, indicating that only part of the catchment was active and that the water was generated relatively far from the weir. Such events can only be modelled when high quality data are available on the spatial distribution of soil parameters and rainfall. These results indicate that the usefulness of LISEM for predictive purposes is limited to events that are large enough to cover the entire catchment. Application of LISEM to a number of rainfall events for which no runoff data were available showed that reasonable results were obtained for those events. Even though LISEM cannot be expected to predict actual runoff amounts it might be able to predict whether or not an event will occur.

Rill erosion intensity was mapped in the field and compared with LISEM simulations of erosion distribution. This comparison shows that the general appearance of simulated and mapped erosion patterns is similar, but also that the patterns are very different in detail. Many causes for this are possible, but it appears that:

- Current process descriptions are not well suited to simulate erosion processes on steep slopes.
- The raster-based approach of LISEM has the advantage to produce detailed erosion patterns, but the disadvantage that abrupt changes in flow conditions give unrealistic results.

- At present the datasets of model input and erosion patterns are not good enough for complex catchments. Especially inaccuracies in input data and the DEM are likely to be important.

The evaluation of catchment soil loss and spatial erosion patterns as simulated by LISEM shows that there are severe limitations in applying such a model to the Chinese Loess Plateau, especially with respect to predicting erosion patterns and future events. Simulation of different land use scenarios might be less problematic if a known event of sufficient size is used for all simulations. Even so, scenario predictions should be done with extreme care and should take into account the factors described above.

## 11 LAND USE SCENARIOS

*Partly based on: Hessel, R., Messing, I., Chen Liding, Ritsema, C.J. & Stolte, J. (in press) Soil erosion simulations of land use scenarios for a small Loess Plateau catchment. Catena.*

### 11.1 Introduction

Soil erosion on the Chinese Loess Plateau is a major problem because on-site it causes loss of arable land, while off-site it can cause silting up of rivers and reservoirs. In 1999, the Chinese government, aided by the Chinese Academy of Sciences (CAS), formulated new ambitious policies about the Loess Plateau. These policies aim to decrease erosion rates through changes in land use. In particular, they aim at a large decrease in cropland area so that all fields on slopes above a certain slope degree should be changed from cropland to other uses. The decrease in cropland should be accompanied by an intensification of the remaining cropland and by an increase in woodland, shrubland and orchards (cash trees). The idea is that in the long term the income of the farmers should increase once they get better yields from the remaining cropland as well as income from fruit trees and other cash trees. Since it takes time before the new land use can start to benefit the farmers, the government is considering paying compensation to the farmers to make the change economically feasible for them.

Not only land use, but also land management influences soil erosion. For China, the number of studies that quantifies these effects is small, although some studies have been conducted on small plots. Shaozhong Kang et al. (2001) studied the effect of different management techniques on runoff and soil erosion for erosion plots in two catchments on the Loess Plateau. They found that erosion rates decreased from bare soil to soil with plant residue to maize. Decreasing slope length was also effective in reducing erosion rates. Erosion rates increased with increasing slope angle, but for very large storms this was no longer the case. Both runoff and erosion were highly correlated with maximum 5-minute interval rain intensity. Gong Shiyang & Jiang Deqi (1979) reported that reforestation and planting grasses had similar effect for small rains, but that planting grasses was less effective for heavy rain. Terracing was found to be more effective than reforestation and was also found to significantly increase crop growth.

The objective of the present study was to evaluate the effects of different land use scenarios on soil erosion in a small catchment on the Loess Plateau in China. The scenarios that were used in the present chapter were developed based on a biophysical resource inventory, farmer's perception and the plans of the authorities on greening the Loess Plateau. The scenarios not only specify land use, but also take into account several kinds of soil and water conservation measures.

To evaluate the effects of the different land use scenarios, the LISEM soil erosion model (de Roo et al., 1996a, Jetten and De Roo, 2001) was applied. LISEM is a process based distributed erosion model that operates on storm basis. Although it has been shown

repeatedly (e.g. Jetten et al., 1999) that such models might not be able to accurately predict future events they may be used to simulate different land use scenarios. In the case of scenarios, the same uncertainty in input data applies to all scenarios and one can therefore assume that the differences produced for the different simulations are in fact a consequence of the applied scenario changes.

## 11.2 Methods

Both arable land and gullies seem to be major sources of sediment during storms (chapter 8). One of the criteria used in selecting the Danangou catchment for research was the fact that up until now the amount of soil conservation measures in the catchment was limited. This allowed us to compare simulation results with a no-conservation situation (the present situation). The farmers are, however, well aware of the erosion problem and are willing to use more conservation measures, but they have so far been unable to do so for financial reasons (Hoang Fagerström et al., in press).

### 11.2.1 Land use

Soil physical properties that are needed for simulation could only be measured for a few land uses: cropland, orchard/cash tree, woodland/shrubland, wild grassland, vegetables and fallow. Figure 11.1 shows the present (1998) distribution of these land uses. The main land uses in the Danangou catchment are wild grassland (wasteland) and cropland. Wild grassland is mainly located on the steeper parts of the gully slopes as well as on the gully bottoms and was until recently used for grazing goats. This practice has ceased, since grazing was prohibited in September 1999. Cropland is located mainly on the hilltops and on the relatively gentle slopes at lower elevation. The most common crops in the area are potato, millet, soybean, buckwheat and maize. Fallow land is mostly situated along the hilltops and woodland in the upper parts of some of the valleys. Chen et al. (2001) used air photos to show that there have been no major changes in land use in the catchment since 1975, though there has been a small decrease in cropland area and a small increase in woodland area.

### 11.2.2 Scenarios

The scenarios used in this chapter were developed based on:

- 1) A biophysical resource inventory in the area (1998/1999, e.g. Messing et al, in press a, b), including soil mapping, soil profile description and land use mapping.
- 2) Farmer's perception as found in participatory approach studies (1998/1999, Hoang Fagerström et al, in press; Messing and Hoang Fagerström, 2001), including their views on soil workability, water availability and crop suitability.
- 3) The plans of the authorities on greening the Loess Plateau. These plans include the gradual restriction of cropland to slopes of less than 15 degrees, and the prohibition of grazing.

Chen et al. (in press) described how land use maps for the different scenarios were developed using soil type, slope angle, aspect, elevation and landscape position criteria.



The resulting scenarios can be divided into 4 groups of 3 scenarios each (Table 11.1). Each group uses a different land use map and the effects of biological measures (such as mulching and improved fallow) and mechanical measures (e.g. contour ridges) were evaluated separately. These measures are relatively simple and inexpensive, but labour-intensive. One group uses the 1998 land use map, the other groups use respectively 25, 20 and 15 degrees as the upper slope limit for cropland. The 15-degree limit scenario is considered a long-term scenario and the 25 and 20-degree limits are therefore short-term intermediate scenarios (Chen et al., in press). The 15-degree cropland limit was already proposed by Fu & Gulinck (1994).

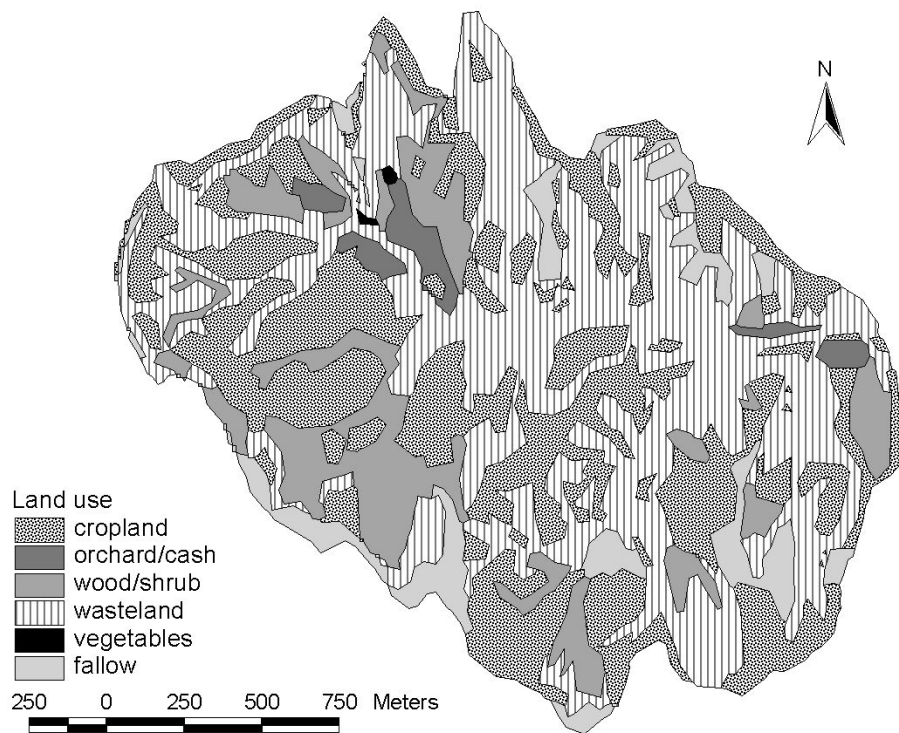


Figure 11.1 Simplified land use map for 1998 (also in Chen et al., in press)

Compared to the present land use (Figure 11.1), the scenario land use maps (15-degree map in Figure 11.2) all have much more woodland/shrubland, while cropland area decreased according to the specified slope limits. The area of orchards also has increased significantly for the 20 and 15-degree scenario groups. Fallow was considered part of the cropland area. Since the proposals suppose an intensification of agriculture on the remaining cropland (e.g. the use of fertilisers, improved fallow) it is likely that the proportion of cropland that is fallow will decrease in the future. In this chapter it was assumed that 1/5 of the cropland will be fallow. The actual distribution of fallow in Figure 11.2 was generated by using randomly distributed fallow areas with minimum size of about 500m<sup>2</sup>. Table 11.2 lists the areas occupied by the different land uses. It shows that for the 25, 20 and 15-degree land use maps there is a gradual decrease in cropland

and fallow land (but maintaining the 4 to 1 ratio between them) and a gradual increase in orchard/cash tree. By definition, the change was limited to areas below 25 degrees. The other land uses (including all slopes of more than 25 degrees) remained unaffected for these scenario groups, so for these land uses and slopes, only the present land use scenario differed. The economic consequences of the large changes in land use specified in table 11.2 were discussed by Chen et al. (in press) and Hoang Fagerström et al. (in press). These studies showed that the new scenarios would require government subsidies to avoid a short-term decrease in farmer income.

Table 11.1 Summary of land use scenarios

Scenario	Description
0	Present land use without conservation measures
0a	Present land use with biological conservation measures on cropland/fallow land
0b	Present land use with mechanical conservation measures on cropland/fallow land
1	Scenario land use with slope angle limit for cropland of 25 degrees, ridges and grass strips on orchard/cash tree land
1a	Scenario land use with slope angle limit for cropland of 25 degrees, with ridges and grass strips on orchard/cash tree land, biological measures on cropland/fallow land
1b	Scenario land use with slope angle limit for cropland of 25 degrees, with ridges and grass strips on orchard/cash tree land, mechanical measures on cropland/fallow land
2	Scenario land use with slope angle limit for cropland of 20 degrees, ridges and grass strips on orchard/cash tree land
2a	Scenario land use with slope angle limit for cropland of 20 degrees, with ridges and grass strips on orchard/cash tree land, biological measures on cropland/fallow land
2b	Scenario land use with slope angle limit for cropland of 20 degrees, with ridges and grass strips on orchard/cash tree land, mechanical measures on cropland/fallow land
3	Scenario land use with slope angle limit for cropland of 15 degrees, ridges and grass strips on orchard/cash tree land
3a	Scenario land use with slope angle limit for cropland of 15 degrees, with ridges and grass strips on orchard/cash tree land, biological measures on cropland/fallow land
3b	Scenario land use with slope angle limit for cropland of 15 degrees, with ridges and grass strips on orchard/cash tree land, mechanical measures on cropland/fallow land

### 11.2.3 LISEM implementation

The LISEM soil erosion model is a process based distributed model. A distributed model has the advantage that it simulates erosion patterns within the catchment as well as sediment yield from the entire catchment. This should give information that can be useful to determine where soil and water conservation measures should be applied. Several recent studies (Takken et al., 1999, Hessel et al., in press a) have shown, however, that the spatial patterns of erosion as simulated with LISEM should be regarded with caution.

LISEM simulates discharge and erosion for individual storms. It produces both an erosion map and a deposition map. Net erosion can be calculated by combining the two maps. For practical reasons we could in this chapter only use the erosion map to present the results.

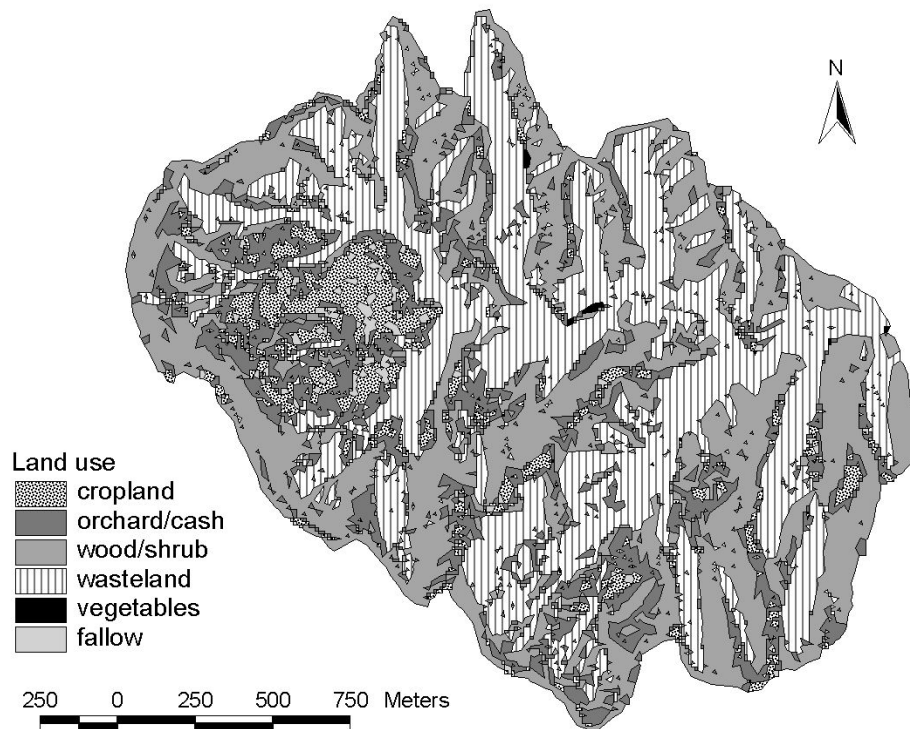


Figure 11.2 Scenario land use (15-degree cropland limit) for the Danangou catchment (also in Chen et al., in press)

Table 11.2 Areas (%) occupied by the different land uses for the different land use maps. Catchment area is 3.52 square kilometres

Land use	Present	25 degree	20 degree	15 degree
Cropland	35.4	21.0	13.0	6.7
Orchard/cash tree	2.4	0.0	9.5	17.8
Wood/shrubland	13.4	38.2	38.4	38.3
Wasteland	41.4	35.5	35.7	35.6
Vegetables	0.1	0.1	0.1	0.1
Fallow	7.3	5.2	3.2	1.6

In the period 1998-1999 data on only three storms could be collected. Calibration on these storms showed that a separate calibration for each storm is preferable (Hessel et al., in press a). This made the use of a so-called design storm less appropriate: such a storm can never be calibrated since it is a hypothetical storm. Therefore, one of the three storms measured had to be used. One of these storms was so small that it did not produce much erosion, while another was too much concentrated in a part of the catchment to make it useful for catchment-wide evaluation of scenarios. The only possibility was therefore to

use the data of the storm of intermediate size that occurred on August 1<sup>st</sup>, 1998. For the simulations the calibrated input data set for the 980801 storm was used (Table 11.3). The effect of the choice of storm will be discussed in section 11.4 by performing the same simulations for the storm that occurred on 000829. The simulations were carried out with LISEM LP.

Table 11.3 LISEM input data set for the event of August 1<sup>st</sup>, 1998

	C	O/C	W/S	WG	V	F <sup>1</sup>
Plant height (m)	0.68	3.66	6.50	0.38	0.68	0.32
Plant Cover	0.38	0.28	0.88	0.52	0.38	0.10
Leaf area index	1.64	3.20	7.37	0.60	1.64	0.78
Cohesion (kg cm <sup>-2</sup> )	0.09	0.11	0.10	0.12	0.09	0.10
Added cohesion (kPa)	2	2	2	2	2	2
Random roughness (cm)	1.16	1.11	0.75	0.90	1.16	1.21
Aggregate Stability (median drop no)	11.1	7.8	28.8	17.3	11.1	8
Manning's n	SD <sup>2</sup>	0.092	0.184	0.091	SD <sup>2</sup>	0.079
Ksat (cm day <sup>-1</sup> )	7.59	33.63	26.24	18.92	7.59	7.59

<sup>1</sup> C = cropland, O/C = orchard/cash tree, W/S = woodland/shrubland, WG = wild grassland, V = vegetables, F = fallow

<sup>2</sup> SD = Slope Dependent, Manning's n is calculated from slope, see Hessel et al (in press b)

Table 11.4 Effects of conservation measures on LISEM input parameters

	Cropland biological	Fallow biological	Cropland mechanical	Orchard ridges with grass strips
Plant height	1	0.5 <sup>1</sup>	1	1
Plant cover	1.05	1.25	1	2
Leaf area index	1.05	1.25	1	2
Cohesion	1	1	1	1
Added cohesion	1	1.25	1	1.25
Random roughness	2	1	1.5	1.5
Aggregate stability	2	1	1	1.25
Manning's n	0.15 <sup>1</sup>	1.1	1.25	1.25
Ksat	1.25	1.25	1.1	1.25

<sup>1</sup> These values are not multiplication factors but real values

The total catchment area of 3.5 km<sup>2</sup> made simulation with pixels smaller than 10 meters impractical. Many soil conservation measures are much smaller than 10 by 10 meters and can therefore not be implemented directly, e.g. by changing the DEM (Digital Elevation Model). Instead, such measures must be incorporated by changing other parameters that will be influenced by the original measure. For example, it can be expected that the use of

contour ridges will increase infiltration because water storage on the slope is increased. Since the ridges cannot be incorporated directly, one can then increase for example saturated conductivity to produce such an increase in infiltration. In this way all the proposed measures were translated into changes of input parameters for the LISEM model (Table 11.4). Table 11.4 gives assumed multiplication factors for the original LISEM input data set (Table 11.3): for example a value of 1.25 for ‘fallow biological’ plant cover means that the data that apply to the 980801 storm were multiplied by 1.25. Hence ‘fallow biological’ plant cover was the product of 0.10 (Table 11.3) and 1.25 (Table 11.4), and equalled 0.125.

### 11.3 Results

Figure 11.3 shows a classified version of the present land use erosion map produced by LISEM. Classification was done using the classification scheme shown in Table 11.5. This was done to improve the map readability. Without classification the map appearance would be totally dominated by a few very high values. It is important to realise that the values for lower and upper boundaries in Table 11.5 apply to the 980801 storm only. For individual storms in the Danangou catchment the lower boundary of severe soil erosion will therefore not always be 100 tonnes ha<sup>-1</sup>. The 980801 storm was not a big storm (its recurrence interval was probably below 1 year), so much larger storms can occur. It is quite possible that for such storms an erosion amount of 100 tonnes ha<sup>-1</sup> should be considered as only a moderate amount.

Table 11.5 Classification scheme for LISEM erosion maps. Erosion is given in tonnes ha<sup>-1</sup>

Erosion class	Lower boundary	Upper boundary
Negligible	0	2.5
Slight	2.5	10
Moderate	10	25
Serious	25	100
Severe	100	2000

For a large area in the southern part of the catchment, no serious erosion was predicted (Figure 11.3). This was caused by the fact that, according to the measured rainfall data, less rain fell in this area during the 980801 event. The amount of erosion therefore also was less. Comparison of Figures 11.3 and 11.1 indicates that other areas with negligible erosion rates for the 980801 storm were mainly woodland areas. A zone along both sides of the main valleys also had little erosion since this area is underlain by bedrock, which has a much higher cohesion, both in reality and in the model. The hilltop areas generally had slight or moderate erosion rates (Figure 11.3), while the steeper parts of the slopes had serious or severe erosion rates. Apart from woodland, not much difference in erosion is visible for the different land uses.

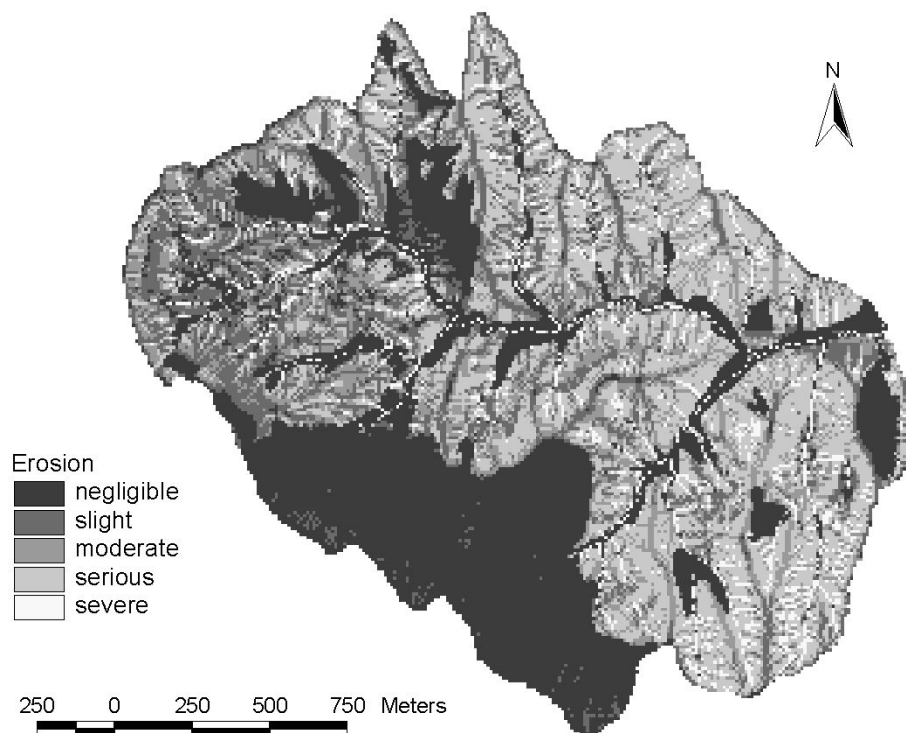


Figure 11.3 Classified LISEM erosion map for the present land use and the August 1<sup>st</sup> 1998 storm

Figure 11.4 shows the results of a scenario run with the present land use, but with biological conservation measures (scenario 0a) on cropland/fallow. In Figure 11.4 the results of scenario 0a are compared to the results of scenario 0. The scenario 0a result was first divided by the scenario 0 result and then classified. Hence, Figure 11.4 shows relative change, so that the actual amounts of erosion involved need not be large. Comparison of Figures 11.4 and 11.1 shows that erosion rates decreased for the cropland and fallow areas and that they remained much the same for the other land uses. In some areas an unexpected increase in erosion was simulated. Since LISEM is a complicated model it is difficult to trace the cause of this increase. One possible explanation would be that the amount of erosion in an upstream pixel was decreased but the amount of water was not, so that there would be a larger transport deficit and more erosion could occur in the pixel than before.

Figure 11.5 shows the results of scenario 3. The classification scheme in Table 11.5 is used, so the map can be compared directly to Figure 11.3. It is evident that the erosion in the catchment has decreased. The area with negligible erosion rates has more than doubled in size, while the other erosion classes have all decreased in area. Comparison with Figure 11.2 shows that like in Figure 11.3 the negligible erosion rates mainly occurred under woodland/shrubland. The large decrease in predicted erosion was therefore probably a direct consequence of the increase in woodland/shrubland area.

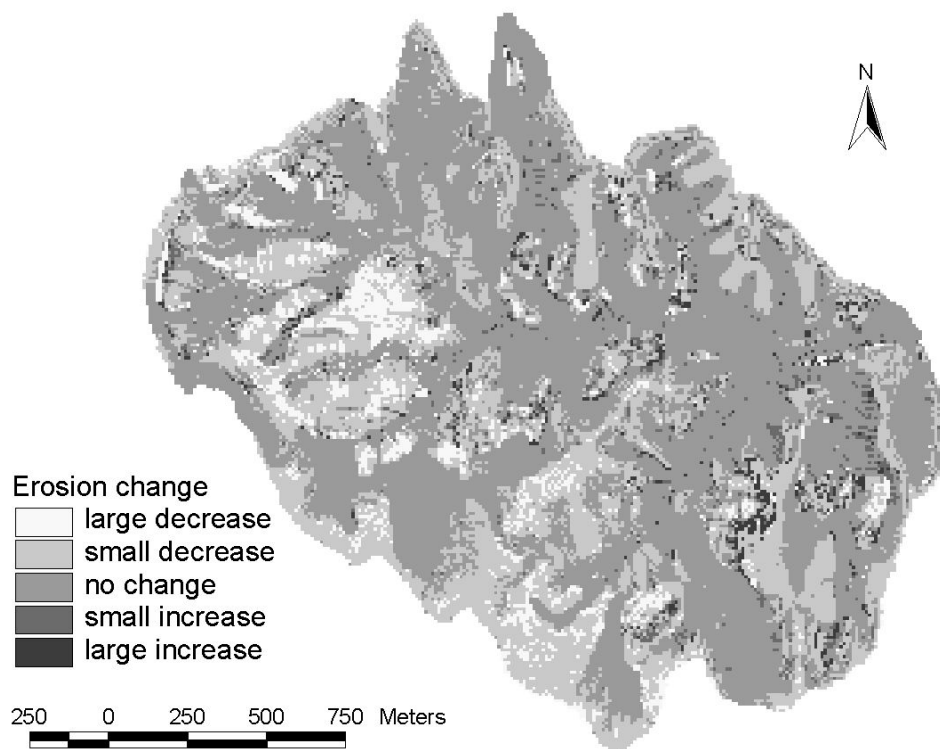


Figure 11.4 Results for the present land use with biological conservation measures (scenario 0a) on cropland/fallow

Table 11.6 shows that erosion in woodland decreased from present land use to the 15-degree scenario, even though woodland area increased significantly (Table 11.2). Comparison of Tables 11.2 and 11.6 shows that erosion for cropland and fallow land steadily decreased with decreasing area occupied by these land uses. Table 11.6 also shows a decrease in erosion for wasteland/wild grassland from the present land use to the 25-degree scenario. However, from the present land use to the 15-degree scenario erosion in the catchment became increasingly dominated by erosion in wasteland/wild grassland. Table 11.7 shows that total soil loss (erosion minus deposition) from the catchment was much larger for scenario 0 than for the other scenarios. The differences in predicted soil loss between scenarios 1, 2 and 3 were, however, relatively small. Since Table 11.2 shows that woodland/shrubland areas in scenarios 1, 2 and 3 were equal, but much smaller in scenario 0 it is very likely that the woodland/shrubland area was indeed the cause of this difference in soil loss between scenario 0 and the other scenarios. Another possible cause would be that cropland was restricted to less steep slopes in scenarios 1 to 3, but Table 11.6 shows that erosion rates for wild grassland were also high. Hence, if the cropland had been replaced by wild grassland there might not have been a decrease in erosion at all. Figure 11.5 also shows that in some areas erosion rates have increased in comparison to scenario 0. Comparison of Figures 11.1 and 11.2 shows that this mainly applied to areas that were woodland/shrubland in scenario 0 and had in scenario 3 become something else, e.g. wild grassland.

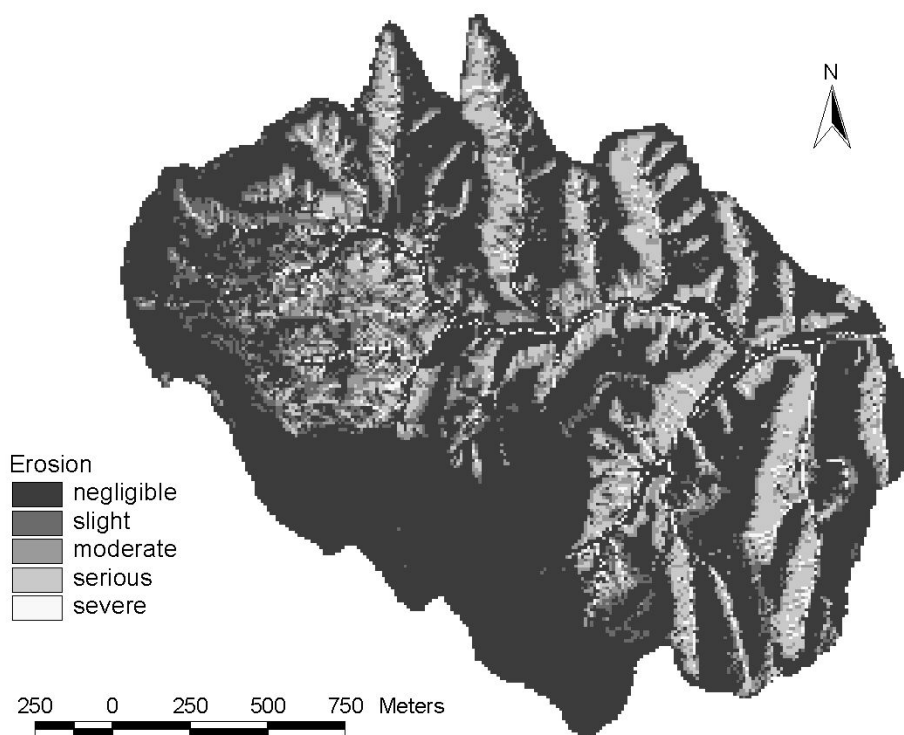


Figure 11.5 Predicted erosion for the scenario land use with 15-degree cropland slope limit (scenario 3)

Table 11.6 Erosion (tonnes) for different land use scenarios

Land use	Present	25 degree	20 degree	15 degree
Cropland	2949	1644	942	437
Orchard/cash tree	97	0	312	524
Wood/shrubland	173	198	173	140
Wasteland	6833	5080	4881	4727
Vegetables	31	62	63	62
Fallow	870	499	360	130
Total	10953	7483	6732	6019

Apart from the erosion/deposition maps, LISEM also generates time series of discharge and erosion for the outlet of the catchment. These data can be used to create hydrographs and sedigraphs for the catchment outlet. The upper 3 curves in Figure 11.6 show that using conservation measures in the present land use (scenario 0) decreased the peak discharge 10 to 18%, while the reduction was much larger when applying scenarios 1, 2 and 3 (40 to 60%). The peak discharge for the alternative scenarios arrived marginally earlier with a lower cropland slope limit (Table 11.7a). This indicated that with the decrease in permissible slope angle the remaining discharge was generated closer to the



stream: since water velocity depends on water height a smaller amount of water would have a lower velocity and a retarded peak. The sedigraphs (not presented here) showed much the same trend as the hydrographs.

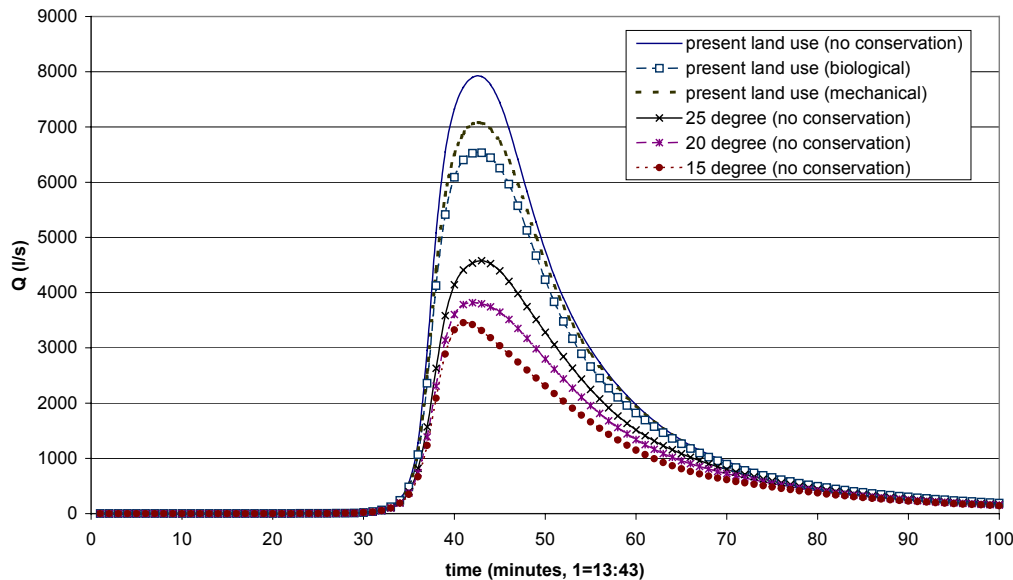


Figure 11.6 Predicted hydrographs for different land use scenarios

Table 11.7 shows that the decrease in total discharge was smaller than the decrease in peak discharge and total soil loss. Total soil loss showed the largest decrease. Relatively small decreases are shown in peak discharge, total discharge and total soil loss for the conservation measures for all scenarios (ranging from 2 to 21%), whereas large decreases (ranging from 33 to 71%) are shown for the alternative land use scenarios compared with scenario 0 (Table 11.7b, 11.7c). The differences between scenarios 1, 2 and 3 were much smaller than those between scenario 1 and scenario 0. These differences between scenarios 1,2 and 3 were caused by conversion of cropland to orchard/cash tree, while the larger difference between scenario 1 and scenario 0 was caused by a major redistribution of land uses. The effect of conservation measures decreased from scenario 0 to 3 (Table 11.7c). This was to be expected since the surface area on which these measures were applied decreased from scenario 0 to 3, while erosion from other parts of the catchment was unaffected by these conservation measures. The biological measures were always more effective than the mechanical measures (Table 11.7c).

#### 11.4 Choice of storm

In section 11.3, only the 980801 storm has been used to simulate the effect of different scenarios. It seems, however, likely that the effect of the different scenarios will depend on which storm is used. To assess this effect two methods were used:

278 Table 11.7 Summary of simulation results for the catchment outlet, 980801 event

a) Simulation results

	scen0	scen0a	scen0b	scen1	scen1a	scen1b	scen2	scen2a	scen2b	scen3	scen3a	scen3b
Time to peak (min)	42.5	42.5	42.75	43	41.5	42.25	42	41.25	41.5	41.25	41.25	41.25
Peak discharge (l/s)	7925	6540	7081	4576	3959	4182	3820	3522	3659	3458	3293	3380
Total discharge (m3)	8901	7766	8320	5924	5220	5611	5144	4589	4918	4441	4054	4291
Total soil loss (tonne)	1723	1360	1531	779	633	712	620	518	577	493	429	468

b) Percentage decrease compared to scen0 results

	scen0	scen0a	scen0b	scen1	scen1a	scen1b	scen2	scen2a	scen2b	scen3	scen3a	scen3b
Time to peak	0.0	0.0	-0.6	-1.2	2.4	0.6	1.2	2.9	2.4	2.9	2.9	2.9
Peak discharge	0.0	17.5	10.6	42.3	50.0	47.2	51.8	55.6	53.8	56.4	58.4	57.4
Total discharge	0.0	12.8	6.5	33.4	41.4	37.0	42.2	48.4	44.7	50.1	54.5	51.8
Total soil loss	0.0	21.1	11.1	54.8	63.3	58.7	64.0	69.9	66.5	71.4	75.1	72.8

c) Percentage decrease compared to the scenarios with no conservation measures

	scen0	scen0a	scen0b	scen1	scen1a	scen1b	scen2	scen2a	scen2b	scen3	scen3a	scen3b
Time to peak	0.0	0.0	-0.6	0.0	3.5	1.7	0.0	1.8	1.2	0.0	0.0	0.0
Peak discharge	0.0	17.5	10.6	0.0	13.5	8.6	0.0	7.8	4.2	0.0	4.8	2.3
Total discharge	0.0	12.8	6.5	0.0	11.9	5.3	0.0	10.8	4.4	0.0	8.7	3.4
Total soil loss	0.0	21.1	11.1	0.0	18.7	8.6	0.0	16.5	6.9	0.0	13.0	5.1

- 1) To vary only the storm size. To do this the rainfall intensities of the 980801 storm were multiplied by certain factors. All other settings remained equal, so that only the effect of storm size could be evaluated. Since the storm that was used is then hypothetical it is not possible to assess in how far its results would reflect reality (section 11.2.3).
- 2) To use another storm. Using this option not only the rainfall data will change, but also the land use map, the plant and soil data and the calibration settings. Thus, differences in scenario results can be due to several causes. On the other hand, a real storm will be used and the results of scenario 0 can be compared to the calibration results for this particular event. The storm of 000829 was chosen for this purpose.

#### 11.4.1 Different size

Table 11.8 shows results that were obtained by multiplying the 980801 storm by different factors. For this analysis the original version of LISEM 1.63 was used. Table 11.8a shows that the LISEM prediction was very sensitive to storm size: a storm of half the size of the original storm produced only 1% of the runoff, while a storm of double size showed a 6.6 fold increase in predicted soil loss. It also shows that total discharge was somewhat less sensitive than peak discharge and soil loss, as was found for the different scenarios. Table 11.8b shows that scenario 1 was most effective for storms of about the size that was

Table 11.8 Effect of storm size (given as multiplication factor) on scenario result

	a) Scenario 0 (% of measured storm)			b) Scenario 1 (% of scenario 0)		
	Qp	Qtot	Soil loss	Qp	Qtot	Soil loss
0.5	1	1	1	89	89	86
0.75	25	33	29	52	59	58
1	100	100	100	52	64	52
1.5	319	267	335	62	67	53
2	612	470	660	70	72	62
3	1284	920	1417	82	81	76

measured. The reason for this is probably that with increasing storm size infiltration becomes less important. On the other hand, for very small storms there will be almost no runoff from the slopes and the only runoff that arrives at the catchment outlet will originate from the channel (which, according to LISEM, is impermeable). Table 11.8b suggests that scenario 1 would be most effective for a storm of a magnitude similar to that of the real storm of 980801. For which storm size the scenarios are most effective is, however, likely to depend on the calibration settings, especially Ksat. In fact, it seems strange that the scenario should be most effective precisely for the storm it is calibrated on. This can be mere coincidence, but might also indicate a dependency on calibration. To find out a similar series of simulations should be done for other measured storms.

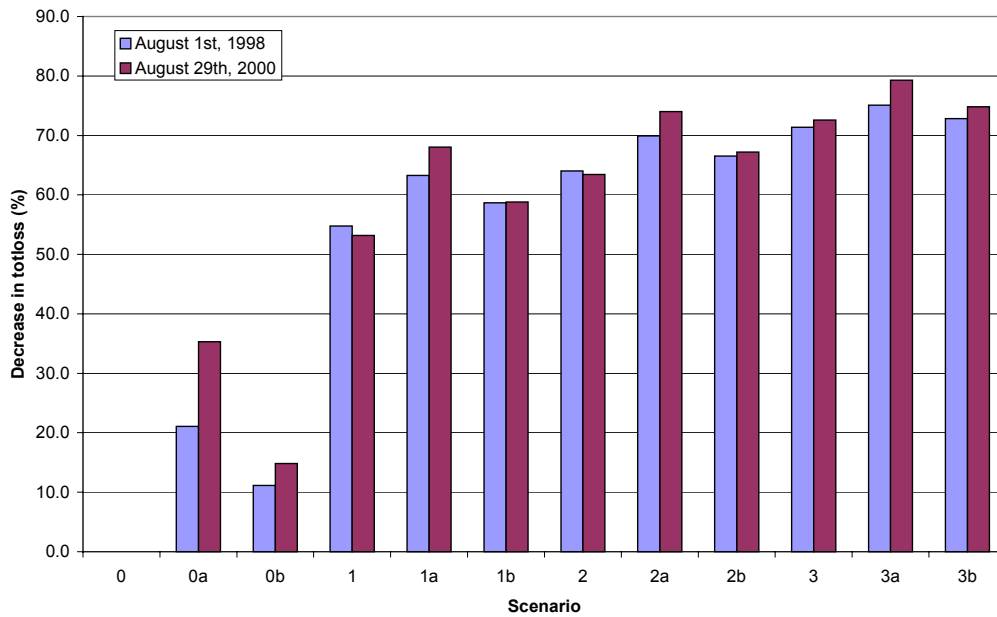


Figure 11.7 Decrease in total soil loss for the different scenarios, 980801 and 000829 storm

#### 11.4.2 Different storm

The results for the 000829 storm are given in Table 11.9, while the results for total soil loss are compared with those obtained for the 980801 storm in figure 11.7. Figure 11.7 clearly shows that for the 000829 event the 0b and especially 0a scenarios were more effective than for the 980801 storm. Tables 11.7c and 11.9c show that this was also true for the other a and b scenarios, but this was less apparent from figure 11.7 because figure 11.7 shows the results expressed as a decrease compared to the scenario 0 results (which corresponds to tables 11.7b and 11.9b). The reason for the larger effect of the a and b scenarios for the 000829 event is probably the fact that the calibrated saturated conductivity for that event was larger than that of the 980801 event (see chapter 10). Thus, if the Ksat is increased by an equal percentage according to table 11.4, the absolute increase will be larger for the 000829 event. Figure 11.7 also shows that the effect of the different land use maps was similar for the 980801 and 000829 events.

Overall, the results for both storms were similar since both showed:

- A continuous decrease in peak discharge, total discharge and soil loss from scenario 0 to scenario 3.
- That the a scenarios (biological measures) are more effective than the b scenarios (mechanical measures)
- That the results of scenarios 1 to 3 clearly differ from that of scenario 0
- Similar absolute values for discharge and soil loss. Chapter 10 showed that for the area upstream of the weir the 980801 and 000829 events are not of similar magnitude. Rainfall data, however, suggest that for the catchment as a whole the events were of similar size (though different intensity). Chapter 10 also showed that soil loss for the 000829 event was considerably underpredicted for the weir,

Table 11.9 Summary of simulation results for the catchment outlet, 000829 event

a) Simulation results

	scen0	scen0a	scen0b	scen1	scen1a	scen1b	scen2	scen2a	scen2b	scen3	scen3a	scen3b
Time to peak (min)	33.75	33.75	34.5	32.5	34	33.25	33	34.25	33.75	33.75	34.5	34
Peak discharge (l/s)	8879	5963	7694	6425	4242	5584	5282	3635	4668	4140	3117	3751
Total discharge (m3)	8142	6455	7472	5511	4392	5097	4715	3825	4401	3930	3302	3716
Total soil loss (tonne)	1617	1046	1377	757	517	666	591	420	530	443	335	407

b) Percentage decrease compared to scen0 results

	scen0	scen0a	scen0b	scen1	scen1a	scen1b	scen2	scen2a	scen2b	scen3	scen3a	scen3b
Time to peak	0.0	0.0	-2.2	3.7	-0.7	1.5	2.2	-1.5	0.0	0.0	-2.2	-0.7
Peak discharge	0.0	32.8	13.3	27.6	52.2	37.1	40.5	59.1	47.4	53.4	64.9	57.8
Total discharge	0.0	20.7	8.2	32.3	46.1	37.4	42.1	53.0	45.9	51.7	59.4	54.4
Total soil loss	0.0	35.3	14.8	53.2	68.0	58.8	63.5	74.0	67.2	72.6	79.3	74.8

c) Percentage decrease compared to the scenarios with no conservation measures

	scen0	scen0a	scen0b	scen1	scen1a	scen1b	scen2	scen2a	scen2b	scen3	scen3a	scen3b
Time to peak	0.0	0.0	-2.2	0.0	-4.6	-2.3	0.0	-3.8	-2.3	0.0	-2.2	-0.7
Peak discharge	0.0	32.8	13.3	0.0	34.0	13.1	0.0	31.2	11.6	0.0	24.7	9.4
Total discharge	0.0	20.7	8.2	0.0	20.3	7.5	0.0	18.9	6.7	0.0	16.0	5.4
Total soil loss	0.0	35.3	14.8	0.0	31.7	12.0	0.0	28.9	10.3	0.0	24.4	8.1

so that the amount predicted for scenario 0 is still well below the amount measured at the weir.

### 11.5 Parameter sensitivity

To evaluate the reliability of the scenario simulation results it is important to investigate the effect of the choice of multiplication factors as shown in table 11.4. The choice of these values is likely to determine the result of the scenario simulation. Thus, physically realistic values should be chosen and the sensitivity of the different parameters should be assessed.

A sensitivity analysis was used to find out which parameters had the largest influence on the results. The multiplication factors were evaluated separately, and were changed for cropland only. The present land use map (scenario 0) was used. Since the only differences between the scenarios 0a, 0b and 0 occur on cropland the results of the sensitivity analysis should give information about what causes the effect of these scenarios. Table 11.2 shows that cropland occupies 35.4% of the total catchment area. To stay as close as possible to table 11.4 the following values for the multiplication values were simulated: 1 (equals scenario 0), 1.1, 1.25, 1.5 and 2. The results are shown in figure 11.8 for total soil loss.

Figure 11.8 shows that the LISEM prediction was most sensitive to changes in saturated conductivity. If Ksat, for example, was increased by 50% (multiplication factor = 1.5) the simulated total soil loss from the catchment decreased by 24% (fraction of original value = 0.76), even though Ksat was only changed for 35% of the catchment area. LISEM was also sensitive to Manning's n and, in a lesser degree, to plant cover and leaf area index. LISEM appeared insensitive to changes in random roughness, aggregate stability and cohesion due to plant roots. Therefore, the differences between scenarios 0, 0a and 0b are mainly due to changes in Ksat and Manning's n. Table 11.7c, for example, shows that scenario 0b decreased total soil loss by 11.1%. Figure 11.8 shows that for the multiplication factors used in that scenario (Table 11.4) both the change in Manning's n and the change in Ksat should result in a decrease of soil loss by about 6%. Jetten et al. (1998) showed that the sensitivity of LISEM can be more completely evaluated by changing combinations of parameters, instead of changing parameters one by one. They also showed that the sensitivity to certain parameters might depend on the level of other parameters and that when the amount of runoff is limited random roughness and cohesion are important, but that if runoff is large Ksat is the most sensitive parameter. Thus, the sensitivities for different individual parameters cannot simply be added up or multiplied to give the combined effect. Nevertheless, a simple sensitivity analysis in which only one parameter value is changed at a time is the easiest way to determine which individual parameters will be most important. Figure 11.8 clearly indicates that the most important parameters are saturated conductivity and Manning's n. The same conclusion has been reached in other sensitivity analyses of the LISEM model (De Roo et al, 1996b; De Roo & Jetten, 1999). The combined effect of plant cover and leaf area index might also be

important since these parameters are related, i.e. if plant cover is high leaf area index is likely to be high too.

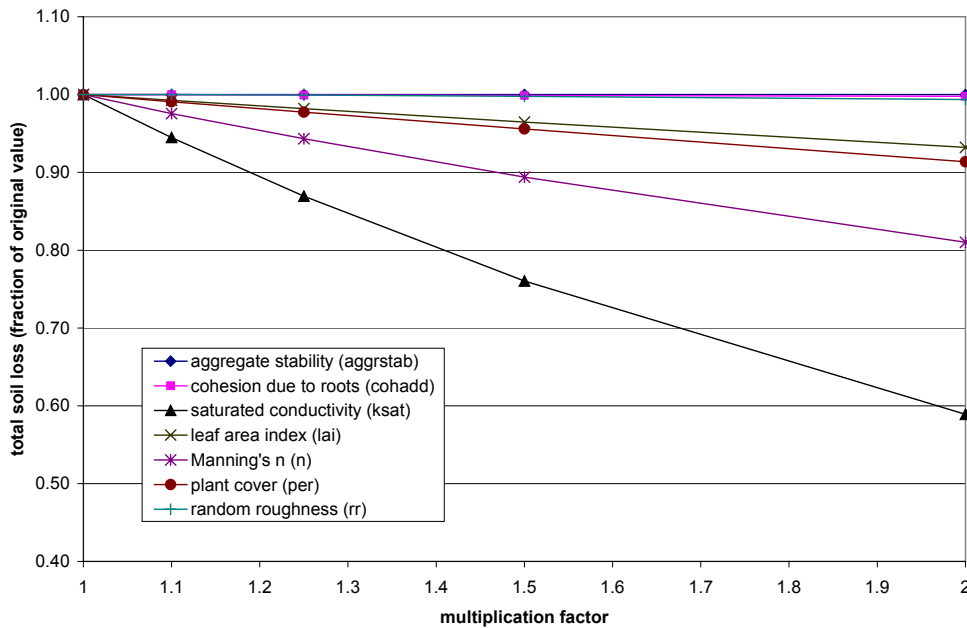


Figure 11.8 Effect of multiplication factors on simulated total soil loss

## 11.6 Discussion

The present study is one of the first attempts to use process based soil erosion modelling as a tool for optimising land use and management strategies to reduce runoff and erosion rates on the Chinese Loess Plateau. To perform the simulations several assumptions were made.

The first is that LISEM can be used for scenario simulations. To evaluate this assumption, further research into the distribution of erosion as simulated by LISEM is needed because several recent studies (Takken et al., 1999; Hessel et al., in press a; Jetten et al, in press) have shown that LISEM might not predict erosion patterns correctly. This might have implications for its use in scenario simulations as well. Another potential problem with LISEM is that total soil loss is often a fairly small difference between large erosion and large deposition values. The erosion amounts shown in Table 11.6 are for example much higher than the total soil loss given in Table 11.7. This means that simulated soil loss from the catchment will be much influenced by simulated deposition, so that conclusions based on simulated erosion might not be applicable to soil loss.

The second assumption is our use of multiplication factors. It is important to realize that the effect that is predicted for SWC measures (when compared to land use change) is determined by the values of the multiplication factors that were assumed (Table 11.4). At present, it is difficult to judge to what degree the values of the multiplication factors used are valid. Section 11.5 showed that the simulation result is especially sensitive to the values of saturated conductivity and Manning's n. More quantitative data on the effect of

SWC measures should be gathered to be able to select values with a higher degree of certainty. Related to this assumption is the assumption that the measured data (Table 11.3) are correct, since the differences in measured values between land uses determine the effect of land use redistribution.

A third assumption is that the selected storm is representative. In reality, it seems likely that the effect of soil and water conservation measures will depend on the intensity and size of a storm. Farmers in the area also indicated that for really large storms it does not matter what conservation measures you have, because there will be severe erosion anyway. In section 11.4 a second storm of comparable magnitude gave results similar to those of the storm originally used. Simulations with increased and decreased rainfall amounts for the measured storm showed that SWC measures would be less effective for both larger and smaller storms. LISEM cannot, however, simulate a decreasing effectiveness of SWC measures with increasing storm size. Such decreasing effectiveness would be plausible for large storms since storage capacities (e.g. of ditches) might be exceeded and SWC measures might be destroyed. In LISEM, the decreasing effectiveness for large storms is only because rainfall intensity is higher, but saturated conductivity remains the same.

Thus, more research is needed before we can say to what degree the simulation results of LISEM reflect reality. LISEM is a state of the art erosion model, and other erosion models will suffer from similar limitations. Therefore, care must be taken not to read too much into scenario simulation results. Scenario simulations with erosion models give us useful insights into what might happen, but they do not tell us what will happen.

## **11.7 Conclusions**

The LISEM scenario simulations predicted that a decrease in runoff volume and erosion amount of about 5-20% can be reached by implementing conservation methods with the present land use distribution (scenarios 0a and 0b). Changing the land use according to the slope-angle-based proposals defined in the scenarios 1, 2 and 3 was predicted to have a much larger effect; discharge decreased by about 40-50%, while erosion decreased by 50-70%. The differences between different maximum permissible slopes for cropland were predicted to be only about 20-25%. The LISEM simulations did not show a clear difference in erosion rates between most land uses; only woodland/shrubland and orchard/cash tree seemed to have clearly lower erosion rates than the other land uses. The large increase in woodland/shrubland area in the scenario 1, 2 and 3 land use maps was therefore a direct cause for the large decrease in predicted erosion, while the decrease from scenario 1 to 3 was caused by conversion of cropland to orchard/cash tree. Simulations using different rainfall data showed that the simulation result for different scenarios might depend on storm size. A sensitivity analysis showed that the simulation results were most sensitivity to saturated conductivity and Manning's n. More research is needed before we can say to what degree the simulation results of LISEM reflect reality.



## 12 SYNTHESIS

As indicated in chapter 1, the Chinese Loess Plateau suffers some of the highest soil erosion rates on earth. This is because it is a semi-arid area with low vegetation cover, erodible soils, steep slopes and occasional high intensity summer storms. In this thesis, a process based distributed soil erosion model was applied to a small catchment on the Chinese Loess Plateau, a type of model that has not often been used there. Several characteristics of the Loess Plateau should be considered to allow successful simulation with such a model. First, the occurrence of very high sediment concentrations can have a pronounced effect on fluid properties. Further, the occurrence of steep slopes that could affect runoff velocity and transport capacity. Finally, many large, permanent gullies are present.

A literature review of the effects of high sediment concentrations (of several hundred grams per litre in the study area) on fluid properties revealed that such concentrations certainly have effects on fluid density, settling velocity and viscosity. For other fluid properties, such as velocity, velocity profile, flow resistance and transport capacity, the evidence is more scant and even partly contradicting. Velocity might be expected to increase due to higher density, but to decrease due to higher viscosity. Flow might become more laminar, but has, on the other hand been reported to remain turbulent. There are indications that for high concentrations transport capacity starts to increase, but no relationships between concentration and transport capacity were found. Present day soil erosion models, however, generally do not consider the effects that high concentrations might have. In this study, these effects were taken into account, but the resulting changes to the LISEM model remained relatively small because of lack of reliable data. Settling velocity was corrected and fluid density calculated, but possible effects on velocity and transport capacity could not be taken into account for lack of data. It was also shown that to compare model results with measurements it is necessary to take into account the volume occupied by the sediment. Present day soil erosion models predict clear water concentration, but do not clearly state that measurement results should in that case be expressed as clear water concentrations too. In this thesis, measured values were converted to clear water values, but it would also be possible to adapt the models so that they yield dirty water values. For erosion models that deal with high concentrations the specific effects of high concentrations cannot be neglected. More data on the effects of high concentrations are, however, needed to fully adapt erosion models to such conditions.

According to the Manning equation, flow velocity should be larger when slopes are steeper. In the Danangou catchment this was found to be the case for those land uses for which the soil is not very erodible. For the erodible cropland, however, flow velocity was almost independent of slope angle. This contradicts the Manning equation and therefore poses problems for erosion modelling. To overcome this problem either the Manning equation should be abandoned or Manning's  $n$  should be allowed to vary with slope angle for erodible soils. To abandon the Manning equation for erodible soils would imply the use of different velocity equations within one model area, which from a modeller's point of view is undesirable because this might lead to discontinuities in the simulated flow. Therefore, the most pragmatic solution is to allow Manning's  $n$  to vary. Obviously, this requires that relationships between slope angle and Manning's  $n$  be developed. This

approach was followed in this study, but the modelling results indicated that using a slope-dependent Manning's  $n$  did not change model results much. This small effect was probably due to two causes: 1) Manning's  $n$  was only changed for cropland, which occupies no more than about 25% of the catchment area, and 2) channels are usually located in wasteland, and never in cropland. Thus, a difference between both methods that exists for cropland might be modified before the water reaches the catchment outlet because of the influence of the channel.

An evaluation of a number of transport equations showed that for the Loess Plateau conditions of steep slopes, fine grain size and high concentrations, most equations tend to overpredict transport rates on steep slopes and underpredict transport rates on gentle slopes. Overprediction on steep slopes is probably caused by the fact that the equations were developed for gentler slopes. Underprediction for gentle slopes occurs probably because most equations were bedload equations, while transport is dominated by suspended load. Another cause could be the reduced settling velocity in high concentration flows, but this effect was taken into account in the evaluation. The results showed that the performance of the different equations not only depends on storm size, but also on what concentration is assumed to be the maximum possible concentration for transport by flowing water. The results further showed that LISEM is very sensitive to the choice of transport equation. For the conditions at Danangou the Govers (1990) equation performed best, but it seems likely that under different circumstances different transport equations will give the best results. Thus, the choice of an appropriate equation is vital in soil erosion modelling.

Because of their widespread occurrence and their large size, gullies can be a major source of sediment in the Danangou catchment. Field observations suggested that gully headcuts are fairly stable on event-basis, and that soil falls on the headcuts and sidewalls are important processes in between events. It proved, however, difficult to determine which percentage of the catchment sediment yield came from the gullies and which from elsewhere. Extensive measurement campaigns are probably needed to obtain a reliable sediment balance. Nevertheless, the model that was developed in chapter 8 shows a possible method to combine a storm based erosion model such as LISEM with a stability model using daily time step. The main problem probably is that the occurrence of soil falls is likely to be governed by local circumstances that cannot be modelled using a catchment model. Mass movements can produce large amounts of loose material, which can potentially (depending on location) be easily entrained by runoff during events, although the actual entrainment rate will be determined by transport capacity. Erosion models that deal with catchments should take such sources of loose sediment into account.

Despite the fact that the LISEM model was, as far as possible, adapted to the local conditions on the Chinese Loess Plateau, calibration of LISEM for a complex catchment such as the Danangou catchment is difficult. Discharge at the outlet can be modelled well by calibrating, but the calibration should at least be different for small and large events, and probably even for each event. The cause could be either flaws in LISEM or inaccuracy in input data. Small events can hardly be modelled, probably because of spatial variability of rainfall. For sediment prediction, the situation is even more difficult, and calibration is less effective than for discharge. Although adequate average concentrations can be obtained, the simulated sedigraph was always different from the

measured one, which might be due to flaws in LISEM, inadequate input or inadequate concentration measurement. Spatial evaluation of distributed models such as LISEM is logical, but revealed that measured and simulated erosion patterns were very different. The reasons can be manifold and include grid-related effects, spatial variability and DEM inaccuracy. For complex catchments it seems almost impossible to obtain sufficient spatially distributed input data. Similar measurement campaigns in catchments with different characteristics would be required. Even so, spatial prediction might well prove to be beyond us.

This also has implications for the use of LISEM in scenario analysis, because if LISEM cannot correctly predict current erosion patterns there is no reason to assume that it can accurately predict the (spatial) effects of using alternative land use and land management scenarios. Furthermore, the effect of scenario simulations will depend on storm size as well as on the way in which the modeller translates scenarios into changes in LISEM input. More research into these dependencies is needed.

These results confirm the now widespread belief that complex process based erosion models have problems predicting erosion. Does this mean that the future for process based erosion models is bleak? It seems likely that such models will indeed be used in fewer practical applications, e.g. as a management tool, than before. For such purposes other types of model might be more suitable, and more care should be taken to select the proper type of model for any particular application. Nevertheless, there are several reasons why we should continue using process based models:

- 1) The fact that until now predictions, and especially spatial predictions, have not been good does not mean that we should stop trying. More attempts are needed, if only to find out what causes the lack of predicting capability: model flaws, inadequate input data or spatial and temporal variability? This requires that different types of catchment are used and that attention is paid to parameter uncertainty and variability. Morgan & Quinton (2001), for example, consider inadequacy of input data (partly caused by spatial variability) and of data used for model evaluation to be more important than flaws in process based models themselves.
- 2) Process based models are the only kind of model that can help us improve our understanding of soil erosion processes. This, however, is not straightforward. Careful analysis and extensive field campaigns are needed to be able to translate model results into process knowledge, because an increased understanding of the model does not necessarily mean an increased understanding of reality. Nevertheless, model behaviour can give clues about processes that might be hard to attain using erosion measurement alone. As Doe & Harmon (2001) and Morgan & Quinton (2001) note research models are not primarily intended for practical use (prediction), but rather to combine our knowledge on individual processes, to explore the dynamics of soil-water processes and to gain insight in complex relationships between variables. If they serve these purposes they should be considered successful, even if predictions are not accurate.
- 3) Though process based models are not synonymous to distributed models, there is a link between process knowledge and spatial & temporal scale. Kirkby (1998), for example, notes that a finer time resolution requires better process understanding, and that this, in turn, generally implies a more detailed spatial scale. Distributed models therefore tend to be process based. Distributed models

are the only kind of model that can produce spatial predictions of erosion. With ever increasing computer power, distributed modelling would seem likely to become more popular. More erosion pattern measurements are, however, needed to compare the results of such models with reality.

Thus, process based models serve different aims than simple models and they also give types of information that cannot be provided by simpler models. Only process based models can provide information on spatial and temporal variability of erosion (Morgan & Quinton, 2001). Therefore, a diversification of models, rather than a replacement of one type with another, seems likely. Different types of model should be used depending on local circumstances at the time of modelling and on what the aim of modelling is.

This thesis aimed at a better understanding of erosion processes in the Danangou catchment and at better erosion predictions by adapting the LISEM model to incorporate this process knowledge. LISEM was thus primarily used as research model, though the scenario simulations were a more practical application with relevance for land management. The results showed the complexities of process based, distributed, soil erosion modelling for catchments on the Loess Plateau. Admittedly, process knowledge regarding the effects of steep slopes, high concentrations and permanent gullies remained incomplete, but nevertheless, process descriptions have improved compared to previous versions of LISEM. Despite this, prediction by the LISEM model was hardly improved. This is probably due to a number of causes. The first is that improvements in one part of the model area might be masked by associated changes elsewhere. Several chapters have, for example, shown how much what happens in the channel affects the simulation result for the catchment outlet. Secondly, theoretical improvements to the model might be nullified by calibration in the sense that it is well possible that models that are worse theoretically can be calibrated to give better predictions. On the other hand, calibration is unavoidable to attain acceptable predictions. This makes it very difficult to determine if an adapted model performs better or worse than the original version. Finally, there is still a lack of data. It is, for example, not known what happens in reality between the point where soil is detached and the catchment outlet. Likewise, there is still insufficient data about the spatial distribution of erosion. Since there is also still a lack of reliable input data with sufficient spatial resolution, and at the appropriate process scale, it is still not possible to determine if incorrect predictions are caused by data inaccuracy or by model errors. It seems likely that the larger and more complex the catchment is, the more difficult these problems will become. Therefore, in case of the Chinese Loess Plateau, more effort should be put into measuring and modelling for single hillslopes, single gullies and subcatchments that are smaller and less complex. Only in such circumstances might it be possible to gain sufficient process knowledge, and to avoid internal model effects that might mask the effects of improved process descriptions.

## SUMMARY

The Chinese Loess Plateau suffers some of the highest soil erosion rates on earth. This is caused by the fact that it can be characterized as a semi-arid area with low vegetation cover, erodible soils, steep slopes and occasional high intensity summer storms. The erosion has large effects, both on-site and off-site. Research of soil erosion on the Loess Plateau is necessary to find ways to reduce the erosion rates.

In this study, the process based distributed soil erosion model LISEM was applied to a small catchment on the Chinese Loess Plateau. This type of model has not been applied to the Loess Plateau often since erosion research in the area has mainly focused on monitoring and on plot studies. Several characteristics specific to the Loess Plateau needed to be taken into account to allow successful simulation with such a model. The most important were:

- The occurrence of very high sediment concentrations that can have a pronounced effect on fluid properties.
- The occurrence of steep slopes. Contrary to regions where soil erosion models have been applied more frequently (Europe and the USA) croplands in the Danangou catchment can be on slopes as steep as 60%. Such slope angles could have pronounced effects on runoff velocity and on transport capacity.
- The presence of large, permanent gullies

### Study area

The study area was Danangou catchment, a 3.5 km<sup>2</sup> catchment in the hilly part of the Loess Plateau located in northern Shaanxi Province. Elevation in the catchment ranges from 1075 to 1370 metres, and slopes are steep. The climate is semi-arid, with average annual precipitation of slightly over 500 mm and with large inter annual variability. Precipitation is concentrated in high intensity summer storms that can occur between June and September. The main land uses in the catchment are wasteland (40%), cropland (28%) and fallow (21%). Vegetation cover is generally low, and the loess soils are erodible, making them susceptible to erosion during storms. Only during the summer storms, runoff from the catchment occurs, and soil loss can be high since discharge can rise to over 10 m<sup>3</sup>/s and sediment concentrations can be 500 g/l or more.

### Data

To study soil erosion in the Danangou catchment several types of measurements were conducted during the period 1998-2000:

- Measurements of parameters that are necessary to run erosion models such as LISEM. Plant and soil characteristics were measured on a fortnightly basis during the period April to October for 1998 and 1999. Soil physical characteristics such as saturated conductivity and relationships between water content, suction and unsaturated conductivity were determined in a few separate campaigns.
- Rainfall was measured continuously from April to October of each year. Six tipping bucket rain gauges were used as well as several simple rain gauges.

- Discharge and sediment concentration were measured at several places. A weir was built at the outlet of a 2 square kilometre catchment and 2 flumes were used to measure at the outlet of a gully and on a steep cropland.
- Erosion was measured/estimated using erosion pins, rill erosion mapping and a gully inventory.

### **High sediment concentrations**

Sediment concentrations in runoff on the Chinese Loess Plateau can become very high, concentrations of up to 1000 g/l occur regularly. Flows with such concentrations take an intermediate position between normal streamflow and debris flow and can be called hyperconcentrated flow. These very high concentrations can probably develop because an erodible material (loess) is present on steep slopes, while loess characteristics as well as climate may play a role too. With increasing concentration fluid properties gradually change: density increases, viscosity increases and settling velocity decreases. These changes also influence flow velocity and transport capacity of the flow. When concentrations become high enough, feedback mechanisms start to operate that cause the fluid to behave differently from normal streamflow. Transport capacity may, for example, increase with increasing concentration. Erosion models that will be used in regions where high concentrations can occur should take these changes in fluid properties into account.

Measured concentrations in the Danangou catchment were up to 500 g/l for the weir, and up to 700 g/l for a smaller plot. Despite the fact that such concentrations change flow properties considerably there was no indication that discharge equations for weir or plot should be changed. However, to compare the measured results with simulated results several corrections were necessary. The first was that when a pressure transducer was used to measure water level the signal should be corrected for fluid density. Furthermore, sediment volume had to be subtracted from fluid volume to obtain a clear water volume that could be compared with model results. For the flume used at the sediment plot, sediment levels had to be subtracted from measured fluid levels. Finally, measured concentrations had to be corrected to give concentrations in terms of grams per litre clear water instead of grams per litre of fluid. At the concentrations measured in the Danangou catchment the settling velocity is already reduced to about 50% of its clear water value. Therefore, a correction for settling velocity is needed in soil erosion models dealing with high sediment concentrations.

### **Flow velocity**

Almost all present day process based erosion models use the Manning equation to calculate flow velocity. To test the validity of the Manning equation a series of 62 flow experiments was carried out, incorporating all major land uses present in the Danangou catchment. Most attention was, however, given to cropland. These tests showed that in the case of cropland Manning's  $n$  was not a constant, but increased with increasing slope angle. The cause of this was soil erosion, which not only increased soil roughness, but also increased flow length. Carrying all the sediment also requires the use of energy that otherwise could have been used to increase flow velocity. The net effect was that on erodible soils in the Danangou catchment the flow velocity did not increase with an increase in slope angle. For less erodible soils (e.g. in woodland) velocity increased with

increasing slope angle and Manning's  $n$  was not a function of slope angle, but of plant cover. A regression equation was developed to predict Manning's  $n$  from slope angle for croplands. This equation was then used to produce an input map for LISEM that had slope-dependent values of Manning's  $n$ .

### **Transport capacity**

Several transport equations were applied to the Danangou catchment by programming the equations into the LISEM model, which was then applied to the entire catchment. The Shields parameter appeared to be unsuitable for the Danangou catchment because the steep slopes, high density flows and small median grainsize of the catchment all contributed to very high values of the Shields parameter. Thus, equations that use Shields overpredicted transport capacity, especially on steep slopes. Likewise, in equations using critical discharge, the critical discharge was very small, so that transport capacity was overpredicted. If the transport threshold was neglected, most equations appeared to be too sensitive to slope angle. The stream power based Govers (1990) equation has relatively low slope dependency and was found to perform best. The Yang equation appeared to be too sensitive to grainsize.

Simulations for the sediment plot showed that the Govers equation also performed well for overland flow for the larger events, when there was sufficient water available, like during the large event of 000829. For small events, however, the transport capacity of overland flow was underpredicted by the Govers equation. This can be due to the large effect gravity will have on transport for such slopes.

These results showed that the Govers equation performed better than the other tested equations for sediment transport by flowing water on steep slopes with small grainsizes. The equation was also suitable for most flow conditions that occur in the Danangou catchment. Since, for modelling, it is preferable to use only one equation for the entire catchment, it is recommended to use the Govers equation for conditions like those in the Danangou catchment.

### **Gullies**

Gully erosion is a very important process on the Chinese Loess Plateau. The Danangou catchment is also heavily dissected by gullies. Repeated observations, however, showed that in the Danangou catchment gully headcuts do not perceptibly retreat during individual events. Rather, loose material tends to accumulate on the gully floors in between rainfall events through soil fall. This loose material can then easily be entrained during the first runoff event. Soil fall is not a process that operates on storm basis; hence it cannot be modelled with soil erosion models such as LISEM. Instead, a daily-based model was developed that simulates soil fall as a function of soil moisture, cohesion and headcut height. The output of this model was a map that specifies the amount of loose material that has accumulated on the gully floors. This map can then be used as an additional source of sediment in storm based simulations of soil erosion.

It proved impossible to develop a reliable sediment balance for the Danangou catchment. This was caused by several problems that were encountered. The first is that in 1998 not

all events were measured at the weir. Therefore, the total soil loss from the catchment is unknown for that year. Second, an inventory of loose material accumulated in the gullies was not complete because many gullies are inaccessible and because the number of gullies is so large that only the larger ones could be visited. Third, loose material not only accumulates due to soil fall, but also due to larger mass movements that occur infrequently but can keep providing sediment to the streams for a long time. Fourth, It was found that sheet erosion rates were quite high. These rates were determined at the sediment plot, but to extrapolate from the plot to the entire catchment was not easy because it was necessary to use a sediment delivery ratio for the plot. Therefore, the resulting sheet erosion rates depended on the choice of sediment delivery ratio. Finally, rill erosion mapping could only be performed on croplands, because on other land uses it was not possible to know if certain erosion features were developed during that particular year. Therefore, erosion rates from wasteland, woodland, orchard and fallow land could only be guessed at. Due to all these uncertainties, cropland erosion could be anything between 20 and 50 % of total erosion, while gully erosion could be estimated at 40 – 70%. For larger events cropland contribution seemed to increase.

### **Adaptations to LISEM**

A number of changes to LISEM were proposed to overcome the modelling problems posed by the steep slopes, high concentrations and permanent gullies of the Danangou catchment. These changes included a slope angle correction, the use of slope dependent Manning's  $n$ , the introduction of a concentration dependent settling velocity, the introduction of a loose material map and the use of sine instead of tangent. These changes were implemented in LISEM and evaluated on the hydrograph and sedigraph at the catchment outlet. They were found to have effects of different magnitude on the LISEM predictions. Predicted discharge decreased by about 50% from applying a slope correction for the calculation of overland flow, but was only marginally affected by using a slope dependent value of Manning's  $n$ . Predicted concentration increased by applying a concentration dependent fall velocity, but was hardly changed by introducing a map with loose material or by using sine instead of tangent in the transport equations. After recalibration the LISEM model simulated measured discharge and sediment yield only slightly better than before.

### **Lisem settings**

An evaluation of the effects of time step length and grid size on simulation results showed that simulated discharge decreased with increasing time step length and grid size. In both cases, this was partly due to the effect of the kinematic wave. Other important causes were a decrease in slope angle with an increase in grid size and the fact that for long time steps rainfall is averaged. The effect of time step length and grid size on simulated erosion was more complex and harder to explain. These results indicated that both time step length and grid size should be chosen before calibration starts.

### **Calibration and validation**

Calibration of the LISEM soil erosion model for the Danangou catchment showed that the LISEM model can in principle be applied to the Chinese Loess Plateau. The results, however, also showed that a separate calibration was needed for low-magnitude and high-



magnitude events and probably even for each event. Small events could not be calibrated well. This need for separate calibrations limits the usefulness of LISEM as a predictor of future discharge. However, application of LISEM to a number of rainfall events for which no runoff data were available showed that reasonable results were obtained for those events. Even though LISEM cannot be expected to predict actual runoff amounts, it might be able to predict whether or not a runoff event will occur.

Rill erosion intensity was mapped in the field and compared to LISEM simulations of erosion distribution. This comparison showed that the general appearance of simulated and mapped erosion patterns was similar, but also that the patterns are very different in detail. Many causes for this are possible, but it appears that:

- Current process descriptions are not well suited to simulate erosion processes on steep slopes.
- The raster-based approach of LISEM has the advantage to produce detailed erosion patterns, but the disadvantage that abrupt changes in flow conditions give unrealistic results.
- At present the datasets of model input and erosion patterns are not good enough for complex catchments. Especially inaccuracies in input data and DEM are likely to be important.

The evaluation of catchment soil loss and spatial erosion patterns as simulated by LISEM showed that there are severe limitations in applying such a model for this environment, especially with respect to predicting erosion patterns and future events. Simulation of different land use scenarios might be less problematic if a known event is used for all simulations, but should nevertheless be done with care.

### **Scenario simulations**

The effect of a number of land use and land management scenarios was simulated with LISEM. The simulations predicted that a decrease in runoff volume and erosion amount of about 5-20% could be reached by implementing conservation methods with the present land use distribution. Changing the land use according to slope-angle-based proposals was predicted to have a much larger effect; discharge decreased by 40-50%, while erosion decreased by 50-70%. The LISEM simulations did not show a clear difference in erosion rates between most land uses; only woodland/shrubland and orchard/cash tree seemed to have clearly lower erosion rates than the other land uses. The large increase in woodland/shrubland area in the scenario land use maps was therefore a direct cause for the large decrease in predicted erosion. Differences between scenarios with equal amounts of woodland were caused by conversion of cropland to orchard/cash tree. Simulations using different rainfall data showed that the simulation result for different scenarios might depend on storm size. A sensitivity analysis showed that the simulation results are most sensitivity to saturated conductivity and Manning's n. More research is needed before we can say to what degree the simulation results of LISEM reflect reality.



# **Bodemerosie modellering in een klein stroomgebied op het Chinese Löss Plateau: toepassing van LISEM onder extreme omstandigheden**

## **Samenvatting**

Het Chinese Löss Plateau is één van de gebieden op aarde met de hoogste erosie snelheden. Dit wordt veroorzaakt door het feit dat het Löss Plateau gekarakteriseerd kan worden als een semi-aride gebied met een lage vegetatiebedekking, erodeerbare bodems, steile hellingen en heftige buien in de zomer. De erosie heeft grote gevolgen, zowel ter plaatse als stroomafwaarts. Onderzoek naar bodemerosie op het Löss Plateau is nodig om manieren te vinden om de erosiesnelheden te verlagen.

In dit onderzoek werd het fysisch-deterministische, gedistribueerde, bodemerosie model LISEM (Limburg Soil Erosion Model) toegepast voor een klein stroomgebied op het Löss Plateau. Dit model simuleert bodemerosie voor individuele buien. Dergelijke modellen zijn nog niet vaak toegepast voor het Löss Plateau. In plaats daarvan heeft tot nu toe de nadruk van het erosieonderzoek gelegen op monitoring en op experimenten op proefveldjes. Om een fysisch-deterministisch erosiemodel toe te passen op het Löss Plateau is het nodig dat een aantal karakteristieken die specifiek zijn voor dit gebied in de beschouwing worden betrokken. De belangrijkste zijn:

- Dat sedimentconcentraties in het water zeer hoog kunnen zijn. Deze concentraties kunnen een groot effect hebben op vloeistofeigenschappen.
- Dat de hellingen steil zijn. In tegenstelling tot gebieden waar bodemerosiemodellen vaker zijn toegepast (Europa en de USA) komen in het Danangou stroomgebied akkers voor op hellingen van 60%. Zulke hellingshoeken kunnen belangrijke gevolgen hebben voor de stroomsnelheid van water en voor de transportcapaciteit van water.
- Dat er veel grote, permanente, gullies zijn.

## **Onderzoeksgebied**

Het onderzoeksgebied was het Danangou stroomgebied, een stroomgebied van 3.5 km<sup>2</sup> in het heuvelachtige deel van het Löss Plateau en gelegen in het noorden van de provincie Shaanxi. De hoogte van het stroomgebied varieert van 1075 tot 1370 meter en de hellingen zijn steil. Het klimaat is semi-aride, met een gemiddelde jaarlijkse neerslag van iets meer dan 500 mm en met grote variaties van jaar tot jaar. Neerslag is geconcentreerd in zomerbuien met een hoge intensiteit die voor kunnen komen tussen juni en september. De belangrijkste landgebruiken in het stroomgebied zijn natuurlijk grasland (40%), akkers (28%) en braakliggende akkers (21%). De vegetatiebedekkingsgraad is over het algemeen laag en omdat de bodems erodeerbaar zijn zijn ze gevoelig voor erosie tijdens de zomerbuien. Er is alleen afvoer tijdens deze buien. Bodemverlies tijdens de buien kan groot zijn omdat de afvoer toe kan nemen tot meer dan 10m<sup>3</sup>/s en sediment concentratie op kan lopen tot tenminste 500 g/l.

## **Gegevens**

Om bodemerrosie in het Danangou stroomgebied te bestuderen werden verschillende typen metingen uitgevoerd in de periode 1998-2000:

- Metingen van parameters die nodig zijn om bodemerrosie modellen zoals LISEM te kunnen gebruiken. Planteigenschappen en bodemeigenschappen werden iedere twee weken gemeten van april tot oktober, zowel in 1998 als in 1999. Bodemfysische eigenschappen zoals verzadigde doorlatendheid en de relaties die bestaan tussen vochtgehalte, zuigspanning en onverzadigde doorlatendheid werden in enkele afzonderlijke campagnes gemeten.
- Neerslag werd continue gemeten van april tot oktober voor alle drie de jaren. Hiervoor werden zowel regenmeters die intensiteiten kunnen meten als regenmeters die alleen de totale hoeveelheid regen meten gebruikt.
- Afvoer en sediment concentratie werden op verschillende plaatsen gemeten. Een V-vormige stuw werd in het stroomgebied gebouwd om de afvoer te meten van de bovenste 2 vierkante kilometer van het stroomgebied. 2 meetgoten werden gebruikt om de afvoer te meten van een gully en van een steile akker.
- Erosie werd gemeten/geschat met erosie pinnen, door het karteren van rills en met een inventarisatie van in het gebied aanwezige gullies.

## **Hoge concentraties**

Sediment concentraties in de afvoer op het Chinese Löss Plateau kunnen heel hoog worden, concentraties van 1000 g/l worden regelmatig gemeten. Bij zulke concentraties neemt de stroming een positie in die inzit tussen normale afvoer in rivieren en puinstromen. Dit type stroming wordt hypergeconcentreerde stroming genoemd. De reden dat dit type stroming in dit gebied veel voorkomt is waarschijnlijk dat erodeerbaar materiaal (löss) aanwezig is op steile hellingen. De eigenschappen van de löss en het klimaat kunnen ook een rol spelen. Met een toename in sediment concentratie gaan vloeistofeigenschappen geleidelijk veranderen: de dichtheid wordt groter, de viscositeit wordt groter en de valsnelheid van sediment wordt kleiner. Deze veranderingen beïnvloeden ook stroomsnelheid en transportcapaciteit van de stroming. Als de concentraties hoog genoeg worden gaan feedbackmechanismen een rol spelen. Deze mechanismen zorgen ervoor dat de stroming zich anders gedraagt dan normale stroming in rivieren. Transportcapaciteit kan bijvoorbeeld toenemen met een toename in concentratie. Als erosiemodellen worden toegepast voor gebieden waar concentraties zo hoog kunnen worden moet rekening gehouden worden met deze veranderingen van vloeistofeigenschappen.

Metingen in het Danangou stroomgebied hebben laten zien dat concentraties bij de stuw op kunnen lopen tot zo'n 500 g/l. Stroming van een akker bevatte zelfs 700 g/l sediment in een bepaald geval. Ondanks het feit dat de concentraties dus behoorlijk hoog waren werden er geen aanwijzingen gevonden die aangaven dat de vergelijkingen die gebruikt zijn om de afvoer te berekenen aangepast zouden moeten worden. Wel was een aantal andere aanpassingen nodig om de modelresultaten te kunnen vergelijken met de meetgegevens. De eerste is dat wanneer een drukopnemer werd gebruikt om de waterhoogte te meten het nodig was om te corrigeren voor de dichtheid van de vloeistof. Ook moet het volume van het sediment afgetrokken worden van het totale

vloeistofvolume om de totale hoeveelheid schoon water te bepalen. De hoeveelheid schoon water kan vergeleken worden met de modelresultaten. Voor de meetgoot die werd gebruikt om afvoer van een akker te meten bleek het nodig om de laag sediment die zich na een bui in de goot had gevormd af te trekken van de gemeten waterniveaus. Tenslotte moeten gemeten concentraties gecorrigeerd worden naar concentraties uitgedrukt als het aantal gram per liter schoon water, in plaats van als het aantal gram per liter vloeistof. Voor de concentraties gemeten in het Danangou stroomgebied is de valsnelheid van sediment nog maar 50% van de valsnelheid in schoon water. Een correctie voor valsnelheid is daarom nodig voor bodemerosie modellen die worden toegepast op gebieden met hoge concentraties.

### **Stroomsnelheid**

Bijna alle huidige fysisch gebaseerde erosiemodellen gebruiken de vergelijking van Manning om de stroomsnelheid uit te rekenen. Om de geldigheid van de Manning vergelijking te testen werd een reeks van 62 afstromingsproeven gedaan, waarbij Manning's n werd gemeten voor alle belangrijke landgebruiken die in het Danangou stroomgebied voorkomen. De meeste aandacht ging echter uit naar akkers. De metingen op de akkers lieten zien dat Manning's n geen constante waarde had, maar dat de waarde toenam met een toename in hellingshoek. De oorzaak hiervan is bodemerosie, die niet alleen de bodemruwheid vergroot maar ook de afstand die het water aflegt vergroot. Ook is er energie nodig om al het sediment te kunnen transporteren. Deze energie kan dus niet gebruikt worden om de stroomsnelheid te vergroten. Het netto effect is dat voor de erodeerbare bodems in het stroomgebied er geen toename was van de stroomsnelheid bij een toename in hellingshoek. Voor bodems die niet erodeerbaar zijn (zoals in bos) was zo'n toename er wel. In die gevallen bleek de stroomsnelheid af te hangen van de bodembedekkingsgraad. Een regressie vergelijking werd gebruikt om voor akkers de waarde van Manning's n uit te rekenen uit de hellingshoek. Deze vergelijking werd vervolgens gebruikt om een kaart te maken met hellingshoekafhankelijke waarden voor Manning's n.

### **Transportcapaciteit**

Verschillende transport vergelijkingen werden toegepast op het Danangou stroomgebied door ze in het LISEM model in te bouwen. Het model werd vervolgens op het hele stroomgebied toegepast. De resultaten lieten zien dat de Shields parameter ongeschikt is voor het stroomgebied. Dat komt door de steile hellingen, de grote vloeistof dichtheid en de kleine korrelgroottes die kenmerkend zijn voor het gebied. Het gevolg is dat vergelijkingen die de Shields parameter gebruiken de transportcapaciteit voor steile hellingen overschatten. Hetzelfde geldt voor vergelijkingen die kritieke afvoer gebruiken. Het blijkt dat in beide gevallen de grenswaarde die nodig is voor transport in de vergelijkingen verwaarloosd kan worden en dat de resulterende vergelijkingen te gevoelig zijn voor hellingshoek. De vergelijking van Govers (1990) hangt minder sterk af van hellingshoek en bleek ook betere voorspellingen te geven dan de andere vergelijkingen. De vergelijking van Yang lijkt te gevoelig te zijn voor korrelgrootte.

Simulaties voor het meetveld op de akker lieten zien dat de vergelijking van Govers voor oppervlakkige afstroming goed presteert voor de grotere buien, zoals de bui van 29

augustus 2000. Voor kleinere buien blijkt echter dat de vergelijking de transportcapaciteit van het water onderschat. Dit heeft mogelijk te maken met de grote invloed die de zwaartekracht kan hebben op sediment transport als de hellingshoek groot is.

Deze resultaten laten zien dat de vergelijking van Govers toegepast kan worden voor de meeste omstandigheden die voorkomen in het onderzoeksgebied. Het gebruik van de vergelijking van Govers wordt daarom aangeraden voor erosiemodellen die worden toegepast voor kleine korrelgroottes op steile hellingen.

### **Gullies**

Gully erosie is een belangrijk proces op het Chinese Löss Plateau. Ook in het Danangou stroomgebied komen veel gullies voor. Herhaalde waarnemingen hebben echter laten zien dat de achterwand van de gullies in het stroomgebied zich nauwelijks terugtrekt tijdens individuele buien. In plaats daarvan accumuleert er los materiaal op de bodem van de gullies doordat er materiaal van de gully-wanden valt tussen buien. Dit losse materiaal kan dan makkelijk worden opgenomen zo gauw er afvoer optreedt. Het proces van afstortend materiaal treedt niet op bui-basis op en kan daarom niet gemodelleerd worden met het LISEM model. In plaats daarvan werd er een model ontwikkeld dat werkt met een dagelijkse tijdstap en dat het afstorten van materiaal simuleert als een functie van bodemvocht, cohesie en de hoogte van de achterwand. Dit model levert een kaart die aangeeft hoeveel los materiaal er is geaccumuleerd op de bodem van de gullies. Deze kaart kan vervolgens dienen als invoer voor bodemerosie simulaties op bui-basis.

Het bleek niet mogelijk om een betrouwbare sedimentbalans voor het Danangou stroomgebied op te stellen. Dat kwam door een aantal problemen. Ten eerste werden in 1998 niet alle buien gemeten bij de stuw. Het gevolg is dat de totale hoeveelheid erosie voor dat jaar onzeker is. Ten tweede was de inventarisatie van de hoeveelheid los materiaal die in de gullies was geaccumuleerd niet compleet omdat veel gullies ontoegankelijk zijn en omdat het totale aantal gullies zo groot is dat ze niet allemaal bezocht konden worden. Ten derde accumuleert los materiaal niet alleen door kleine afstortingen, maar ook door grotere massabewegingen. Zulke massabewegingen komen niet vaak voor, maar als ze optreden kunnen ze lang materiaal blijven leveren tijdens buien. Ook bleek dat de erosiesnelheden voor oppervlakkige erosie hoog waren. Deze snelheden werden gemeten op een akker, maar om de daar gemeten snelheden te extrapoleren naar het hele stroomgebied was het nodig om een ratio te gebruiken die aangeeft welk deel van het geërodeerde materiaal ook daadwerkelijk de akker verlaat. Er zijn geen harde gegevens over die ratio, terwijl de keuze voor een bepaalde waarde van die ratio wel grote gevolgen heeft voor de schatting van de totale hoeveelheid oppervlakkige erosie. Tenslotte was kartering van rill erosie alleen mogelijk op akkers omdat voor andere landgebruiken het onbekend is of daar aanwezige rills wel tijdens een bepaald jaar gevormd zijn. Als gevolg daarvan kunnen de erosiesnelheden voor grasland, bos, boomgaard en braakliggende akkers alleen geschat worden.

Vanwege deze onzekerheden is het niet mogelijk een nauwkeurige schatting te maken van hoeveel materiaal er uit de gullies komt en hoeveel van de akkers. De best mogelijke schatting zou zijn dat 20-50% van het materiaal dat het stroomgebied verlaat van de akkers komt, terwijl 40-70% uit de gullies komt.

### **Aanpassingen van LISEM**

Een aantal veranderingen was nodig om het LISEM model toe te kunnen passen voor de steile hellingen, hoge concentraties en permanente gullies van het onderzoeksgebied. Deze veranderingen omvatten een correctie voor hellingshoek, het gebruik van een hellingshoek afhankelijke waarde voor Manning's  $n$ , de correctie van de valsnelheid van sediment, het gebruik van een kaart die aangeeft hoeveel los materiaal er in het gebied aanwezig is en het gebruik van de sinus in plaats van de tangens van de hellingshoek. Deze veranderingen werden aangebracht in LISEM, en de effecten van de veranderingen werden onderzocht. Het bleek dat sommige veranderingen grote gevolgen hadden, terwijl het resultaat van andere gering was. De gesimuleerde afvoer nam af met 50% door het toepassen van een helling correctie, maar werd nauwelijks beïnvloed door het gebruik van een variabele waarde voor Manning's  $n$ . Voorspelde sediment concentraties namen toe door het gebruik van een correctie op de valsnelheid, maar veranderden nauwelijks bij het gebruik van een kaart met los materiaal, of door het gebruik van sinus in plaats van tangens. Het bleek dat de voorspellingen van LISEM na hercalibratie van het model niet veel beter waren dan voordat de veranderingen werden doorgevoerd.

### **Instellingen van LISEM**

Er werd onderzocht wat het effect is van de keuze van de LISEM instellingen pixel grootte en lengte van de tijdstap in het model. Beiden bleken grote invloed te hebben op de voorspellingen van het model. Voor de afvoer voorspelling bleek in beide gevallen de kinematische-golf vergelijking (kinematic wave) een gedeeltelijke verklaring te zijn. Andere belangrijke oorzaken waren de verandering van hellingshoek bij een verandering van pixel grootte en het feit dat voor lange tijdstappen de regengegevens gemiddeld werden. Het effect op de voorspelling van erosie was complexer en moeilijker te verklaren. Deze resultaten laten in ieder geval zien dat zowel pixel grootte als de lengte van de tijdstap gekozen moeten worden voordat het model gecalibreerd wordt.

### **Calibratie en validatie**

Calibratie van het LISEM model liet zien dat het model in principe gebruikt kan worden voor het Löss Plateau. De resultaten lieten echter ook zien dat een aparte calibratie nodig is voor grote en kleine buien, en mogelijk zelfs voor iedere bui. Het bleek ook moeilijk om kleine buien te calibreren. Deze aparte calibraties betekenen dat het moeilijk is om LISEM te gebruiken om de afvoer van toekomstige buien te voorspellen. LISEM werd ook toegepast op een aantal buien waarvoor geen kwantitatieve afvoergegevens beschikbaar waren. Deze simulaties gaven redelijke resultaten en suggereerden dat hoewel LISEM niet gebruikt kan worden om de hoeveelheid afvoer nauwkeurig te voorspellen het wel gebruikt kan worden om te voorspellen of er wel of geen afvoer optreedt.

De intensiteit van rill erosie werd in het veld gekarteerd en vergeleken met voorspellingen van het LISEM model. Deze vergelijking liet zien dat de erosiepatronen in grote lijnen wel overeen kwamen, maar dat er toch op kleinere schaal grote verschillen waren. Daar zijn verschillende redenen voor aan te voeren, maar de belangrijkste zijn waarschijnlijk dat:

- Huidige procesbeschrijvingen niet erg geschikt zijn voor erosie processen op steile hellingen.
- De pixel benadering van LISEM weliswaar als voordeel heeft dat gedetailleerde erosiepatronen voorspeld kunnen worden, maar als nadeel dat er abrupte overgangen in hellingshoek op kunnen treden, die onrealistische resultaten kunnen veroorzaken doordat de stromingscondities te snel veranderen.
- Tot nu toe de gegevens die beschikbaar zijn van onvoldoende kwaliteit zijn om erosie patronen correct te kunnen voorspellen. Vooral onnauwkeurigheden in het digitale hoogtemodel kunnen belangrijk zijn.

De evaluatie van de LISEM resultaten voor bodemverlies uit het stroomgebied, en voor erosie patronen in het stroomgebied liet zien dat er grote beperkingen zijn voor het toepassen van een dergelijk model voor Löss Plateau omstandigheden. Deze beperkingen gelden vooral de voorspelling van toekomstige buien en van erosie patronen. Voor scenario simulaties zijn de beperkingen kleiner, maar toch moeten zulke analyses met voorzichtigheid gebeuren.

### **Simulatie van scenario's**

Het effect van een aantal landgebruik en land management scenario's werd met LISEM gesimuleerd. Deze simulaties voorspelden dat door het toepassen van anti-erosie maatregelen voor het huidige landgebruik de hoeveelheid erosie met 5-20% verkleind kan worden. Er werd ook voorspeld dat een verandering van het landgebruik zelf tot grotere reducties kan leiden: afvoer nam volgens het model af met 40-50% en erosie met 50-70% voor alternatieve landgebruiken die waren gebaseerd op het beperken van akkers tot minder steile hellingen. De simulatie resultaten lieten echter geen duidelijk verschil in erosie zien voor de meeste landgebruiken, alleen bos/struikgewas en boomgaard bleken duidelijk lagere erosiesnelheden te hebben dan de andere landgebruiken. Volgens de scenario's neemt het bos oppervlak aanzienlijk toe. De voorspelde afname in erosie is hiervan een direct gevolg. Verschillen tussen scenario's met gelijke hoeveelheden bos werden veroorzaakt door de omzetting van akkers in boomgaard. Simulaties waarbij andere buien werden gebruikt lieten zien dat de resultaten afhankelijk kunnen zijn van de grootte van de bui. Een gevoeligheidsanalyse liet zien dat de modelvoorspellingen het meest gevoelig waren voor verzadigde doorlatendheid en voor de waarde van Manning's n. Er is meer onderzoek nodig voordat duidelijk kan worden in hoeverre deze simulatie resultaten de werkelijkheid weerspiegelen.



# 中国黄土高原小流域土壤侵蚀模拟 —极端条件下 LISEM 模型的应用

## （摘要）

中国黄土高原是世界上水土流失最为严重的地区。这主要是由于黄土高原地处半干旱地区、植被稀疏、土壤可蚀性强、地形陡峭以及夏季偶发暴雨所造成的。土壤侵蚀严重地影响了黄土高原当地和下游环境。因此，研究黄土高原的土壤侵蚀，对于水土流失治理具有十分重要的意义。

本项研究，应用空间分布式土壤侵蚀物理模型 LISEM，研究中国黄土高原小流域的土壤侵蚀。在黄土高原地区，土壤侵蚀研究主要集中在土壤侵蚀监测和径流小区试验方面，有关这类空间分布式土壤侵蚀物理模型的应用尚未见报道。为了能成功地应用 LISEM 模型模拟该区的土壤侵蚀，必须考虑黄土高原的几个特殊性质。

其中，最重要的特征为：

- 极高浓度的泥沙含量可能对流体特征产生显著的影响；
- 地形陡峭。与壤侵蚀模型经常应用的地区（欧洲和美国）相反，大南沟小流域的坡耕地一般大于 60%。这么陡峭的坡度可能对径流速度及其运移力产生显著的影响；
- 大量永久性切沟广泛分布。

## 研究区域

研究地点在中国陕北黄土丘陵沟壑区大南沟小流域，面积约 3.5 平方公里。该小流域海拔为 1075—1370 米，坡度很大。气候为半干旱气候，年均降雨量为 500 毫米左右，年际变化较大。降雨主要集中在 6—9 月份，多为夏季高强度暴雨。该小流域主要的土地利用方式为荒草地（40%）、农地（28%）和休闲地（21%）。该小流域植被盖度低、黄土可蚀性强，在暴雨过程中极易发生土壤侵蚀。但是，只有在夏季暴雨过程中，整个小流域才可能产生径流。流速很高（>10 立方米/秒），造成土壤流失也很严重，泥沙含量最少可高达 500 克/升。

## 数据的获取

为了研究大南沟小流域的土壤侵蚀，在 1998—2000 年共三年间，观测并收集了下述几方面数据：

- LISEM 模型参数。1998 年和 1999 年每年 4 月至 10 月，每两周一次对植物和土壤特征进行了观测。另外，还单独观测了诸项土壤物理性质，如饱和导水率以及土壤含水量、持水力和非饱和导水率的相互关系。
- 降雨。每年 4 月—10 月，采用 6 个翻斗式自动雨量记和几个人工雨量筒观测降雨。

- 径流量和泥沙含量：在大南沟小流域内选取了一个约 2 平方公里的小流域，并在其出口修建了一个量水堰；在一个切沟出口和一个坡耕地上分别安装了一个径流槽。分别在这三个地方观测径流量和泥沙含量。
- 土壤侵蚀量。分别采用侵蚀测针观测（Erosion pin）、细沟侵蚀图绘制和切沟调查法，估测土壤侵蚀量。

### 泥沙含量高

在中国黄土高原地区，径流中的泥沙含量十分高，经常高达 1000 克/升。这种泥沙含量的水流介于正常河流和泥石流之间，被称为高含沙水流

（hyperconcentrated flow）。这种高含沙水流的形成，一方面可归因于广泛分布在陡坡上的易蚀物质（黄土），另一方面黄土的特殊性质及其特殊气候条件也是重要的影响因子。一般说来，随着泥沙含量的增高，流体特征也发生相应的变化，即密度增加、粘度增加、沉积速度降低。这些变化也将影响到流速及其运移力。当泥沙含量足够高时，反馈机制开始起作用，导致流体表现出与正常河流显著不同的行为特征。例如，水流的运移力随着泥沙含量的增高而增强。显然，在高含沙水流地区应用土壤侵蚀模型时，必须考虑这些流体特征。

在大南沟小流域，流域出口观测到的泥沙含量为 500 克/升，径流小区高达 700 克/升。尽管从理论上说，这种高浓度泥沙含量会显著改变水流性质，但研究表明，水坝或小区的流量方程并不需要改用其他方程。但是，为了把测量结果和模拟结果进行比较，必须进行下述几个方面的修正。首先，当采用压力变频器

（pressure transducer）测量水位时，应该用流体密度来对信号进行修正。第二，应该用整个浑水体积减去泥沙体积，得到纯粹的水体积，以便与模型的模拟结果进行比较。对径流小区的水槽来说，也应该从整个浑水总量中减去泥沙总量。最后，所观测到的泥沙含量应该换算为纯水中的泥沙含量（克/升）而不是整个浑水中的泥沙含量（克/升）。研究表明，在大南沟小流域所观测的高泥沙含量的情况下，沉积速度（settling velocity）经过换算可减少为其纯水体积的 50%。因此，在模拟高泥沙含量的土壤侵蚀模型中，必须依据泥沙含量对沉积速度进行修正。

### 水流速度

现在，几乎所有基于物理过程的土壤侵蚀模型都采用曼宁方程（Manning equation）来计算水流速度。为了验证曼宁方程的有效性，根据大南沟小流域的主要土地利用类型，总共进行了 62 次水流试验。其中，绝大多数试验是在农地上进行的。这些试验结果表明，农地的曼宁系数并不是一个常数，而是随着坡度的增加而增大。这主要归因于土壤侵蚀，即随着坡度增大土壤侵蚀增强，从而导致土壤粗糙度增加、水流路径增长。携带这些泥沙同样需要耗费大量能量，而这些能量本可以用来提高水流速度的。大南沟小流域的研究表明，在可蚀较强的土壤（农地）上，水流速度并没有随着坡度的增大而增加；相反在可蚀性较弱的土壤（如林地）上，水流速度随着坡度的增大而增加，曼宁系数与坡度无关，却表现出与地表覆盖存在显著相关性。据此，本文构建了一个一元回归方程，利用该方程可根据坡度预测农地的曼宁系数。本文利用该方程计算了整个小流域中农地的曼宁系数，并生成

了曼宁系数分布图，做为 LISEM 模型的输入参数。可见，在本项研究中，LISEM 模型的曼宁系数是随着坡度的改变而变化的。

## 运移能力

通过编程，在 LISEM 模型中预置了下述几个运移方程（transport equation），并用于整个大南沟小流域的土壤侵蚀模拟。研究发现，Shield 参数并不适用于大南沟小流域。这是因为该小流域坡度较大、水流密度较高、土壤粒径较小，所有这些都导致 Shield 参数值太高。因此，在运移方程中使用 Shield 参数，就会高估运移力，尤其在估计陡坡水流运移力时更为严重。同理，因为临界径流值（critical discharge）非常小，所以如果用于估计运移力，也会高估运移力。研究表明，如果忽略运移临界值，绝大多数运移方程对坡度变化都过于敏感。根据 Govers（1990）方程计算的河流运移力与坡度的关系不显著，相对来说其估测效果最好。另外，Yang 方程对土壤粒径变化过于敏感。

径流小区的模拟表明，当有效水分充足时，比如在 2000 年 8 月 29 日的暴雨事件中，Govers 方程对地表径流（overland flow）运移能力的估测精度比较高。但是对于小降雨事件来说，Govers 方程会低估地表径流的运移能力。这是因为，重力作用对陡坡上的运移力具有重要影响。

上述结果表明，对于坡度较大、粒径较小的土壤来说，Govers 方程比其他方程能更好地估测水流的泥沙运移能力。研究发现，该方程也同样适用于大南沟小流域的大多数水流条件。因此，既然在模拟时只使用一个方程式来估测全流域运移力的效果会更好，那么在大南沟小流域这种条件下，建议使用 Govers 方程。

## 切沟

在中国黄土高原地区，切沟侵蚀是一个非常重要的侵蚀和地貌过程。大南沟小流域也不例外，被切沟切割得支离破碎。但是，大南沟小流域的重复观测表明，在每次暴雨事件中，切沟的向源切割（headcuts）推移现象并不明显。相反，在两次降雨间期，土壤坍塌（soil fall）导致疏松物质（土壤）容易在切沟地表累积。然而，这些疏松物质在第一次降雨产流过程中也容易被冲走。土壤坍塌并不是在暴雨过程中发生的，因此不能采用诸如 LISEM 之类的土壤侵蚀模型来模拟。相反，可以构建一个以天为步长的模型来模拟土壤坍塌，该模型认为土壤坍塌是土壤含水量、粘结力（Cohesion）和向源切割高度的函数。该模型的输出结果是一张图，详细标明了在切沟地表上堆积的疏松物质数量。在次降雨土壤侵蚀模拟过程中，该图可用来模拟额外的泥沙来源。

事实证明，几乎不可能在大南沟小流域建立一个可靠的泥沙平衡。这是由以下几个问题所造成的。首先，在 1998 年没有观测到小流域出口的所有产流过程，因此无法估算该流域 1998 年全年的土壤流失总量。第二，对堆积在切沟地表的疏松物质的调查也不完全。因为有许多切沟没有办法调查，而且切沟的数量太多，只能调查较大的切沟。第三，土壤坍塌可以导致疏松物质在切沟的累积，另外偶发的大规模土壤运移（larger mass movement）不仅可以造成疏松物质的累积，而且还可以长期为河流输送泥沙。第四，本研究发现该小流域的土壤面蚀强度也很高。面蚀强度是在径流小区上观测的，但是很难把该观测结果外推到整个小流域，因为这

必须应用泥沙传递比（sediment delivery ratio）。因此，土壤面蚀强度的估算值在很大程度上决定于泥沙传递比值的选择。最后一点，只能绘制该小流域农地的细沟侵蚀图。对其他土地利用方式而言，很难确定其侵蚀特征的具体发生年份。因此，对荒草地、林地、果园和休闲地上的土壤侵蚀强度而言，只能采取估计的方法。在上述这些不确定性的情况下，本文所估测的农地土壤侵蚀约占全部土壤侵蚀的20%—50%。同理，切沟侵蚀占40%-70%。对较大强度的降雨事件而言，农地土壤侵蚀所占的比重可能会增加。

### **LISEM 模型的改进**

正如前述，在大南沟小流域，坡度陡峭、泥沙含量高和永久切沟广泛分布影响了土壤侵蚀模拟精度。因此，本文采取了一系列措施来改进 LISEM 模型，包括地表径流计算中的坡度修正，采用坡度有关的曼宁系数，引入与泥沙含量相关的沉积速度，引进疏松物质分布图，在运移方程中使用正弦代替正切。本项研究，首先在 LISEM 模型操作中实施这些改进措施，然后根据小流域出口的水文图和泥沙图来评价改进效果。研究表明，改进措施不同，对 LISEM 模型预测值的影响也不同。当应用坡度修正法计算地表径流时，流域出口的径流预测值比原来降低了50%；但是采用与坡度相关的曼宁系数时，径流预测结果变化较小。当应用与泥沙含量有关的沉积速度时，流域出口泥沙含量的预测值增加；但是通过引进疏松物质分布图或在运移方程中使用正弦代替正切，泥沙含量的预测结果几乎不变。整体说来，在对 LISEM 模型进行重校准后，径流量和产沙量的模拟精度提高很小。

### **LISEM 模型的设置**

通过评价时间步长和像元大小对模拟结果的影响发现，随着时间步长增长和像元增大，流域出口的径流模拟值降低。在这两种情况下，部分原因是由于运动波（kinematic wave）的影响。其他重要原因还有：坡度随着像元大小的增大而降低，降雨随着时间步长的增长而趋于平均。时间步长和像元大小对侵蚀量模拟值的影响更加复杂，而且很难解释。所有这些结果表明，在模型校准之前，就需要提前确定时间步长和像元大小。

### **校准与校正**

经过校准发现，LISEM 土壤侵蚀模型原则上可以应用于中国黄土高原地区小流域的土壤侵蚀模拟，但是对高强降雨和低强度降雨事件需要分别单独校准，甚至可能对每次降雨事件都需要重新校准。一般说来，对低强度降雨的校准效果不是很理想。这些表明，LISEM 不能用于黄土高原地区未来降雨事件的径流和侵蚀预报。但是，通过对大量降雨事件的模拟发现，LISEM 模型可以获得比较合理的模拟结果。尽管 LISEM 模型不能预测实际的径流量，但它至少可以预测某次降雨是否产流。

在野外调查并绘制了细沟侵蚀强度图，并把它和 LISEM 模型预测的侵蚀强度分布图相比较。结果表明，LISEM 预测结果和调查结果整体上比较相似，但是其分布细节相差很大。原因是多方面的，包括：

- 当前 LISEM 模型中所使用的侵蚀过程，并不适宜于模拟陡坡上的侵蚀过程；
- 栅格式土壤侵蚀模型的主要优点是可以生成细致的侵蚀空间分布格局，但是这类模型的缺点是不能对水流状态的突变给出合理的模拟结果；
- 目前，LISEM 模型的输入数据集和侵蚀过程存在一些问题，尚不能对复杂小流域环境的土壤侵蚀过程进行较好的模拟。尤其以模型输入数据和 DEM 图的准确度问题最为重要。

通过对整个小流域的土壤侵蚀总量和侵蚀空间分布模拟结果的评价表明，大南沟小流域这种环境条件，严重地限制了 LISEM 模型的应用。尤其在对侵蚀空间分布格局和未来降雨事件进行模拟和预测时，LISEM 模型的局限性更为显著。但 LISEM 可以用于模拟不同土地利用方案在同一次观测降雨事件中的水土流失效应，当然也要小心谨慎。

### 情景 (scenarios) 模拟

应用 LISEM 模型，模拟了大量土地利用方式和土地管理措施的水土流失效应。模拟结果表明，保持土地利用现状，采用相应的水土保持措施，径流量和泥沙量可以减少 5—20%。陡坡农地退耕情景的水土保持效应更为显著，径流量降低 40-50%，侵蚀量降低 50-70%。LISEM 模型的预测结果表明，一般说来，土地利用方式之间土壤侵蚀强度的差异很小；只有林地/灌木地和果园/经济林的土壤侵蚀强度显著低于比其他几种土地利用方式。显然，在农地退耕情景模拟中，整个小流域出口水土流失模拟值减少的主要原因，是由林地/灌木地面积的大量增加所造成的。林地/灌木地数量相同的不同土地利用情景之间，其水土流失模拟值的差异是因为农地向果园/经济林的转变所引起的。利用不同降雨数据的模拟结果表明，暴雨大小在一定程度上决定了不同土地利用情景的模拟结果。敏感性分析表明，模拟结果与饱和导水率和曼宁系数  $n$  最为敏感。显然，要进一步提高 LISEM 模型的模拟精度，还需要进一步的深入研究。



## REFERENCES

- Abrahams, A.D., A.J. Parsons & Shiu-Hung Luk (1986), Field measurement of the velocity of overland flow using dye tracing. *Earth Surface Processes and Landforms* 11, pp. 653-657
- Abrahams, A.D., A.J. Parsons & Shiu-Hung Luk (1990), Field experiments on the resistance to overland flow on desert hillslopes. *IAHS Publication* 189, pp. 1-18
- Abrahams, A.D., G. Li, C. Krishnan & J.F. Atkinson (2001), A sediment transport equation for interrill overland flow on rough surfaces. *Earth Surface Processes and Landforms* 26, pp. 1443-1459
- Alonso, C.V., W.H. Neibling & G.R. Foster (1981), Estimating sediment transport capacity in watershed modeling. *Transactions of the ASAE* 24, pp. 1211-1220, 1226
- Bagnold, R.A. (1980) An empirical correlation of bedload transport rates in flumes and natural rivers. *Proceedings of the Royal Society of London A* 372, pp. 453-473
- Batalla, R.J., C. de Jong, P. Ergenzinger & M. Sala (1999), Field observations on hyperconcentrated flows in mountain torrents. *Earth Surface Processes and Landforms* 24, pp. 247-253
- Belmans, C., J.G. Wesseling & R.A. Feddes (1983), Simulation model of the water balance of a cropped soil: SWATRE. *Journal of Hydrology* 63, pp. 271-286
- Beschta, R.L. (1987), Conceptual models of sediment transport in streams. In: Thorne, C.R., J.C. Bathurst & R.D. Hey (eds.) *Sediment transport in Gravel-bed rivers*, pp. 387-419
- Beuselinck, L., G. Govers, J. Poesen, G. Degraer & L. Froyen (1998), Grain-size analysis by laser diffractometry: comparison with the sieve-pipette method. *Catena* 32, pp. 193-208
- Beven, K. (2001), On modelling as collective intelligence. *Hydrological Processes* 15, pp. 2205-2207
- Beven, K. (2002), Towards an alternative blueprint for a physically based digitally simulated hydrologic response modeling system. *Hydrological Processes* 16, pp. 189-206
- Beven, K.J., E.F. Wood & M. Sivapalan (1988), On hydrological heterogeneity-catchment morphology and catchment response. *Journal of hydrology* 100, pp. 353-375
- Billard, A., T. Muxart, A. Andrieu & E. Derbyshire (2000), Loess and water. Ch. 4 in: Derbyshire, E., Xingmin Meng & T.A. Dijkstra (eds.) *Landslides in the thick loess terrain of north-west China*. Chichester: Wiley, pp. 91-130
- Bocco V., G.H.R. (1990), Gully erosion analysis using remote sensing and geographic information systems. A case study in central Mexico. Ph.D. thesis. University of Amsterdam
- Borges, A., S. Brochot & M. Meunier (1995), Modèle hydrosédimentologique des écoulements hyperconcentrés d'un petit torrent des Alpes du sud. In : Meunier, M. (ed.) *Compte-rendu de recherches N° 3*. BVRE de Draix. Equipements pour l'eau et l'environnement 21. Cemagref, pp. 203-221
- Bos, M.G. (ed., 1989), *Discharge Measurement Structures*. ILRI publication 20, 3rd edition. ILRI, Wageningen
- Bradley, J.B. & S.C. McCutcheon (1987), Influence of large suspended sediment concentrations in rivers. In: Thorne, C.R., J.C. Bathurst & R.D. Hey (eds.) *Sediment transport in gravel bed rivers*. Chichester: Wiley, pp. 645-689
- Braun, P., T. Molnar, H.-B. Kleeberg (1997), The problem of scaling in grid-related hydrological process modelling. *Hydrological Processes* 11, pp. 1219-1230
- Brazier, R.E., K.J. Beven, J. Freer & J.S. Rowan (2000), Equifinality and uncertainty in physically based soil erosion models: Application of the GLUE methodology to WEPP – The water erosion prediction project – for sites in the UK and USA. *Earth Surface Processes and Landforms* 25, pp. 825-845

- Bryan, R.B (1987), Processes and significance of rill development. In: Bryan, R.B. (ed.) *Rill Erosion: Processes and significance*. Catena Supplement 8, pp. 1-15
- Bull, L.J. & M.J. Kirkby (1997), Gully processes and modelling. *Progress in Physical Geography* 21, pp. 354-374
- Burkard, M.B. & R.A. Kostaschuk (1997), Patterns and controls of gully growth along the shoreline of Lake Huron. *Earth Surface Processes and Landforms* 22, pp. 901-911
- Cantón, Y., F. Domingo, A. Solé-Benet & J. Puigdefàbregas (2001), Hydrological and erosion response of a badlands system in semiarid SE Spain. *Journal of Hydrology* 252, pp. 65-84
- Cerdan, O., Y. Le Bissonnais, V. Souchère, P. Martin & V. Lecomte (2002), Sediment concentration in interrill flow: Interactions between soil surface conditions, vegetation and rainfall. *Earth Surface Processes and Landforms* 27, pp. 193-205
- Chen, L., Jun Wang, Bojie Fu & Yang Qiu (2001), Land-use change in a small catchment of northern Loess Plateau, China. *Agriculture, Ecosystems and Environment* 86, pp. 163-172
- Chen, L., I. Messing, S. Zhang, B. Fu & S. Ledin (in press), Land use evaluation and scenario analysis towards sustainable planning on the Loess Plateau in China - case study in a small catchment. *Catena*
- Collison, A. (1996), Unsaturated strength and preferential flow as controls on gully head development. In: Anderson, M.G. & S.M. Brooks (eds.) *Advances in Hillslope Processes*. Vol. 2. Chichester: Wiley, pp. 753-769
- Collison, A.J.C. (2001), The cycle of instability: stress release and fissure flow as controls on gully head retreat. *Hydrological Processes* 15, pp. 3-12
- Costa, J.E. (1988), Rheologic, geomorphic, and sedimentologic differentiation of water floods, hyperconcentrated flows, and debris flows. Chapter 7 in: Baker, V.R., R.C. Kochel & P.C. Patton (eds.) *Flood Geomorphology*. New York: Wiley, pp. 113-122
- Crouch, R.J. (1987), The relationship of gully sidewall shape to sediment production. *Australian Journal Soil Research* 25, pp. 531-539
- Crouch, R.J. & T. Novruzzi (1989), Threshold conditions for rill initiation on a vertisol, Gunnedah, N.S.W., Australia. *Catena* 16, pp. 101-110
- Derbyshire, E. (1989), Mud or dust. Erosion of the Chinese loess. *Geography Review*, November 1989, pp. 31-35
- Derbyshire, E. & X. Meng (2000), Loess as a geological material. Ch 3 in: Derbyshire, E., Xingmin Meng & T.A. Dijkstra (eds.) *Landslides in the thick loess terrain of north-west China*. Chichester: Wiley, pp. 47-90
- Derbyshire, E., J. Wang, Z. Jin, A. Billard, Y. Egels, M. Kasser, D.K.C. Jones, T. Muxart & L. Owen (1991), Landslides in the Gansu loess of China. In: Okuda, S. et al. (eds.) *Loess Geomorphological hazards and processes*. Catena supplement 20, pp. 119-145
- Derbyshire, E., T.A. Dijkstra, A. Billard, T. Muxart, I.J. Smalley & Young-Jin Li (1993), Thresholds in a sensitive landscape: the loess region of central China. In: Thomas, D.S.G. & R.J. Allison (Eds.) *Landscape Sensitivity*. Chichester: Wiley, pp. 97-127
- Derbyshire, E., Xingmin Meng, A. Billard, T. Muxart & T.A. Dijkstra (2000), The environment: geology, geomorphology, climate and land use. Ch. 2 in: Derbyshire, E., Xingmin Meng & T.A. Dijkstra (eds.) *Landslides in the thick loess terrain of north-west China*. Chichester: Wiley, pp. 21-46
- De Roo, A.P.J. & V.G. Jetten (1999), Calibrating and validating the LISEM model for two data sets from the Netherlands and South Africa. *Catena* 37, pp. 477-493
- De Roo, A.P.J., C.G. Wesseling, N.H.D.T. Cremers, R.J.E. Offermans, C.J. Ritsema & K. van Oostindie (1994), LISEM: a new physically-based hydrological and soil erosion model in a GIS-environment, theory and implementation. *IAHS publication* 224, pp. 439-448



- De Roo, A.P.J., C.G. Wesseling & C.J. Ritsema (1996a), LISEM: a single-event physically based hydrological and soil erosion model for drainage basins: I: Theory, input and output. *Hydrological Processes* 10, pp. 1107-1117
- De Roo, A.P.J., R.J.E. Offermans & N.H.D.T. Cremers (1996b), LISEM: a single-event, physically based hydrological and soil erosion model for drainage basins. II: Sensitivity analysis, validation and application. *Hydrological Processes* 10, pp. 1119-1126
- DiCenzo, P.D. & Shiu-hung Luk (1997), Gully erosion and sediment transport in a small subtropical catchment, South China. *Catena* 29, pp. 161-176
- Dietrich, W.E. & T. Dunne (1993), The channel head. In: Beven, K. & M.J. Kirkby (eds.) *Channel network hydrology*. Chichester: Wiley, pp.175-219
- Dijkstra, T.A., C.D.F. Rogers, I.J. Smalley, E. Derbyshire, Li Yong Jin & Meng Xing Min (1994) The loess of north-central China: geotechnical properties and their relation to slope stability. *Engineering Geology* 36, pp. 153-171
- Dijkstra, T.A., F.E. Rappange, T.W.J. Van Asch, Yongjin Li & Boa Xing Li (2000), Laboratory and in situ shear strength parameters of Lanzhou loess. Ch. 5 in: Derbyshire, E., Xingmin Meng & T.A. Dijkstra (eds.) *Landslides in the thick loess terrain of north-west China*. Chichester: Wiley, pp. 131-172
- Doe, W.W. & R.S. Harmon (2001), Introduction to soil erosion and landscape evolution modeling. Ch 1 in: Harmon, R.S. & W.W. Doe (Eds.) *Landscape erosion and evolution modeling*. New York: Kluwer Academic/Plenum, pp. 1-14
- Douglas, I. (1989), Land degradation, soil conservation and the sediment load of the Yellow River, China: review and assessment. *Land degradation and rehabilitation* 1, pp. 141-151
- Dunkerly, D. (2001), Estimating the mean speed of laminar overland flow using dye tracing injection-uncertainty on rough surfaces. *Earth Surface Processes and Landforms* 26, pp. 363-374
- Einstein, H.A. & N. Chien (1955), effects of heavy sediment concentration near the bed on the velocity and sediment distribution. M.R.D. Sediment series 8, Missouri River Division, U.S. Corps of Engineers
- Elliot, W.J. (1988), A process-based rill erosion model. PhD thesis, Iowa State University
- Emmett, W.M. (1970), The hydraulics of overland flow on hillslopes. Geological Survey Professional Paper 662-A
- Engman, E.T. (1986), Roughness coefficients for routing surface runoff. *Journal of Irrigation and Drainage Engineering* 112, pp. 39-53
- Everaert, W. (1991), Empirical relations for the sediment transport capacity of interrill flow. *Earth Surface Processes and Landforms* 16, pp. 513-532
- Fang Zhengsan, Zhou Piehua, Liu Qiande, Liu Baihe, Ren Letian & Zhang Hanxiong (1981), Terraces in the Loess Plateau of China. In: Morgan, R.P.C. (ed.) *Soil Conservation: Problems and prospects*. Chichester: Wiley, pp. 481-513
- Favis-Mortlock, D., T. Guerra & J. Boardman (1998), A self-organizing systems approach to hillslope rill initiation and growth: model development and validation. IAHS publication 249, pp. 53-61
- Favis-Mortlock, D., J. Boardman & V. MacMillan (2001), The limits of erosion modeling: Why we should proceed with care. In: Harmon, R.S. & W.W. Doe (Eds.) *Landscape Erosion and Evolution Modeling*. New York: Kluwer Academic/Plenum, pp. 477-516
- Flanagan, D.C., J.C. Ascough, M.A. Nearing & J.M. Laflen (2001), The Water Erosion Prediction Project (WEPP) model. In: Harmon, R.S. & W.W. Doe (Eds.) *Landscape Erosion and Evolution Modeling*. New York: Kluwer Academic/Plenum, pp. 145-199
- Fread, D.L. (1985), Channel routing. Ch 14 in: Anderson, M.G. & T.P. Burt (Eds.) *Hydrological Forecasting*. Chichester: Wiley

- Fread, D.L. (1993), Flow routing. Ch 10 in: Maidment, D.R. (Ed.) Handbook of hydrology. New York: McGraw-Hill.
- Fu, B. & H. Gulinck (1994) Land evaluation in an area of severe erosion: the Loess Plateau of China. *Land Degradation & Rehabilitation* 5, pp. 33-40
- Garbrecht, J. & L. Martz (1994), Grid size dependency of parameters extracted from digital elevation models. *Computers & Geosciences* 20, pp. 85-87
- Gerits, J., A.C. Imeson, J.M. Verstraten & R.B. Bryan (1987), Rill development and badland regolith properties. In: Bryan, R.B. (ed.) *Rill Erosion: Processes and significance*. *Catena Supplement* 8, pp. 141-160
- Giménez, R. & G. Govers (2001), Interaction between bed roughness and flow hydraulics in eroding rills. *Water Resources Research* 37, pp. 791-799
- Gilley, J.E., D.C. Flanagan, E.R. Kottwitz & M.A. Weltz (1992), Darcy-Weisbach roughness coefficients for overland flow. In: Parsons, A.J. & A.D. Abrahams (eds.) *Overland flow hydraulics and erosion mechanics*. London: UCL Press, pp. 25-52
- Gong Shiyang & Jiang Deqi (1979), Soil erosion and its control in small watersheds of the loess plateau. *Scientia Sinica* 22, pp. 1302-1313
- Govers, G. (1987), Spatial and temporal variability in rill development processes at the Huldenberg experimental site. In: Bryan, R.B. (ed.) *Rill Erosion: Processes and significance*. *Catena Supplement* 8, pp. 17-34
- Govers, G. (1990), Empirical relationships for the transport capacity of overland flow. *IAHS publication* 189, pp. 45-63
- Govers, G. (1992a), Evaluation of transporting capacity formulae for overland flow. Chapter 11 in: Parsons, A.J. and A.D. Abrahams (eds.) *Overland Flow: hydraulics and erosion mechanics*. London: UCL Press
- Govers, G. (1992b), Relationships between discharge, velocity and flow area for rills eroding loose, non-layered materials. *Earth Surface Processes and Landforms* 17, pp. 515-528
- Graf, W.L. (1988), *Fluvial processes in dryland rivers*. Berlin: Springer
- Guy, B.T., W.T. Dickinson & R.P. Rudra (1992), Evaluation of fluvial sediment transport equations for overland flow. *Transactions of the ASAE* 35, pp. 545-555
- Haan, C.T., B.J. Barfield & J.C. Hayes (1994), *Design hydrology and sedimentology for small catchments*. San Diego: Academic Press
- Halbertsma, J.M. & G.J. Veerman (1997), Determination of the unsaturated conductivity and water retention characteristic using the Wind's evaporation method. In: Stolte, J. (ed.) *Manual for soil physical measurements*. Technical Document 37, DLO Winand Staring Centre, Wageningen, pp. 47-55
- Handy, R.L. (1973), Collapsible loess in Iowa. *Soil Science Society of America Proceedings* 37, pp. 281-284
- Harvey, A.M. (1994), Influence of Slope/Stream Coupling on Process Interactions on Eroding Gully Slopes: Hawgill Fells, Northwest England. In: Kirkby, M.J. (ed.) *Process models and theoretical geomorphology*. British Geomorphological Research Group Symposia Series 8. Chichester: Wiley, pp. 247-270
- Hessel, R., V. Jetten, Liu Baoyuan, Zhang Yan & J. Stolte (in press a), Calibration of the Lisem model for a small Loess Plateau catchment. *Catena*
- Hessel, R., V. Jetten, Zhang Guanghui, (in press b), Estimating Manning's n for steep slopes. *Catena*
- Hoang Fagerström, M.H., I. Messing, Z.M. Wen, K.O. Trouwborst, M.X. Xu, X.P. Zang, C. Olsson, C. Andersson (in press), A participatory approach for integrated conservation planning in a small catchment in Loess Plateau, China- Part II: Analysis and findings. *Catena*

- Horton, R.E. (1945), Erosional development of streams and their drainage basins; hydrophysical approach to quantitative morphology. *Bulletin of the Geological Society of America* 56, pp. 275-370
- Hossain, M.M. & M.L. Rahman (1998), Sediment transport functions and their evaluation using data from large alluvial rivers of Bangladesh. IAHS publication 249, pp. 375-382
- Hsieh Wen Shen & P.Y. Julien (1993), erosion and sediment transport. Chapter 5 in: Maidment, D.R. (ed.) *Handbook of Hydrology*. New York: McGraw-Hill
- Huang, C. (1995), Empirical analysis of slope and runoff for sediment delivery from interrill areas. *Soil Science Society of America Journal* 59, pp. 982-990
- Huang, C., L.K. Wells & L.D. Norton (1999), Sediment transport capacity and erosion processes: model concepts and reality. *Earth Surface Processes and Landforms* 24, pp. 503-516
- Huang, C.C., J. Pang & J. Zhao (2000), Chinese loess and the evolution of the east Asian monsoon. *Progress in Physical Geography* 24, pp. 75-96
- Imeson, A.C & F.J.P.M. Kwaad (1980), Gully types and gully prediction. *Geografisch Tijdschrift* 14, pp. 430-441
- Jetten, V. & A.P.J. de Roo (2001), Spatial Analysis of erosion conservation measures with LISEM. In: Harmon, R. & W.W. Doe (eds.) *Landscape Erosion and Evolution Modeling*. New York: Kluwer Academic/Plenum, pp. 429-445
- Jetten, V., J. Boiffin & A. de Roo (1996), Defining monitoring strategies for runoff and erosion studies in agricultural catchments: a simulation approach. *European Journal of Soil Science* 47, pp. 579-592
- Jetten, V., A. de Roo & J. Guérif (1998), Sensitivity of the model Lisem to variables related to agriculture. In: Boardman, J. & D. Favis-Mortlock (eds.) *Modelling soil erosion by water*. NATO ASI Series I 55. Berlin: Springer, pp. 339-349
- Jetten, V., A. de Roo & D. Favis-Mortlock (1999), Evaluation of field-scale and catchment-scale soil erosion models. *Catena* 37, pp. 521-541
- Jetten, V., G. Govers & R. Hessel (in press), Erosion models: quality of spatial predictions. *Hydrological Processes*.
- Jiang Deqi, Qi Leidi & Tan Jiesheng (1981), Soil erosion and conservation in the Wuding River Valley, China. In: Morgan, R.P.C. (ed.) *Soil Conservation: Problems and prospects*. Chichester: Wiley, pp. 461-479
- Jin, C.-X., M.J.M. Römken & F. Griffioen (2000), Estimating Manning's roughness coefficient for shallow overland flow in non-submerged vegetative filter strips. *Transactions of the ASAE* 43, pp. 1459-1466
- Julien, P.Y. & D.B. Simons (1985), Sediment transport capacity of overland flow. *Transactions of the ASAE* 28, pp.755-762
- Kalman, R. (1976), Etude expérimentale de l'érosion par griffes. *Revue de géographie physique et de géologie dynamique, série 2*, 18, pp. 395-406
- King, D., D.M. Fox, Y. le Bissonnais & V. Danneels (1998), Scale issues and a scale transfer method for erosion modelling. Ch 15 in: Boardman, J. & D. Favis-Mortlock (Eds.) *Modelling soil erosion by water*. NATO ASI series I 55. Berlin: Springer, pp. 201-212
- Kirkby, M.J (1994), Thresholds and Instability in Stream Head Hollows: A Model of Magnitude and Frequency for Wash Processes. In: Kirkby, M.J. (ed.) *Process models and theoretical geomorphology*. British Geomorphological Research Group Symposia Series 8. Chichester: Wiley
- Kirkby, M. (1998), Modelling across scales: the MEDALUS family of models. In: Boardman, J. & D. Favis-Mortlock (Eds.) *Modelling soil erosion by water*. NATO ASI Series I 55. Berlin: Springer, pp. 161-173

- Knisel, W.G. (1991), CREAMS/GLEAMS: a development overview. In: Beasley, D.B., W.G. Knisel & A.P. Rice (eds.) Proceedings of the CREAMS/GLEAMS symposium. Publication 4, Agricultural Engineering Department, University of Georgia, Athens, USA, pp. 9-17
- Kukla, G. & Z. An (1989), Loess stratigraphy in central China. *Palaeogeography, Palaeoclimatology, Palaeoecology* 72, pp. 203-225
- Leger, M. (1990), Loess Landforms. *Quaternary International* 7/8, pp. 53-61
- Li, G. & A.D. Abrahams (1997), Effect of saltating sediment load on the determination of the mean velocity of overland flow. *Water Resources Research* 33, pp. 341-347
- Lin, Z. & W. Liang (1982), Engineering properties and zoning of loess and loess-like soils in China. *Canadian Geotechnical Journal* 19, pp. 76-91
- Linyuan, Z., D. Xuerong, S. Zhengtao (1991), The sources of loess material and the formation of the Loess Plateau in China. In: Okuda, S et al. (eds.) *Loess Geomorphological hazards and processes*. *Catena supplement* 20, pp. 1-14
- Liu Guobin, Xu Mingxiang & Wen Zhongming (in press), Study on soil characteristics in a small watershed in the hilly-gullied area on the Loess Plateau in China.
- Loch, R.J. & E.C. Thomas (1987), Resistance to rill erosion: observations on the efficiency of rill erosion on tilled clay soil under simulated rain and run-on water. In: Bryan, R.B. (ed.) *Rill Erosion: Processes and significance*. *Catena Supplement* 8, pp. 71-83
- Lohnes, R.A. & R.L. Handy (1968), Slope angles in friable loess. *The Journal of Geology* 76, pp. 247-258
- Long Yuqian & Xiong Guishu (1981), Sediment measurement in the Yellow River. IAHS publication 133, pp. 275-285
- Low, A.J. (1954), The study of soil structure in the field and in the laboratory. *Journal of Soil Science* 5, pp. 57-74
- Low, H.S. (1989), effect of sediment density on bed-load transport. *Journal of hydraulic engineering* 115, pp. 124-138
- Loughran, R.J. (1989), The measurement of soil erosion. *Progress in Physical Geography* 13, pp. 216-233
- Lu, H. & D. Sun (2000), Pathways of dust input to the Chinese Loess Plateau during the last glacial and interglacial periods. *Catena* 40, pp. 251-261
- Lu, J.Y., E.A. Cassol & W.C. Moldenhauer (1989), Sediment transport relationships for sand and silt loam soils. *Transactions of the ASAE* 32, pp. 1923-1931
- Ludwig, B., J. Daroussin, D. King & V. Souchère (1996), Using GIS to predict concentrated flow erosion in cultivated catchments. IAHS Publication 235, pp. 429-436
- Madsen, H., G. Wilson & H.C. Ammentorp (2002), Comparison of different automated strategies for calibration of rainfall-runoff models. *Journal of Hydrology* 261, pp. 48-59
- Mathys, N. (1995), Caractérisation des matières en suspension. Mise au point d'une méthode rapide d'estimation des concentrations des prélèvements. In: Meunier, M. (coord.) *Compte-rendu de recherches N° 3*. BVRE de Draix. Equipements pour l'eau et l'environnement 21. Cemagref, pp. 25-41
- Messing, I., M.H. Hoang Fagerström (2001), Using farmers' knowledge for defining criteria for land qualities in biophysical land evaluation. *Land Degradation and Development* 12, pp. 541-553.
- Messing, I., Chen Liding & R. Hessel (in press a), Soil conditions in a small catchment on the Loess Plateau in China. *Catena*.
- Messing, I., M.H. Hoang Fagerström, C. Liding, B. Fu (in press b), Criteria for land suitability evaluation in a small catchment on the Loess Plateau in China. *Catena*
- Miao, T.D. & Z.G. Wang (1991), Deformation mechanism of collapsible loess in consideration of the microstructure instability. In: Okuda, S. et al. (eds.) *Loess Geomorphological hazards and processes*. *Catena supplement* 20, pp. 93-105

- Mohamoud, Y.M. (1992), Evaluating Manning's roughness coefficients for tilled soils. *Journal of Hydrology* 135, pp. 143-156
- Montgomery, D.R. & W.E. Dietrich (1992), Channel initiation and the problem of landscape scale. *Science* 255, pp. 826-830
- Montgomery, D.R. & W.E. Dietrich (1994), Landscape dissection and Drainage Area-Slope Thresholds. In: Kirkby, M.J. (ed.) *Process models and theoretical geomorphology*. British Geomorphological Research Group Symposia Series 8. Chichester: Wiley, pp. 221-246
- Morgan, R.P.C. (1996), *Soil erosion & conservation*. Second edition. Longman, Harlow, UK
- Morgan, R.P.C. & J.N. Quinton (2001), Erosion modelling. Ch 6 in: Harmon, R.S. & W.W. Doe (Eds.) *Landscape erosion and evolution modeling*. New York: Kluwer Academic/Plenum, pp. 117-143
- Morgan, R.P.C., J.N. Quinton, R.E. Smith, G. Govers, J.W.A. Poesen, K. Auerswald, G. Chisci, D. Torri & M.E. Styczen (1998a), The European Soil Erosion Model (EUROSEM): A dynamic approach for predicting sediment transport from fields and small catchments. *Earth Surface Processes and Landforms* 23, pp. 527-544
- Morgan, R.P.C., J.N. Quinton, R.E. Smith, G. Govers, J.W.A. Poesen, K. Auerswald, G. Chisci, D. Torri, M.E. Styczen & A.J.V. Folly (1998b), *The European Soil Erosion Model (EUROSEM): documentation and user guide, version 3.6*. Silsoe College, Cranfield University
- Mou Jinze (1981), The establishment of experimental plots for studying runoff and soil loss in the rolling loess regions of China. *IAHS publication* 133, pp. 467-477
- Muxart, T., A. Billard, E. Derbyshire & J. Wang (1994), Variation in runoff on steep, unstable loess slopes near Lanzhou, China: Initial results using rainfall simulation. In: Kirkby, M.J. (ed.) *Process models and theoretical geomorphology*. British Geomorphological Research Group Symposia Series 8. Chichester: Wiley, pp. 337-355
- Nachtergaele, J., J. Poesen, L. Vandekerckhove, D. Oostwoud Wijdenes & M. Roxo (2001), Testing the ephemeral gully erosion model (EGEM) for two Mediterranean Environments. *Earth Surface Processes and Landforms* 26, pp. 17-30
- Nearing, M.A. (1998), Why soil erosion models over-predict small soil losses and under-predict large soil losses. *Catena* 32, pp. 15-22
- Nearing, M.A., L.D. Norton, D.A. Bulgakov, G.A. Larionov, L.T. West & K.M. Dontsova (1997), Hydraulics and erosion in eroding rills. *Water Resources Research* 33, pp. 865-876
- Nearing, M.A., J.R. Simanton, L.D. Norton, S.J. Bulygin & J. Stone (1999), Soil erosion by surface water flow on a stony, semiarid hillslope. *Earth Surface Processes and Landforms* 24, pp. 677-686
- Nir, D. & M. Klein (1974), Gully erosion induced in land use in a semi-arid terrain (Nahal Shiqma, Israel). *Zeitschrift für Geomorphologie Supplementband* 21, pp. 191-201
- Nordström, K. (1988), Gully erosion in the Lesotho lowlands. A geomorphological study of interactions between intrinsic and extrinsic variables. *UNGI rapport* 69
- NSERL (1995), *Technical Documentation USDA-Water Erosion Prediction Project (WEPP)*. NSERL report 10. USDA-ARS National Soil Erosion Research Laboratory: West Lafayette.
- Olivier, J. & J. Pebay Peyroula (1995), L'Ellan, un limnographe adapte aux mesures en conditions difficiles. In: Meunier, M. (coord.) *Compte-rendu de recherches N° 3*. BVRE de Draix. Equipements pour l'eau et l'environnement 21. Cemagref, pp. 12-24
- Oostwoud Wijdenes, D.J. & R. Bryan (2001), Gully-head erosion processes on a semi-arid valley floor in Kenya: a case study into temporal variation and sediment budgeting. *Earth Surface Processes and Landforms* 26, pp. 911-933
- Petryk, S. & G. Bosmajian (1975), Analysis of flow through vegetation. *Journal of the hydraulics division, ASCE* 101, pp. 871-884

- Poesen, J. (1993), Gully typology and gully control measures in the European loess belt. In: Wicherek, S. (Ed.) *Farm land erosion in temperate plains environment and hills*. Amsterdam: Elsevier, pp. 221-239
- Poesen, J., K. Vandaele & B. van Wesemael (1998), Gully erosion: importance and model implications. In: Boardman, J & D. Favis-Mortlock (eds.) *Modelling soil erosion by water*. NATO ASI series I 55, Berlin: Springer, pp. 285-311
- Prosser, I.P. (1996), Thresholds of Channel Initiation in Historical and Holocene Times, Southeastern Australia. In: Anderson, M.G. & S.M. Brooks (eds.) *Advances in Hillslope Processes*. Vol. 2. Chichester: Wiley, pp. 687-708
- Prosser, I.P. & W.E. Dietrich (1995), Field experiments on erosion by overland flow and their implication for a digital terrain model of channel initiation. *Water Resources Research* 31, pp. 2867-2876
- Prosser, I.P. & P. Rustomji (2000), sediment transport capacity relations for overland flow. *Progress in Physical Geography* 24, pp. 179-193
- Pye, K. (1987), *Aeolian dust and dust deposits*. Academic Press, London
- Pye, K. & D. Sherwin (1999), Loess. Ch 10 in: Goudie, A.S., I. Livingstone & S. Stokes (Eds.) *Aeolian environments, sediments and landforms*. Chichester: Wiley, pp. 213-238
- Rauws, G. (1987), The initiation of rills on plane beds of non-cohesive materials. In: Bryan, R.B. (ed.) *Rill Erosion: Processes and significance*. Catena Supplement 8, pp. 107-118
- Reid, I., J.C. Bathurst, P.A. Carling, D.E. Walling & B.W. Webb (1997), Sediment erosion, transport and deposition. Ch 5 in: Thorne, C.R., R.D. Hey & M.D. Newson (eds.), *Applied fluvial geomorphology for river engineering and management*, Chichester: Wiley, pp. 95-135
- Renard, K.G., G.R. Foster, G.A. Weesies, D.K. McCool & D.C. Yoder, coordinators (1997), *Predicting soil erosion by water: a guide to conservation planning with the Revised Universal Soil Loss Equation (RUSLE)*. US Department of Agriculture, Agriculture Handbook 703
- Ren Mei-e & Zhu Xianmo (1994), Anthropogenic influences on changes in the sediment load of the Yellow River, China, during the Holocene. *The Holocene* 4, pp. 314-320
- Rhoads, B.L. (1987), Stream power terminology. *Professional Geographer* 39, pp. 189-195
- Rickenmann, D. (1991), Hyperconcentrated flow and sediment transport at steep slopes. *Journal of hydraulic engineering* 117, pp. 1419-1439
- Rose, C.W. (1985), Developments in soil erosion and deposition models. In: Stewart, B.A. (ed.) *Advances in soil science*, volume 2, New York: Springer, pp. 1-65
- Rouhipour, H., C.W. Rose, B. Yu & H. Ghadiri (1999), Roughness coefficients and velocity estimation in well-inundated sheet and rilled flow without strongly eroding bed forms. *Earth Surface Processes and Landforms* 24, pp. 233-245
- Schoorl, J.M., M.P.W. Sonneveld & A. Veldkamp (2000), Three-dimensional landscape process modelling: the effect of DEM resolution. *Earth Surface Processes and Landforms* 25, pp. 1025-1034
- Scott, K.M. (1988), Origins, behavior, and sedimentology of lahars and lahar-runout flows in the Toutle-Cowlitz river system. U.S. Geological Survey professional paper 1447-A
- Selby, M.J. (1993), *Hillslope materials and processes*. Second edition. Oxford University Press, Oxford.
- Shaozhong Kang, Lu Zhang, Xiaoyu Song, Shuhan Zhang, Xianzhao Liu, Yinli Liang & Shiqing Zheng (2001), Runoff and sediment loss responses to rainfall and land use in two agricultural catchments on the Loess Plateau of China. *Hydrological Processes* 15, pp. 977-988
- Sidorchuk, A. (1999), Dynamic and static models of gully erosion. *Catena* 37, pp. 401-414
- Sidorchuk, A. & A. Sidorchuk (1998), Model for estimating gully morphology. IAHS publication 249, pp. 333-343
- Singh, V.P. (1997), *Kinematic wave modeling in water resources*. Environmental hydrology. Wiley

- Singh, V.P. (2002), Is hydrology kinematic? *Hydrological Processes* 16, pp. 667-716
- Smart, G.M. & M.N.R. Jaeggi (1983), Sediment transport on steep slopes. *Mitteilungen der Versuchsanstalt für Wasserbau, Hydrologie und Glaziologie* 64. Technische Hochschule Zurich.
- Smith, R.E., D.C. Goodrich & J.N. Quinton (1995), Dynamic, distributed simulation of watershed erosion: The KINEROS2 and EUROSEM models. *Journal of Soil and Water Conservation* 50, pp. 517-520
- Smith, T.R. & F.P. Bretherton (1972), Stability and the conservation of mass in drainage basin evolution. *Water Resources Research* 8, pp. 1506-1529
- Steenen, A. & G. Govers (2001), Correction factors for estimating suspended sediment export from loess catchments. *Earth Surface Processes and Landforms* 26, pp. 441-449
- Stolte, J., B. van Venrooij, Zhang Guanghui, K.O. Trouwborst, Liu Guobin, C.J. Ritsema & R. Hessel (in press), Land-use induced spatial heterogeneity of soil hydraulic properties on the Loess Plateau of China. *Catena*
- Summer, W. & Wei Zhang (1998), sediment transport analysed by energy derived concepts. IAHS publication 249, pp. 355-362
- Takken, I. & G. Govers (2000), Hydraulics of interrill overland flow on rough, bare soil surfaces. *Earth Surface Processes and Landforms* 25, pp. 1387-1402
- Takken, I., G. Govers, C.A.A. Ciesiolka, D.M. Silburn & R.J. Loch (1998), Factors influencing the velocity-discharge relationships in rills. IAHS Publication 249, pp. 63-69
- Takken, I., L. Beuselinck, J. Nachtergaele, G. Govers, J. Poesen & G. Degraer (1999), Spatial evaluation of a physically-based distributed erosion model (LISEM). *Catena* 37, pp. 431-447
- Tan, T.K. (1988), Fundamental properties of loess from northwestern China. *Engineering Geology* 25, pp. 103-122
- Torri, D. & L. Borselli (1991), Overland flow and soil erosion: some processes and their interactions. *Catena supplement* 19, pp. 129-137
- Torri, D., M. Sfalanga & G. Chisci (1987), Threshold conditions for incipient rilling. In: Bryan, R.B. (ed.) *Rill Erosion: Processes and significance*. *Catena Supplement* 8, pp. 97-105
- Vandaele, K., J. Poesen, G. Govers & B. van Wesemael (1996), Geomorphic threshold conditions for ephemeral gully incision. *Geomorphology* 16, pp. 161-173
- Vandekerckhove, L., J. Poesen, D. Oostwoud Wijdenes & G. Gysels (2001), Short-term bank gully retreat rates in Mediterranean environments. *Catena* 44, pp. 133-161
- Van den Berg, J.H. & A. van Gelder (1993), Prediction of suspended bed material transport in flows over silt and very fine sand. *Water Resources Research* 29, pp. 1393-1404
- Van den Elsen, H.G.M., Liu Baoyuan, Wu Yongqiu, K. Trouwborst & C.J. Ritsema (in press a), Intensive water content and discharge measurements in a hillslope erosion gully in China. *Catena*
- Van den Elsen, H.G.M., R. Hessel, Liu Baoyun, K.O. Trouwborst, C.J. Ritsema & H. Blijenberg (in press b), Discharge measurements at the outlet of a watershed on the Loess Plateau of China. *Catena*
- Van Dijck, S. (2000), Effects of agricultural land use on surface runoff and erosion in a Mediterranean area. *Netherlands Geographical Studies* 263
- Van Rijn, L.C. (1993), Principles of sediment transport in rivers, estuaries and coastal seas. Aqua publications- I11
- Vázquez, R.F., L. Feyen, J. Feyen & J.C. Refsgaard (2002), Effect of grid size on effective parameters and model performance of the MIKE-SHE code. *Hydrological Processes* 16, pp. 355-372
- Ven Te Chow (1959), *Open-Channel Hydraulics*. Auckland: McGraw-Hill
- Ven Te Chow, D.R. Maidment & L.W. Mays (1988), *Applied hydrology*. New York: McGraw-Hill

- Wagner, L.E. & Yiming Yu (1991), Digitization of profile meter photographs. *Transactions of the ASAE* 34, pp. 412-416
- Wen Qizhong, Diao Guiyi & Yu Suhua (1987), Geochemical environment of loess in China. In: Pécsi, M. (Ed.) *Loess and environment*. *Catena supplement* 9, pp. 35-46
- Wesseling, C.G., D. Karssenbergh, P.A. Burrough & W.P.A. van Deursen (1996), Integrating dynamic environmental models in GIS: The development of a Dynamic Modelling language. *Transactions in GIS* 1, pp. 40-48
- Wischmeier, W.H. & D.D. Smith (1978), Predicting rainfall erosion losses – a guide to conservation planning. US Department of Agriculture, Agricultural Research Service Handbook 537
- Woodward, D. (1999), Method to predict cropland ephemeral gully erosion. *Catena* 37, pp. 393-399
- Wu Yongqiu, Kunqing Xie, Zhang Qingchun, Zhang Yan, Xie Yun & C.J. Ritsema (in press), Plant characteristics and their temporal change on the Loess Plateau of China.
- Xu Jiongxin (1999a), Erosion caused by hyperconcentrated flow on the Loess Plateau of China. *Catena* 36, pp. 1-19
- Xu Jiongxin (1999b), Grain-size characteristics of suspended sediment in the Yellow River, China. *Catena* 38, pp. 243-263
- Xu Jiongxin (2001), Historical bank-breaching of the lower Yellow River as influenced by drainage basin factors. *Catena* 45, pp. 1-17
- Yalin, M.S. (1963), An expression for bedload transportation. *Journal of the Hydraulics Division, Proceedings of the American Society of Civil Engineers* 89, pp. 221-250
- Yang, C.T. (1973), Incipient motion and sediment transport. *Journal of the Hydraulics Division, Proceedings of the American Society of Civil Engineers* 99, pp. 1679-1703
- Zhang, J., W.W. Huang & M.C. Shi (1990), Huanghe (Yellow River) and its estuary: sediment origin, transport and deposition. *Journal of hydrology* 120, pp. 203-223.
- Zhang, X., D.E. Walling, T.A. Quine & A. Wen (1997), Use of reservoir deposits and caesium-137 measurements to investigate the erosional response of a small drainage basin in the rolling loess Plateau region of China. *Land degradation & Development* 8, pp. 1-16
- Zhaohui Wan & Zhaoyin Wang (1994), *Hyperconcentrated flow*. IAHR Monograph, Rotterdam: Balkema
- Zhi-Yong Yin & Xinhao Wang (1999), A cross-scale comparison of drainage basin characteristics derived from digital elevation models. *Earth Surface Processes and Landforms* 24, pp. 557-562
- Zhu, T.X. (1997), deep-seated, complex tunnel systems – a hydrological study in a semi-arid catchment, Loess Plateau, China. *Geomorphology* 20, pp. 255-267
- Zhu, T.X., Q.G. Cai & B.Q. Zeng (1997), Runoff generation on a semi-arid agricultural catchment: field and experimental studies. *Journal of Hydrology* 196, pp. 99-118
- Zhu, T.X., S.H. Luk, Q.G. Cai (2002), Tunnel erosion and sediment production in the hilly loess region, North China. *Journal of Hydrology* 257, pp. 78-90



## **CURRICULUM VITAE**

Rudi Hessel was born on January 28<sup>th</sup>, 1972 in Utrecht (The Netherlands). After graduating from secondary school in 1990, he studied Physical Geography at Utrecht University from 1990-1996, specialising in land degradation and hydrology. He started work on this PhD thesis in January 1998. To gather the data presented in this thesis he went to China 6 times in the next three years, with a total duration of stay of about 11 months. His frequent travels to China also gave him the opportunity to visit the second lowest place on Earth: Lake Aydingkol in Qinghai Province (-154 m).

He presented part of the research described in this thesis at the following international conferences: the first international symposium on gully erosion under global change, held in Leuven, Belgium (2000), the second international symposium on gully erosion under global change, held in Chengdu, China (2002) and the 12<sup>th</sup> ISCO conference, held in Beijing, China (2002).

Since 2001, he is also employed by Alterra Green World Research, Wageningen, the Netherlands, where he is currently involved in the application of the LISEM model to catchments in Kenya and Tanzania. During a stay in Tanzania in 2001, he extended his altitude range to over 6000 m by climbing Mount Kilimanjaro (5895 m).

